The Design of Ligands for Aluminium Oxy/hydroxide Surfaces

David K. Henderson

Doctor of Philosophy

University of Edinburgh

2001

Contents.

Preface and Declaration.

Since graduating from the University of Edinburgh in 1997 with a BSc. (Hons) degree in Chemistry, the author has been engaged in a programme of full time research under the supervision of Professor P. A. Tasker of the University of Edinburgh and Professor R. E. P. Winpenny, formerly of the University of Edinburgh now at the University of Manchester.

I declare that this thesis has been entirely composed by myself and that the work described herein is my own work except where clearly mentioned either in acknowledgement, reference or text. No part of the work referred to in this thesis has been submitted in support of an application for another degree or qualification from this or any other University or institute of learning. Certain of the results have been published previously.

Abstract.

This work deals with the design, synthesis and evaluation of ligands to bind to lightly oxidised metal surfaces, particularly those of aluminium. Chapter 1 provides some information on the properties, production, uses, and compounds of aluminium and on protocols currently in use as pre-treatments which generally involve aggressive, environmentally unsound processes. The concept of using surface-modifying ligands in more benign pre-treatments is discussed.

1,3,5-triazine derivatives are considered as potentially polynucleating surface-ligands in chapter 2. Synthetic routes to novel hydroxy and thiol functionalised, alkylamino containing triazines were developed. A range of such compounds with different subtitution patterns has been characterised. X-ray structure determination of 6-(diethylamino)-1,3,5-triazine-2,4-dithione (H_2SSta) and 6-(diethylamino)-1,3,5-triazine-2-thione-4-one (H_2OSta) showed them to be present in the thione/one tautomeric forms. All the crystallographically characterised triazines show strong intermolecular hydrogen bonding. Formation of transition metal complexes was found to be accompanied by ligand rearangement. Condensation reactions, forming novel thioether bridged ligands *in-situ*, have been observed in the crystallographically characterised complexes $[Ni\{(Sta)S(S_2ta)\}]$ and $[Co_6NaO(OStaH)_7\{S(Ota)_2\}_2(O_2CPh)_2(H_2O)_2]$. The instability of these compounds in solution in the presence of metal Lewis acids limits their study by isotherm determination and makes them poor candidates for the rational development of surface treatments for aluminium. The structurally related ligands 2-hydroxypyridine and uracil were shown by the isotherm studies to adsorb only weakly onto an $Al(OH)_3$ surface.

Known carboxylic acid-based corrosion inhibitors for iron are considered in aluminium chemistry in chapter 3. Isotherm studies on the 3-ketocarboxylic acid, 3-(4-methylbenzoyl)-propionic acid and its non keto analogue 4-*p*-tolyl-butyric acid have reinforced the concept that secondary interactions, such as hydrogen bonding to surface hydroxides, can play an important role in determining the binding characteristics of surface ligands. In accordance with a survey of the Cambridge

Crystallographic Database which revealed that there are few examples of carboxylic acids functioning as polynucleating ligands for aluminium(III), it was found impossible to isolate crystalline aluminium(III) complexes. However, the coordination chemistry of 3-ketocarboxylic acids was extended by the synthesis of two mixed ligand, 3-benzoyl-propionoic acid (Hbpa)/ 6-x-2-hydroxypyridine [Hxhp, where x = m (methyl) or c (chloro)], polynuclear nickel clusters, $[Ni_3(chp)_4(bpa)_2(MeOH)_6].2MeOH$ and $[Ni_6Na_2Cl_2(OH)_6(Hmhp)_6(bpa)_6]$.

Simple phosphorus acid-based ligands are considered in chapter 4. Isotherm studies demonstrated that phosphonic acids bind strongly to $Al(OH)_3$. Their development (chapter 5) by incorporating carbonyl or additional phosphonic acid groups has revealed the increased surface coverage and improved surface passivation properties (chapter 6) of (3-oxo-3-phenyl-propyl)-phosphonic acid and (3-oxo-3-*p*-tolyl-propyl)-phosphonic acid over the non carbonyl analogue (3-phenyl-propyl)-phosphonic acid again implicate the important role played by the carbonyl group in surface binding. A potential binding mode of the ligand 4-methyl-2,6-bis(phosphonomethyl)phenol (H_5mbpp) was suggested by the crystal structure of the tetranuclear copper complex, $[Cu_4(Hmbpp)_2(H_2NC(O)NH_2)_2(H_2O)_8].4H_2O$.

Of the ligand classes studied, phosphonic acids, and in particular the 3-keto derivatised phosphonic acids have the greatest potential for use as surface modifying agents.

Acknowledgements.

My supervisors Prof. Peter Tasker and Prof. Richard. E. P. Winpenny who gave me the chance to do a PhD and for their constant support, ideas and guidance throughout.

Dr Phil Bailey for giving me a space in his lab for a year and for not giving me too hard a time in my first year viva.

Dr Dave White, Dr Paul Lovatt and Dr David Nation for advice and discussions at various stages of my PhD.

Dr Tim Higgs because he always claims that he merits a paragraph of his own.

Dr Simon Parsons, Dr Bob Coxall and Andy Parkin for all of the X-ray crystallography, often against the odds with poor quality crystals (and occasionally the wrong ones – Andy!).

John Millar and Wesley Kerr for NMR, Lorna Eades, Stuart Franklin and Tim Calder for elemental analysis and Alan Taylor and Harry Mackenzie for mass spectrometry.

Dr Neil Robertson for the conductivity measurements, Paul Snelson at Avecia for the hydrogen evolution data, Dr Eric McInnes at Manchester University for the EPR spectra and Alasdair Graham for running the SQUID samples.

All of the people that I have worked with during the time I have been at Edinburgh, particularly those in lab's 94, 85, 86, 2.16 and 2.17.

Billy (great name for a Rangers fan) Gordon, because life would be much duller without his daily (blue tinged) view of the world and Sonali De Silva, who thought chapter 1 was a bit dull and so coloured in a couple of the diagrams for me.

And finally my Mum and Dad for their support and for putting up with me all these years.

Abbreviations.

δ	chemical shift
λ	wavelength
ν	wavenumber
ε	extinction coefficient
°	degree
θ	circle diffraction angle
°C	degree centigrade
χ_M	molar susceptibility
μm	micrometre
$\{(Sta)S(S_2ta)\}^{2-}$	4-diethylamino-6-(4-diethylamino-6-disulfanyl-[1,3,5]triazin-2-ylsulfanyl)-[1,3,5]triazine-2-thiol
$\{S(Ota)_2\}^{2-}$	2,2'-thiobis-{6-(diethylamino)-1,3,5-triazine-4-ol}
2-opepa	(2-oxo-2-phenyl-ethyl)-phosphonic acid
3-pppa	(3-phenyl-propyl)-phosphonic acid
4-nbpa	4-nitrobenzyl phosphonic acid
4-nbpampa	[(4-nitro-benzyl-phosphonomethyl-amino)-methyl]-phosphonic acid
Å	angstrom
acac	2, 4-pentanedione
Al_{13}	term referring to a class of polynuclear cluster containing 13 aluminium atoms
Alk	alkyl
Al_{P2}	"$Al_{24}O_{72}$"
Ar	aryl
bpa	3-benzoylpropionic acid
br	broad
ca	*circa*
$CDCl_3$	deuterated chloroform

chp	anion of 6-chloro-2-hydroxypyridine
cis	*cisoid*
cm^{-1}	wavenumber
CSD	Cambridge Structural Database
d (NMR)	doublet
D_2O	deuterated water
d_6-DMSO	deuterated dimethyl sulfoxide
dd	doublet of doublets
dpa	diphenylacetic acid
dppp	bis(diphenylphosphino)propane
ed.	editor
EIMS	electron impact mass spectroscopy
EPR	electron paramagnetic resonance
et al	*et alli* (and others)
EtOH	ethanol
FABMS	fast atom bombardment mass spectroscopy
g	gram
g (EPR)	*g* value (for a free electron, $g_e = 2.0023$)
h	hour
H_2O_2ta	6-(isopropylamino)-1,3,5-triazine-2,4-dione
H_2OSta	6-(diethylamino)-1,3,5-triazine-2-thione-4-one
H_2SSta	6-(diethylamino)-1,3,5-triazine-2,4-dithione
H_3heidi	$N(CH_2CO_2H)_2(CH_2CH_2OH)$
H_5mbpp	4-methyl-2,6-bis(phosphonomethyl)phenol
IR	infra-red
Irg-419	3-(4-methylbenzoyl)-propionic acid
Irg-78	4-p-tolyl-butyric acid
Irgacor 252	2-(benzothiazol-2-ylsulfanyl)-succinic acid
K	kelvin
K	equilibrium constant
m	*meta*
m (IR)	medium

m (NMR)	multiplet
m.p.	melting point
m/z	mass per unit charge
MeCN	acetonitrile
MeOH	methanol
mhp	anion of 6-methyl -2-hydroxypyridine
MHz	mega hertz
min	minute
ml	millilitre
mmHg	millimetres of mercury
mmol	milli moles
mol	moles
NMR	nuclear magnetic resonance
o	*ortho*
OH	hydroxide anion
p	*para*
p-419	(3-oxo-3-*p*-tolyl-propyl)-phosphonic acid
p-bpa	(3-oxo-3-phenyl-propyl)-phosphonic acid
pH	negative logarithm (base ten) of the hydrogen ion concentration
Ph	phenyl
pK_a	negative logarithm (base ten) of the acid dissociation constant
ppa	phenylphosphonic acid
q (NMR)	quartet
QCM	quartz crystal microbalance
S	siemens ($ohms^{-1}$)
s (IR)	strong
s (NMR)	singlet
SBU	secondary building unit
T	temperature
t (NMR)	triplet

THF	tetrahydrofuran
tma	trimethylacetic acid
tpa	triphenylacetic acid
trans	*transoid*
UV/vis	ultra violet/visible
VBATDT	6-[(4-vinylbenzyl)propylamino]-1,3,5-triazine-2,4-dithione
w (IR)	weak
Z	number of asymmetric units per unit cell

Publications.

1. Inter-ligand reactions: *in-situ* formation of new polydentate ligands, Robert A. Coxall, Steven G. Harris, David K. Henderson, Simon Parsons, Peter A. Tasker and Richard E. P. Winpenny, *J. Chem. Soc. Dalton Trans.*, 2000, 2349.

Chapter 1:

Introduction.

Contents.

1.1 Aluminium: History, Properties, Occurrence, Production and Uses.

The Danish chemist Hans Christian Oersted was the first to isolate aluminium in 1825 using a process involving potassium amalgam. Friedrich Wohler, a German chemist improved the process, by the use of metallic potassium and was the first to measure the specific gravity of aluminium. In 1854 Henri Sainte-Claire Deville produced aluminium by the reduction of aluminium chloride with sodium. With the financial backing of Napoleon III, who saw its potential for use as lightweight body-armour, he built an experimental plant and presented a display of pure aluminium at the Paris Exposition of 1855. A breakthrough in aluminium production came in 1886 when, independently, Charles Martin Hall in the USA and Paul L. T. Heroult in France discovered that aluminium oxide (Al_2O_3) dissolved in molten cryolite ($Na_3[AlF_6]$) and could then be decomposed electrolytically to a crude molten metal. This process is still the main method for the commercial production of aluminium, although the purity of the product has been increased since the original efforts.[1,2]

Aluminium is a hard, strong, lightweight, non-magnetic, silvery metal, which although highly electropositive, is resistant to corrosion, due to the formation of a protective oxide layer on exposure to air. Some fundamental atomic and physical properties of aluminium are listed (Table 1.1).

Atomic Properties		Physical Properties	
Atomic number	13	m.p./ °C	660.37
No. of naturally occurring isotopes	1	b.p./ °C	2467
		Density (20°C)/ g cm^{-3}	2.699
Atomic weight	26.98154	Hardness (Mohs)	2.75
Electronic configuration	$[Ne]3s^23p^1$	ΔH_{fus}/ kJ mol^{-1}	10.50
		ΔH_{vap}/ kJ mol^{-1}	290.8
Ionization energy/ kJ mol^{-1}	577.4	ΔH_f (monoatomic gas)/ kJ mol^{-1}	321.7
	1816.1		
	2744.1	Electrical resistivity/ μohm cm^{-1}	2.655
Metal radius/ pm	143		
Ionic radius/ pm (6-coord.)	53.5	$E°$ ($M^{3+} + 3e^- = M(s)$/ V	-1.66
		$E°$ ($M^+ + e^- = M(s)$/ V	0.55
		Electronegativity χ	1.5

Table 1.1: Fundamental atomic and physical properties of aluminium.[3]

Aluminium is the third most abundant element and the most common metal in the Earth's crust at 8.8 mass %. It does not occur in the metallic state because of its strong affinity for oxygen but is widespread in minerals and rocks, particularly in chemical combination with silicon oxides such as feldspars, mica and clays. Other minerals containing oxides of aluminium, e.g. spinel ($MgAl_2O_4$), garnet [$Ca_3Al_2(SiO_4)_3$], beryl ($Be_3Al_2Si_6O_{18}$) and turquoise [$Al_2(OH)_3PO_4.H_2O/Cu$] are rare. Corundum (Al_2O_3), at 52.9 % aluminium, has the highest known aluminium content and is one of the hardest substances known. Many gemstones are impure forms of Al_2O_3, e.g. ruby (Cr) and sapphire (Co). Aluminium also occurs in a number of other ores and minerals, including, hydroxide, oxide-hydroxide, phosphate, fluoride and sulfate.[2,3,4,5]

The weathering of feldspars and other aluminium silicates is known as kaolinization and leads to the formation of clay minerals such as kaolinite [$Al_2(OH)_4Si_2O_5$], montmorillonite [$(Na,Ca)_{0.3}(Al,Mg)_2Si_4O_{10}(OH)_2.nH_2O$] and vermiculite [$(Mg,Fe(II),Al)_3(Al,Si)_4O_{10}(OH)_2.4H_2O$], via the leaching of the more soluble constituents, sodium, potassium, calcium, magnesium and some silicon. Under certain conditions, mainly in tropical and subtropical regions, the weathering can continue beyond the kaolinization process. The silicates are further broken down and silica leached out forming bauxites, $AlO_x(OH)_{3-2x}$ ($0 < x < 1$). Bauxites contain a minimum of 40 % alumina and are commercially the most important aluminium-containing minerals.[3,4]

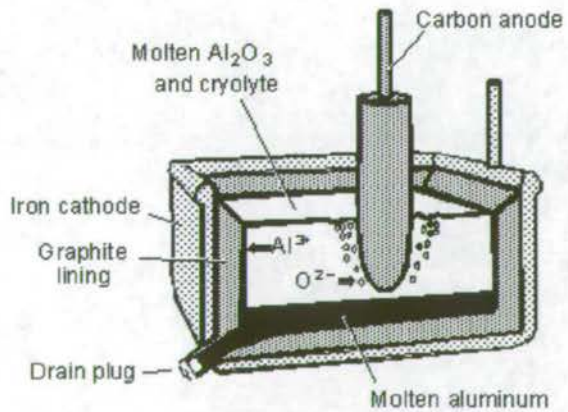

Cathode: $4\ Al^{3+} + 12\ e^- \longrightarrow 4\ Al(l)$

Anode: $6\ O^{2-} \longrightarrow 3\ O_2(g) + 12\ e^-$

Net: $4\ Al^{3+} \longrightarrow 4\ Al(l) + 3\ O_2(g)$

Figure 1.1: Production of aluminium metal by electolysis.[6]

Aluminium metal is prepared by the electrolysis of Al_2O_3 dissolved in molten cryolite (Figure 1.1). The Al_2O_3 is obtained by calcination of aluminium trihydroxide, normally gibbsite, prepared by the Bayer process. In the Bayer process (Figure 1.2), crushed bauxite is treated with caustic aluminate solutions containing NaOH (100-300 g l^{-1}). The reaction is carried out at elevated temperature (140-280 °C) and under pressure (≤ 35 atm). The caustic solution only reacts with the alumina, leaving the impurities to be separated by filtration, giving a clear solution. The dissolved aluminium hydroxide is recovered by dilution and cooling of the solution to 50-70 °C. The aluminium hydroxide is precipitated by addition of large quantities of seed particles of gibbsite and agitation in large crystallisers for three days. The product slurry is clarified and the course fraction separated and passed on to the next stage, while the finer fraction is recycled as seed for future crystallisations. The filtered solution, still containing approximately half its original alumina content, is sent back to the extraction system via the evaporators.[4,7]

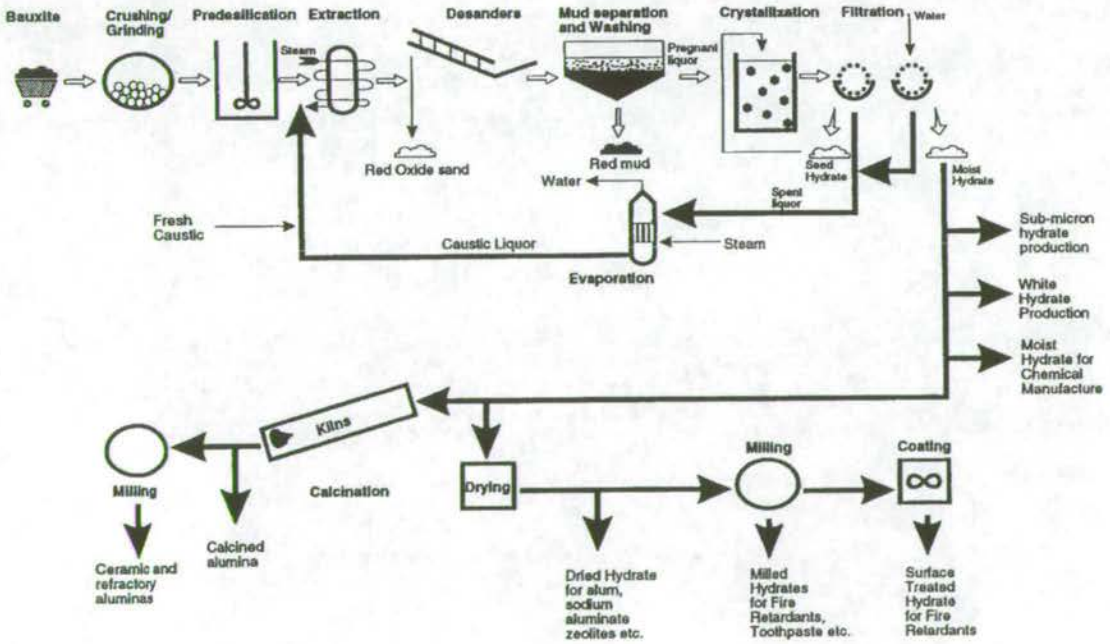

Figure 1.2: The Bayer process.[4]

Worldwide production of aluminium hydroxide exceeds 55 million tonnes per year and approximately 90 % is calcined to aluminium oxide, most of which is used in the production of aluminium metal.[4]

Aluminium is widely used in industry and in America alone, in 1996, primary aluminium production was 3.6 million tonnes with an estimated value of $5.6 billion. This figure however accounts for only 17 % of the total world production, the other two largest producers being Russia (14 %) and Canada (11 %). In addition to this, secondary production, recovery from scrap, in America amounted to around 3.3 million tonnes. These figures demonstrate the scale and importance of aluminium in industry.[8]

American domestic use of aluminium in 1996 included the transport industry (32 %), containers and packaging (26 %), building and construction (16 %), electrical and consumer durables (8 % each) and other uses (10 %).[8]

The automobile industry is becoming an increasingly important user of aluminium as demonstrated by Audi launching the world's first mass produced all aluminium car in 1995, the A8 (Figure 1.3), followed in 2000 by the A2.

Figure 1.3: Audi A8.

1.2 Aluminium Oxide/Hydroxides: Structures,[9] Production and Uses.[4,7]

Aluminium forms a wide range of oxides and hydroxides. Some of these are well characterised crystalline compounds, while others are amorphous and ill-defined. There are three main types of aluminium oxide/hydroxide, aluminium oxide

[Al_2O_3], aluminium oxy/hydroxide [Al(O)(OH)] and aluminium hydroxide [$Al(OH)_3$], each of which can be subdivided into α and γ forms (Table 1.2). Other forms such as tohdite ($5Al_2O_3.H_2O$) exist but are less well documented.

Oxide/hydroxide	α-form	γ-form
Al_2O_3	corundum	γ-alumina
Al(O)(OH)	diaspore	boehmite
$Al(OH)_3$	bayerite	gibbsite

Table 1.2: Common forms of aluminium oxide/hyroxides.

The structure of corundum is composed of hexagonal close-packed layers of oxygen ions with two-thirds of the octahedral holes occupied statistically by aluminium ions. This is the most thermodynamically stable of the aluminium oxide/hydroxides and is the final product of thermal or dehydroxylation treatments of all the oxides/hydroxides. It has a Mohs' hardness of 9 and a density of 3.98 g cm^{-3}.

γ-Alumina has no single defined structure and instead represents a collection of phases which are based on a defective spinel ($M^{2+}M^{3+}{}_2O_4$) structure where the oxygen atoms are essentially cubic close packed and the aluminium ions are disordered within this lattice. A substantial number of these transition phases are observed before ultimate reconstruction of the lattice to that of corundum (Figure 1.4).

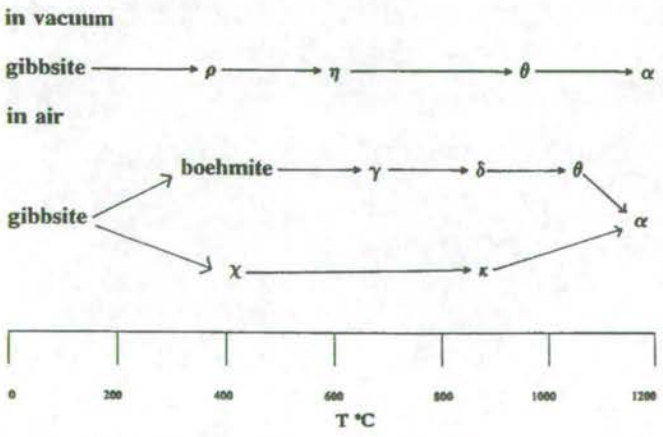

Figure 1.4: Phase changes of aluminium oxide/hydroxides on heating.[4]

Diaspore (Figure 1.5) is isostructural with α-Fe(O)(OH) (goethite) and contains two independent oxygen atoms (O_I oxo and O_{II} hydroxyl). All aluminium ions are octahedral and bound to three O_I and three O_{II} (Al-O_I 1.85 Å and Al-O_{II} 1.98 Å). The resulting octahedra share edges to form "double rutile strings". These are connected to each other by corner shared oxygens forming a 3-D network.

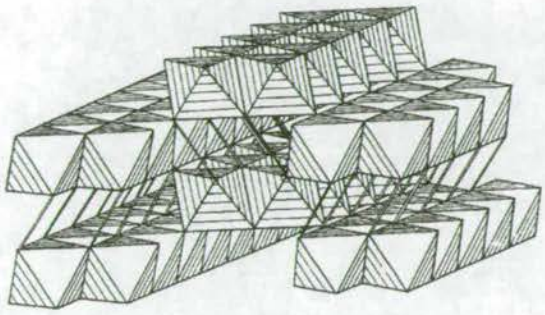

Figure 1.5: Structure of diaspore.

The structure of boehmite (Figure 1.6) as a whole is not close packed, but the oxygen atoms within a layer are cubic close packed. As in diaspore there are two types of oxygen (O_I oxo and O_{II} hydroxyl). The structure can essentially be regarded as an Al/O_I sheet backbone with $O_{II}H$ on the periphery of the sheet hydrogen bonded to $O_{II}H$ of the adjacent sheet.

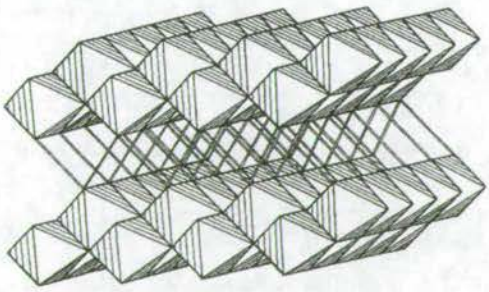

Figure 1.6: Structure of boehmite.

All forms of aluminium trihydroxide are built around the same basic unit, layers of $\{Al(OH)_3\}_n$, and the differences between them result from the nature of the stacking of these layers. The layer can be described as a system of $Al(OH)_6$ octahedra each sharing three edges, or as close-packed sheets of hydroxide ions stabilised by aluminium ions situated in two-thirds of the octahedral interstitial holes.

Bayerite contains approximately hexagonal close-packed anions with an interlayer spacing of 4.72 Å. The structure is monoclinic.

In the structure of gibbsite (Figure 1.7) the layers are open-packed with neighbouring pairs, with the whole structure having approximately hexagonal symmetry. The interlayer spacing is larger than in bayerite at 4.85 Å. Gibbsite is usually monoclinic, but a triclinic form also exists.

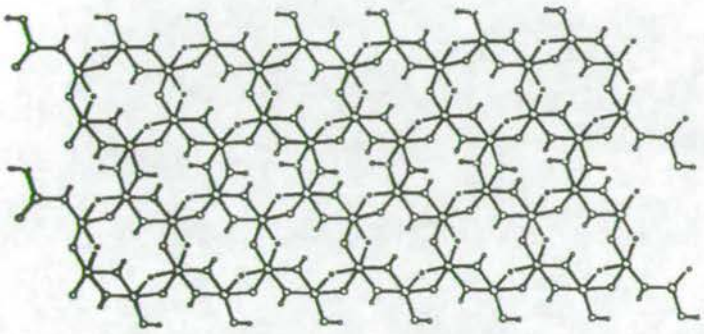

Figure 1.7: Structure of gibbsite. [10]

Nordstrandite represents an intermediate case of the two main aluminium trihydroxide structures with an interlayer spacing of 4.79 Å.

As described previously the Bayer process produces aluminium oxides and hydroxides, most of the annual production going to make aluminium metal. Approximately 3.6 million tonnes of aluminium hydroxide per year is used outside of aluminium metal production. Much of this is used to make other aluminium compounds including, zeolites, aluminium sulfate for use in paper making and water treatment, aluminium fluoride, aluminium nitrate, aluminium chloride, poly(aluminium silicate sulfate), sodium aluminate, catalysts and titania pigment coating.

There are also many direct applications of aluminium hydroxide, which account for several hundred thousand tonnes annually. Approximately 200,000 tonnes per year worldwide is used as the basis of fire retardants in plastics. The fire retardant properties of aluminium hydroxide are due to its interference with the primary combustion stage. On heating to above 200 °C it decomposes to give alumina and water vapour (Scheme 1.1). This reaction is strongly endothermic, absorbing 1.97 kJ g^{-1} of aluminium hydroxide, thus removing heat from the reaction

zone of the polymer and slowing the rate of decomposition. The water vapour (34.6 % by wt of $Al(OH)_3$) released also dilutes any combustible gases evolved and hinders the access of oxygen to the polymer thereby suppressing the fire.

$$2\ Al(OH)_3(s) \xrightarrow{> 200°C} Al_2O_3(s) + 3\ H_2O(g)$$

Scheme 1.1: Mechanism of fire retardance of $Al(OH)_3$.

Toothpastes can contain up to 50 % by weight of aluminium hydroxide, as an abrasive filler. Aluminium hydroxide is particularly good in this regard as it has excellent cleansing properties but causes less damage to tooth enamel than other commonly used fillers such as chalk and calcium diphosphate. The degree of abrasivity and cleaning properties can be controlled by choice of particle size. Its non-toxicity, insolubility and compatibility with fluorides also enhance its suitability.

The paper industry uses aluminium hydroxide as both a filler and a coating. It has very high retention and dispersibility characteristics during paper manufacture and improves the retention behaviour of other fillers and pigments. As a coating it imparts high brightness, high opacity, high gloss, and good ink receptivity.

Aluminium hydroxide is used as a cheaper alternative to titania in paint formulations. It has been shown that a 25 % replacement of the titania can be made without loss of opacity.

High purity amorphous aluminium hydroxide gel is used in the pharmaceutical industry in antacid preparations and in medicines for the control of phosphate levels.

Alumina ceramics have superb resistance to heat, wear and chemicals, which means that they have a multiplicity of application in many areas of industry. These include laboratory ware (e.g. crucibles), spark plugs, electronics (e.g. integrated circuits), bioceramics (e.g bone substitutes in joints and dental implants), armour (e.g. bullet-proof jackets), tableware and cutting tools.

High purity aluminas are used in the manufacture of synthetic gemstones such as rubies and yttrium aluminium garnets for lasers and sapphires for instrument windows and lasers.

1.3 Coordination Chemistry of Aluminium.[11]

Aluminium can combine with almost all nonmetallic elements to form complexes in its +3 oxidation state. It has an exceptional affinity for oxygen and therefore oxygen donor ligands dominate the coordination chemistry. While aluminium compounds with three coordination are known, these species are strong Lewis acids and usually achieve four coordination through formation of three-centre bonds, e.g. aluminium trichloride exists in the gas phase in its dimeric Al_2Cl_6 form with two bridging chlorides. Aluminium is not restricted to an octet of electrons in its valence shell and so compounds with five and six coordination are also common.

Aluminium is a sluggishly labile metal ion and so intermolecular reactions such as ligand substitution or water exchange are relatively slow.[12]

1.4 Polynuclear Aluminium Complexes.

The complexation chemistry of aluminium has been widely studied and there are many structurally characterised complexes known. This section will not attempt to describe all of the areas of aluminium complex chemistry but will concentrate on large polynuclear complexes and those which have structural relationships with aluminium oxide/hydroxides. Aluminium carboxylates, phosphinates and phosphonates will be dealt with separately in Chapter 3, Section 3.1.2, Chapter 4, Sections 4.1.2 and 4.1.3, and Chapter 5, Section 5.1.1 respectively.

1.4.1 Alumoxanes.

Alumoxane is the generic term given to a class of aluminium oxide containing macromolecules formed by the controlled hydrolysis of aluminium compounds or salts of formula AlX_3, where X = R, OR, $OSiR_3$ or O_2CR.[13]

Alkylalumoxane compounds, where X = R, were extensively studied in the 1960's as active catalysts in polymerisation processes[14] but little was known about the nature of their structures. Interest in these compounds was renewed in the 1980's

primarily through the work of Kaminsky,[14] who incorporated them into active catalysts for the polymerisation of ethylene and propylene. The first structural model for alkylalumoxanes was the $[Al_7O_6Me_{16}]^-$ (Figure 1.8) anion, synthesised by Atwood *et al*,[15] consisting of an Al_6O_6 ring with a central aluminium atom bonded to three alternate oxygen atoms in the ring. A methyl group is also coordinated to the central aluminium. Several other compounds containing simple Al_3O_3 rings have also been synthesised,[16,17,18,19] e.g $[(^tBu)_2Al(\mu\text{-}OH)]_3$ (Figure 1.8).

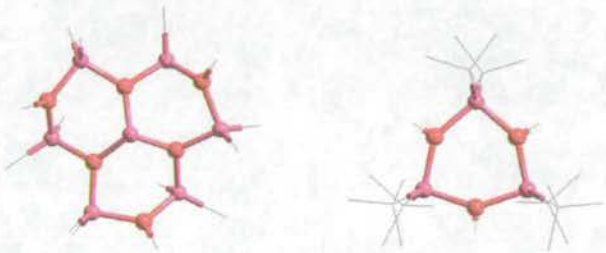

Figure 1.8: Crystal structures of $[Al_7O_6Me_{16}]^-$ and $[(^tBu)_2Al(\mu\text{-}OH)]_3$. Al-pink, O-red, C-grey.

The use of Al^tBu_3 has been particularly successful in producing[13,16,20,21,22,23] polynuclear alkylalumoxanes. The structures of some of these are shown (Figure 1.9). Two, $[(^tBu)Al(\mu_3\text{-}O)]_6$ and $[Al_5(^tBu)_7(\mu_3\text{-}O)_3(\mu\text{-}OH)_2]$ share structural features with the mineral boehmite (Figure 1.10).

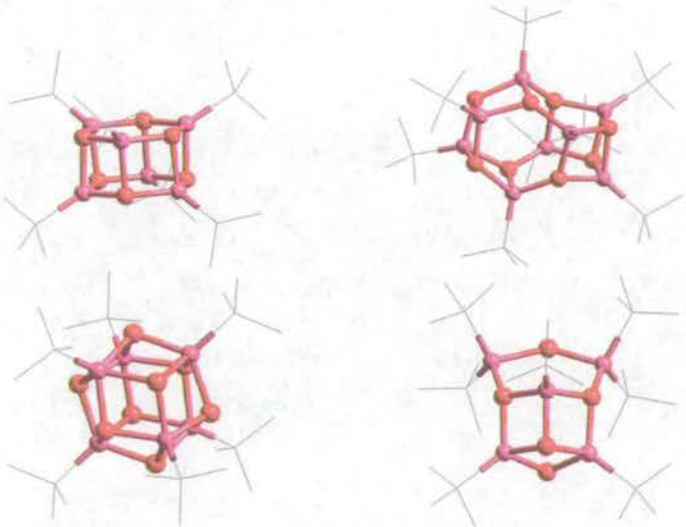

Figure 1.9: Crystal structures of some ^{t}Bu substituted alumoxanes, clockwise form top left: $[(^tBu)Al(\mu_3\text{-}O)]_6$, $[(^tBu)Al(\mu_3\text{-}O)]_8$, $[Al_5(^tBu)_7(\mu_3\text{-}O)_3(\mu\text{-}OH)_2]$ and $[Al_6(^tBu)_6(\mu_3\text{-}O)_4(\mu_3\text{-}OH)_4]$. Al-pink, O-red, C-grey.

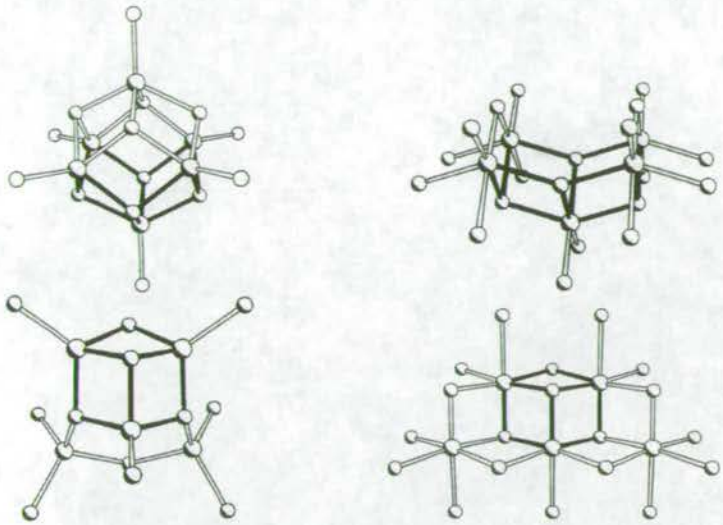

Figure 1.10: Cores of $[(^{t}Bu)Al(\mu_3\text{-}O)]_6$ and $[Al_5(^{t}Bu)_7(\mu_3\text{-}O)_3(\mu\text{-}OH)_2]$ (left) and their structural relationship with a fragments of boehmite (right).[13,22]

Other alkyl containing alumoxanes include[24] $(Mes^*AlO)_4$ and $[Al_6(Mes^*)_4(Et)_6(\mu_3\text{-}OH)_4]$, where Mes* is $(C_6H_2\text{-}2,4,6\text{-}^{t}Bu_3)$.

The partial hydrolysis of aluminium alkoxides and siloxides has also led to the discovery of several large polynuclear aluminium complexes.

The decanuclear complex $Al_{10}O_4(OEt)_{22}$ (Figure 1.11) was prepared[25] by crystallisation, from carbon disulfide, of the waxy solid obtained after allowing $Al(OEt)_3$ to "swell" in benzene over a prolonged time. The μ_3-hydroxides within the structure are believed to have been introduced during the swelling period and are formed from water in the benzene.

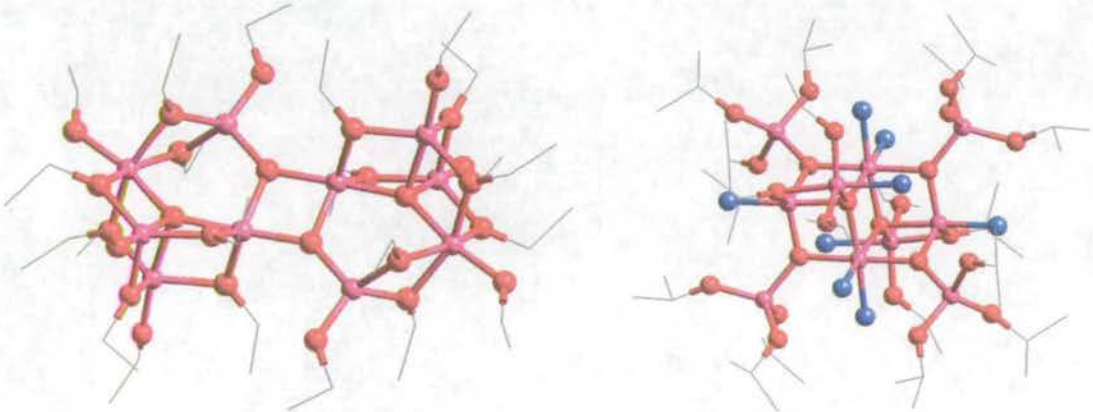

Figure 1.11: Crystal structures of $Al_{10}O_4(OEt)_{22}$ and $[Al_{10}O_6(O^{i}Pr)_{18}(NH_3)_8]$. Al-pink, O-red, N-blue, C-grey.

Ammonolysis of aluminium isopropoxide by passing a stream of ammonia gas through a toluene solution produced[26] the decanuclear complex $[Al_{10}O_6(O^iPr)_{18}(NH_3)_8]$ (Figure 1.11). The core of the structure contains four aluminium atoms, forming two face sharing defective cubanes each missing one vertex. Four "$OAl(O^iPr)_3$" units form the outer vertices of the defective cubanes. The eight ammonia ligands fill the vacant coordination sites of the aluminium atoms.

Unusually both of the Al_{10} clusters have four, five and six coordinate aluminium environments present within their structures.

Partial hydrolysis of $Al(OSiEt_3)_3$ produced the decanuclear alumoxane complex[27] $Al_{10}(OH)_{16}(OSiEt_3)_{14}$ (Figure 1.12). The structure consists of four defective face sharing cubanes each missing one vertex, formed by six aluminium atoms. In addition there are two terminal "$AlO(OSiEt_3)_3$" groups and two "$Al(OSiEt_3)_2O_2$" groups which bridge faces of the cubanes. This core of this cluster has structural similarities with both diaspore and boehmite (Figure 1.13).

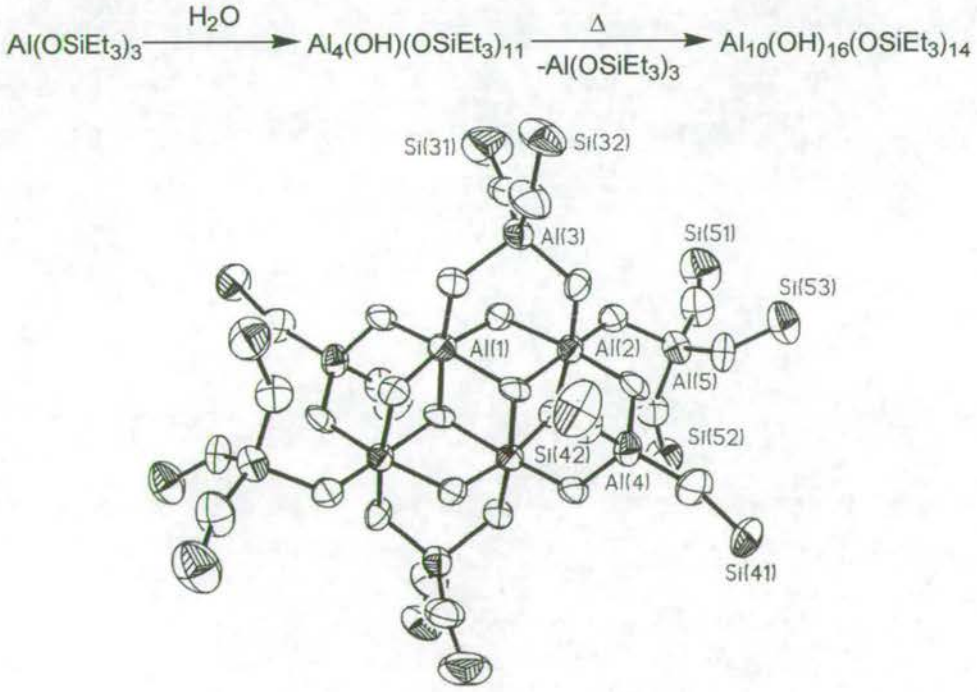

Figure 1.12: Proposed route for formation and crystal structure of $Al_{10}(OH)_{16}(OSiEt_3)_{14}$.[27]

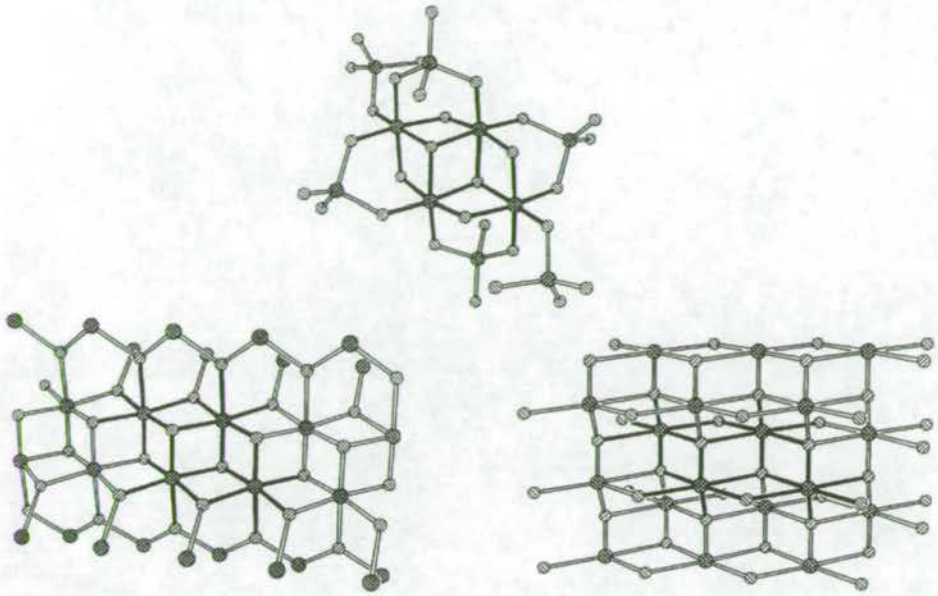

Figure 1.13: Structural similarities between the core of $Al_{10}(OH)_{16}(OSiEt_3)_{14}$, diaspore and boemite.[27]

1.4.2 Aluminium$_{13}$ Clusters.

While in most cases thirteen is considered an unlucky number, this is definitely not the case in aluminium chemistry. Indeed thirteen appears to be a common number for large polynuclear aluminium clusters, with several structurally characterised and two distinct structural types emerging.

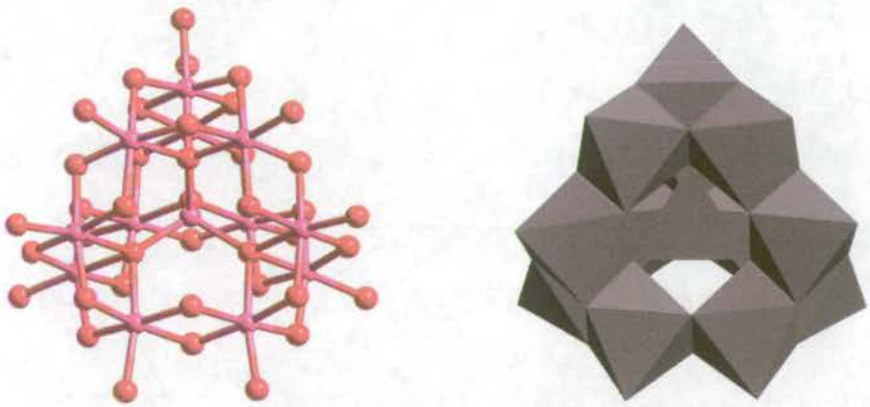

Figure 1.14: Crystal structure of $[Al_{13}O_4(OH)_{24}(H_2O)_{12}]^{7+}$ and its commonly used polyhedral representation. Al-pink, O-red.

The first to be synthesised[28,29] was the oxy/hydroxide cluster $Na[Al_{13}O_4(OH)_{24}(H_2O)_{12}](SO_4)_4$ in 1960 by Johansson *et al.* This has the Keggin[30] structure familiar to polyoxometallate chemistry, with the central tetrahedrally

coordinated aluminium surrounded by twelve edge-linked octahedral aluminiums. Since the structure was first published it has been found that while the basic structure does not change, the complex can be crystallised in several different forms depending on the conditions and counter ion used. A summary of these is given (Table 1.3).

Formula	Space Group
$Na[Al_{13}O_4(OH)_{24}(H_2O)_{12}](SO_4)_4$	$P4_232$
$Na[Al_{13}O_4(OH)_{24}(H_2O)_{12}](SO_4)_4$	$P\bar{1}$
$Na[Al_{13}O_4(OH)_{24}(H_2O)_{12}](SeO_4)_4$	T_d-$F\bar{4}3m$
$[Al_{13}O_4(OH)_{25}(H_2O)_{11}](SO_4)_3$	P2/n or Pn and P2/a or Pa *
$(NH_4)_7[Al_{13}O_4(OH)_{24}(H_2O)_{12}](SO_4)_7$	4/m
$[Al_{13}O_4(OH)_{24}(H_2O)_{12}][Al(OH)_6Mo_6O_{18}]_2(OH)$	C2/c

Table 1.3: Different forms of the "Al_{13}" polycation.[28,29,31,32,33] * Crystals are unstable and can spontaneously convert to the larger unit cell with no visible change in the appearance of the crystal.

In addition to the pure aluminium forms, it has been discovered that other metals can replace the central aluminium. Schonherr *et al*[34] were able to crystallise a germanium analogue $[GeO_4Al_{12}(OH)_{24}(H_2O)_{12}](SO_4)_4$. The gallium subsituted analogue $[GaO_4Al_{12}(OH)_{24}(H_2O)_{12}]^{7+}$ has been studied in solution by ^{27}Al NMR[35] and its selenate salt form by powder X-ray diffraction.[36] There have been attempts to substitute a number of other metal ions[37,38] into the tetrahedral site but evidence of their success is limited. A patent[39] by Vaughan claims the substitution of more than twenty elements into the Al_{13} Keggin structure, in both the tetrahedral and octahedral positions, but does not provide any clear cut evidence for their formation.

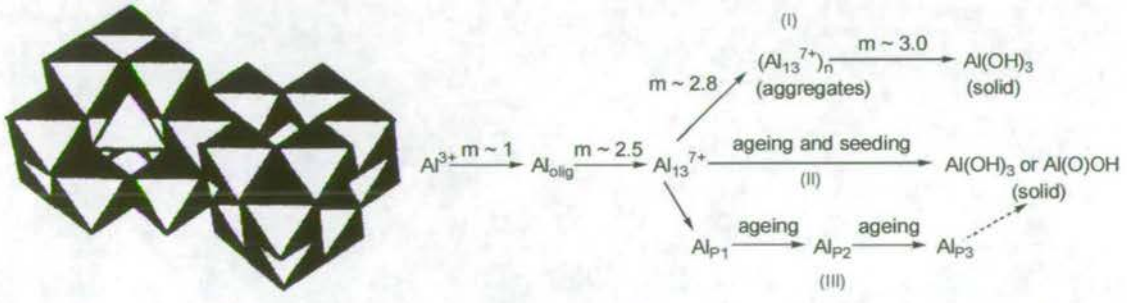

Figure 1.15: Proposed structure of and route to "$Al_{24}O_{72}$" (Al_{P2}) and larger polycations.[40]

^{27}Al NMR evidence[40] has suggested that on heating a solution containing pure $[Al_{13}O_4(OH)_{24}(H_2O)_{12}]Cl_7$ it can condense via loss of one of the twelve outer aluminiums forming a larger polycation of proposed formula "$Al_{24}O_{72}$" (Al_{P2}). The formation of even larger polycations may also be possible through this mechanism (Figure 1.15).

Recently Taulelle *et al*[41] and Nazer *et al*[42] independently published the structure of $[Al_{30}O_8(OH)_{56}(H_2O)_{24}](SO_4)_9$, (Figure 1.16) the largest aluminium oxy-hydroxide polycation so far. It consists of two Al_{13} Keggin units linked by four AlO_6 octahedra and has an overall charge of +18, requiring nine sulfate counter ions. It has been suggested[42] that this may in fact be the correct form of Al_{P2} in solution.

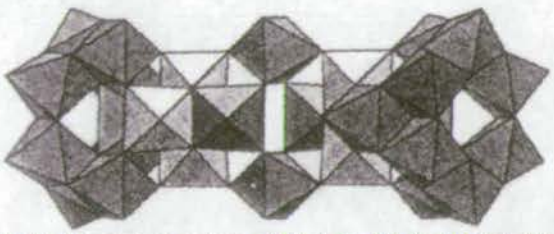

Figure 1.16: Crystal structure of $[Al_{30}O_8(OH)_{56}(H_2O)_{24}](SO_4)_9$.[41]

Substitution of the terminal water molecules for organic ligands in Keggin and other similar structures has been successfully achieved in poloxometallate chemistry[43] but there have been no reports so far of similar reactions for Al_{13}.

Currently the only crystal structure containing Al_{13} and organic molecules is that of Raston *et al.*[44] This consists of the Al_{13}^{7+} polycation co-crystallising with a supramolecular assembly consisting of a sodium ion containing 18-crown-6, associated with two sulfonated calixarines (Figure 1.17).

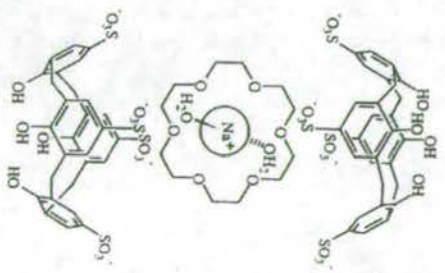

Figure 1.17: 18-crown-6 associated with two sulfonated calixarines.[44]

The second structural type of Al_{13} cluster was synthesised by Powell *et al.*[45] $[Al_{13}(\mu_3\text{-}OH)_6(\mu_2\text{-}OH)_{12}(heidi)_6(H_2O)_6](NO_3)_3$ (Figure 1.18), where H_3heidi = $N(CH_2CO_2H)_2(CH_2CH_2OH)$, is currently the largest aluminium hydroxide cluster containing organic ligands. The cluster is flatter and more disc shaped than the Keggin structure. It consists of a central octahedral aluminium atom surrounded by a ring of six aluminium atoms. The ligand coordination modes within this structure are discussed further in Chapter 3, Section 3.1.2. The related oxy-hydroxide cluster $[Al_{13}(OH)_{24}(H_2O)_{24}]Cl_{15}.13H_2O$[46] (Figure 1.18) shares the same core structure, but with the six heidi ligands replaced by six μ_2-OH groups and twelve terminal water molecules.

Removal of the central aluminium from the Al_7O_{12} core of these clusters creates a $\{Al_6(\mu_2\text{-}OH)_{12}\}$ring, as found in gibbsite (Figure 1.18).

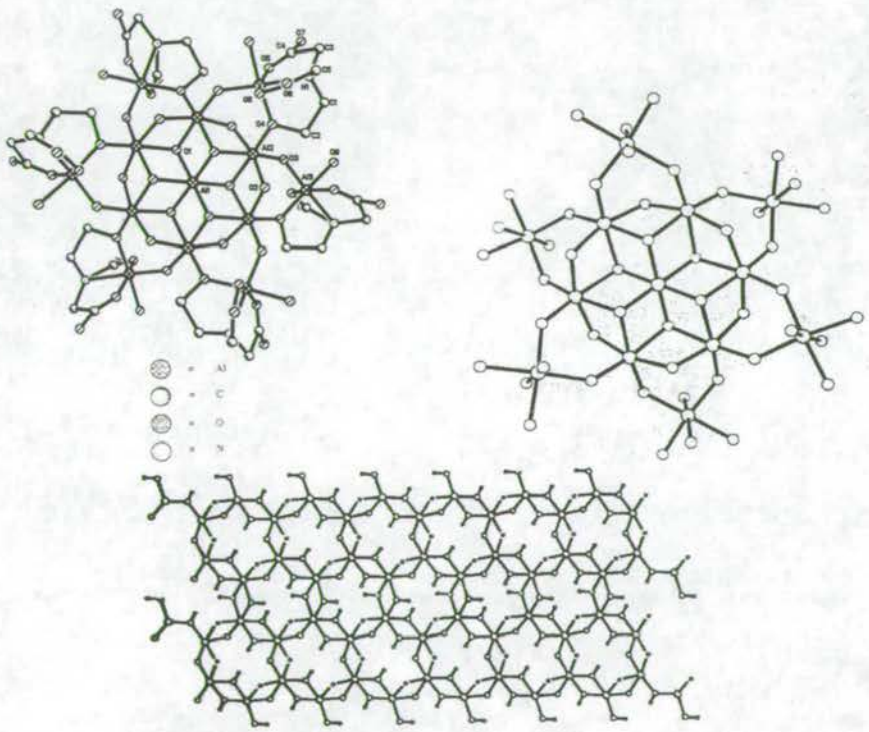

Figure 1.18: Crystal structures of $[Al_{13}(\mu_3\text{-}OH)_6(\mu_2\text{-}OH)_{12}(heidi)_6(H_2O)_6]^{3+}$ and $[Al_{13}(OH)_{24}(H_2O)_{24}]Cl_{15}.13H_2O$ and their similarity to the structure of the mineral gibbsite.[10,45,46]

Although this type of cluster has not yet found use as a model for aluminium oxide surfaces, a similar fragment, Al_8O_{12}, has been used in *ab-initio* calculations involving the interaction of water molecules[47] and the chemisorption of carbon

monoxide[48] onto the α-$Al_2O_3(0001)$ surface. Al_8O_{12} can be created from the Al_7O_{12} core of Al_{13} by removal of the central aluminium and replacing it with two aluminiums capping the triangular faces of the oxygens.

1.5 Surface Treatment of Aluminium.

The thin oxide layer that forms on the surface of aluminium, on exposure to air usually gives sufficient natural corrosion protection, in the pH range 4.5 – 8.5. The growth of this layer is self-limiting, with its maximum thickness (~10 nm) dependent on conditions and exposure time.[2] The nature of this layer is not fully understood, but is believed to consist of non-crystalline amorphous aluminium oxide (Al_2O_3) with short range cubic order.[49,50] Upon exposure to moisture, hydration of Al_2O_3 to boehmite [Al(O)OH] occurs, followed by growth of bayerite [$Al(OH)_3$] crystallites on the plates of the boehmite phase.[50] The mechanism, dissolution-redeposition or nucleation, of this conversion from boehmite to bayerite is unknown.[50] The natural oxide layer is not suitable for coatings or adhesively bonding aluminium and it is therefore necessary to pre-treat[51] the aluminium surfaces before attempting adhesive bonding or coating. The aerospace industry has been adhesively bonding aluminium for decades using a complex series of chemical pre-treatments that are described below.

1.5.1 The Forest Products Laboratory Process (FPL).[52]

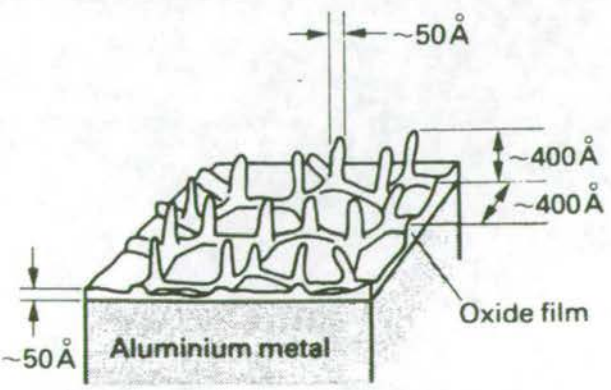

Figure 1.19: Oxide structure of FPL treated aluminium.[51]

Following degassing and an alkaline cleaning treatment, aluminium panels are immersed in a solution containing $Na_2Cr_2O_7$, H_2SO_4 and H_2O (ratio 1:10:30) for 15-30 minutes at a temperature of 68 °C. This process reduces the thickness of the natural oxide layer and increases the roughness of the surface allowing mechanical locking with the adhesive layer. Surface roughness is known to be important factor in determining adhesion at the epoxy-oxide interface. An isometric drawing (Figure 1.19) of the oxide structure produced by the FPL process is shown. The surface is characterised by its high concentration of 50 Å thick, 400 Å high oxide whiskers that protrude from the surface.[51]

1.5.2 Boeing Phosphoric Acid Anodise Process (PAA).[53]

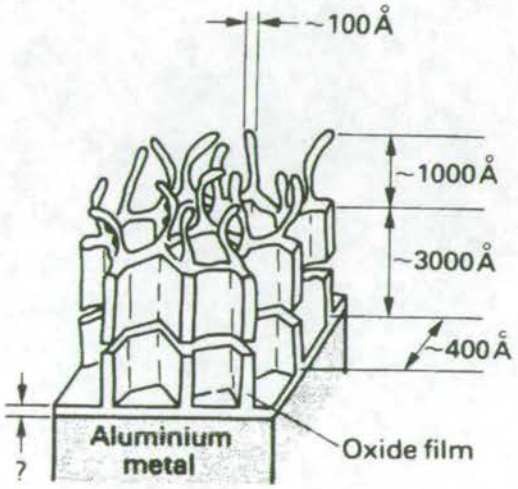

Figure 1.20: Oxide structure of PAA treated aluminium.[51]

Aluminium panels are first treated by the FPL process, then anodised at 10V for 40 minutes in an aqueous solution of 10 % by weight of H_3PO_4 at a temperature of 24 °C. The surface oxide (Figure 1.20) obtained is considerably thicker than that produced by the FPL process and contains hollow hexagonal cells. Above these are 100 Å thick, 1000 Å high fibrous oxide fingers that make the surface rough and give excellent mechanical interlocking to the adhesive layer. The total thickness of the oxide layer is 4000 Å and so provides better corrosion inhibition than the FPL surface.[51]

1.5.3 Chromic Acid Anodise Process (CAA).[54]

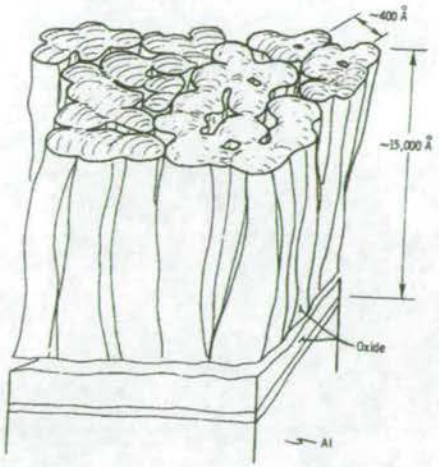

Figure 1.21: Oxide structure of CAA treated aluminium.[51]

Aluminium panels are again first treated by the FPL process, then anodised, this time at 49 V for 40 minutes in an aqueous solution of 5 % by weight of CrO_3 at a temperature of 35 °C. The surface oxide (Figure 1.21) is denser, smoother and much thicker than that produced by either the FPL or PAA processes. The lack of surface roughness means that this treatment is less suitable for mechanical interlocking to the adhesive layer, but the denser oxide structure gives it increased corrosion resistance.[51] Scanning electron microscopy (SEM) has been used[55] to show that extensive penetration by the adhesive into the PAA oxide surface occurs, while only partial penetration was evident for the CAA oxide surface.

1.6 Surface Ligands.

All of the surface pre-treatments described in the preceding section require the use of chromic acid and as a result produce considerable quantities of chromic waste which is difficult to dispose of. Additionally the surface produced is fragile and must be handled with care. Thus high volume production of surface modified aluminium requires an alternative pre-treatment to anodising.

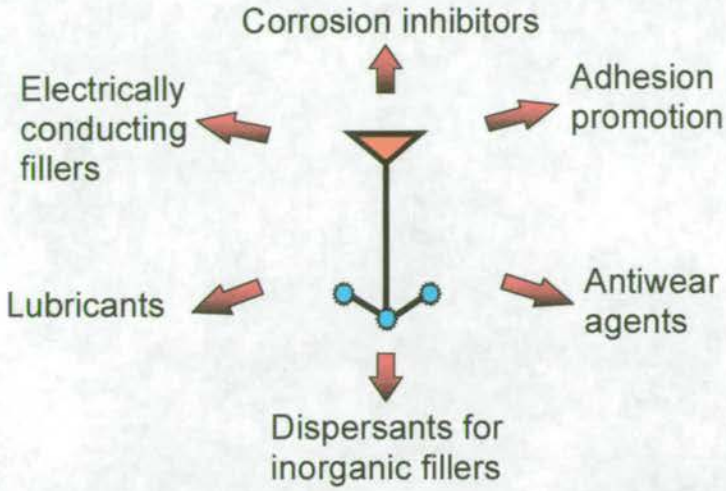

Figure 1.22: Applications for surface ligands.

One such alternative could involve the use of organic molecules "surface ligands" that can attach themselves to the metal oxide surface. These ligands contain a "head" group consisting of a functional group tailored to bind strongly to the surface that is being addressed and a "tail" group which can be modified depending on the application (Figure 1.22) required. For example corrosion inhibition may simply require the attachment of large bulky groups to provide a physical barrier to corrosive ions on the surface, while ligands designed as adhesion promoters can have functional groups, such as vinyl or epoxides, that can cross link into the poymer based adhesives (Figure 1.23).

As has been mentioned previously adhesion promotion is particularly relevant to aluminium, while corrosion inhibition is less important due to the protecting effect of the naturally formed oxide layer.

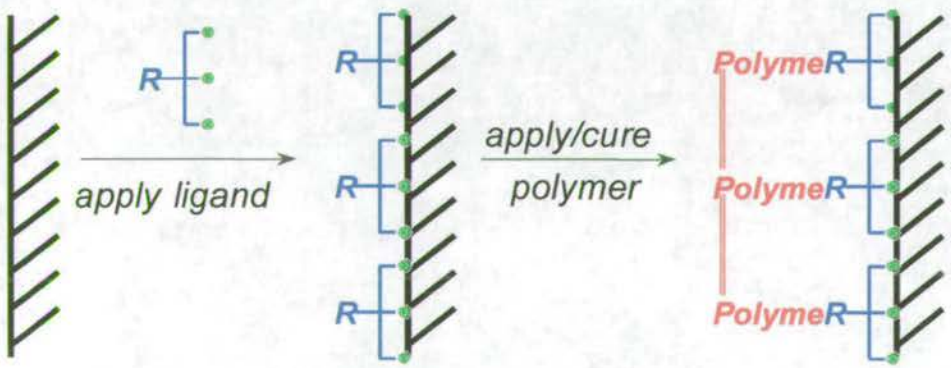

Figure 1.23: Crosslinking of ligand into polymer.

In this thesis our approach to surface modification is to design polynucleating ligands which will recognise arrays of metals on surface oxide structures. Such ligands could form complexes with very high kinetic and thermodynamic stabilities (Figure 1.24).

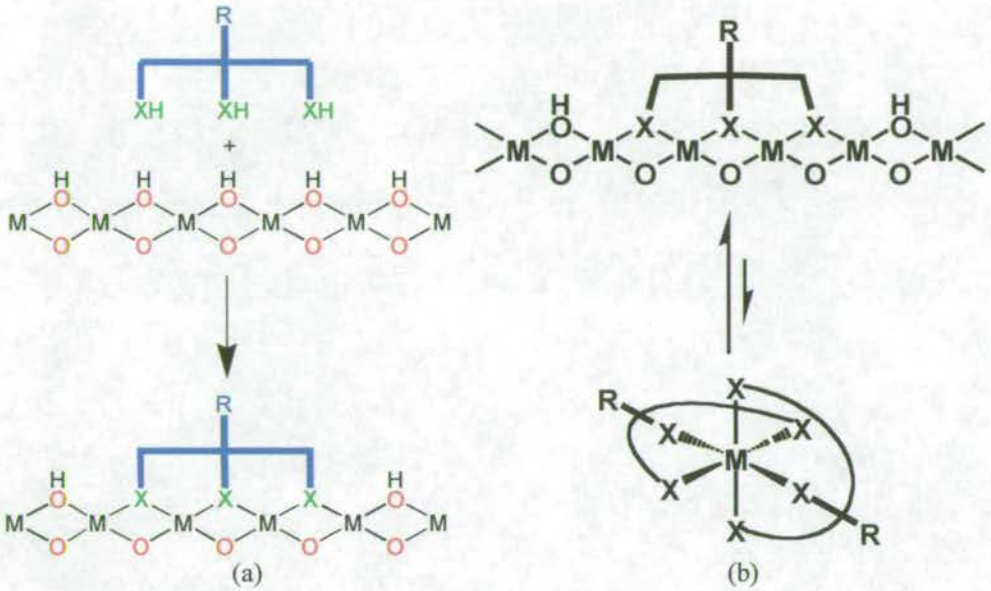

Figure 1.24: (a) Coordination of a polynucleating ligand to a metal oxide surface. (b) The equilibrium between adsorption of ligand onto the surface and sequestration of metal ions into solution.

To optimise the thermodynamic stability of these complexes we need to maximise the number of ligand-to-surface metal interactions by designing polynucleating head groups which contain a high density of donor functions. In order to prevent the ligand sequestering metal atoms into solution and thus degrading the surface, it is also necessary to minimise the chelating (Figure 1.24) abilities of the ligand donor set. This might be achieved by incorporating the donor atoms in a rigid framework and so preventing two donors converging onto one metal site i.e. acting as a conventional chelating agent. The size of any putative "chelate ring" could be controlled to exclude the possibility of formation of favourable five or six-membered rings.

1.7 Adsorption isotherms.

Adsorption isotherms are commonly used to elucidate the adsorption characteristics of an adsorbate onto a metal oxide surface. Adsorption isotherms can provide information on (1) the equilibrium constant for adsorption/desorption, (2) the number of available adsorption sites for monolayer coverage, (3) the strength of binding of a ligand, (4) the required surface area for a single ligand (if the surface area of the substrate is known) and (5) the orientation of the ligand on the surface.

1.7.1 Isotherm Types. [56,57,58,59]

Isotherms for the adsorption of organic solutes can be divided into four main classes, *S*, *L*, *H* and *C* curves, according to the shape of the slope of the initial portion of the curve. These classes can then be divided further into sub-groups (Figure 1.25) as defined by the shape of the isotherm farther from the origin.

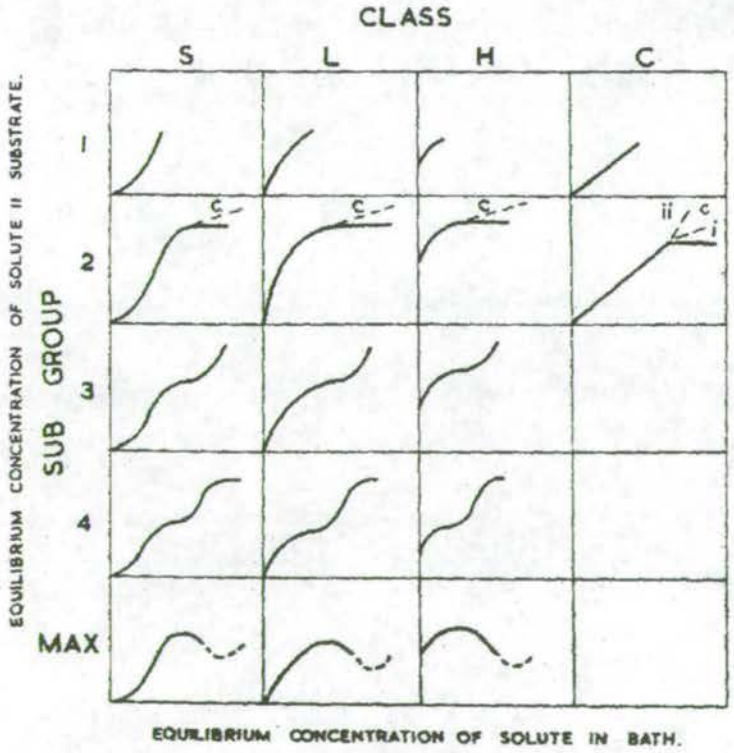

Figure 1.25: Classes of adsorption isotherms – Main classes along the x-axis and sub groups along the y-axis.[56]

The initial slope of an isotherm depends on the rate of change of site availability with increase in solute adsorbed. As more solute is adsorbed, there is usually progressively less chance that an approaching solute molecule will find a suitable site on which it can adsorb. This case applies in normal *L* curves and in the latter stages of *S* and *H* curves. For the initial slope of *S* curves the opposite condition applies and the more solute already adsorbed makes it easier for additional solute molecules to adsorb. This implies cooperative behaviour of the adsorbed molecules on the surface. In the case of *C* curves the availability of adsorption sites remains constant at all concentrations up to saturation. The probable causes for these effects are described below.

For *S* curve isotherms, in the initial stage, adsorption becomes easier as concentration increases. This generally occurs when three conditions are met. The solute molecule (1) is monofunctional, (2) has moderate intermolecular interaction, causing it to pack vertically in a regular array and (3) meets strong competition from solvent molecules or another adsorbed species. This type of isotherm indicates a tendency for the adsorbed molecules to associate rather than remain as isolated units.

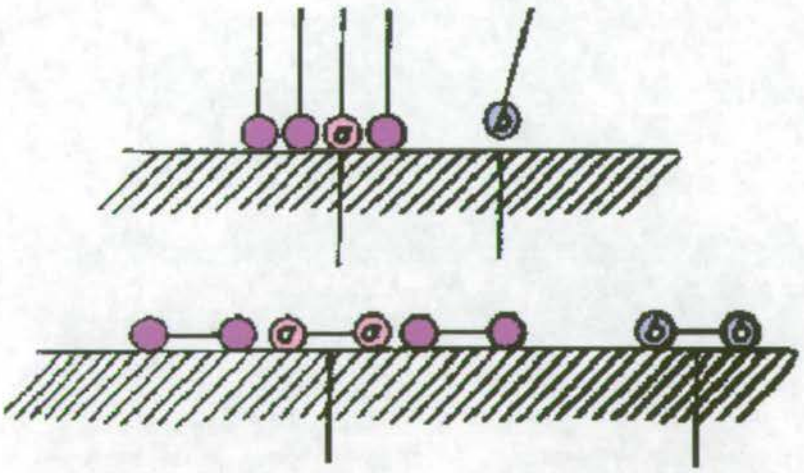

Figure 1.26: Top; Conditions for S curve isotherms – the solute molecule is more stable adsorbed at site a, adjacent to another adsorbed molecule than in isolation at site b. Bottom; Conditions for L curve isotherms – The bifunctional molecule is equally stable adsorbed at site a or b.[58]

For *L* curves the initial slope shows that as more sites are filled it becomes more difficult for solute molecules to find a vacant site. This can mean that the

molecule is not vertically orientated to the surface or alternatively there is little or no competition from solvent molecules.

The *H* curve is a special case of the *L* curve, in which the solute has such a high affinity for the surface in dilute solutions that it is completely adsorbed. This gives a vertical initial slope to the isotherm.

C curve isotherms are characterised by a constant partition of solute between solution and the substrate, up to the point of maximum adsorption. At this point the graph becomes a horizontal plateau. The conditions that favour the *C* curve isotherm are (1) a porous substrate with flexible molecules and regions of differing crystallinity, (2) a solute with higher affinity than the solvent for the substrate, and (3) with better penetrating power due to condition (2) and of molecular gometry, into the crystalline regions of the substrate.

The linearity of the isotherm indicates that the number of sites available for adsorption remains constant, i.e., as sites are filled more are created. This can happen if the solute can penetrate the substrate, breaking inter-substrate bonds, so that more sites are made available. This action has been compared with the opening of a zip fastener, where the fastenings represent the inter-substrate bonds and the slider the first molecule to penetrate the substrate. This opens up the structure, allowing more molecules to penetrate.

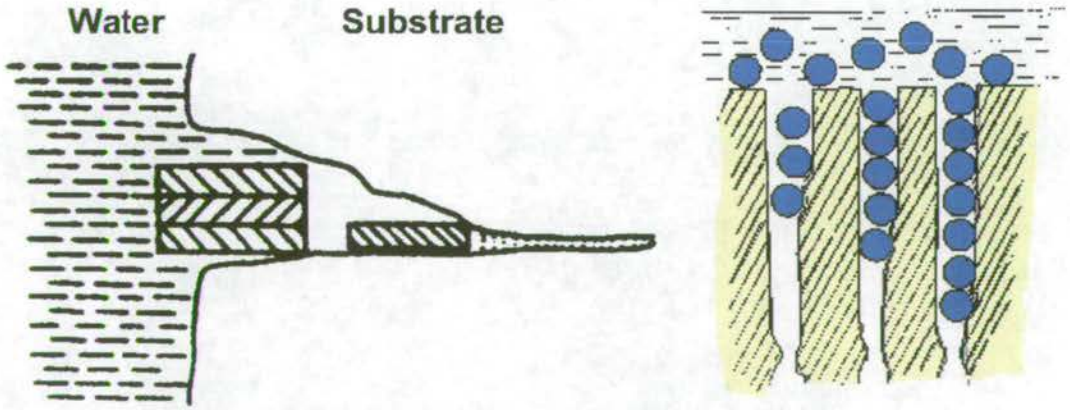

Figure 1.27: Two representations of the conditions required for *C* curve isotherms – solute molecule penetrating the substrate leaving more vacant sites to be filled.[56,58]

1.7.2 Interpretation of Isotherms.[60,61]

The simplest and most common equation used for the interpretation of adsorption isotherms is the Langmuir isotherm model (Figure 1.28).

1) $n + [HL] \overset{K}{\rightleftharpoons} n_A$

n = concentration of unnocupied surface sites mol l^{-1}

$[HL]$ = concentration of adsorbate in solution mol l^{-1}

n_A = concentration of adsorbate on surface sites mol l^{-1}

Applying the mass law to this equation gives :

2) $$\frac{n_A}{n[HL]} = K = \exp\left(-\frac{\Delta G^{\circ}_{ads}}{RT}\right)$$

The maximum concentration of surface sites n_M is therefore given by :

3) $n_M = n + n_A$

Thus :

4) $$n_A = n_M \frac{K[HL]}{1 + K[HL]}$$

The equation can also be written either as :

5) $$\theta = \frac{K[HL]}{1 + K[HL]}$$ where 6) $$\theta = \frac{n_A}{n_M}$$ or 7) $$K[HL] = \frac{\theta}{1 - \theta}$$

Figure 1.28: Derivation of the Langmuir equation.

The Langmuir model was originally developed for solid-gas systems but has been modified for use in solid-solution systems. It is derived from the assumption that the adsorption sites on the surface of a solid (adsorbent) become occupied by an adsorbate from the solution $[HL]$. This implies a 1:1 adsorbate to adsorbent stoichiometry. Other assumptions made are that all available sites are equivalent and that the ability of a ligand to bind to them is independent of the occupation or otherwise of neighbouring sites, i.e. the model does not take into account cooperative binding.

From the value for n_M, if the surface area of the substrate is known, then the required surface area per ligand can be calculated (Figure 1.29).

$$\text{Required surface area per molecule} = \frac{\text{Surface area of substrate}}{n_M}$$

Figure 1.29: Formula for required surface area per molecule.

As the Langmuir model was initially developed for solid-gas systems before it was modified for use in solid-solution systems, it does not take into account charge, either on the ligand being adsorbed or on the surface. The validity of the Langmuir model also breaks down when the system becomes more complicated than described in equation (1), for example when there is more than one competing ligand in solution or when the ligand has two or more competing binding modes. Another limitation of the model is that it assumes full monolayer coverage of the ligand on the surface will occur. With strongly binding ligands this is not a problem, however weakly binding ligands may not give full monolayer coverage, leading to an apparently lower number of available surface sites and thus an overestimation of the required surface area per ligand. These factors limit the application of the Langmuir model to the evaluation of simple *L* curve isotherms. The model can be expanded to take into account an adsorbent with two binding sites of different affinities. This gives the double Langmuir equation (Figure 1.30).

$$n_A = n_1 \frac{K_1[HL]}{1 + K_1[HL]} + n_2 \frac{K_2[HL]}{1 + K_2[HL]}$$

Figure 1.30: The double Langmuir equation for an adsorbent with two binding sites.

Several other models have been developed for more complex behaviour. One of these is the Frumkin equation (Figure 1.31), also known as the Frumkin-Fowler-Gugenheim (FFG) equation. This takes into account lateral interactions at the surface, such as charged ions repelling each other within the adsorbed layer, by the addition to the Langmuir model of the $\exp(-2a\theta)$ term, which reflects the extent of these interactions. An interaction coefficient of $a > 0$ indicates attraction, while $a < 0$ means repulsion.

$$K[HL] = \frac{\theta}{1-\theta} \exp(-2a\theta)$$

Figure 1.31: The Frumkin equation.

1.8 References.

1 "Aluminum," Microsoft® Encarta® Online Encyclopedia 2000 http://encarta.msn.com © 1997-2000 Microsoft Corporation. All rights reserved.

2 *Chemistry of Aluminium, Gallium, Indium and Thallium*, edited by A. J. Downs, published by Blackie Academic & Professional an Imprint of Chapman & Hall, 1993.

3 N. N. Greenwood and A. Earnshaw, *Chemistry of the Elements*, 2nd Ed, published by Oxford: Butterworth-Heinemann, 1997

4 R. Thompson, *Industrial Inorganic Chemicals: Production and Uses*, published by The Royal Society of Chemistry, 1995.

5 F. A. Cotton and G. Wilkinson, *Advanced Inorganic Chemistry*, 5th Ed, published by Wiley Interscience, 1988.

6 http://scifun.chem.wisc.edu/CHEMWEEK/Aluminum/ALUMINUM.html

7 K. A. Evans and N. Brown, *Speciality Inorganic Chemicals*, edited by R. Thompson, published by The Royal Society of Chemistry, 1981.

8 U.S. Geological Survey-Minerals Information by P.A. Plunkert, 1996.

9 A. F. Wells, *Structural Inorganic Chemistry*, 5th Ed, Oxford University Press, 1984.

10 A. K. Powell and S. L. Heath, *Coord. Chem. Rev.*, 1996, **149**, 59.

11 A. W. Apblet, Aluminium: Inorganic Chemistry, *Encyclopedia of Inorganic Chemistry*, Volume 1, Ed. R. B. King, published by John Wiley & Sons. Ltd, 1994

12 G. H. Robinson, *Coordination Chemistry of Aluminium*, published by VCH Publishers Inc, 1993

13 C. J. Harlan, M. R. Mason and A. R. Barron, *Organometallics*, 1994, **13**, 2957-2969.

14 S. Pasynkiewicz, *Polyhedron*,1990, **9**, 429 and references within.

15 J. L. Atwood, D. C. Hrncir, R. D. Priester and R. D. Rogers, *Organometallics*, 1983, **2**, 985.

[16] M. R. Mason, J. M. Smith, S. G. Bott and A. R. Barron, *J. Am. Chem. Soc.*, 1993, **115**, 4971.

[17] T. Gelbrich, U. Dumichen and P. Jorchel, *Acta Crystallogr., Sect. C*, 1999, **55**, 856.

[18] H. D. Hausen, G. Schmoger and W. Schwarz, *J. Organomet. Chem.*, 1978, **153**, 271.

[19] J. Storre, C. Schnitter, H. W. Roesky, H. G. Schmidt, M. Noltemeyer and R. Fleischer, *J. Am. Chem. Soc.*, 1997, **119**, 7505.

[20] C. J. Harlan, S. G. Bott and A. R. Barron, *J. Am. Chem. Soc.*, 1995, **117**, 6465

[21] C. C. Landry, C. J. Harlan, S. G. Bott and A. R. Barron, *Angew. Chem. Int. Ed.*, 1995, **34**, 1201.

[22] Y. Koide and A. R. Barron, *Organometallics*, 1995, **14**, 4026.

[23] C. J. Harlan, S. G. Bot, B. Wu, R. W. Lenz and A. R. Barron, *Chem. Commun.*, 1997, 2183.

[24] R. J. Wehmschulte and P. P. Power, *J. Am. Chem. Soc.*, 1997, **119**, 8387.

[25] A. I. Yanovsky, N. Y. Turova and N. I. Kozlova, *Koord. Khim.*, 1987, **13**, 242.

[26] U. M. Tripathi, A. Schier and H. Schnidbaur, *Z. Naturforsch., Tiel B*, 1998, **53**, 434.

[27] A. W. Apblett, A. C. Warren and A. R. Barron, *Chem. Mater.*, 1992, **4**, 167-182.

[28] G. Johansson, G. Lundgren, L. G. Sillen and R. Soderquist. *Acta. Chem. Scand.*, 1960, **14**, 769.

[29] G. Johansson. *Acta. Chem. Scand.*, 1960, **14**, 771.

[30] J. F. Keggin, *Nature*, 1933, **131**, 908.

[31] G. Johansson, *Ark. Kemi.*, 1963, **20**, 321.

[32] G. Johansson, *Ark. Kemi.*, 1962, **20**, 305.

[33] J-H. Son, H. Choi and Y-U, Kwon, *J. Am. Chem. Soc.*, 2000, **122**, 7432.

[34] V. S. Schonherr and H. Gorz, *Z. Anorg. Allg. Chem.*, 1983, **583**, 37.

[35] B. Thomas, H. Gorz and S. Schonherr, *Z. Chem.*, 1987, **27**, 183.

[36] S. M. Bradley, R. A. Kydd and C. A. Fyfe, *Inorg. Chem.*, 1992, **31**, 1181.

[37] J. B. Nagy, J-C. Bertrand, I. Palinko and I. Kiricsi, *J. Chem. Soc., Chem.*

Commun., 1995, 2269.

38 W. O. Parker, R, Millini and I. Kiricski, *Inorg. Chem.*, 1997, **36**, 571.

39 D. E. Vaughan, US Patent 4,666,877, Exxon Research and Engineering Company, 1987.

40 G. Fu, L. F. Nazar and A. D. Bain, *Chem. Mater.*, 1991, **3**, 602.

41 L. Allouche, C. Gerardin, T. Loiseau, G. Ferey and F. Taulelle, *Angew. Chem. Int. Ed.*, 2000, **39**, 511.

42 J. Rowsell and L. F. Nazar, *J. Am. Chem. Soc.*, 2000, **122**, 3777.

43 For examples see M. I. Khan and J. Zubietta, *Progress in Inorganic Chemistry*, **43**, 1 and references within.

44 A. Drljaca, M. J. Hardie and C. L. Raston, *J. Chem. Soc., Dalton Trans.*, 1999, 3639.

45 S. L. Heath, P. A. Jordan, I. D. Johnson, G. R. Moore, A. K. Powell and M. Helliwell. *Journal of Inorganic Biochemistry*. 1995, **59**, 785.

46 W. Seichter, H. Mogel, P. Brand and D. Salah, *Eur. J. Inorg. Chem.*, 1998, 795.

47 J. M. Wittbrodt, W. L. Hase and H. B. Schlegel, *J. Phys. Chem B*, 1998, **102**, 5511.

48 M. Casarin, C. Maccato and A. Vittadini, *Inorg. Chem.*, 2000, **39**, 5232.

49 H. P. Godard, W. B. Jepson, M. R. Bothwell and R. L. Kane, *The Corrosion of Light Metals*, published by John Wiley & Sons, Inc.

50 R. G. Schmidt and J. P. Bell, *Advances in Polymer Science*, 1985, **75**, 32 and references within.

51 J. D. Venables, D. K. McNamara, J. M. Chen, T. S. Sun and R. Hopping, *Applications of Surface Science 3,* 1979, 88 and references within.

52 H. W. Eicher and W. E. Schowalter, *Forest Products Laboratory Report no* 1813 (1950).

53 G. S. Kabayashi and D. J. Donelly, *Boeing Co. report no.* DG-41517 (February, 1974).

54 N. L. Rogers, *US Patent* 414,489.

55 R. J. Davies and M. D. Richie, *J. Adhesion*, 1992, **38**, 243.

[56] C. H. Giles, D. Smith and A. Huitson, *J. Colloid and Interface Sci.*, 1974, **47**, 755.

[57] C. H. Giles, A. P. D'Silva and I. A. Easton, *J. Colloid and Interface Sci.*, 1974, **47**, 766.

[58] C. H. Giles, T. H. MacEwan, S. N. Nakhwa and D. Smith, *J. Chem. Soc.*, 1960, 3973.

[59] G. D. Parfitt and C. H. Rochester, *Adsorption from Solution at the Solid/Liquid Interface*, published by Academic Press, 1983.

[60] Werner Stumm, *Chemistry of the Solid-Water Interface: processes at the mineral-water and particle-water interface in natural systems*, published by Wiley-Interscience, 1992.

[61] R. L. Parfitt, *Advances in Agronomy*, 1978, **30**, 1.

Chapter 2:

Functionalised 1,3,5-Triazine Derivatives.

Contents.

2.1 Introduction.

2.1.1 Background.

This chapter reports the synthesis of a range of 1,3,5-triazine-based ligands and their complexes with 1st row transition metals (Ni and Co) as well as a novel sodium cage. It also describes the difficulties in the use of triazines as surface modifying ligands and presents isotherm data for two model compounds, 2-hydroxypyridine and uracil.

1,3,5-triazines have been known[1,2] for around two hundred years and were formerly known as symmetric or *s*-triazines. They are six membered heterocyclic rings with three nitrogens in the 1-, 3- and 5- positions. The most common starting material for the synthesis of 1,3,5-triazine derivatives is 2,4,6-trichloro-1,3,5-triazine, more commonly known as cyanuric chloride (Figure 2.1). It has been demonstrated previously[3,4,5] that cyanuric chloride can be derivatised in a stepwise manner with displacement of one, two or three chloride ions via control of the reaction temperature and/or pH. It is this strategy which will be employed to produce a range of new compounds, varying the ligating properties of the molecules systematically. The "tail" group can likewise be altered in this way in, to tailor the ligand for different applications.

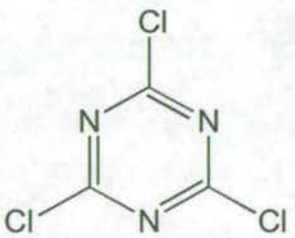

Figure 2.1: Cyanuric chloride.

Analogies can be drawn between 1,3,5-triazines and 2-hydroxy pyridonate derivatives (Figure 2.2). These have proved[6] to be highly successful in the synthesis of high nuclearity transition metal cages, due in part to their ability to display at least nine different binding modes. Functionalised triazines should also be capable of a similar number of binding modes. Successful synthesis of high nuclearity clusters

with triazine derivatives should provide valuable information on their mode of action on a metal oxide surface.

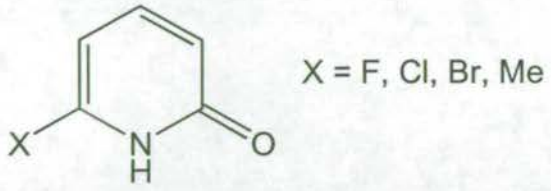

Figure 2.2: 2-hydroxy pyridonates.

2.1.2 1,3,5-Triazines as Surface Ligands.

Triazine thiones have previously been shown to inhibit corrosion and improve adhesion of copper. In particular the compound 6-[(4-vinylbenzyl)propylamino]-1,3,5-triazine-2,4-dithione (VBATDT), (Figure 2.3), has proved to be a good corrosion inhibitor[7] due to the presence of the vinyl group which can be polymerised, providing a further barrier against attack. VBATDT has also been used[8] to improve the adhesion strength of dental alloys.

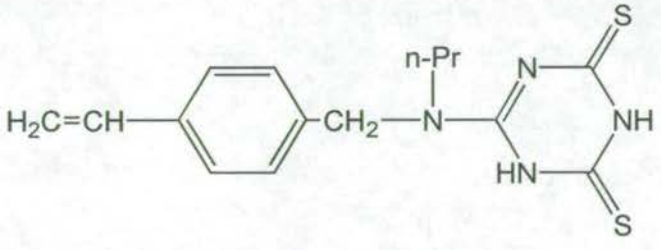

Figure 2.3: VBATDT.

Surface-enhanced Raman spectroscopy (SERS) has been used to establish that the amine functionalised triazine, 2,4-diamino-6-phenyl-1,3,5-triazine (DPT) can adsorb on to a silver colloidal surface.[9]

The surface coordinating properties of oxygen functionalised and mixed donor triazines have not been explored.

2.1.3 Naming Conventions.

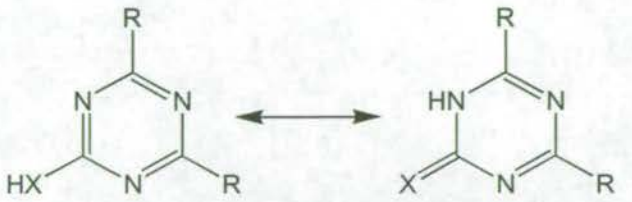

Figure 2.4: Tautomerism of oxygen and sulfur functionalised triazines.

Oxygen and sulfur substituted triazines can exist in several tautomeric forms[3,10] (Figure 2.4). This creates difficulties when naming this class of compounds. The early literature in particular can be confusing, with several different naming conventions used. Recently Mizuno *et al* proved[10] conclusively that the molecule VBATDT, which can potentially exist in three different tautomers, triazine-dithiol, triazine-dithione and triazine-thione-thiol (Figure 2.5), has the dithione structure, both in the solid state and in acetone solution. Therefore all oxygen and sulfur substituted triazines synthesised in this chapter will be named as one/thione as opposed to hydroxy/mercapto.

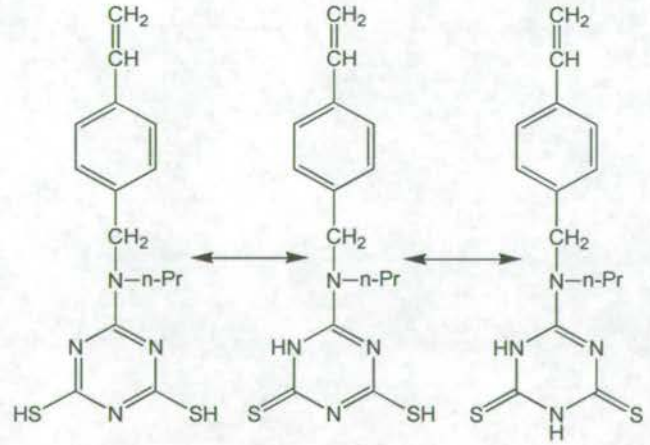

Figure 2.5: Tautomerism of VBATDT.

2.1.4 1,3,5-Triazine Complexes.

There have been few 1st row transition metal complexes synthesised with functionalised triazine ligands; of these most contain cyanuric acid and fall into two

categories, mononuclear with one ligand[11,12,13,] and mononuclear with two ligands[14,15,16] (Figure 2.6).

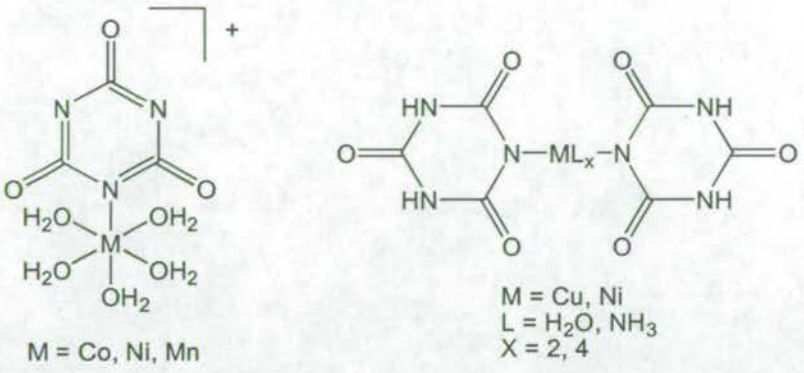

Figure 2.6: Two categories of cyanuric acid complexes.

Other cyanuric acid complexes in the literature include the mononuclear nickel complex $[K_2\{Ni(C_3H_2N_3O_3)_4\}.5H_2O]$ of Palade *et al*[17] containing four ligands bound through an oxygen donor to one nickel and the polymeric mixed copper/sodium complex $[Na_2Cu(C_3H_2N_3O_3)_4.6H_2O]$ of Hart *et al*[18] discovered as a purple crystalline deposit in an Australian swimming pool.

There have been several transition metal (nickel,[19,20] cobalt[21] and copper[22]) and four gold[23,24] complexes made with the sulfur analogue of cyanuric acid, trithiocyanuric acid. However, there is only one reported cobalt structure, $[\{Co(en)_2\}_2(\mu\text{-dtcy})]I_3$ (where en = ethane-1,3-diamine and H_3dtcy = 4-oxo-1,3,5-triazine-2,6-dithione), with a mixed oxygen/sulfur functionalised triazine.[21]

2.1.5 The Harris Notation.[25,26]

The Harris notation was developed at Edinburgh by Dr S. G. Harris as a simpler and more intuitive alternative to conventional binding mode descriptions to differentiate between the binding modes of pyridonate based ligands. In this system the binding mode is referred to as $X.Y_1Y_2Y_3\ldots Y_n$ where X is the overall number of metals bound by the whole ligand, and each value of Y refers to the number of metal atoms attached to the different donor atoms. The system will be used throughout this thesis to describe both the binding modes of pyridonates and 1,3,5-triazine based ligands.

2.2 Synthesis and Characterisation of 1,3,5-Triazine Derivatives.

As stated in the introduction the most common method of synthesising functionalised triazines is via stepwise substitution of the chloride groups of cyanuric chloride. Our strategy was to first substitute an amine group and use this amine-dichloro-triazine as a starting material to build up a library of compounds incorporating different functional group combinations. The 1,3,5-triazines prepared in this chapter and any abbreviations used in the text are shown (Table 2.1). Full experimental details and characterisation data for all triazines are given in Section 2.6.2.

Structure	Name	Abbreviation (where used)
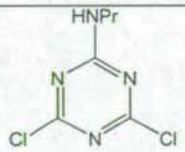	6-(*n*-propylamino)-2,4-dichloro-1,3,5-triazine	-
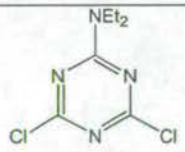	6-(diethylamino)-2,4-dichloro-1,3,5-triazine	-
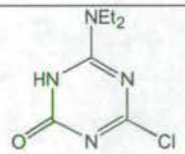	6-(diethylamino)-4-chloro-1,3,5-triazine-2-one	-
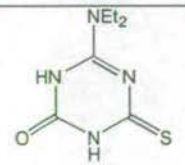	6-(diethylamino)-1,3,5-triazine-2-thione-4-one	H_2OSta
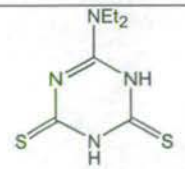	6-(diethylamino)-1,3,5-triazine-2,4-dithione	H_2SSta

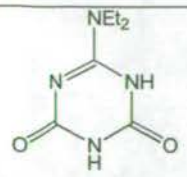	6-(diethylamino)-1,3,5-triazine-2,4-dione	-
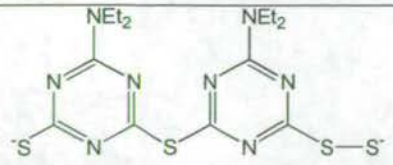	4-diethylamino-6-(4-diethylamino-6-disulfanyl-[1,3,5]triazin-2-ylsulfanyl)-[1,3,5]triazine-2-thiol	$\{(Sta)S(S_2ta)\}^{2-}$
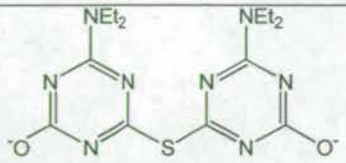	2,2'-thiobis-{6-(diethylamino)-1,3,5-triazine-4-ol}	$\{S(Ota)_2\}^{2-}$
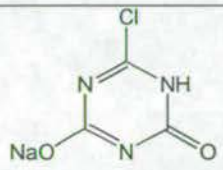	2-chloro-4,6-dihydroxy-1,3,5-triazine-(Na salt)	-
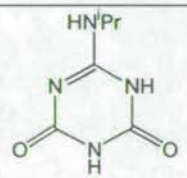	6-(isopropylamino)-1,3,5-triazine-2,4-dione	H_2O_2ta
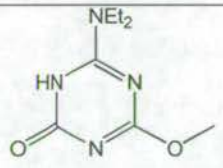	6-(diethylamino)-4-methoxy-1,3,5-triazine-2-one	-

Table 2.1: 1,3,5-Triazine ligands synthesised within this chapter.

Initially the primary amine, *n*-propylamine was used. The reaction to produce 6-(*n*-propylamino)-2,4-dichloro-1,3,5-triazine (Scheme 2.1), was both temperature and pH sensitive. Allowing the temperature to rise over 5 °C gave a product with multiple amine substitution. If the reaction was taken over pH 7 then this resulted in hydrolysis and loss of the amine group from the final product.

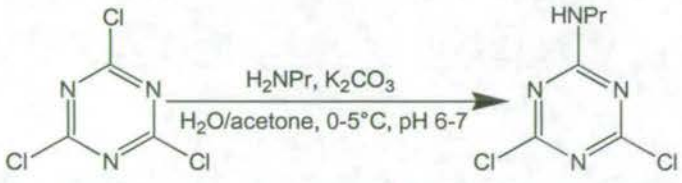

Scheme 2.1: Reaction scheme for 6-(*n*-propylamino)-2,4-dichloro-1,3,5-triazine.

Dichlorotriazines with secondary amine substituents are also known to be prone to unwanted hydrolysis and decomposition, giving off HCl gas, generally over a period of a few days. The reason for the reactivity of this class of compound is that they can exist as two different tautomers. Either tautomeric form is capable of hydrogen bonding to a water molecule, facilitating attack on the ring chlorides.[3] This hydrogen bonding to water also makes the compounds difficult to dry, increasing the decomposition problem. It was therefore impossible to obtain the product, 6-(*n*-propylamino)-2,4-dichloro-1,3,5-triazine in a pure form. This, combined with the inability to store the compound for more than a few days, made it a poor candidate as a starting material.

Tertiary amine derivatives are much more stable to hydrolysis as they do not contain an amino hydrogen and therefore cannot tautomerise or undergo hydrogen bonding interactions.[3] This makes them much easier to work with as they can be readily dried and stored over a longer time period.

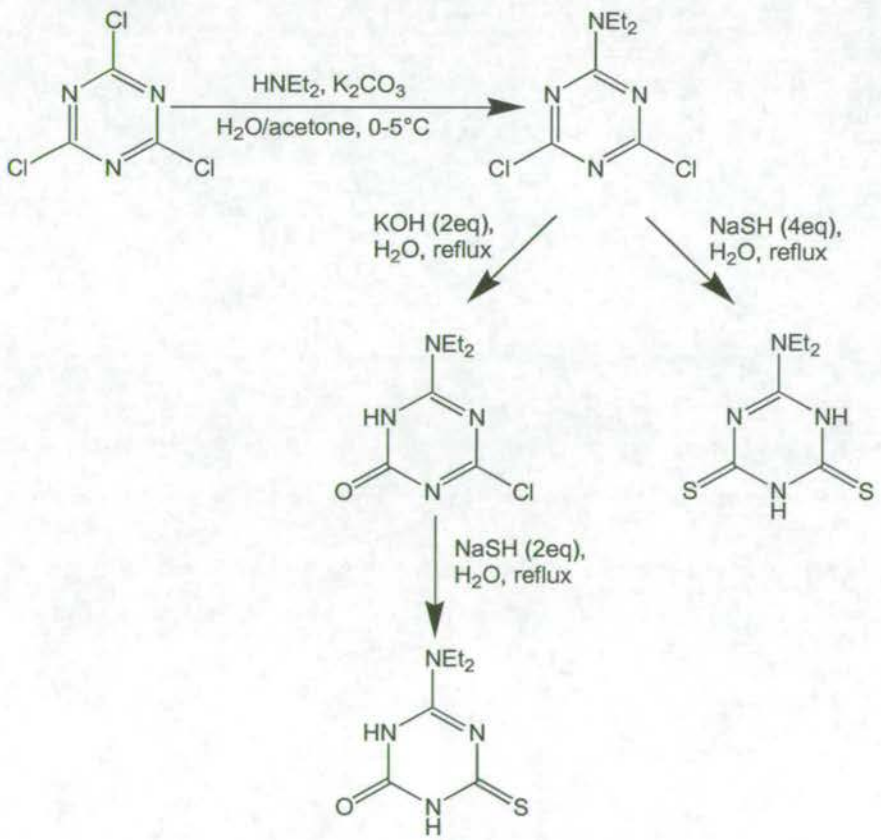

Scheme 2.2: Reaction scheme for triazines.

6-(Diethylamino)-2,4-dichloro-1,3,5-triazine was synthesised[3] in high yield (67 %), and the reaction scheme (Scheme 2.2) is shown above. The reaction is not pH sensitive, in contrast to that for 6-(propylamino)-2,4-dichloro-1,3,5-triazine. However, care still has to be taken not to allow the reaction to warm up before completion or multiple amine substitution occurs. The compound proved to be considerably more resilient to hydrolysis, with no significant decomposition observed even after storage for several months. Large X-ray quality crystals were obtained by slow evaporation of an ethanol solution. Crystallographic data (Table 1) and significant bond lengths and angles (Table 2) are given in the appendix.

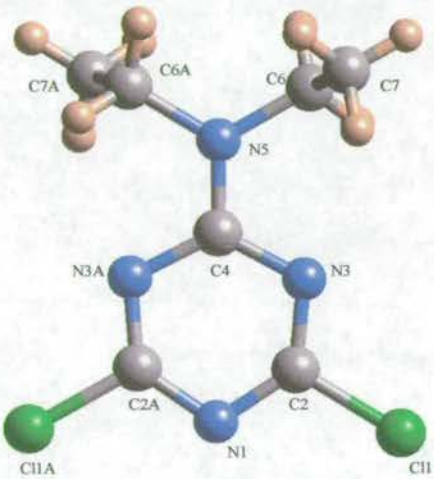

Figure 2.7: Crystal structure of 6-(diethylamino)-2,4-dichloro-1,3,5-triazine.

6-(Diethylamino)-2,4-dichloro-1,3,5-triazine crystallises in a layered arrangement with π-stacking between the layers in the form of π-stacked dimers. The X-ray structure (Figure 2.7) reveals an unusually short exocyclic C(4)-N(5) bond of 1.329(2) Å. This compares to the average exocyclic C-N bond lengths[27] in 2-chloro-4,6-bis and 2,4,6-tris(N,N-diisopropylamino)-1,3,5-triazines of 1.348 Å and 1.367 Å respectively. This can be explained by the partial double bond character of the C(4)-N(5) bond. Further evidence for this explanation is that the sum of the angles around N(5) is 360°, which indicates the sp^2-hybridised nature of the nitrogen. In addition the endocyclic bonds C(2)-N(3) and C(2A)-N(3A) at 1.305 Å are the shortest lending weight to the argument that the structure exists as a resonance hybrid with a substantial contribution from the *N*-diethyliminium form (Figure 2.8). This

explanation is given by Dastagiri Reddy *et al*[28] in their description of the related compound 6-(*N*-ethyl-*N*-isopropylamino)-2,4-dichloro-1,3,5-triazine. The reported[28] exocyclic C-N bond length of 1.329(3) of this compound is statistically identical to that found in 6-(diethylamino)-2,4-dichloro-1,3,5-triazine.

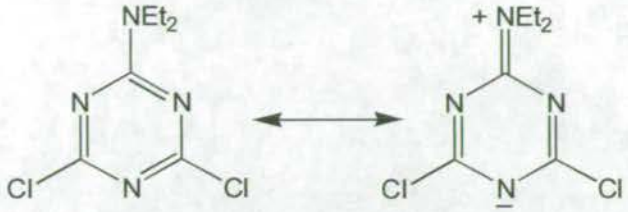

Figure 2.8: Resonance hybridisation of 6-(diethylamino)-2,4-dichloro-1,3,5-triazine.

6-(Diethylamino)-4-chloro-1,3,5-triazine-2-one (Figure 2.9) has not previously been reported. However, a related compound, 6-(methylamino)-4-chloro-1,3,5-triazine-2-one was made[29] by Talebian *et al*. Their method, using four equivalents of sodium hydroxide at 0 °C in water/acetonitrile solvent proved unsuccessful for the synthesis of 6-(diethylamino)-4-chloro-1,3,5-triazine-2-one. A new method (Scheme 2.2) was developed, in which the starting material, 6-(diethylamino)-2,4-dichloro-1,3,5-triazine, was refluxed in a solution of KOH (or NaOH) until it had nearly all dissolved. Filtering off unreacted starting material, followed by acidification of the filtrate with dilute HCl afforded the desired product in good yield, with no further purification necessary.

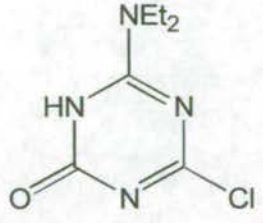

Figure 2.9: 6-(diethylamino)-4-chloro-1,3,5-triazine-2-one.

^{1}H and ^{13}C NMR results for this compound were surprising, both providing evidence that the two ethyl groups were inequivalent, indicating that rotation of the diethylamine group is restricted. This could be explained by a similar resonance hybrid effect to that in 6-(diethylamino)-2,4-dichloro-1,3,5-triazine, the partial

double bond character of the exocyclic C-N bond restricting the rotation of the diethylamine group. Unfortunately, despite repeated attempts, we were unable to grow X-ray quality crystals of this compound in order to check this. It is interesting to note that the effect was not recorded for 6-(methylamino)-4-chloro-1,3,5-triazine-2-one.[29] One feature of the ^{13}C NMR (Figure 2.10) that is repeated for both compounds is the overlap of the ring carbon signals making assignment of the peaks difficult.

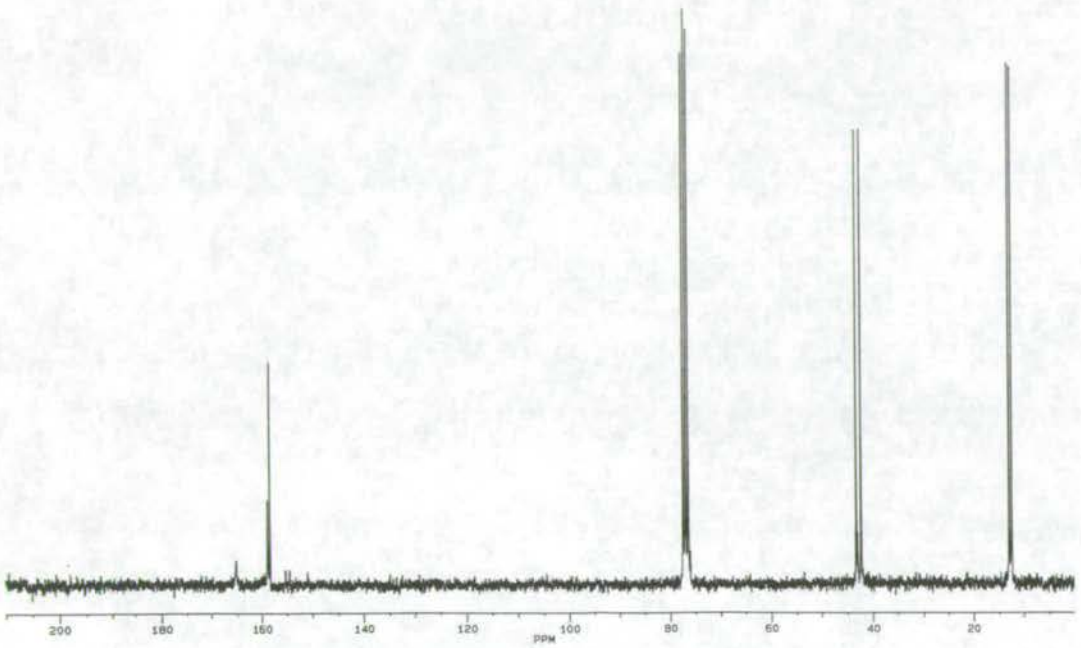

Figure 2.10: ^{13}C NMR of 6-(diethylamino)-4-chloro-1,3,5-triazine-2-one.

6-(Diethylamino)-1,3,5-triazine-2-thione-4-one was synthesised (Scheme 2.2) by refluxing a solution of 6-(diethylamino)-4-chloro-1,3,5-triazine-2-one and NaSH, allowing it to cool and precipitating the product by acidifying with dilute HCl. This afforded the crude product in excellent (90 %) yield. Although nearly pure the compound was found by EIMS to contain a small quantity of elemental sulfur (S_8), probably formed by oxidation of the NaSH during the reaction. This impurity proved difficult to remove, requiring several recrystallisations, resulting in the lowering of the overall yield to 41 %. Crystals suitable for X-ray analysis were obtained by slow evaporation of a methanol solution. Crystallographic data (Table 3) and significant bond lengths and angles (Table 4) are given in the appendix.

The structure of 6-(diethylamino)-1,3,5-triazine-2-thione-4-one (Figure 2.11) shows a "head-to-tail" interaction involving H-bonding between S(6) and N(1) in neighbouring molecules. In addition there is a "head-to-tail" interaction between O(2) and N(3) and a third molecule, leading to H-bonded strands within the structure. This H-bonded network helps to explain the relative insolubility of the compound. The N...S distance of 3.339(5) Å is similar to that found in 2,4,6-trithiocyanuric acid,[30] while the N...O distance of 2.799(5) Å is similar to those found[31] in dimers of 2-pyridone derivatives.

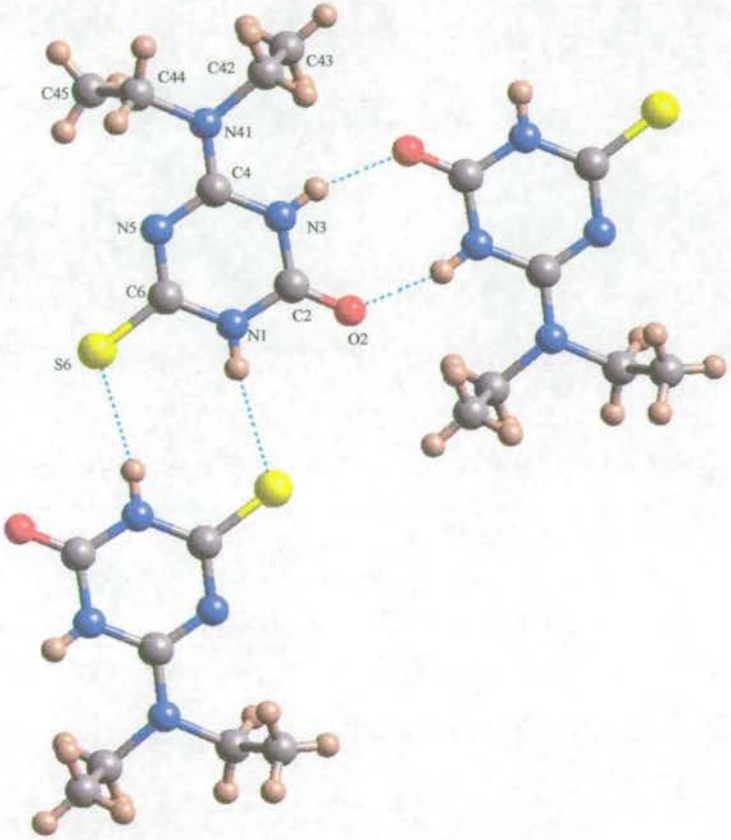

Figure 2.11: Crystal structure of 6-(diethylamino)-1,3,5-triazine-2-thione-4-one.

6-(Diethylamino)-1,3,5-triazine-2,4-thione was obtained simply by refluxing a solution of 6-(diethylamino)-2,4-dichloro-1,3,5-triazine and NaSH (Scheme 2.2) and acidifying, after cooling, using dilute HCl. This afforded the crude product in good yield. As with 6-(diethylamino)-1,3,5-triazine-2-thione-4-one the product was found to be contaminated with elemental sulfur and required several recrystallisations to purify. Crystals suitable for X-ray analysis were obtained by

slow evaporation of an ethanol solution. Crystallographic data (Table 5) and significant bond lengths and angles (Table 6) are given in the appendix.

The structure of 6-(diethylamino)-1,3,5-triazine-2,4-dithione (Figure 2.12) reveals that N(1) and S(6) atoms form a "head-to-tail" pair of interactions with the equivalent atoms in a neighbouring molecule leading to a dimer. The N...S distance of 3.272(5) Å is statistically identical to that in 6-(diethylamino)-1,3,5-triazine-2-thione-4-one. In both compounds the hydrogen atoms were not located and were placed in calculated positions in the refinement (attached to the more electronegative nitrogen atom with a hydrogen bond to the neighbouring sulfur atom). Therefore, it is not possible from the X-ray structure to state whether the mercapto or thione tautomer is present. In 6-(diethylamino)-1,3,5-triazine-2-thione-4-one the C-O bond length (1.22 Å) suggests the keto tautomer is present rather than the hydroxo.

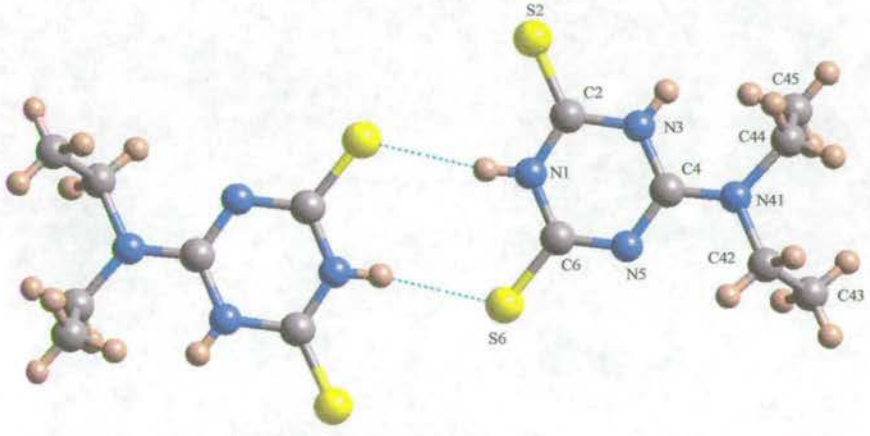

Figure 2.12: Crystal structure of 6-(diethylamino)-1,3,5-triazine-2,4-dithione.

6-(Diethylamino)-1,3,5-triazine-2,4-dione should have been easily synthesised in the same manner as 6-(diethylamino)-1,3,5-triazine-2,4-dithione by reaction with four equivalents of sodium hydroxide. However, acidification of the reaction solution with dilute hydrochloric acid did not precipitate the product as expected. Removal of the solvent gave the desired product as confirmed by IR, EIMS, ^{1}H and ^{13}C NMR but elemental analysis showed that it contained a considerable amount of impurity, probably sodium chloride formed by neutralisation of the excess sodium hydroxide. Although a small quantity of X-ray quality crystals were obtained from a THF solution, it proved impossible to obtain the compound in a pure form in large quantities. The structure of 6-(diethylamino)-1,3,5-triazine-2,4-

dione has a similar "head to tail" dimeric arrangement to that of 6-(diethylamino)-1,3,5-triazine-2,4-dithione. The N...O distance is 2.78 Å while the C-O bond lengths of 1.22 Å and 1.23 Å indicate that the keto tautomer is present. Crystallographic data (Table 7) and significant bond lengths and angles (Table 8) are given in the appendix.

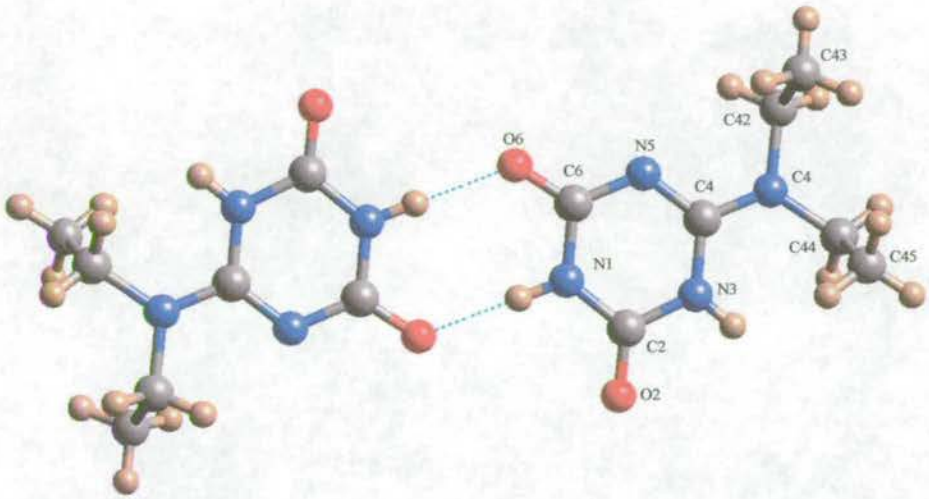

Figure 2.13: Crystal structure of 6-(diethylamino)-1,3,5-triazine-2,4-dione.

Talebian *et al*[29] reports that 6-(methylamino)-1,3,5-triazine-2,4-dione can be formed readily by refluxing 6-(methylamino)-4-chloro-1,3,5-triazine-2-one in water for only 15 min. This procedure was attempted for 6-(diethylamino)-4-chloro-1,3,5-triazine-2-one but the compound was found to be resistant to hydrolysis and remained unchanged even after refluxing for several hours.

2.3 Reaction of 1,3,5-Triazines with 1st Row Transition Metals.

2.3.1 Synthesis and Structure of [Ni{(Sta)S(S_2ta)}].[26]

The sodium salt of 6-(diethylamino)-1,3,5-triazine-2,4-thione (H_2SSta) was formed by reaction with Na(OMe) in methanol, followed by evaporation to dryness. This was reacted with nickel(II) chloride hexahydrate in the presence of sodium pivalate. It has previously been found[32] that addition of carboxylate salts can solubilise otherwise intractable reactants, which assists in formation of crystalline material, even where the carboxylate is not incorporated in the final product. Evaporation of the MeOH solution gave a black powder. This was extracted with MeCN, to give a dark red solution, from which green/yellow needles of [Ni{(Sta)S(S_2ta)}] grew after several weeks. It was necessary to recrystallise this material further from CH_2Cl_2/hexane to produce crystals suitable for X-ray studies. The need to carry out two low-yielding recrystallisations, led to formation of [Ni{(Sta)S(S_2ta)}] in low (10 %) yield. We were unable to characterise materials in the dark red solution unambiguously.

Elemental analysis suggests one nickel bound to two ligands, but X-ray analysis, shows that while this stoichiometry is maintained, the two ligands condensed to produce the complex [Ni{(Sta)S(S_2ta)}] (Figure 2.14) derived from a quadradentate ligand {H_2(Sta)S(S_2ta)} (Table 2.1). Crystallographic data (Table 9) and significant bond lengths and angles (Table 10) are given in the appendix. The nickel is four-coordinate, bound to two nitrogen donors from the triazines, and two sulfur atoms, one from the disulfide, and the second from the thiol group of a triazine. The resulting coordination geometry is very distorted square planar, with *cis*-angles varying from 73.5 to 96.0°, and *trans*-angles of around 169°. The bond lengths to the Ni centre show considerable variation. The shortest is the Ni-N(1A) bond [1.841(5) Å], to the nitrogen atom of the triazine to which the thiol group is attached. This is considerably shorter than the Ni-N(1B) bond [1.913(5) Å] to the other triazine. There is also a significant difference between the two Ni-S bonds, with the bond to the disulfide sulfur, Ni-S(3B), shorter at 2.131(2) Å than the bond to

the thiol sulfur [2.240(2) Å]. The Ni-S(disulfide) bond is typical of previous examples containing this feature,[33,34,35,36,37] as is the S-S bond of 2.049(3) Å.

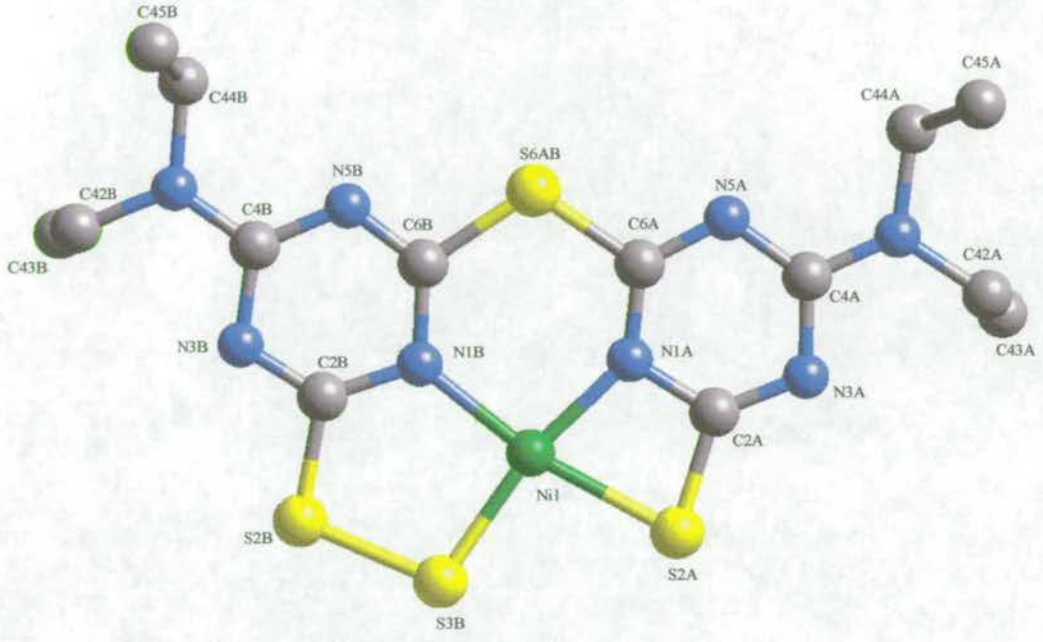

Figure 2.14: Crystal structure of [Ni{(Sta)S(S_2ta)}].

The crystal structure also shows that there is an orientational disorder (Figure 2.15) of the whole complex *via* a two-fold rotation about an axis which pases approximately through Ni(1) and S(6AB).

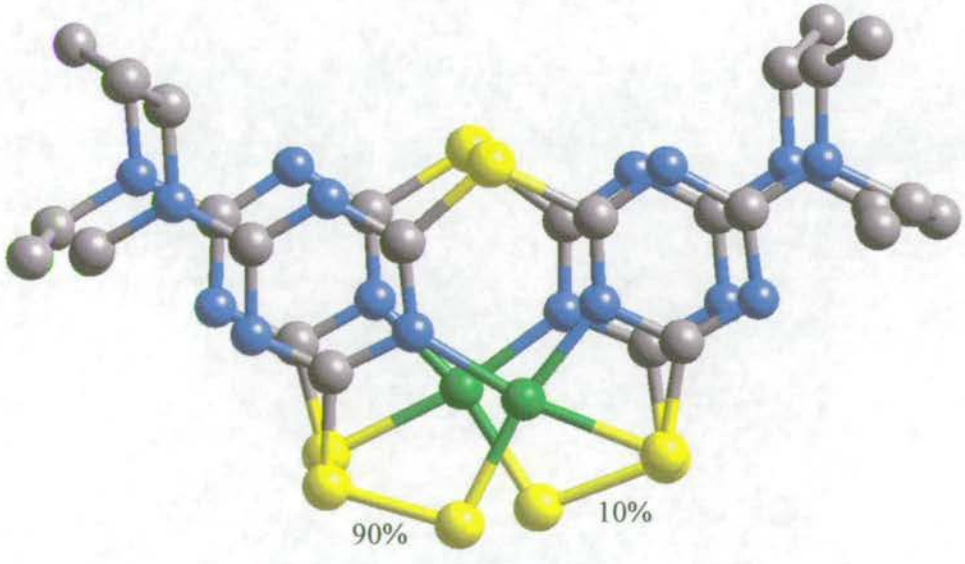

Figure 2.15: Representation of the disorder of [Ni{(Sta)S(S_2ta)}].

The molecules of [Ni{(Sta)S(S_2ta)}] stack in the solid state (Figure 2.16). The most significant inter-molecule interactions are between the nickel centres [e.g. Ni(1) or Ni(1A)] and the bridge-head sulfur [e.g. S(6AA) or S(6AB)]. This contact of 3.27 Å is close to the sum of the Van der Waals radii of the two elements. The arrangement of the molecules is such that the triazine rings are directly above one another within these dimers. The distance between the centroids of neighbouring triazines is 3.41 Å, which represents a weak "graphitic" interaction. These weak interactions create "dimers" within the stacks. The closest "inter-dimer" interaction is a Ni…Ni contact of 3.58 Å [Ni(1)…Ni(1B) (Figure 2.16)].

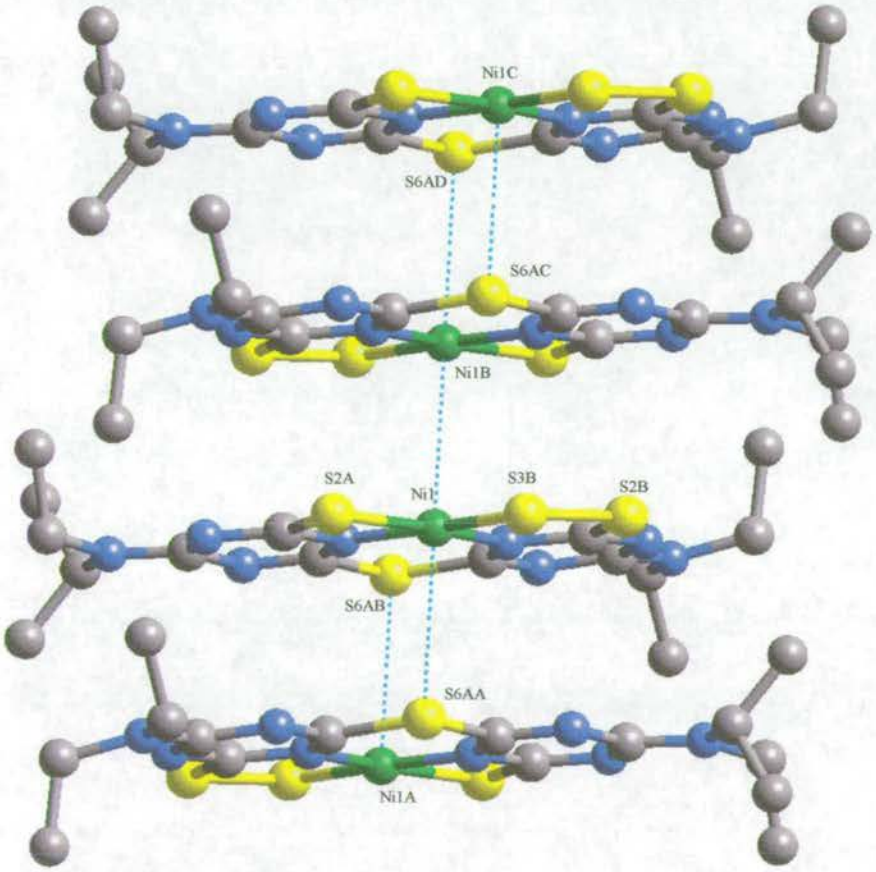

Figure 2.16: Stacking of [Ni{(Sta)S(S_2ta)}].

All routes to the ligand $\{(Sta)S(S_2ta)\}^{2-}$ require a multi-step mechanism. One possibility is shown (Scheme 2.3). The first two steps proposed are formation of a disulfide bridge between two triazine ligands, and nucleophilic substitution reaction

involving displacement of one thiol from an S_2ta ligand by a thiol from a second triazine. The same product results whichever step is taken first. The final step is then nucleophilic displacement of the disulfide by an incoming S_2ta group, giving $\{(Sta)S(S_2ta)\}^{2-}$ and $\{(Sta)_2S\}^{2-}$ as products. While the former is found in formation of the complex $[Ni\{(Sta)S(S_2ta)\}]$, a product related to the latter group is found in $[Co_6NaO(OStaH)_7\{S(Ota)_2\}_2(O_2CPh)_2(H_2O)_2]$ (see section 2.3.2). Formation of the disulfide bridge is an oxidation of the ligand, which is presumably carried out by atmospheric oxygen. We were unable to improve the yield of $[Ni\{(Sta)S(S_2ta)\}]$ by bubbling dry oxygen through the solution.

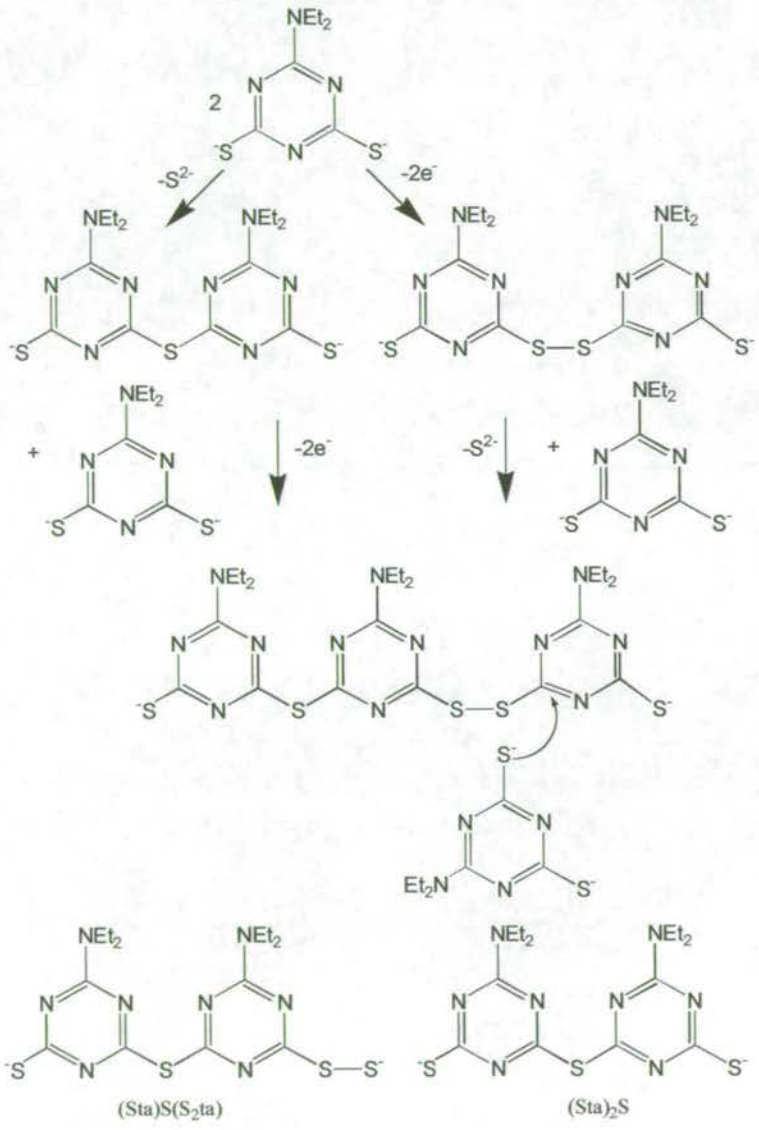

Scheme 2.3: Possible reaction path to give $\{(Sta)S(S_2ta)\}^{2-}$.

2.3.2 Conductivity of [Ni{(Sta)S(S_2ta)}].

Because of the stacking and intermolecular interactions displayed by [Ni{(Sta)S(S_2ta)}] (Figure 2.16), it was considered that it may have an increased conductivity over a simple molecular solid. The conductivity of a single crystal (Figure 2.17) of [Ni{(Sta)S(S_2ta)}] was measured by an a.c. conductivity measurement using the four probe method at room temperature by Dr N. Robertson. The value obtained was 1×10^{-5} S cm^{-1}. This is typical of a non-doped molecular conductor with strong intermolecular interactions. Doped molecular conductors typically have values in the range 0.1-1 S cm^{-1}, while simple molecular solids have much lower values, $< 1 \times 10^{-7}$ S cm^{-1}.[38] For comparison the conductivity of various materials is shown (Figure 2.18).

Figure 2.17: Crystals of [Ni{(Sta)S(S_2ta)}].

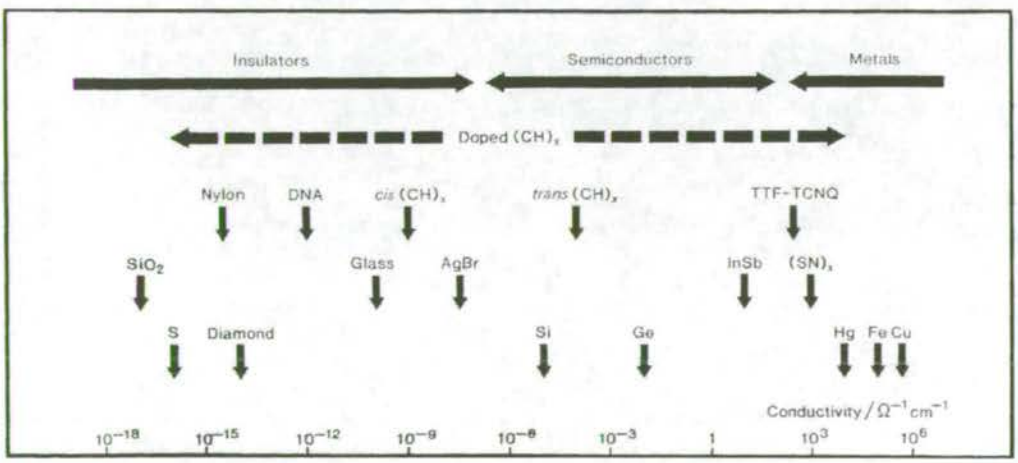

Figure 2.18: Conductivity of various materials.[38]

2.3.3 Synthesis and Structure of $[Co_6NaO(OStaH)_7\{S(Ota)_2\}_2(O_2CPh)_2(H_2O)_2]$ and $[Co(OStaH)_3]$.[26]

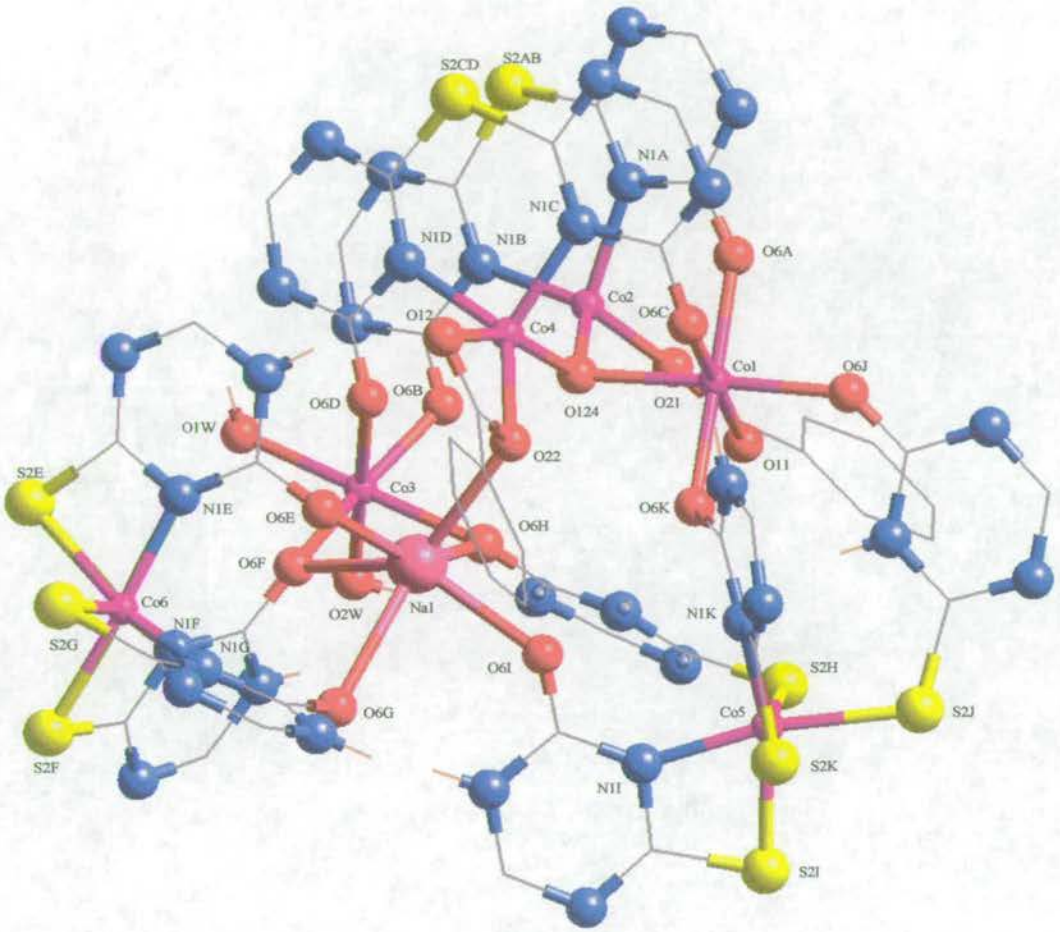

Figure 2.19: Crystal structure of $[Co_6NaO(OStaH)_7\{S(Ota)_2\}_2(O_2CPh)_2(H_2O)_2]$.

Reaction of the sodium salt of 6-(diethylamino)-1,3,5-triazine-2-thione-4-one (H_2OSta) with cobalt chloride and $Na(O_2CPh)$ in MeOH, followed by evaporation to dryness and recrystallisation from MeCN, gives the product, $[Co_6NaO(OStaH)_7\{S(Ota)_2\}_2(O_2CPh)_2(H_2O)_2]$ (Figure 2.19). Once again transformation of some of the triazine ligands by condensation reactions, generates a new ligand $\{S(Ota)_2\}^{2-}$ (Table 2.1) but in this case the product, as characterised by X-ray diffraction, is a great deal more complicated. As in the synthesis of $[Ni\{(Sta)S(S_2ta)\}]$, the yield is poor due to the recrystallisation step. The major product is a black solid which forms before the crystals and which, despite repeated efforts to crystallise, has not yet been characterised unambiguously. Crystallographic

data (Table 11) and significant bond lengths and angles (Table 12) are given in the appendix.

The ligand reaction is more straightforward, and not all ligands present have condensed. Two $\{S(Ota)_2\}^{2-}$ ligands (Figure 2.20) are found in which a sulfur from one triazine has displaced a sulfur from a second, thus linking two oxygen-substituted triazines. These ligands lie almost co-planar within the cage [see ligands involving S(2AB), N(1B), O(6B), N(1A), O(6A) and S(2CD), N(1D), O(6D), N(1C), O(6C)] and forming six-membered chelate rings with Co(2) and Co(4) respectively, using triazine nitrogen donors. One oxygen atom [O(6A) and O(6C)] from each binds to Co(1), and the second oxygen donor [O(6B) and O(6D)] from each binds to Co(3). A difference is that the oxygen atoms bind to Co(1) in a *syn*-fashion, but to Co(3) as *anti*. A μ_3-oxide [O(124)] also bridges Co(2), Co(4) and Co(1).

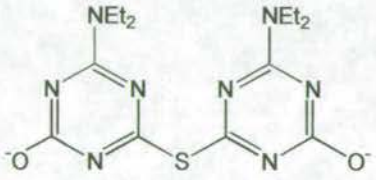

Figure 2.20: $\{S(Ota)_2\}^{2-}$.

While this segment of the cage is comparatively ordered, the remaining three metal sites are irregularly distributed. Co(5) is attached to the cage through two OStaH$^-$ ligands, which bind to Co(1) through the oxygen donor [O(6K) or O(6J)] and to Co(5) through the sulfur [S(2K) or S(2J)]. The nitrogen atom between the two exocyclic groups is protonated, and in both cases is involved in H-bonds. Co(6) is attached to three OSta$^-$ ligands, with each ligand chelating to Co(6) through the sulfur atom and the N(1) site of the triazine, to give a *fac*-octahedral geometry. This is a similar mode of coordination to that observed for cobalt coordinated to 2-mercaptopyridine. The tris-chelate around Co(6) thus has three O-atoms to act as donors to other metals, and these oxygen atoms [O(6E), O(6F) and O(6G)] all bind to a sodium atom [Na(1)] with one of the oxygen atoms [O(6F)] bridging further to Co(3). The sodium site is bridged to Co(5) through two OSta$^-$ ligands, both of which bind to the sodium through the oxygen donor [O(6I) or O(6H)], while one

coordinates to Co(5) through both nitrogen and sulfur donors [N(1I) and S(2I)], while the second binds to Co(5) through the exocyclic sulfur alone [S(2H)]. Two benzoates are also found in the structure. One chelates to Co(1) through O(11) and O(21), and also bridging to Co(2) through O(21). The second chelates to Co(4) through O(12) and O(22), with O(22) forming a bridge to Na(1).

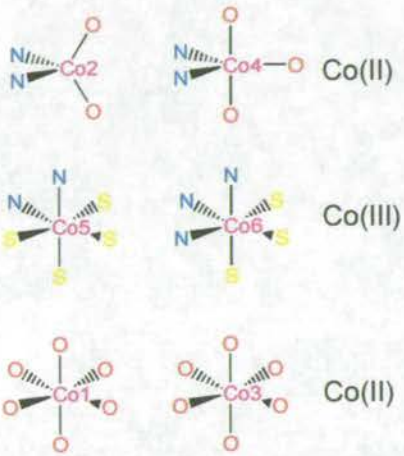

Figure 2.21: Cobalt coordination environments in $[Co_6NaO(OStaH)_7\{S(Ota)_2\}_2(O_2CPh)_2(H_2O)_2]$.

The metal coordination sites are extremely varied (Figure 2.21). Co(1) and Co(3) are each bound to six oxygen donors, having fairly regular octahedral geometries. Co(2) is bound to two nitrogen and two oxygen donors, with a distorted tetrahedral geometry. Co(4) has three oxygen and two nitrogen donors in its coordination sphere. The Co(4)-O(12) bond is significantly longer than the remaining four bonds, and the geometry is best regarded as a capped-tetrahedron. Co(5) is bound to the nitrogen and sulfur donors of two chelating OStaH$^-$ ligands, and to two further sulfur atoms. The geometry is based on octahedral, but is severely distorted by the two chelating groups. Co(6) is bound to the nitrogen and sulfur donors of three chelating OStaH$^-$ ligands. The geometry is distorted octahedral. The sodium site has seven oxygen donors within bonding distance, with a predictably distorted geometry.

Assigning charge is not straightforward. Consideration of the bridging modes and H-bonding involving the OStaH$^-$ ligands, led us to consider all of them to be singly deprotonated anions. These ligands display four binding modes, two of which involve binding through a triazine nitrogen, and two which do not (Figure 2.22). The

2.1_11_21 mode involves chelating to one metal through the N(1) position and the exocyclic sulfur, while bridging to a second metal through the oxygen donor. This is displayed by two of the three OSta$^-$ ligands attached to Co(6), and by two of the four ligands bound to Co(5). The second mode ($3.1_12_{23}1_1$) is closely related, differing in that the oxygen donor binds to two metals. This is displayed exclusively by one ligand attached to Co(6) through N(1F) and S(2F), while O(6F) bridges between Co(3) and Na(1). The third coordination mode (2.110) involves bridging between two metals, with the S-atom [S(2J)] attached to one metal [Co(5)] and the oxygen atom [O(6J)] attached to a second [Co(1)]. The fourth (3.120) is very similar, with the sulfur atom [S(2H)] bound to one metal [Co(5)], and the oxygen [O(6H)] bridging between two metals [Co(3) and Na(1)].

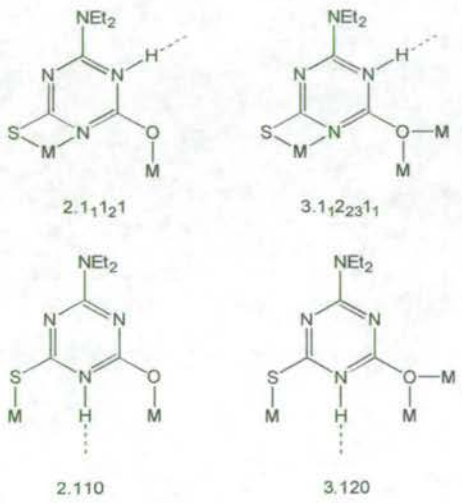

Figure 2.22: OSta binding modes in $[Co_6NaO(OStaH)_7\{S(Ota)_2\}_2(O_2CPh)_2(H_2O)_2]$.

Within the cage there is a complicated series of hydrogen-bonds (Figure 2.23). For the ligands which show the 2.110 and 3.120 binding modes, the N(1) nitrogen of the triazine is protonated, and acts a hydrogen bond donor, with the hydrogen bond acceptor the exocyclic oxygen of a neighbouring OSta$^-$ ligand. The N...O distances vary from 2.85 to 2.98 Å. For the ligands where N(1) is bound, the N(5) nitrogen (i.e. the nitrogen *para* to the exocyclic sulfur) is protonated, and acts as an H-bond donor, with the acceptor an oxygen derived from a coordinated water, a benzoate or an OSta$^-$ ligand. Here the N...O distances vary from 2.69 to 2.86 Å. The final hydrogen bonds involve the condensed $\{S(Ota)_2\}^{2-}$ ligands, where a water

molecule [O(1W)] is the hydrogen bond donor to the N(5) nitrogen in the triazine ring nearest [N…O distances 2.79 and 2.91 Å].

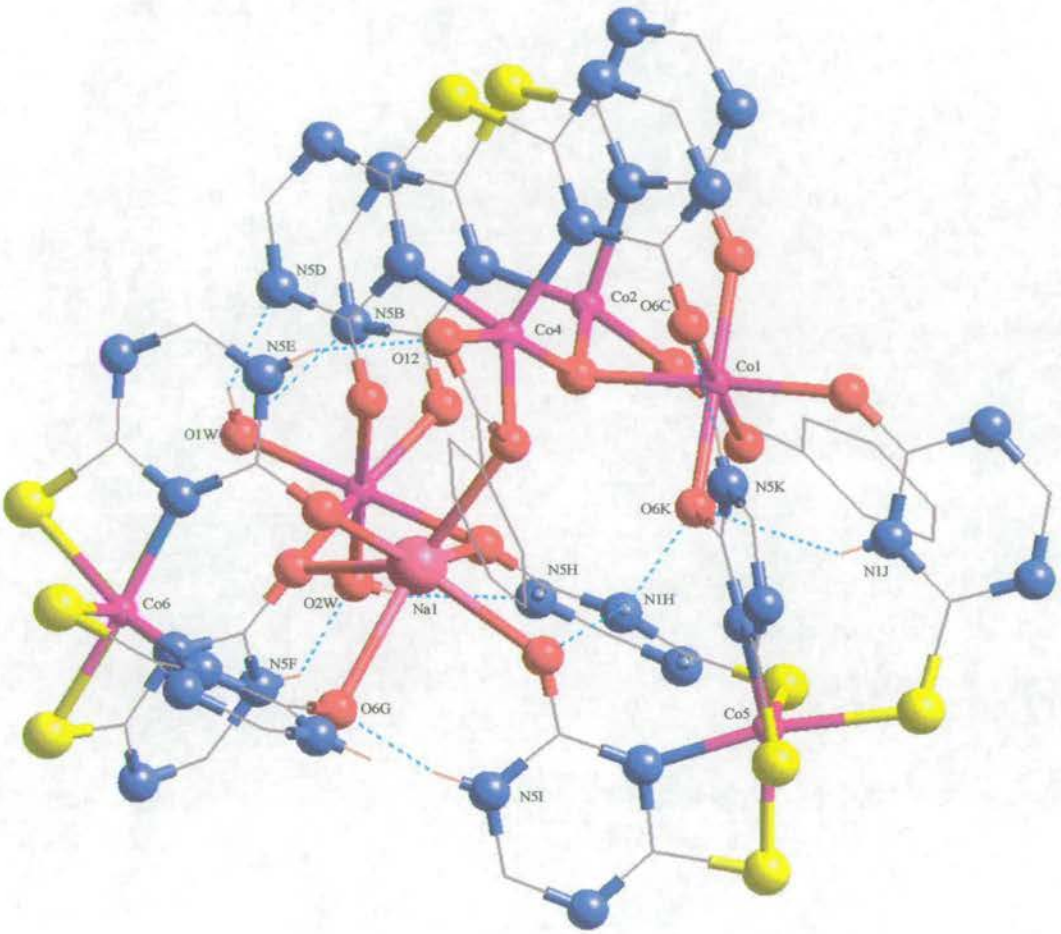

Figure 2.23: Hydrogen-bonding in $[Co_6NaO(OStaH)_7\{S(Ota)_2\}_2(O_2CPh)_2(H_2O)_2]$.

This assignment of charge to the $OStaH^-$ ligands requires that two of the six cobalt sites in the cage are Co(III), while the remaining four sites are Co(II). While Co(2) and Co(4) can probably be assigned as Co(II) due to their approximately tetrahedral coordination geometry, assigning oxidation states to the other sites is more complicated. The similarities between the bond lengths at the Co(5) and Co(6) sites [Co-S 2.277 - 2.320(5), Co-N 1.929 - 1.960(10) Å], and the bond lengths in tris(2-mercaptopyridine)cobalt(III) [Co-S 2.285 - 2.307(5), Co-N 1.904 - 1.938(6) Å],[39,40] rather than the bond lengths in the anionic complex tris(2-mercaptopyridine)cobalt(II) [Co-S 2.552 - 2.585(6), Co-N 2.094 - 2.135(8) Å],[41] supports assignment of these centres to the higher oxidation state. This assignment

leaves Co(1) and Co(3) as Co(II). It is interesting that the higher oxidation state is to be bound to the "softer" sulfur and nitrogen donor groups, while Co(1) and Co(3), in the lower oxidation state are bound exclusively to oxygen donors.

Further evidence for this assignment of oxidation state comes from the crystallisation of $[Co(OStaH)_3]$. This compound crystallised from the reaction mixture that gave $[Co_6NaO(OStaH)_7\{S(Ota)_2\}_2(O_2CPh)_2(H_2O)_2]$ in very low yield. The structure (Figure 2.24) contains a Co(III) site bound to the sulfur and nitrogen donors of three chelating $OStaH^-$ ligands. The geometry is distorted octahedral, with the three sulfur and three nitrogen donor atoms in a *fac*-arrangement. The bond lengths [Co-S 2.249 - 2.311(11), Co-N 1.84 - 1.98(3) Å] fall in the same ranges as those for the Co(5) and Co(6) sites in $[Co_6NaO(OStaH)_7\{S(Ota)_2\}_2(O_2CPh)_2(H_2O)_2]$. Crystallographic data (Table 13) and significant bond lengths and angles (Table 14) are given in the appendix.

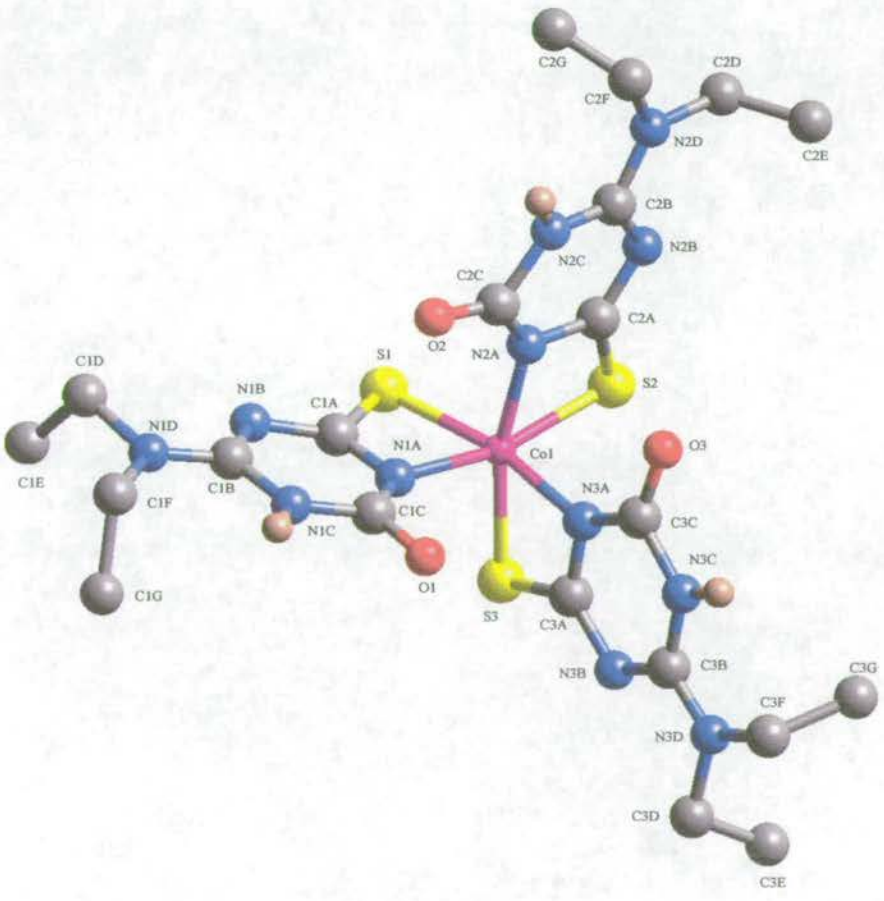

Figure 2.24: Crystal structure of $[Co(OStaH)_3]$.

A curious feature of the structure of $[Co(OStaH)_3]$ is the presence of eight crystallographically independent molecules within the asymmetric unit. These eight molecules form two supra-molecular tetrahedral aggregates, one of which is shown (Figure 2.25). Four $[Co(OStaH)_3]$ units lie with the cobalt centres at the vertices of a tetrahedron. The molecules are held together by pairs of hydrogen bonds between the nitrogen atom *para* to the sulfur donor, and the exocyclic oxygen, e.g. N(2C)...O(5) and O(2)...N(5C) (Figure 2.25). Four molecules of MeCN lie at the centres of the faces of the tetrahedral aggregate. These are not shown in the diagram.

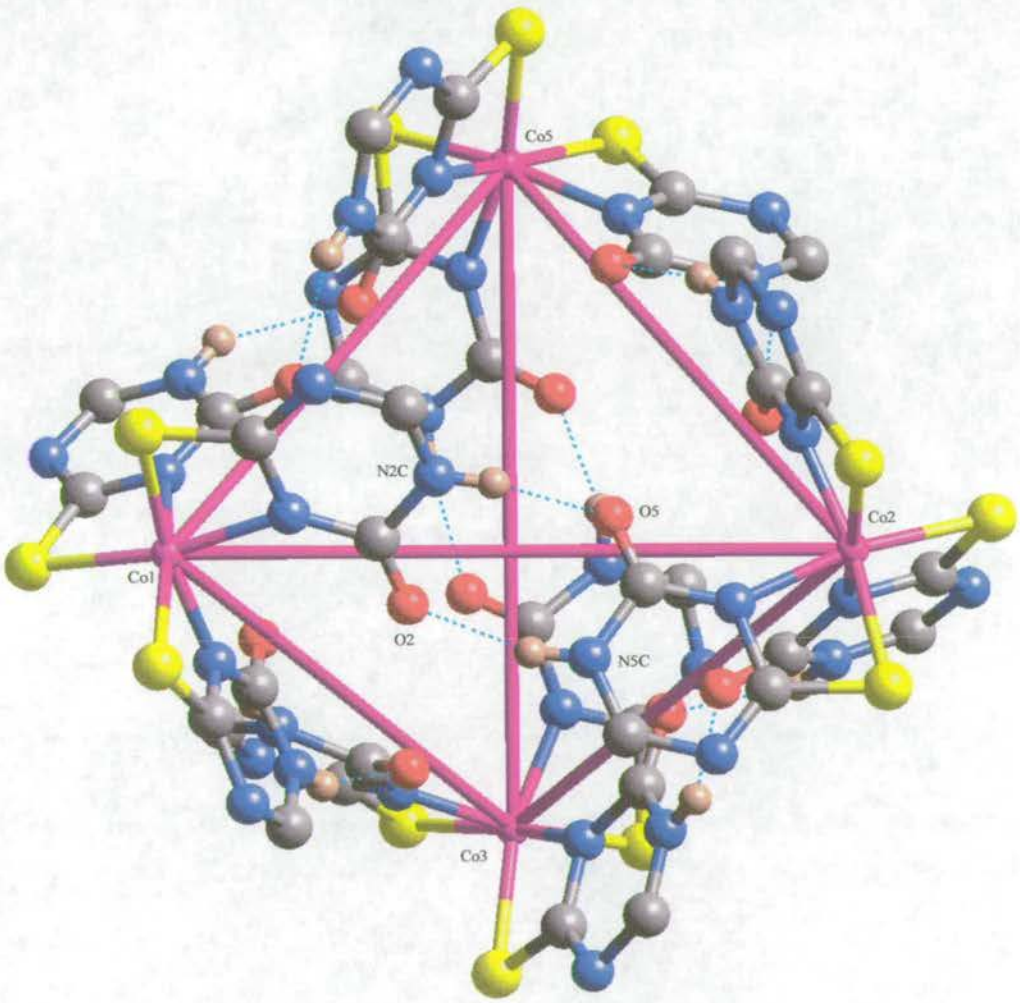

Figure 2.25: One of two tetrahedral aggregates of molecules of $[Co(OStaH)_3]$.

In both $[Co_6NaO(OStaH)_7\{S(Ota)_2\}_2(O_2CPh)_2(H_2O)_2]$ and $[Co(OStaH)_3]$there is evidence for oxidation of Co(II) to Co(III). We assume this oxidation has been caused by atmospheric oxygen, but have not yet been able to improve the yield of

either compound by addition of oxidants or by bubbling dry oxygen through reactant or recrystallisation solutions.

2.3.4 Synthesis and Structure of $[Na_6(HO_2ta)_6(H_2O_2ta)_6(CH_3OH)_8(H_2O)_2].2CH_3OH.H_2O$.

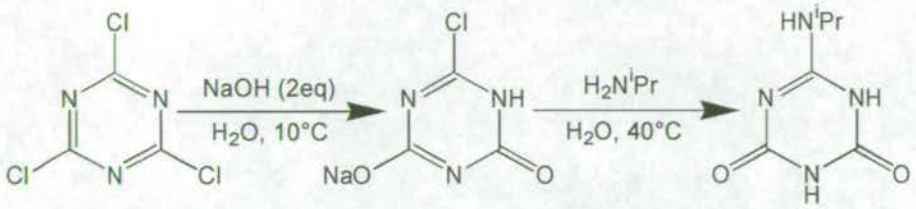

Scheme 2.4: Reaction scheme for 6-(isopropylamino)-1,3,5-triazine-2,4-dione.

After the problems encountered synthesising pure dihydroxy functionalised triazines by the initial route, an alternative method (Scheme 2.4), via the dihydroxy species, then substituting the remaining chloride with the required amine was attempted. 2-Chloro-4,6-dihydroxy-1,3,5-triazine-(Na salt).$2H_2O$ was synthesised in 48 % yield by the method of Horrobin.[42] The amine substitution was carried out using a similar method to Kataoka.[43] The presence of the desired product was confirmed by electron impact mass spec, however purification by recrystallisation from methanol yielded both the protonated and deprotonated ligand as part of a hexameric sodium complex $[Na_6(HO_2ta)_6(H_2O_2ta)_6(CH_3OH)_8(H_2O)_2].2CH_3OH.H_2O$ (Figure 2.26).

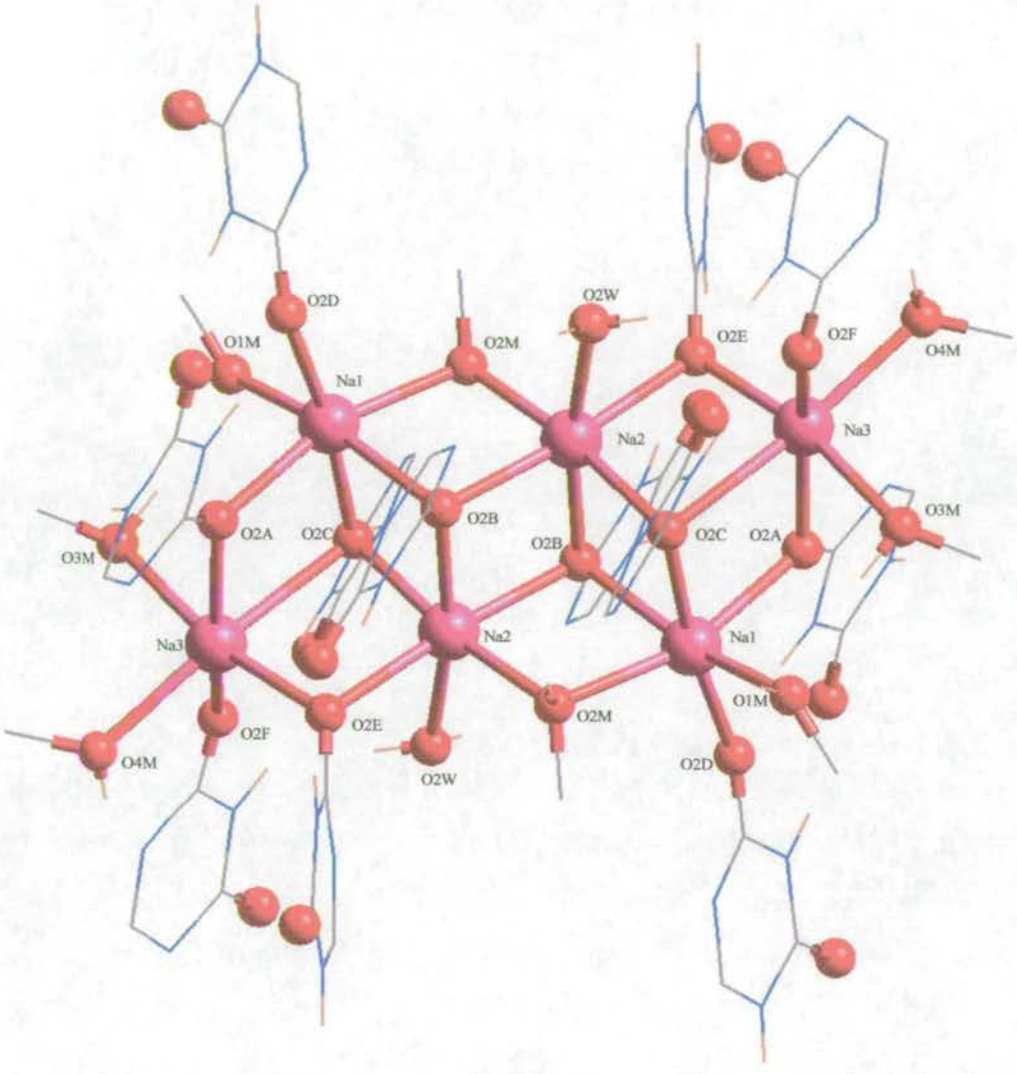

Figure 2.26: Crystal structure of $[Na_6(HO_2ta)_6(H_2O_2ta)_6(CH_3OH)_8(H_2O)_2].2CH_3OH.H_2O$.

Crystallographic data (Table 15) and selected bond lengths and angles (table 16) for $[Na_6(HO_2ta)_6(H_2O_2ta)_6(CH_3OH)_8(H_2O)_2].2CH_3OH.H_2O$ are given in the appendix. The complex contains six sodium atoms and twelve 6-(isopropylamino)-1,3,5-triazine-2,4-dione (H_2O_2ta) ligands, six of which are deprotonated (HO_2ta) in order to maintain charge balance. The ligands display three binding modes (Figure 2.27), terminal co-ordination to one sodium, μ_2-bridging to two sodiums and μ_3-bridging to three sodiums. In all cases only one oxygen atom of the ligand is involved in bonding to the metal centres. Both protonated and deprotonated ligands show all three modes. The co-ordination of the ligands is further complicated by the fact that four (B and E) contain a half occupied hydrogen on N(5). The Na-O (ligand) bonds range from 2.338(3) - 2.773(2) Å, with an average of 2.439 Å.

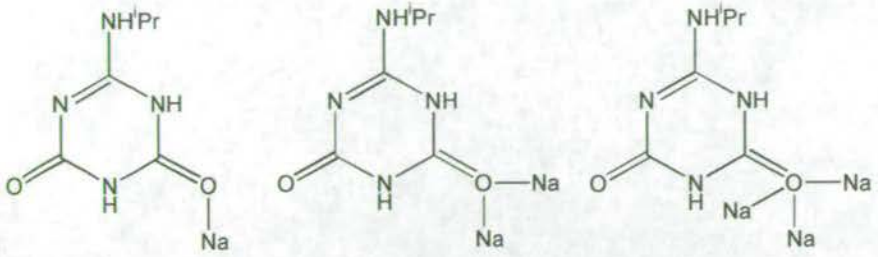

Figure 2.27: Ligand binding modes in $[Na_6(HO_2ta)_6(H_2O_2ta)_6(CH_3OH)_8(H_2O)_2].2CH_3OH.H_2O$.

Eight methanols, six terminal and two μ_2-bridging and two terminal water molecules complete the co-ordination around the cluster. Methanol(4) bonded to Na(3) is disordered over two positions.

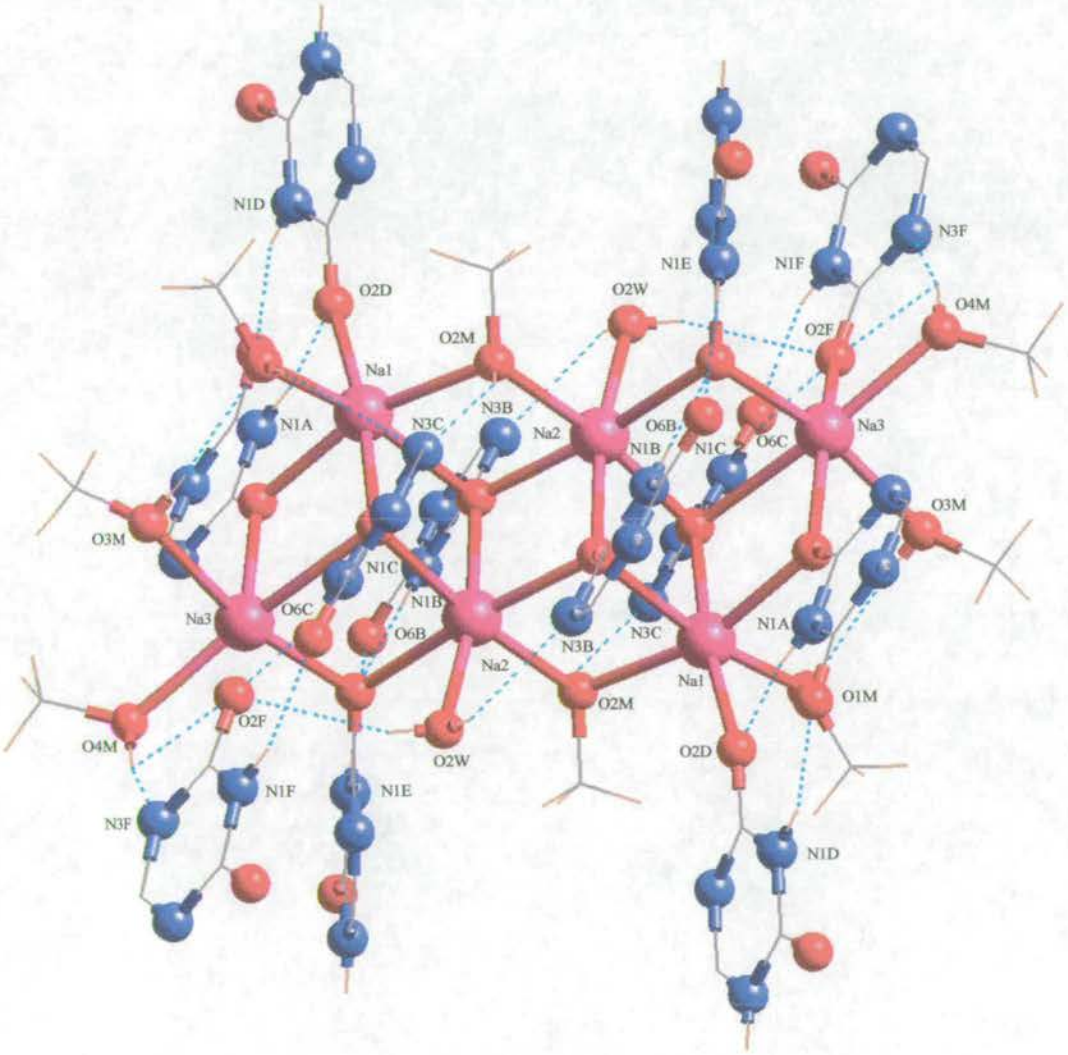

Figure 2.28: Hydrogen bonding network of $[Na_6(HO_2ta)_6(H_2O_2ta)_6(CH_3OH)_8(H_2O)_2].2CH_3OH.H_2O$.

The hydrogen-bonding network (Figure 2.28) around the complex is complicated. The ligands A and D, B and E, and C and F all form dimers via "head to tail" pairs of similar N-H…O hydrogen bonds (Figure 2.29). For ligands D and E, these are the only hydrogen bonding interactions in which they are involved. Additional hydrogen bonds are seen for ligands A, B, C and F. Ligand B forms a O-H...N interaction with O(2W). Ligand C has a bifurcated hydrogen bond of the type O-H…N between N(3C) and methanols (1 and 2), while ligand F forms an additional hydrogen bond of type O-H…N to O(2W). The disordered nature of methanol (4) means that in one position it forms a hydrogen bond with ligand A and in the other position with ligand F. Both bonds are of type O-H…N. There is also a O-H…O bond present between methanols (1 and 3). All hydrogen bond contacts and distances are given (Table 2.2).

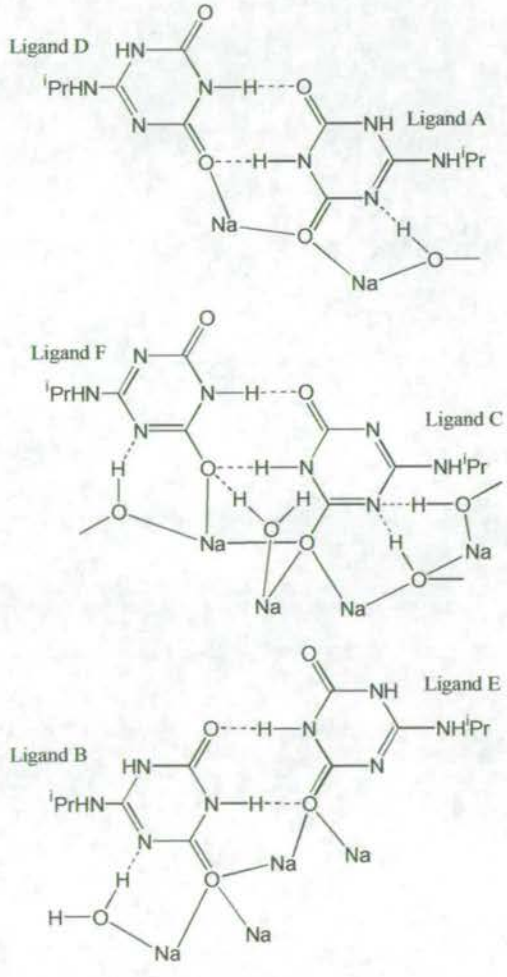

Figure 2.29: Schematic diagram of the hydrogen bonded pairs in $[Na_6(HO_2ta)_6(H_2O_2ta)_6(CH_3OH)_8(H_2O)_2].2CH_3OH.H_2O$.

Bond type	Donor atom	Acceptor atom	Bond length (Å)
N-H...O	N(1D)	O(6A)	3.067
N-H...O	N(1A)	O(2D)	2.712
N-H...O	N(1A)	O(2E)	2.891
N-H...O	N(1E)	O(6B	3.183
O-H...N	O(2W)	N(3B)	3.136
N-H...O	N(1C)	O(2F)	2.744
N-H...O	N(1F)	O(6C)	2.996
O-H...N	O(1M)	N(3C)	3.321
O-H...N	O(2M)	N(3C)	2.816
O-H...N	O(4M)	N(3F)	2.835
O-H...N	O(4M')	N(3A)	2.834
O-H...N	O(2W)	O(2F)	3.281
O-H...O	O(3M)	O(1M)	3.032

Table 2.2: Hydrogen bond contacts in $[Na_6(HO_2ta)_6(H_2O_2ta)_6(CH_3OH)_8(H_2O)_2].2CH_3OH.H_2O$.

All of the sodium atoms are in a distorted octahedral environment, co-ordinated by six oxygen atoms. The central Na_6O_{10} core (Figure 2.30) can be described as four face sharing cubanes, each missing one vertex. The Na...Na contacts have a range of 3.4311(17) to 3.7339(17) Å, with an average of 3.565 Å. The central core arrangement is very similar to that found in the of the Na_6 cluster of Bock *et al*,[44] formed using tetraphenyl imidodiphosphate, $(HN[PO(OC_6H_5)_2]_2)$. The defective cubanes in this complex however are less regularly cubic than those in $[Na_6(HO_2ta)_6(H_2O_2ta)_6(CH_3OH)_8(H_2O)_2].2CH_3OH.H_2O$. A similar core can also be found in the mixed metal nickel/ sodium cluster $[Ni_4Na_4(mhp)_{12}(Hmhp)_2]$ (Hmhp = 6-methyl-2-hydroxypyridonate).[45] In this case, while the central two defective cubane units are identical, forming a "chair" like structure, nickel atoms fill the sodium sites in the outer units. The complex contains two additional defective cubane units formed by the other two nickel atoms. This produces a centrosymmetric structure containing four chemically identical $[Ni(mhp)_3]^-$ units surrounding the central sodium "chair". Two other Na_6 clusters are known, however these have cores consisting of two fully formed cubanes.[46,47]

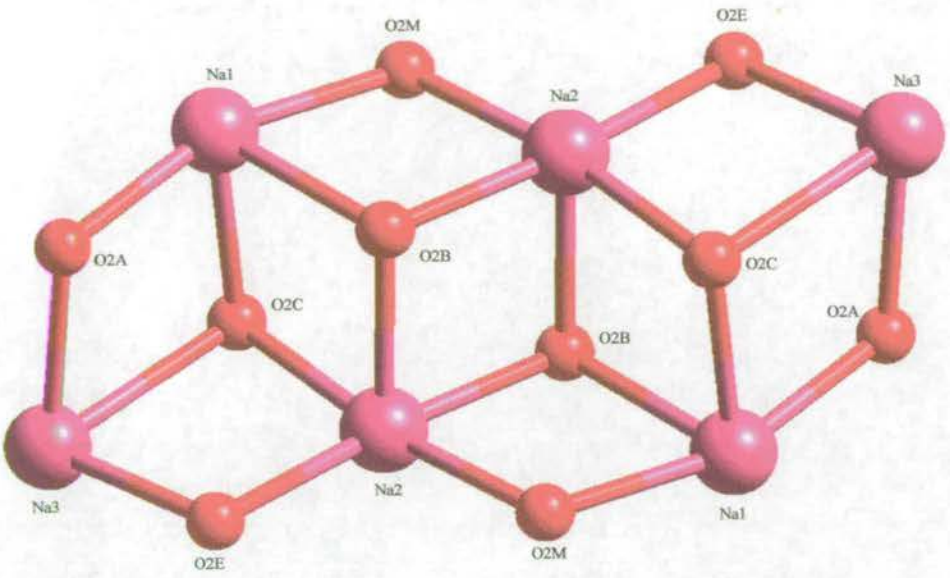

Figure 2.30: Na_6O_{10} core of $[Na_6(HO_2ta)_6(H_2O_2ta)_6(CH_3OH)_8(H_2O)_2].2CH_3OH.H_2O$.

More relevant to this project, the core shares structural features with the minerals boehmite and diaspore, the two polymorphs of $Al(O)(OH)_2$ (Figure 2.31), and the defective cubane structure features in several polynuclear aluminium complexes.[48,49]

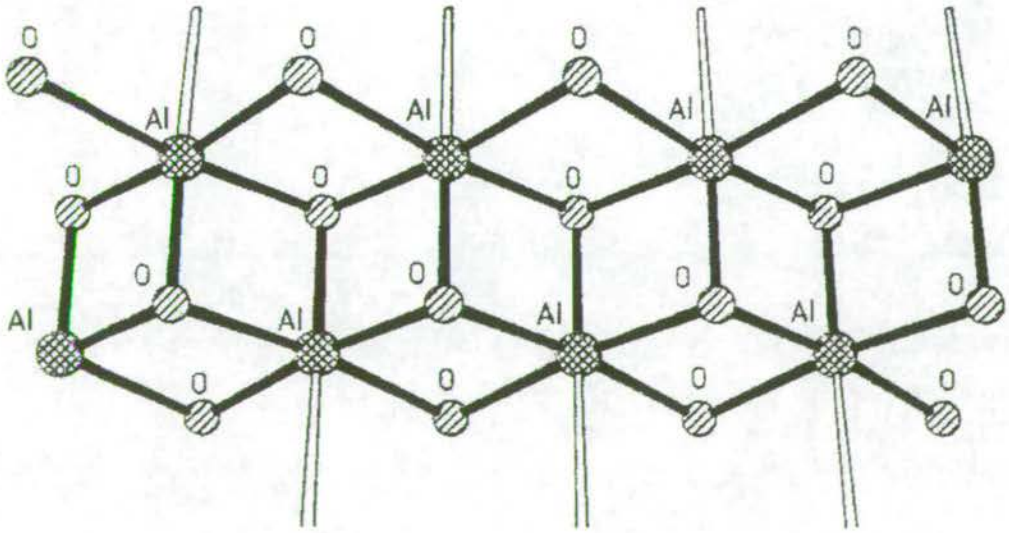

Figure 2.31: The structure of $Al(O)(OH)_2$.[49]

2.4 Isotherm Studies.

2.4.1 Problems.

As can be seen from the preceding sections the complex formation reactions of sulfur functionalised triazines are not straightforward, leading to formation of polydentate ligands via *in situ* inter-ligand reactions. The lability of the compounds 6-(diethylamino)-1,3,5-triazine-2,4-thione and 6-(diethylamino)-1,3,5-triazine-2-thione-4-one severely limits their utility as surface ligands.

The lability of triazine based ligands is also highlighted in the reaction of aluminium nitrate nonahydrate with 6-(diethylamino)-4-chloro-1,3,5-triazine-2-one. Instead of forming the expected $Al(L_3)$ complex, crystals of a new ligand 6-(diethylamino)-4-methoxy-1,3,5-triazine-2-one (Figure 2.32) were obtained, in which a methoxy group from the solvent methanol has substituted the remaining chloride atom. Crystallographic data (Table 17) and significant bond lengths and angles (Table 18) are given in the appendix. The compound adopts a hydrogen bonded [N(1)-H....O(21) 2.773 Å] dimeric arrangement similar to that observed for other triazines in the solid state.

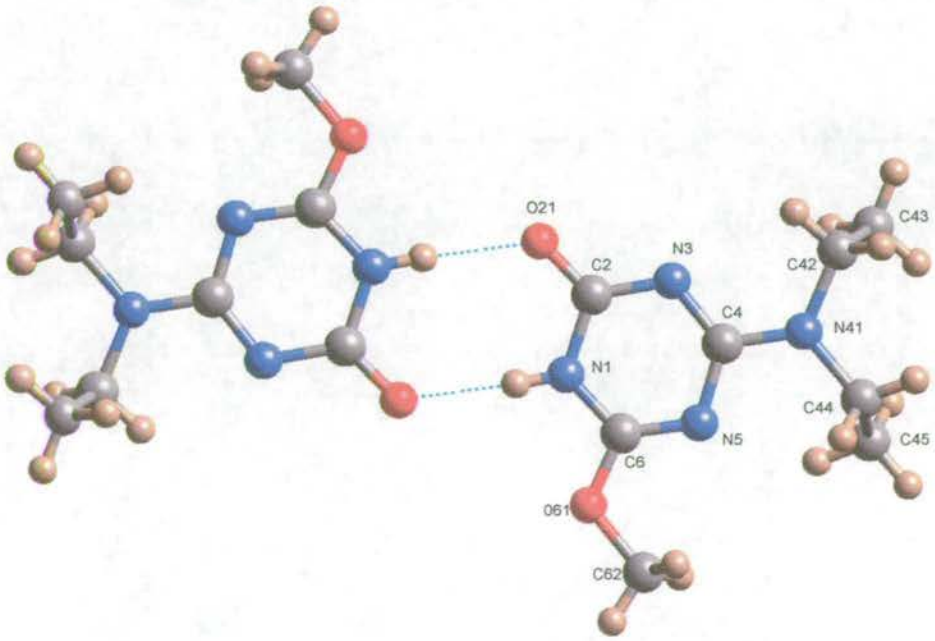

Figure 2.32: Crystal structure of 6-(diethylamino)-4-methoxy-1,3,5-triazine-2-one.

This shows that the ligands, instead of modifying the surface as intended are capable of being modified themselves by a surface. This means that they cannot reliably be used in isotherm experiments as they rely on the ligand remaining unchanged throughout the experiment.

The obvious choice as the best triazine candidate as a surface ligand for aluminium are the oxygen substituted dione compounds. However, using our synthetic routes these proved difficult to obtain pure in large quantities. The formation of the hexameric sodium cluster $[Na_6(HO_2ta)_6(H_2O_2ta)_6(CH_3OH)_8(H_2O)_2].2CH_3OH.H_2O$ highlights the difficulty in purification of this type of compound. A sample of 6-(*p*-tolyl)-1,3,5-triazine 2,4-dione (Figure 2.33) was obtained from Zeneca, but this proved to be insoluble in the solvent system used for the experiment.

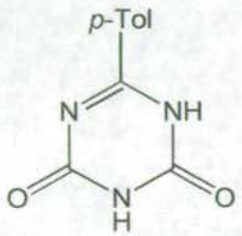

Figure 2.33: 6-(*p*-tolyl)-1,3,5-triazine 2,4-dione.

2.4.2 Isotherm Results.

Given that the most favourable donor atom for aluminium is oxygen, two compounds, 2-hydroxypyridine and uracil (Figure 2.34) were used as "model triazines". These can present a similar donor array and have the required solubility.

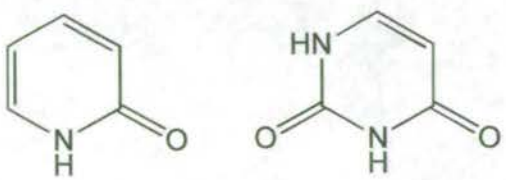

Figure 2.34: 2-hydroxypyridine and uracil.

Data for the calibration and isotherm experiments in this section are given in the appendix, Tables 31-34.

The UV/vis spectra of 2-hydroxypyridine and uracil were recorded in 95/5 % methanol/water and their extinction coefficients determined (Table 2.3) using the Beer-Lambert Law.

Compound	UV/vis bands, λ (nm)	Extinction coefficient ε
2-hydroxypyridine	227, 298	5420(50), (λ = 298)
uracil	205, 259	8160(40), (λ = 259)

Table 2.3: Electronic spectra for ligands in 95 % methanol/water (standard deviations in parenthesis).

The adsorption isotherms were determined as described in Section 2.6.3 and are plotted (Figure 2.35). All isotherms within this thesis will be plotted on the same scale to allow for easier comparison.

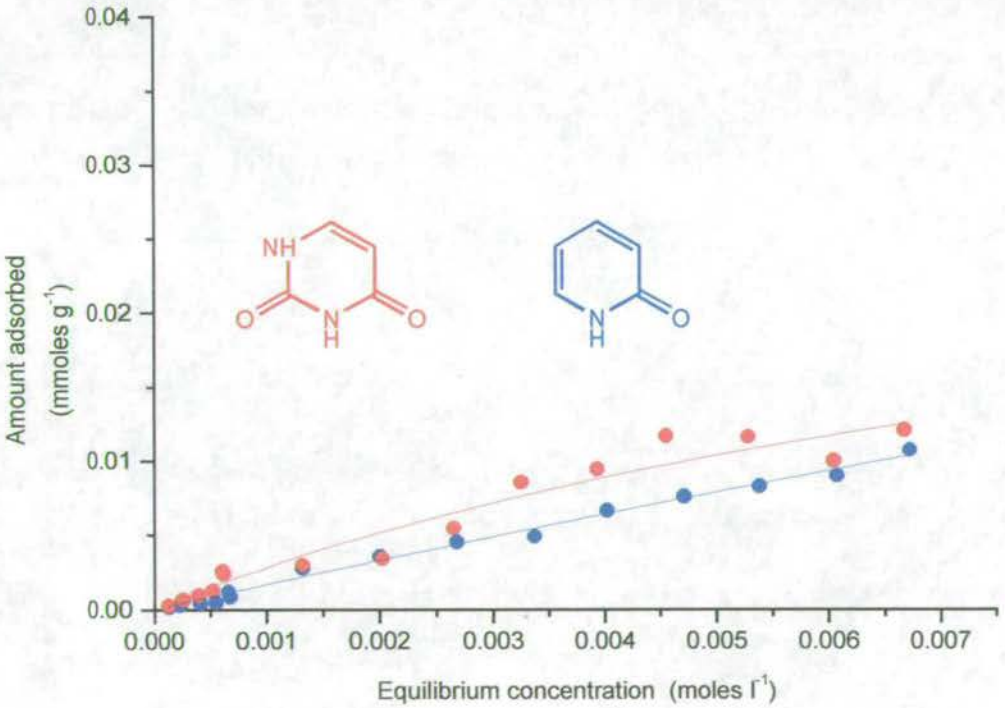

Figure 2.35: Adsorption isotherms for 2-hydroxypyridine (blue) and uracil (red).

The equilibrium adsorption constants (Table 2.4) obtained from curve fitting the isotherms are very low for both compounds, with uracil slightly better than 2-

hydroxypyridine, indicating that they do not bind strongly to $Al(OH)_3$. The figures however are not very useful in this case as neither isotherm conforms well to the Langmuir adsorption model, as shown by the large standard deviations. This is due to the scattering of the points in the uracil plot and the unusually linear nature of the curve in the 2-hydroxypyridine graph. In particular, while the monolayer coverage (Table 2.4) gives a reasonable value for the area occupied on the surface by a single molecule of uracil of 39(13) $Å^2$ $molecule^{-1}$, the value of 12(10) $Å^2$ $molecule^{-1}$ obtained for 2-hydroxypyridine is far too small and can be ignored. These figures are calculated from the surface area of the $Al(OH)_3$ which is known[50] to be 7 m^2 g^{-1}. It should be noted that given the very weak nature of the binding it is unlikely that monolayer coverage can be attained by either of these two compounds, even if the experiments were to be performed at much higher concentrations.

Qualitative information can be obtained from the shape of the isotherm, in particular in the low concentration region where the slope is proportional to the binding strength. It is obvious from the graphs that while, as a result of its extra functional group, uracil is better than 2-hydroxypyridine, neither can be considered a good surface ligand. From these results it can be inferred that nitrogen donor sets and soft sulfur donor sets would be even less favourable at binding to aluminium. Indeed preliminary isotherm studies of the nitrogen donors 6-methyl- and 6-phenyl-2,4-diamino-1,3,5-triazine gave graphs which scattered about zero, indicating that virtually no binding of the ligands was taking place.

Compound	Amount of ligand adsorbed at monolayer coverage (n_M) 10^5 [mol g^{-1}]	Equilibrium adsorption constant (K) [L mol^{-1}]
2-hydroxypyridine	10(8)	20 (10)
uracil	3(1)	100 (50)

Table 2.4: Adsorption isotherm data (standard deviations in parenthesis).

2.5 Conclusions.

Several novel functionalised 1,3,5-triazine ligands were synthesised, however this class of compounds were found to be poor candidates as surface ligands for aluminium oxide surfaces, due both to the instability of the ligands and their low binding strength to $Al(OH)_3$, as demonstrated in the isotherm experiments by the model compounds, 2-hydroxypyridine and uracil. As these compounds contain theoretically the best functional group sets for binding to aluminium, it can be assumed that other donor sets containing nitrogen and/or sulfur would be inferior.

The reaction chemistry of the sulfur substituted triazines, 6-(diethylamine)-1,3,5-triazine-2,4-thione and 6-(diethylamine)-1,3,5-triazine-2-thione-4-one with the 1st row transition metals nickel and cobalt was found to be more complicated than anticipated, with the formation of mono- and polynuclear complexes containing novel polydentate ligands formed *in situ*.

2.6 Experimental.

2.6.1 Chemicals and Instrumentation.

All reagents were used as obtained from Aldrich, Acros or Lancaster. Solvents were used as received. High surface area "superfine $Al(OH)_3$" was supplied by Alcan. Water was distilled before use.

Analytical data were obtained on a Perkin-Elmer 2400 Elemental analyser by the University of Edinburgh Microanalytical Service.

Melting points were determined using a Gallenkamp melting point apparatus and are uncorrected.

^{1}H and ^{13}C NMR were obtained using Bruker WP200 and AC250 spectrometers at ambient temperature. Chemical shifts (δ) are reported in parts per million (ppm) relative to residual solvent protons as internal standards.

Electron impact mass spectrometry (EIMS) was carried out on a Kratos MS50TC spectrometer. Fast atom bombardment mass spectrometry (FABMS) was carried out using a Kratos MS50TC spectrometer a 3-nitrobenzyl alcohol (NOBA) or thioglycerol matrix.

The infra-red spectra were obtained as potassium bromide discs using a Perkin Elmer Paragon 1000 FT-IR spectrometer.

Electronic spectra were measured on an ATI UNICAM UV/vis spectrometer with 1cm path length quartz cuvettes.

Curve fitting were performed using the programs Origin 5.0 © Microcal Software Inc and SigmaPlot 2000 (demo version) © 1986-2000 SPSS Inc.

With the exception of $[Co_6NaO(OStaH)_7\{S(Ota)_2\}_2(O_2CPh)_2(H_2O)_2]$ crystal data for all compounds were collected on a Stoe Stadi-4 diffractometer equipped with an Oxford Cryosystems low-temperature device. Data for $[Co_6NaO(OStaH)_7\{S(Ota)_2\}_2(O_2CPh)_2(H_2O)_2]$ were collected by Dr Simon Coles (EPSRC National Crytallographic Service, The University of Southampton), on a Nonius Kappa-CCD diffractometer. Full listings of atomic positions and thermal parameters are provided electronically on the CD accompanying this thesis.

Conductivity measurements were carried out by Dr N. Robertson at Imperial College, London.

2.6.2 Synthesis.

6-(*n*-Propylamino)-2,4,-dichloro-1,3,5-triazine.

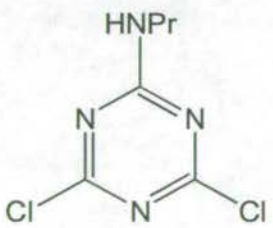

A solution of cyanuric chloride (28.7 g, 155.9 mmol) in hot acetone (100 ml) was poured onto a well stirred solution of ice water (100 ml) to produce a fine slurry. A solution of propylamine (15 ml, 157.5 mmol) and distilled water (50 ml) was added dropwise, maintaining the temperature of the suspension at 0-5 °C and the pH

at 6-7. The suspension was filtered and the precipitate washed with acetone. The product was dried in a vacuum desiccator to give a white powder (23.9 g, 74 %).

EIMS *m/z* 207 (L); IR (cm^{-1}, KBr disc) ν 3263s (NH), 2977s & 2935m (CH), 2874m, 1629s (C=N), 1514s, 1460s, 1435s, 1409s, 1349m, 1323s, 1235s, 1183s, 1140m, 1098m, 986w, 940w, 876w, 854s, 795s, 649w, 571w. Due to decomposition problems with this compound no further analysis was carried out.

6-(Diethylamino)-2,4-dichloro-1,3,5-triazine.

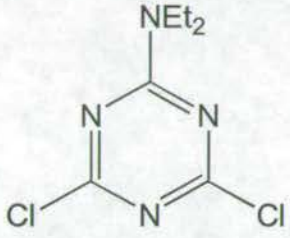

A solution of cyanuric chloride (30.6 g, 165.9 mmol) in hot acetone (100 ml) was poured onto a well-stirred solution of ice water (100 ml) to produce a fine slurry. The suspension was cooled in an ice bath to ~0 °C. Diethylamine (18.5 ml, 166.7 mmol) in a K_2CO_3 solution (165 ml of a 1M solution, 165 mmol) was added dropwise, maintaining the temperature of the suspension between 0 and 5°C. The suspension was then stirred at 0 – 5 °C for a further hour before it was neutralised with 1M HCl. The suspension was filtered and the precipitate washed with cold distilled water then cold ethanol. The product was dried under vacuum to give a white powder (24.1 g, 66 %).

m.p. 77-79 °C (lit.[3] 78-79 °C); (Found C, 38.4; H, 4.7; N, 25.5 %; $C_7H_{10}N_4Cl_2$ requires C, 38.0; H, 4.5; N, 25.3 %); ^{1}H NMR ($CDCl_3$, 200MHz): δ 3.61 (q, 4H, 2 x CH_2), 1.20 (t, 6H, 2 x CH_3); ^{13}C NMR ($CDCl_3$, 63MHz) δ 169.73 (2 x C-Cl), 163.70 (C-N), 42.36 (2 x CH_2), 12.44 (2 x CH_3); EIMS m/z 220 (L), 205 (L-CH_3), 193 (L-CH_2CH_3); IR (cm^{-1}, KBr disc) ν 2986m & 2953m & 2935m (CH), 2875m, 1586s (C=N), 1563s, 1475s, 1434s, 1377m, 1348s, 1327s, 1228s, 1156s, 1092w, 1076m, 1040m, 981w, 944w, 848m, 834m, 793s, 668w, 594w, 556w, 502w. Crystals suitable for X-ray analysis were grown by slow evaporation of the ethanol filtrate.

6-(Diethylamino)-4-chloro-1,3,5-triazine-2-one.

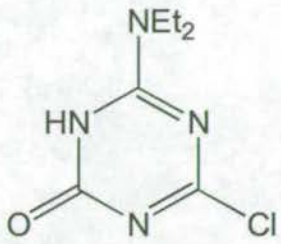

6-(Diethylamino)-2,4-dichloro-1,3,5-triazine (15.1 g, 62.3 mmol) was added to a solution of KOH (65 ml of a 2M solution, 130 mmol) in distilled water (80 ml). The suspension was heated under reflux for 1 hour, then cooled to room temperature and filtered to remove unreacted starting material. The filtrate was acidified with 1M HCl and the white precipitate filtered. The product was then dried under vacuum to give a white powder (11.3 g, 89 %).

m.p. 162-163 °C; (Found: C, 41.4; H, 5.5; N, 27.6 %; $C_7H_{11}N_4OCl$ requires C, 41.5; H, 5.4; N, 27.7 %); ^{1}H NMR (d_6-DMSO, 200MHz) δ 11.54 (s, 1H, NH), 11.13 (s, 1H, NH), 3.53 (dq, 4H, 2 x CH_2), 1.09 (dt, 6H, 2 x CH_3); ^{13}C NMR ($CDCl_3$, 63MHz) 158.72 (1C) and 158.25 (2C, overlapping C=O, C-Cl, C-N), 43.20 (CH_2), 42.26 (CH_2), 12.95 (CH_3), 12.44 (CH_3); EIMS *m/z* 202 (L), 187 (L-CH_3), 173 (L-CH_2CH_3), 167 (L-Cl); IR (cm^{-1}, KBr disc) ν 3116m (NH), 3030m, 2978s & 2943m & 2925m (CH), 1687s (C=O), 1603s (C=N), 1537s, 1492s, 1458s, 1444s, 1412s, 1382m, 1361s, 1325s, 1268s, 1184s, 1088m, 1070w, 1002s, 975s, 937w, 845w, 819w, 786m, 735w, 638w, 609w, 559w, 496w.

6-(Diethylamino)-1,3,5-triazine-2-thione-4-one (H_2OSta).

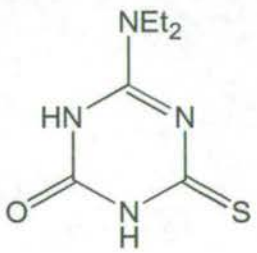

6-(Diethylamino)-4-chloro-1,3,5-triazine-2-one (10.0 g, 49.5 mmol) was added to an aqueous solution of NaSH (50 ml of a 2M solution, 100 mmol). The suspension was heated under reflux for two hours, then cooled to room temperature and the product filtered. The yield of crude product was 8.4 g. This was recrystallised twice from methanol, then dried under vacuum to give a white crystalline product (4.0 g, 41 %).

m.p. 246-248 °C (decomposition); (Found: C, 41.7; H, 6.0; N, 27.7 %; $C_7H_{12}N_4OS$ requires C, 42.0; H, 6.0; N, 28.0 %); ^{1}H NMR (d_6-DMSO, 200MHz) δ 11.76 (s, 1H, NH), 11.44 (s, 1H, NH), 3.5 (broad m, 4H, 2 x CH_2), 1.09 (t, 6H, 2 x CH_3); ^{13}C NMR (d_6-DMSO, 63MHz) δ 183.6 (C=S), 151.82 and 149.36 (C-N and C=O), 42.17 (2 x CH_2), 13.04 (2 x CH_3); EIMS *m/z* 200 (L); IR (cm^{-1}, KBr disc) ν 3072m, 3014m & 2997m & 2930m (CH), 1724s (C=O), 1610s (C=N), 1515s, 1400m, 1362m, 1262m, 1153s (C=S), 1092w, 1010w, 816w, 718w, 588w, 523w, 492w, 470w. Crystals suitable for X-ray analysis were grown by slow evaporation of a methanol solution.

6-(Diethylamino)-1,3,5-triazine-2,4-dithione (H_2S_2ta).

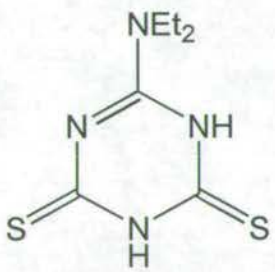

6-(Diethylamino)-2,4-dichloro-1,3,5-triazine (3.0 g, 13.6 mmol) was added to an aqueous solution of NaSH (55 ml of a 1M solution, 55 mmol). The suspension was heated under reflux overnight, then cooled to room temperature, and filtered to remove unreacted starting material. The filtrate was acidified with 1M HCl and the precipitate filtered. The yield of crude product was 2.6 g. This was recrystallised from ethanol, then dried under vacuum to give a white crystalline product (1.3 g, 45 %).

m.p. 240-242 °C (decomposition); (Found: C, 38.8; H, 5.6; N, 25.9 %; $C_7H_{12}N_4S_2$ requires C, 38.9; H, 5.6; N, 25.9 %); ^{1}H NMR (d_6-DMSO, 200MHz) δ 12.82 (s, 2H - very broad, NH), 3.57 (q, 4H, 2 x CH_2), 1.10 (t, 6H, 2 x CH_3); ^{13}C NMR (d_6-DMSO, 63MHz) δ 177.95 (2 x C=S), 148.71 (C-N), 42.43 (2 x CH_2), 13.04 (2 x CH_3); EIMS *m/z* 216 (L), 201 (L-CH_3), 187 (L-CH_2CH_3); IR (cm^{-1}, KBr disc) ν 3097m, 3055m, 2968m & 2905m (CH), 1601s (C=N), 1540s, 1504s, 1482s, 1435s, 1382m, 1359m, 1270m, 1210m, 1197m, 1166w, 1140s (C=S), 1098w, 1080m, 1047w, 985w, 937w, 887m, 832w, 792w, 776w, 738m, 691w, 652w. Crystals suitable for X-ray analysis were grown by slow evaporation of an ethanol solution.

6-(Diethylamino)-1,3,5-triazine-2,4-dione.

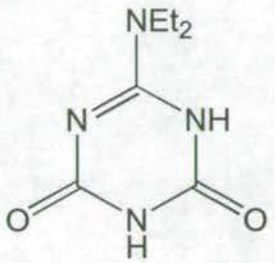

6-(Diethylamino)-2,4-dichloro-1,3,5-triazine (4.07 g, 18.4 mmol) was added to an aqueous solution of NaOH (37 ml of a 2M solution, 74 mmol). The suspension was heated under reflux for one hour until all starting material had dissolved, then for a further six hours to allow the reaction to go to completion. The solution was cooled to room temperature and acidified with 1M HCl. The solvent was removed on a rotary evaporator to give a white solid which was extracted with ethanol, filtered and the solvent removed on a rotary evaporator. The product was dried under vacuum to give a white solid (1.76 g).

^{1}H NMR (D_2O, 200MHz) δ 3.58 (q, 4H, 2 x CH_2), δ 1.21 (t, 6H, 2 x CH_3); ^{13}C NMR (D_2O, 63MHz) δ 150.79 (C-N), δ 150.58 (2 x C=O), δ 44.83 (2 x CH_2), 12.86 (2 x CH_3); EIMS *m/z* 184(L); IR (cm^{-1}, KBr disc) ν 3186m, 2974m(CH), 1728s (C=O), 1692s (C=O), 1664s, 1581s (C=N), 1509w, 1458w, 1388s, 1360m,

1296m, 1088w, 1049w, 973w, 779m, 720w, 637w, 550m, 451w. Crystals suitable for X-ray analysis were grown from a THF solution.

[Ni{(Sta)S(S_2ta)}].

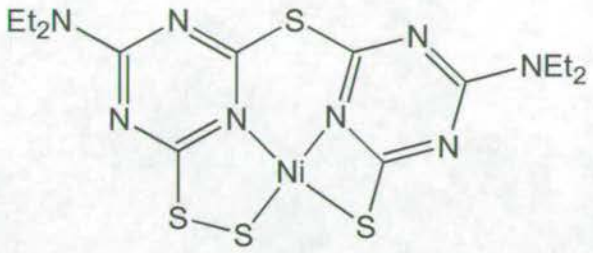

6-(Diethylamino)-1,3,5-triazine-2,4-dithione was deprotonated by reaction with one equivalent of Na(OMe) in methanol, followed by evaporation to dryness. This sodium salt (1.02 g, 4.2 mmol) was reacted with hydrated nickel chloride (0.50 g, 2.1 mmol) in the presence of sodium pivalate (0.52 g, 4.2 mmol) in MeOH (20 ml). The reaction was evaporated to dryness, and the resulting black powder redissolved in MeCN to give a dark red solution. Upon standing for several weeks, green/yellow needles formed (0.10 g, 10 %).

m.p. 282-284 °C (decomposition); (Found: C, 34.5; H, 3.9; N, 22.9 %; $C_{14}H_{20}N_8NiS_4$ requires C, 34.5; H, 4.1; N, 23.0 %); ^{1}H NMR ($CDCl_3$, 200MHz); δ 3.59-3.44 (m, 8H, 4 x CH_2), δ 1.17-1.10 (m, 12H, 4 x CH_3) ^{13}C NMR ($CDCl_3$, 63MHz) δ 196.09 (1C), δ 186.19 (1C), δ 172.86 (1C), δ 165.70 (1C), δ 159.31 (1C), δ 155.17 (1C), δ 42.31 (CH_2), δ 42.21 (CH_2), δ 42.13 (CH_2), δ 41.99 (CH_2), δ 12.78 (CH_3), δ 12.71 (CH_3), δ 12.60 (2 x CH_3); FABMS *m/z* 487 (L); IR (cm^{-1}, KBr disc) ν 2974w & 2930w (CH), 2868w, 1560s (C=N), 1533s, 1482s, 1456s, 1442s, 1429s, 1379s, 1360s, 1333m, 1310m, 1273m, 1219m, 1205m, 1172m, 1159m (C-S), 1097w, 1079m, 1070m, 1057m, 1019w, 949w, 872w, 820w, 778m, 770s, 592w, 576w, 535w. Crystals suitable for X-ray analysis were grown by redissolving these crystals in CH_2Cl_2 and layering the solution with hexane.

$[Co_6NaO(OStaH)_7\{S(Ota)_2\}_2(O_2CPh)_2(H_2O)_2]$ and $[Co(OStaH)_3]$.

6-(Diethylamino)-1,3,5-triazine-2-thione-4-one was deprotonated by reaction with one equivalent of Na(OMe) in methanol, followed by evaporation to dryness. This sodium salt (1.02 g, 4.6 mmol) was reacted with cobalt(II) chloride (0.3 g, 2.3 mmol) and $Na(O_2CPh)$ (0.67 g, 4.6 mmol) in MeOH (50 ml), followed by evaporation to dryness and recrystallisation from MeCN. Crystals of $[Co_6NaO(OStaH)_7\{S(Ota)_2\}_2(O_2CPh)_2(H_2O)_2]$ suitable for X-ray diffraction studies grew from MeCN after a period of two weeks (5 %). The mother liquor was allowed to stand, and after a further period of nine months, green crystals of $[Co(OStaH)_3]$ formed in very low yield.

2-Chloro-4,6-dihydroxy-1,3,5-triazine-(Na salt).$2H_2O$.

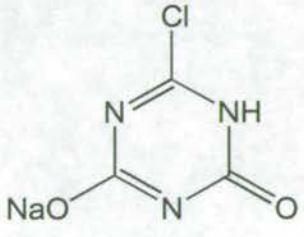

Cyanuric chloride (5.1 g, 27.5 mmol) was added in portions to a stirred, cooled (~10 °C) solution of NaOH (55 mmol of a 2M solution, 110 mmol) over a period of 30min. The reaction was stirred at 5-10 °C for one hour until almost all of the cyanuric chloride had dissolved. The solution was filtered to remove unreacted cyanuric chloride and left to stand at room temperature overnight. The pH was adjusted to 8 with 1M HCl and the solution cooled in an ice bath to give a white precipitate. The product was filtered off and dried under vacuum to give a white powder (2.7 g, 48 %).

m.p. >310 °C; (Found C, 17.4; H, 2.4; N, 20.1 %; $C_3H_5N_3O_4NaCl$ requires C, 17.5; H, 2.4; N, 20.4 %); EIMS *m/z* 147 (L); IR (cm^{-1}, KBr disc) ν 3414(br)s (OH), 2975m, 2825m, 1690s (C=O), 1527s, 1455s, 1414s, 1261s, 1007s, 857w, 795m, 668w, 607(br)m, 477s.

$[Na_6(HO_2ta)_6(H_2O_2ta)_6(CH_3OH)_8(H_2O)_2].2CH_3OH.H_2O$.

2-Chloro-4,6-dihydroxy-1,3,5-triazine-(Na salt).$2H_2O$ (1.0 g, 6.0 mmol) was dissolved in a solution of isopropylamine (7 ml, 82.2 mmol) and distilled water (5 ml). The solution was heated to 40 °C for two and a half hours, then cooled to room temperature. The solvent was removed on a rotary evaporator to give a white powder. Recrystallisation of this powder from methanol resulted in the formation of a small quantity (ca 20 % yield) of colourless rod-like crystals that on examination by X-ray diffraction were found to be $[Na_6(HO_2ta)_6(H_2O_2ta)_6(CH_3OH)_8(H_2O)_2].2CH_3OH.H_2O$.

(Found C, 36.6; H, 5.5; N, 27.5 %; $C_{82}H_{160}N_{48}O_{37}Na_6$ requires C: 38.6, H: 6.3, N: 26.4 %); IR (cm^{-1}, KBr disc) ν 3291m (NH), 2979s CH), 1734s (C=O), 1674s (C=O), 1635s, 1604s (C=N), 1570s, 1501s, 1458s, 1368s, 1305m, 1256w, 1179w, 1115w, 1070w, 981w, 940w, 852w, 801m, 748w, 668m, 576w, 546m, 464m.

6-(Diethylamino)-4-methoxy-1,3,5-triazine-2-one.

Aluminium nitrate nonahydrate (0.15 g, 0.4 mmol) and 6-(diethylamino)-4-chloro-1,3,5-triazine-2-one (0.24 g, 1.2 mmol) were dissolved in methanol/water (50 ml 10:1). NaOH (1.3 ml of a 1M solution, 1.3 mmol) was added slowly. The solution turned cloudy, then became clear after ~ two days. Colourless crystals suitable for X-ray analysis formed after two weeks on slow evaporation of the reaction solution (0.11 g, 46 %).

m.p. 181-183 °C; (Found C, 47.5; H, 7.2; N, 27.8 %; $C_8H_{14}N_4O_2$ requires C: 48.5, H: 7.1, N: 28.3 %); ^1H NMR ($CDCl_3$, 200MHz); δ 3.92 (s, 3H, OCH_3), δ 3.60 (broad m, 4H, 2 x CH_2), δ 1.18 (t, 6H, 2 x CH_3); ^{13}C NMR (D_2O, 63MHz) δ 162.94 (1C) and δ 159.98 (2C, overlapping C=O, C-OCH_3 and C-N), δ 54.54 (OCH_3), δ

42.30 (CH_2), δ 42.01 (CH_2), δ 13.14 (CH_3), δ 12.81 (CH_3); FABMS *m/z* 199 (LH); IR (cm^{-1}, KBr disc) ν 3468s (OH), 2979s & 2970s & 2961s & 2944s (CH), 1662s (C=O), 1625s (C=N), 1567s, 1515s, 1445s, 1421s, 1378s, 1335s, 1320s, 1271m (COC), 1218m, 1098m, 1086m, 1003w, 982w, 940m, 919m, 847w, 796s, 758w, 636s, 752m, 534w, 496m.

2.6.3 Adsorption isotherm measurements.

Preweighed quantities of $Al(OH)_3$ (0.40 g) in polycarbonate centrifuge tubes were stirred with the desired concentration of ligand in methanol/water (10 ml, 95:5 v/v) for two hours at 25 °C. The suspensions were centrifuged and flittered, and the supernatant diluted if necessary, for absorbance measurement by UV spectrometry. The measured absorbance was related to the concentration of the ligand remaining in solution by reference to calibration curves. The amount of ligand adsorbed was then calculated from the difference between initial and final concentration. From this plots of amount of ligand adsorbed versus equilibrium concentration were obtained.

2.7 References.

1 J. M. E. Quirke, *Comprehensive Heterocyclic Chemistry*,1984 **2**, 457.

2 D. Bartholemew, *Comprehensive Heterocyclic Chemistry*, 1996, **6**, 575.

3 J. T. Thurston, J. R. Dudley, D. W. Kaiser, I. Hechenbleikner, F. C. Schaefer and D. Holm-Hansen. *J. Am. Chem Soc.*, 1951, **73**, 7, 2981.

4 W. M. Pearlman and C. K. Banks. *J. Am. Chem Soc.*, 1948, **70**, 3726.

5 W. F. Beech. *J. Chem Soc. (C).* 1967, 466.

6 S. Parsons and R. E. P. Winpenny. *Acc. Chem. Res.* 1997, **30**, 89 and references within.

7 M. Mori and Y. Nakamura. *J. Polymer Science-Polymer Letters*, 1983, **21**, 889.

8 K. Kojima, Y. Kadoma and Y. Imai. *J. Dent. Mater.*, 1987, **6**, 702.

9 S. Cinta, T. Illiescu, M. Venter and O. Cozar. *Journal of Molecular Structure*, 1997, **410-411**, 189.

[10] A. Mizuno, Y. Toda, M. Itoh, K. Kojima and Y. Kadoma, *Journal of Molecular Structure*, 1998, **441**, 149.

[11] V. M. Agre, T. F. Sisoeva, V. K. Trunov, M. Z. Gurevich and M. Z. Branzburg, *Koord. Khim.*, 1986, **12**, 122.

[12] L. R. Falvello, I. Pascual and M. Tomas, *Inorg. Chim. Acta*, 1995, **229**, 135.

[13] M. Z. Branzburg, T. F. Sisoeva, N. F. Shugal, N. M. Dyatlova, V. M. Agre and M. Z. Gurevich, *Koord. Khim.*, 1986, **12**, 1658.

[14] P. G. Slade, M. Raupach and E. W. Radoslovich, *Acta Crystallogr., Sect. B*, 1973, **29**, 279.

[15] L. R. Falvello, I. Pascual, M. Tomas and E. P. Urriolabeitia, *J. Am. Chem. Soc.*, 1997, **119**, 11894.

[16] S. Shi-Bao, C. Chang-Zhang, H. Xiao-Ying, G. Dong-Shou, L. Zhou-Bin and L. Ding, *Chinese J. Struct. Chem. (Jiegou Huaxue)*, 1996, **15**, 246.

[17] T. Palade and M. Nutiu, *Revista de Chimie (Bucharest)*, 1986, **37**, 80.

[18] R. D. Hart, B. W. Skelton and A. H. White, *Aust. J. Chem.*, 1992, **45**, 1927.

[19] P. Kopel, Z. Travnicek, R. Panchartkova and M. Biler, *Transition Met. Chem.*, 1999, **24**, 239.

[20] P. Kopel, Z. Travnicek, L. Kvitek, R. Panchartkova, M. Biler, J. Marek and M. Nadvornik, *Polyhedron*, 1999, **18**, 1779.

[21] K. Yamanari, Y. Kushi, M. Yamamoto, A. Fuyuhiro, S. Kaizaki, T. Kawamoto and Y. Kushi, *J. Chem. Soc, Dalton Trans.*, 1993, 3715.

[22] C. Chan, K. Cheung and C. Che, *Chem.Commun.*, 1996, 227.

[23] W. J. Hunks, M. C. Jennings and R. J. Puddephatt, *Inorg. Chem.*, 1999, **38**, 5930.

[24] B. Tzeng, C. Che and S. Peng, *Chem.Commun.*, 1997, 1771.

[25] S. G. Harris, University of Edinburgh, PhD thesis, 1999.

[26] R. A. Coxall, S. G. Harris, D. K. Henderson, S. Parsons, P. A. Tasker and R. E. P. Winpenny, *J. Chem. Soc., Dalton Trans.*, 2000, 2349.

[27] A. R. Katrizky, I. Ghiviriga, P. J. Steel and D. C. Oniciu, *J. Chem. Soc. Perkin Trans. 2*, 1996, 443.

[28] N. Dastagriri Reddy, A. J. Elias and A. Vij, *J. Chem Research (M)*, 1998, 2028.

[29] A. Talebian, A. Ghiorghis, C. F. Hammer, E. A. Murril and F. Pallis, *J.*

Heterocyclic Chem., 1992, **29**, 979.

30 V. R. Pedireddi, S. Chatterjee, A. Ranganathan and C. N. R. Rao, *J. Am. Chem. Soc.*, 1997, **119**, 10867.

31 A. Kvick, *Acta. Cryst., Sect. B,* 1976, **32**, 220.

32 R. E. P. Winpenny, *Comm. Inorg. Chem.*, 1999, **20**, 233.

33 D. Coucouvanis, P. R. Patil, M. G. Kanatzidis, B. Detering and N. C. Baenziger, *Inorg. Chem.*, 1985, **24**, 24.

34 M. Bonamico, G. Dessy, V. Fares and L. Scaramuzza, *J. Chem. Soc. A*, 1971, 3191.

35 J. P. Fackler Jr., J. A. Fetchin and D. C. Fries, *J. Am. Chem. Soc.*, 1972, **94**, 7323.

36 J. Piotraschke, P. Strauch, G. Zahn and E. Hoyer, *Z. Anorg. Allg. Chem.*, 1994, **620**, 505.

37 J. Piotraschke, P. Strauch, S. Abram and U. Abram, *Z. Anorg. Allg. Chem.*, 1994, **620**, 1659.

38 R. Munn, *Chemistry In Britain*, 1984, 518.

39 H. Kang, G. Ofori-Okai and J. Zubieta, *Inorg. Chim. Acta.*, 1991, **188**, 61.

40 E. C. Constable, C. A. Palmer and I. A. Tocher, *Inorg. Chim. Acta.*, 1990, **176**, 57.

41 P. Yu, B. Zhuang, L. Huang and B. Pan, *Acta Cryst C,* 1996, **52**, 630.

42 S. Horrobin. *J. Chem Soc.*, 1963, 4130.

43 H. Kataoka. *Chemical Abstracts*, 1966, **64**, 736.

44 H. Bock, H. Schodel, Z. Havlas and E. Herrmann, *Angew. Chem., Int. Ed. Engl.*, **34**,12, 1995, 1355.

45 E. K. Brechin, L.M. Gilby, R. O. Gould, S. G. Harris, S. Parsons and R. E. P. Winpenny, *J. Chem. Soc. Dalton Trans.*, 1998, 2657.

46 M. P. Hogerheide, S. N. Ringelberg, M. D. Janssen, J. Boersma, A. L. Spek and G. van Koten, *Inorg. Chem.*, **35**, 1996, 1195.

47 M. Kunert, E. Dinjus, M. Nauck and J. Sieler, *Chem. Ber.*, **130**, 1997, 1461.

48 U. M. Tripathi, A. Schier and H. Schnidbaur, *Z. Naturforsch., Tiel B*, 1998, **53**, 434.

49 A. W. Apblett, A. C. Warren and A. R. Barron, *Chem. Mater.*, 1992, **4**, 167.

[50] Surface area of $Al(OH)_3$ determined by Alcan for a particular batch of "superfine $Al(OH)_3$", S. Ingham, private communication, 1997.

Chapter 3:

Carboxylic Acids.

Contents.

3.1 Introduction.

3.1.1 Background.

Aluminium carboxylates are used in a wide variety of applications such as finishing agents for the water-proofing of cloth, mordants in the dyeing of textiles, pharmaceutical preparations (because of their antiseptic and astringent properties) and in the manufacture of cosmetics due to the gelling properties of some of the higher molecular weight aluminium carboxylates.[1]

The literature was surveyed to establish the modes of binding of carboxylate groups in both simple and polynuclear aluminium(III) complexes. The results are presented in sections 3.1.2 – 3.1.4 below.

3.1.2 Polynuclear Aluminium Carboxylate Complexes.

In comparison with iron(III) there are relatively few crystographically characterised aluminium(III) carboxylate compounds. Carboxylates are potentially capable of adopting a large number of different binding modes to aluminium, however only four are observed in the Cambridge Structural Database (CSD) (Figure 3.1). The surprising absence of a chelating mode is discussed further in section 3.2.

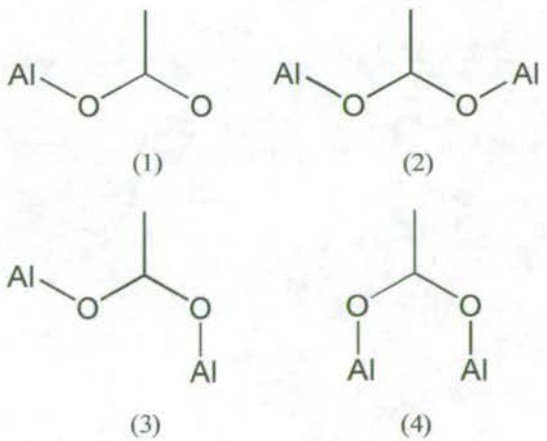

Figure 3.1: Binding modes observed for carboxylates with aluminium in the CSD.

A search of the CSD using the fragment [AlOC(C)O] gave seventy four hits. After removing hits arising from esters, sugars and mixed metal complexes this left forty five structurally characterised aluminium carboxylates, of which twenty five were monomeric species. Of the twenty remaining polynuclear complexes, there are eleven dimers, two trimers, two tetramers, one pentamer, two hexamers and two polymers. Thirteen of the polynuclear complexes are organometallic.

The optimal binding mode to an aluminium surface would be 1,3 bridging as this mode would maximise the number of donor/metal interactions and reduce the chance of the carboxylate sequestering aluminium into solution, thus degrading the surface. Twelve complexes contain carboxylate ligands which display this binding mode. Of these, six are interesting to us as they also contain a bridging oxide or hydroxide thus mimicking a mode of coordination which could readily occur at an aluminium oxide surface.

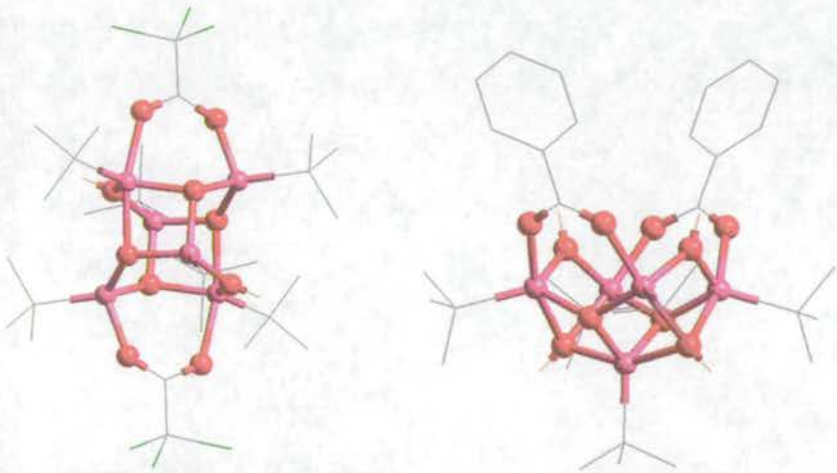

Figure 3.2: Crystal structure of $[(^t\text{Bu})_6\text{Al}_6(\mu_3\text{-O})_4(\mu\text{-OH})_2(\mu\text{-O}_2\text{CCCl}_3)_2]$ and $[\text{Al}_5(^t\text{Bu})_5(\mu_3\text{-O})_2(\mu_3\text{-OH})_2(\mu\text{-OH})_2(\mu\text{-O}_2\text{CPh})_2]$. Al-pink, O-red, C-grey, Cl-green, H-beige.

Two of these complexes have been synthesised by Barron *et al.* The hexanuclear compound $[(^t\text{Bu})_6\text{Al}_6(\mu_3\text{-O})_4(\mu\text{-OH})_2(\mu\text{-O}_2\text{CCCl}_3)_2]$ (Figure 3.2) was prepared[2] by reaction of $[(^t\text{Bu})\text{Al}(\mu_3\text{-O})]_6$ with trichloroacetic acid as a model for the interaction of $[\text{Pd(OAc)}_2\text{(dppp)}]$ (dppp = bis(diphenylphosphino)propane) with $[(^t\text{Bu})\text{Al}(\mu_3\text{-O})]_6$. This reaction is important in the palladium catalysed copolymerisation of carbon monoxide and ethylene to give polyketone polymers. The structure consists of an Al_6O_6 core with the trichloroacetate groups on opposite

sides of the cage, each bridging two aluminium atoms. The second pentanuclear compound $[Al_5(^tBu)_5(\mu_3\text{-}O)_2(\mu_3\text{-}OH)_2(\mu\text{-}OH)_2(\mu\text{-}O_2CPh)_2]$ (Figure 3.2) was made[3] as a model for the interaction of carboxylic acids with boehmite and its structure can be considered as an inverted square pyramid of aluminium atoms. A comparison of the core structure of $[Al_5(^tBu)_5(\mu_3\text{-}O)_2(\mu_3\text{-}OH)_2(\mu\text{-}OH)_2(\mu\text{-}O_2CPh)_2]$ with a fragment of the boehmite structure (Figure 3.3) shows their similarity.

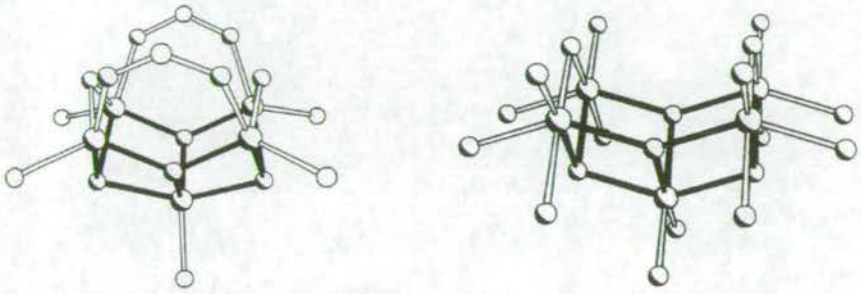

Figure 3.3: Diagram of the core structure of $[Al_5(^tBu)_5(\mu_3\text{-}O)_2(\mu_3\text{-}OH)_2(\mu\text{-}OH)_2(\mu\text{-}O_2CPh)_2]$ and a fragment of boehmite.[3]

The presence of hydroxide ions in the structure was explained by trace quantities of water remaining in the benzoic acid used.

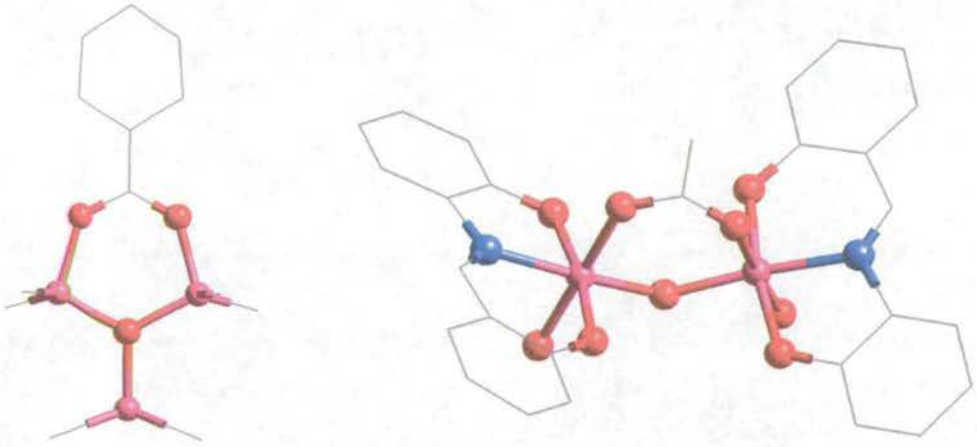

Figure 3.4: Crystal structure of $[PhCO_2(AlMe_2)_2OAlMe_3]^-$ and $[\{(H_2O)(L)Al(\mu\text{-}MeCO_2)\}_2(\mu\text{-}OH)]$. Al-pink, O-red, N-blue, C-grey.

Two examples[4,5] of aluminium carboxylates feature as components of clathrate systems $[PhCO_2(AlMe_2)_2OAlMe_3]^-$ (Figure 3.4) and $[\{(H_2O)(L)Al(\mu\text{-}MeCO_2)\}_2(\mu\text{-}OH)]$ (Figure 3.4), where H_2L = *N*-salicylidene-*o*-aminophenol.

Clathrates are crystalline inclusion compounds with host structures comprised of separate molecules, linked together by hydrogen bonds to form cavities. The cavities are connected by channels and can contain small guest molecules.[6]

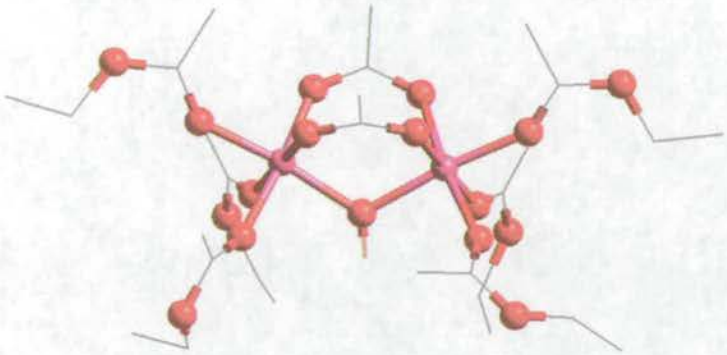

Figure 3.5: Crystal structure of $[(CH_3CO_2C_2H_5)_3Al(\mu\text{-}CH_3CO_2)_2(\mu\text{-}OH)Al(CH_3CO_2C_2H_5)_3]^{3+}$. Al-pink, O-red, C-grey, H-beige.

The complex $[(CH_3CO_2C_2H_5)_3Al(\mu\text{-}CH_3CO_2)_2(\mu\text{-}OH)Al(CH_3CO_2C_2H_5)_3][AlCl_4]_3$ (Figure 3.5) was the unexpected result of a study[7] into the interaction of ester molecules with components of the Ziegler-Natta catalyst system. The formation of acetate and the presence of hydroxide in the product are attributed to the influence of moisture leaking slowly into the crystallisation vessel. This compound has been proposed as a possible analogue to the binuclear iron centre in proteins such as haemerythrin.[8]

The final example from the CSD search is the heterobimetallic complex $[Pb_2Al_5(O)_2(O^iPr)_{12}(OAc)_3]$[9] (Figure 3.6).

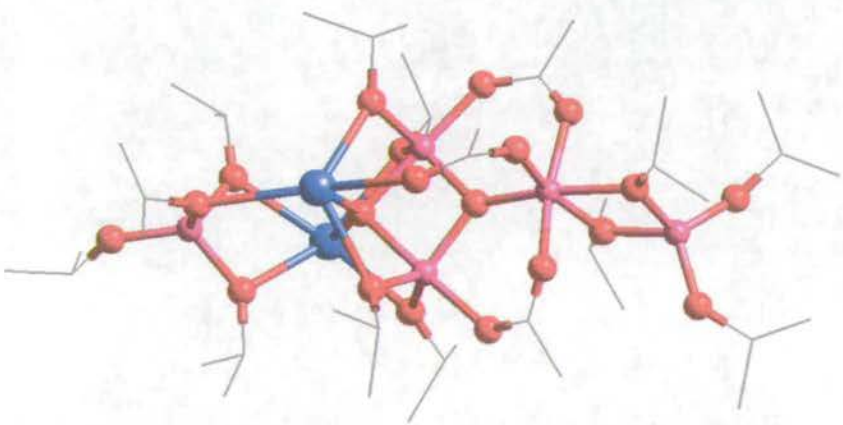

Figure 3.6: Crystal structure of $[Pb_2Al_5(O)_2(O^iPr)_{12}(OAc)_3]$. Al-pink, O-red, Pb-blue, C-grey.

One important aluminium carboxylate complex which has not been placed on the CSD is the tridecanuclear $[Al_{13}(\mu_3\text{-}OH)_6(\mu_2\text{-}OH)_{12}(heidi)_6(H_2O)_6]^{3+}$ (Figure 3.7) ($H_3heidi = N(CH_2CO_2H)_2(CH_2CH_2OH)$) synthesised by Powell *et al.* [10] This is the largest aluminium hydroxide cluster containing organic ligands. The cluster has a central octahedral aluminium atom surrounded by a ring of six aluminium atoms. The peripheral six aluminium atoms are involved in an unusual binding mode where an "AlO_2" unit bridges two core aluminium atoms. This type of bridging mode is also observed[11,12] for $[Al_3(H_{-1}Cit)_3(OH)(H_2O)](NO_3)_3$, a trinuclear aluminium citrate complex and the related oxy-hydroxide cluster $[Al_{13}(OH)_{24}(H_2O)_{24}]Cl_{15}.13H_2O$ which shares the same core structure. All of the carboxyate functionalities in the complex are monodentate while the alkoxides bridge two aluminium atoms.

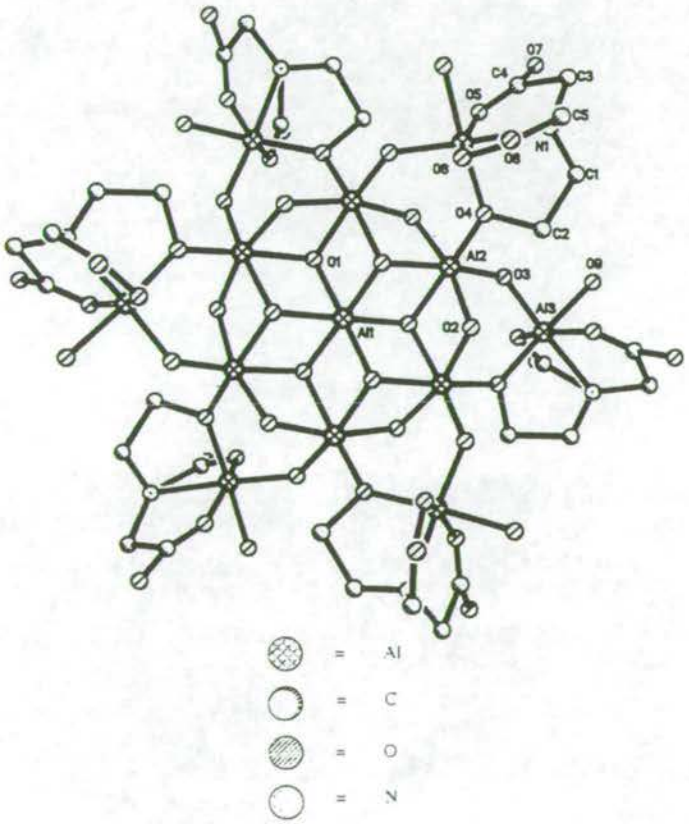

Figure 3.7: Crystal structure of $[Al_{13}(\mu_3\text{-}OH)_6(\mu_2\text{-}OH)_{12}(heidi)_6(H_2O)_6]^{3+}$.[10]

3.1.3 Carboxylic Acids as Surface Ligands.

Previous studies[13] on the adsorption of carboxylic acids onto metal oxide surfaces include the use of electrochemical techniques to investigate the abilities of a series of straight chain mono and α,ω-dicarboxylic acids to inhibit corrosion of mild steel, copper and aluminium. The work showed that there was a strong dependence of corrosion inhibition with chain length. The optimal chain length for corrosion inhibition of mild steel was found to be ($C_nH_{2n+1}CO_2^-$) where ($6 \leq n \leq 10$) for monocarboxylates and ($^-O_2C(CH_2)_nCO_2^-$) where ($3 \leq n \leq 8$) for dicarboxylates. For copper n = 10 was found to be best for monocarboxylates and for dicarboxylates corrosion inhibition increased with increasing n. Aluminium was discovered to be similar to copper with "peak" inhibition occurring at n = 11 for monocarboxylates and inhibition increasing with increasing n for dicarboxylates.

Quartz crystal microbalance (QCM) techniques, electronic and electron loss spectroscopies in ultrahigh vacuum have been used[14] to study the adsorption of *n*-octanoic acid onto the native oxide surface of aluminium. Under these conditions the alkanoic acids adsorb weakly onto the native oxide surface, and it was found that treating the oxide surface first with a zirconium alkoxide provides for strong subsequent adsorption of the acid (Figure 3.8).

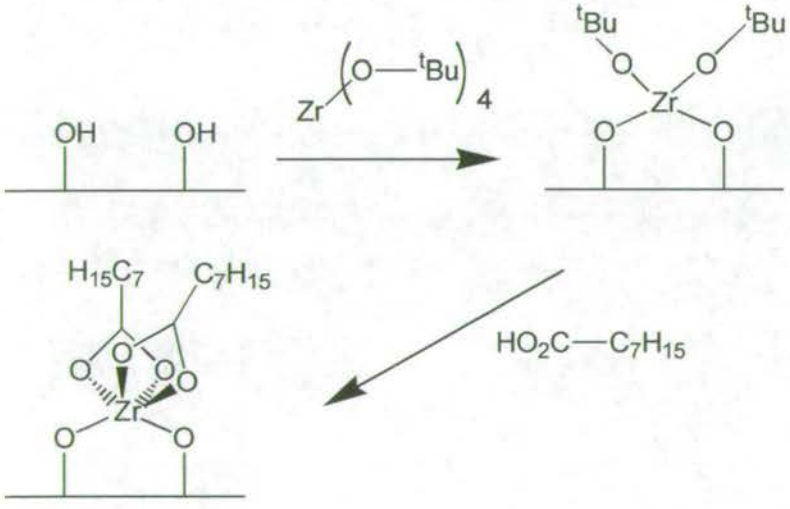

Figure 3.8: Adsorption of *n*-octanoic acid onto a Zr alkoxide-treated Al surface.

3.1.4 Irgacor-419, A Known Corrosion Inhibitor for Iron.

The compound 3-(4-methylbenzoyl)-propionic acid (Irgacor-419) produced by Ciba Speciality Chemicals is an effective corrosion inhibitor for mild steel when used in waterborne polymeric coatings. It is thought to bind to lightly oxidised iron surfaces in its deprotonated form, creating a passivating film. This barrier prevents aggressive ions from attacking the surface. Testing of this compound and its related derivatives (Figure 3.9) reveals[15] that the presence of both the methyl group in the *para* position of the aromatic ring and the carbonyl group give rise to a greater effectiveness as a corrosion inhibitor in protective coatings than compounds which lack the carbonyl functionality or with different types and positions of aromatic substituents.

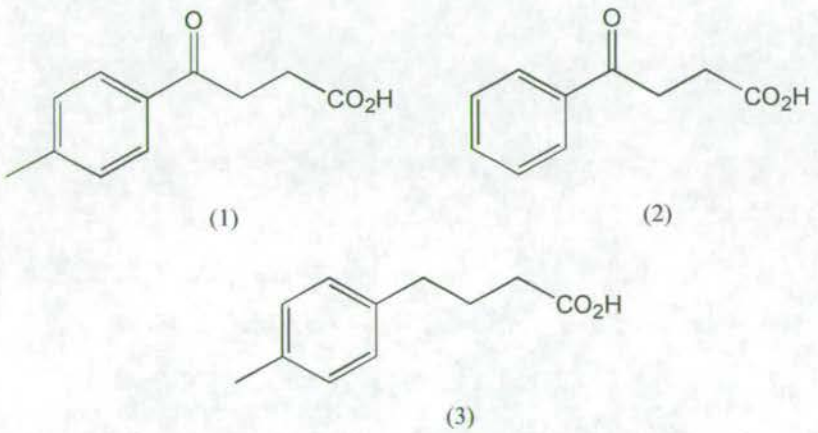

Figure 3.9: Structure of the ligands (1) 3-(4-methylbenzoyl)-propionic acid (Irg-419), (2) 3-benzoyl propionic acid (bpa), (3) 4-p-tolyl-butyric acid (Irg-78).

The "mode of action" of Irg-419 was investigated[16,17,18] at Edinburgh by Dr Steve Harris and Dr David Nation using a combination of adsorption isotherm, crystallographic and molecular modelling techniques.

The isotherms (Figure 3.10) on goethite indicate (Table 3.1) that Irg-419 and bpa have similar binding characteristics within experimental error, while Irg-78 has both a lower surface coverage and binding strength. This shows that while the carbonyl functionality has a dramatic effect on binding strength, the role the methyl group in surface passivation is more subtle.

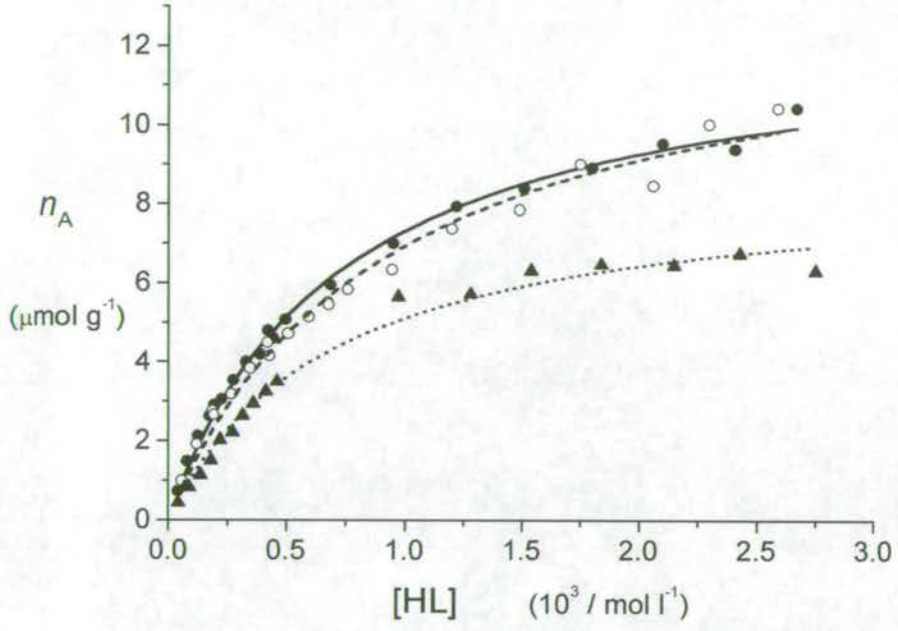

Figure 3.10: Adsorption isotherms for • Irg-419, ▲ Irg-78 and o bpa.

Compound	Amount of ligand adsorbed (n_M) 10^5 [mol g^{-1}]	Equilibrium adsorption constant (K) 10^{-3} [L mol^{-1}]
Irg-419	1.26(2)	1.4(1)
Bpa	1.32(5)	1.1(1)
Irg-78	0.87(4)	1.4(1)

Table 3.1: Adsorption isotherm data.

A polynuclear iron cage complex $[Fe_{11}(O)_6(OH)_6(Irg\text{-}419)_{15}]$ containing the Irg-419 ligand was synthesised via the trinuclear species $[Fe_3(O)(Irg\text{-}419)_6(H_2O)_3]$.(Irg-419)], and its structure (Figure 3.11) was determined by X-ray crystallography. The cluster contains fifteen Irg-419 ligands, all of which bind in a 1,3-bridging mode to two iron centres. Four of the ligands show an additional hydrogen bonding interaction between the carbonyl functionality and a bridging hydroxide of the cage. This suggests that the carbonyl in Irg-419 could enhance its performance as a corrosion inhibitor due to this ability to hydrogen bond to hydroxide groups on an oxidised metal surface, leading to stronger binding at the surface.

Analysis[18] of the structure shows that the four Irg-419 ligands which feature this hydrogen bond *via* their 3-carbonyl group show very similar coordination geometries and ligand conformation in the dinuclear units (Figure 3.12).

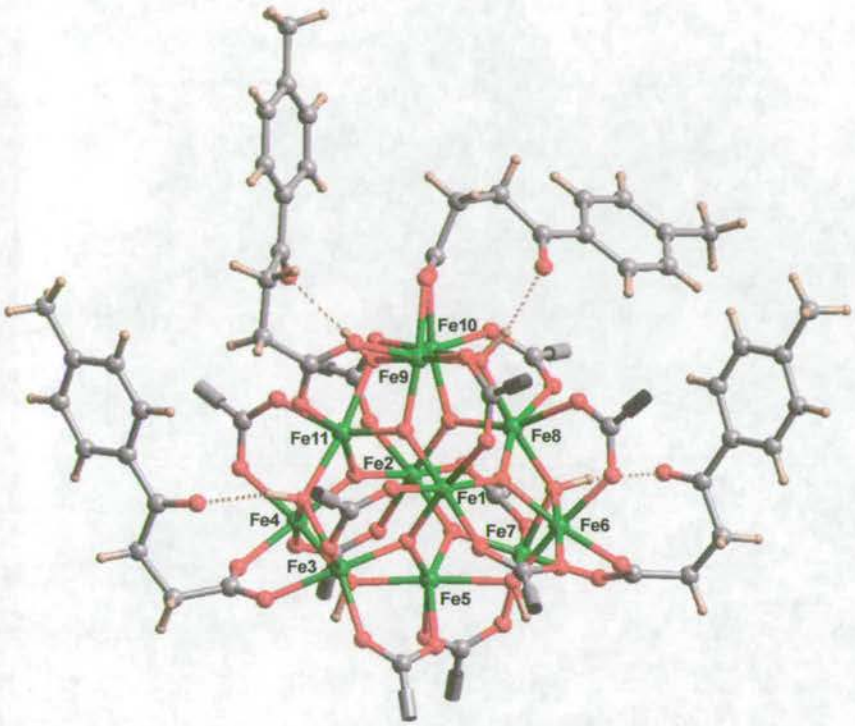

Figure 3.11: Crystal structure of $[Fe_{11}(O)_6(OH)_6(Irg\text{-}419)_{15}]$. The organic tail group of eleven of the Irg-419 ligands are excluded for clarity.

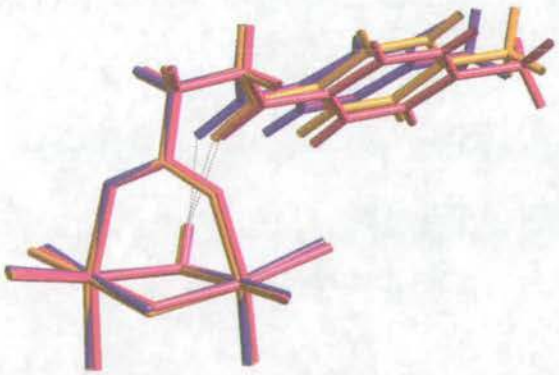

Figure 3.12: Conformation of Irg-419 observed in the hydrogen bonded units in $[Fe_{11}(O)_6(OH)_6(Irg\text{-}419)_{15}]$.

Using the 021 surface of lepidocrocite, a common form of iron oxide found in rust, an Irg-419 molecule can be attached (Figure 3.13) in a very similar configuration to that found in the model complex. When this orientation is used in a

computer generated monolayer (Figure 3.14), very good surface coverage is obtained with efficient packing (ca 50 $Å^2$ per Irg-419). This packing could provide a hydrophobic barrier to the ingress and egress of ionic species. The potential role of the *para*-methyl substituent also becomes clearer, as its removal creates gaps in the barrier through which ions can diffuse.

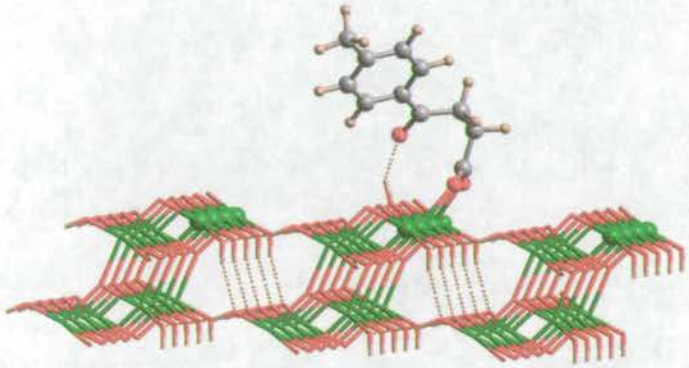

Figure 3.13: Binding of a single molecule of Irg-419 to the 021 surface of lepidocrocite.

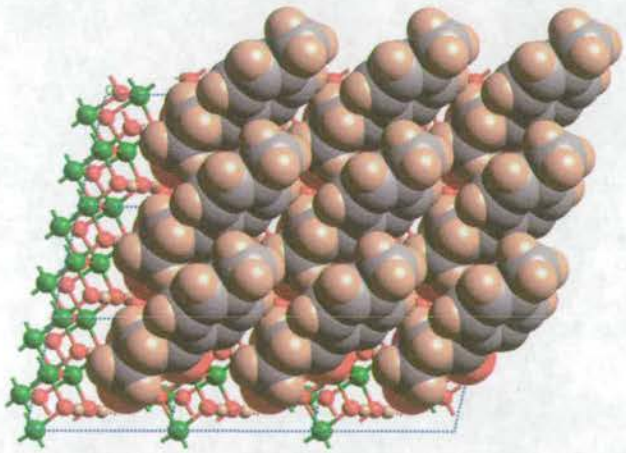

Figure 3.14: Packing of nine Irg-419 ligands on the 021 surface of lepidocrocite.

This strategy, a combination of synthesis of model complexes and molecular modelling, works well for proposing a mode of action of a surface modifier for iron. The work described in this chapter extends this approach in two directions. Firstly, we have attempted to make polynuclear aluminium cages as models for the interaction of carboxylates with aluminium surfaces. Secondly, we have examined the coordination chemistry of keto-carboxylates with other metals to see if the hydrogen bonding found with the iron clusters is a common motif in other metals.

3.2 Attempts to Synthesise Polynuclear Aluminium Carboxylate Complexes.

Several strategies were used in an attempt to prepare polynuclear carboxylate complexes with aluminium. It was hoped that such complexes could be used as models for the interaction of carboxylates at an aluminium oxide surface.

Mixing of carboxylic acids with simple aluminium salts such as chloride or nitrate in aqueous solution under a variety of conditions generally led to immediate precipitates or solutions which on slow evaporation gave uncharacterisable solids.

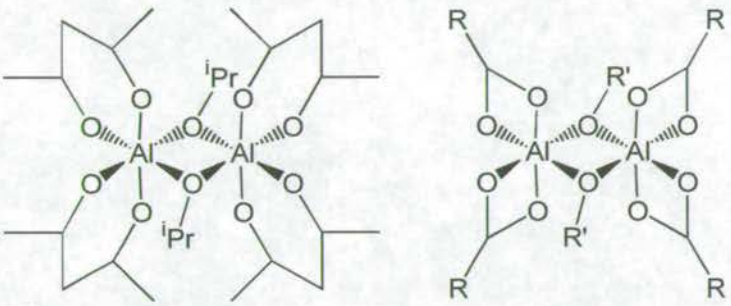

Figure 3.15: $[Al(acac)_2(O^iPr)]_2$ dimer and proposed structure of aluminium alkoxide/carboxylate dimers.

Aluminium alkoxides were reacted with a series of carboxylic acids in order to try to form dimers of the type $[Al(OR)(O_2CR')_2]_2$ similar to the mixed ligand acac/ isopropoxide dimers synthesised by Wengrovius *et al*[19] (Figure 3.15). The general reaction method is shown (Scheme 3.1) and a summary of the reactions carried out is given (Table 3.2). It was hoped that these compounds could be used as a starting point to build larger polynuclear complexes.

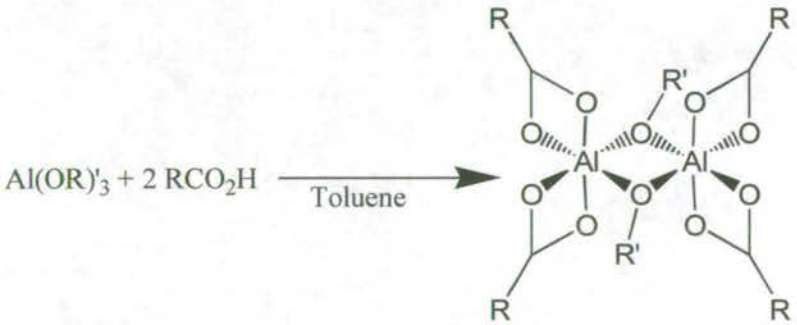

Scheme 3.1: General reaction scheme for the formation of aluminium alkoxide/carboxylate dimers.

Aluminium alkoxide	Carboxylic acid
Aluminium isopropoxide	benzoic acid trimethylacetic acid (tma) diphenylacetic acid (dpa) triphenylacetic acid (tpa) 3-benzoylpropionic acid (bpa)
Aluminium *t*-butoxide	benzoic acid trimethylacetic acid (tma) diphenylacetic acid (dpa) triphenylacetic acid (tpa)

Table 3.2: Combinations of aluminium alkoxides and carboxylic acids used in attempts to prepare dinuclear aluminium complexes.

Characterisation of the products obtained from these reactions proved difficult for a number of reasons. The complexes formed with benzoic acid and tma were completely insoluble in common organic solvents. Complexes formed using aluminium isopropoxide and dpa, tpa and bpa were shown by ^{1}H NMR to contain a 2:1 ratio of carboxylate to isopropoxide, consistent with the formula expected, however in all cases FAB mass spectrometry failed to give useful information on speciation. Elemental analysis proved similarly unhelpful in characterisation. In general the analysis showed the carbon and hydrogen content of the compound was lower than that required for compounds of formula $[Al(OR)(O_2CR')_2]_2$.

Much effort was put into crystallising the soluble complexes in the series. However, in general crystallisations led to powders, colourless films or gelatinous products. In particular the material resulting from the reaction of aluminium isopropoxide with dpa was capable of forming a thick gel in chloroform solution within two days inside a parafilm-sealed NMR tube.

Our inability to isolate crystalline dimeric carboxylate complexes is perhaps not surprising given that no examples of a carboxylate ligand chelating to aluminium can be found in the literature and a study[20] by Barron *et al* has indicated that this coordination mode may be very unfavourable as a result of steric strain. In his study of 1,3-diaryltriazeneido compounds, e.g. 1,3-diphenyltriazene (Figure 3.16) with

aluminium he observed that the N-N-N angle in a monoanionic triazenide ligand is reduced from ~112° to ~106°. He reasons that a similar chelate geometry would be expected for both the carboxylate and triazenide ligands. However the O-C-O bond angle in free acid is ~123° and therefore on coordination would be reduced by ~18°, imposing significant ring strain on the system. A search of the CSD found only two examples[21,22] of compounds containing an AlOCO chelating binding mode. Both compounds contain the N, N-diisopropylcarbamato ($HO_2CN^iPr_2$) ligand. The O-C-O chelate angles are ca 115° which is larger than that predicted by Barron *et al.*

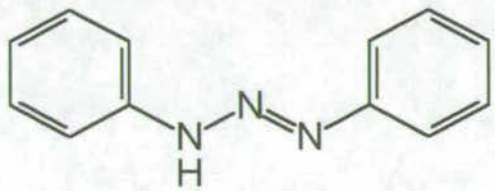

Figure 3.16: 1,3-diphenyltriazene.

One interesting observation obtained from the current work came from the reaction between aluminium *t*-butoxide and diphenylacetic acid (dpa). ^{1}H NMR clearly revealed the presence of isopropoxide in the product, with the ratio of isoproxide to *t*-butoxide in the NMR spectra being ~ 2:1. It is unclear how this reaction could have occurred and no explanation was actively sought.

There have been no structurally characterised aluminium(III) carboxylate μ_3-oxo-centred trinuclear complexes of the type shown (Figure 3.17). Indeed, evidence for the existence of such species is limited[23] with the most convincing evidence coming from acid-base titration studies in glacial acetic acid.[24] This is very different from iron(III) chemistry where there have been many such complexes identified and structurally characterised. Despite the lack of literature information on such trinuclear aluminium carboxylate complexes it was decided that their synthesis was worth attempting as metal carboxylates (Figure 3.17) have proved to be very successful as starting materials in the synthesis of polynuclear cages, for example $[Fe_{11}(O)_6(OH)_6(Irg\text{-}419)_{15}]$ (Figure 3.11). A particularly successful method which has resulted in the formation of many novel polynuclear metal cages[25,26,27,28] is

heating of the trinuclear complexes under inert atmosphere, followed by recrystallisation of the product from an appropriate solvent.

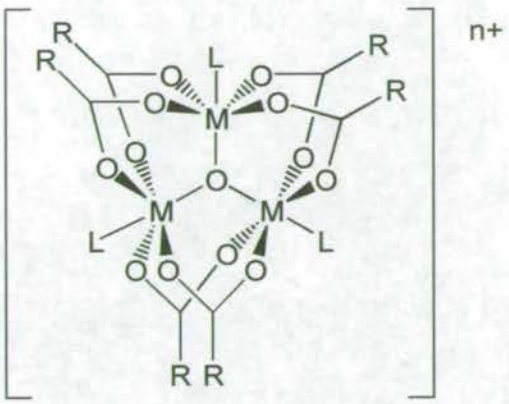

Figure 3.17: General structure of trinuclear complexes of formula $[M_3O(RCO_2)_6L_3]^{n+}$.

Two compounds were synthesised from benzoic and trimethylacetic acid, from a procedure[27] for the preparation of chromium trimers. Elemental analysis gave formulae consistent with the formation of trinuclear complexes of formula $[Al_3O(RCO_2)_6(H_2O)_3]^+$. A comparison of the IR spectra (Table 3.3) of $[Al_3O(tma)_6(H_2O)_3](NO_3)$ and the analogous trimeric iron complex $[Fe_3O(tma)_6(H_2O)_3](NO_3)$ shows a number of common bands although as most of these arise from the carboxylate ligand a definitive assignment of the oxo centred trimeric structure to the aluminium complex is not possible. Mass spectrometry failed to give additional information on speciation. The complexes were insoluble in common organic solvents and on heating to 200-400 °C under a stream of nitrogen produced grey or black powders, depending on temperature, which were similarly insoluble. Loss of carboxylic acid and water was observed during the reactions but the products showed little change in their IR spectra from that of the starting complexes.

ν (cm^{-1})		Assignment of bands
$[Al_3O(tma)_6(H_2O)_3](NO_3)$	$[Fe_3O(tma)_6(H_2O)_3](NO_3)$	
3701	-	
3426(br)w	3570(br)w	OH
2966m	2966m	CH(alk)
2930w	2932w	CH(alk)
1588s	1572s	CO_2^- (bridging tma)
-	1512w	
1492s	1488s	CO_2^- (bridging tma)
-	1459w	
1445s	1425s	CO_2^- (bridging tma)
1384m	1381s	NO_3^-
1364m	1365m	
-	1311w	
1236m	1229m	
-	1038w	
987m	-	
-	940w	
-	899w	
794w	787w	
628m	608m	possibly M_3O
525w	-	

Table 3.3: Comparison of the bands in the IR spectra of the trimeric complexes $[Al_3O(tma)_6(H_2O)_3](NO_3)$ and $[Fe_3O(tma)_6(H_2O)_3](NO_3)$.

3.3 Nickel Complexes with 3-Benzoyl-propionic Acid.

The lack of success in characterising aluminium complexes of relevant carboxylates was frustrating. Given the lack of literature on coordination complexes of 3-ketocarboxylates, other than previous work[16,17] from this group on iron clusters, it was felt that synthesis of complexes featuring other metals might illustrate the binding modes of the 3-ketocarboxylates.

3.3.1 Synthesis and Structure of $[Ni_3(chp)_4(bpa)_2(MeOH)_6]$ .2MeOH.

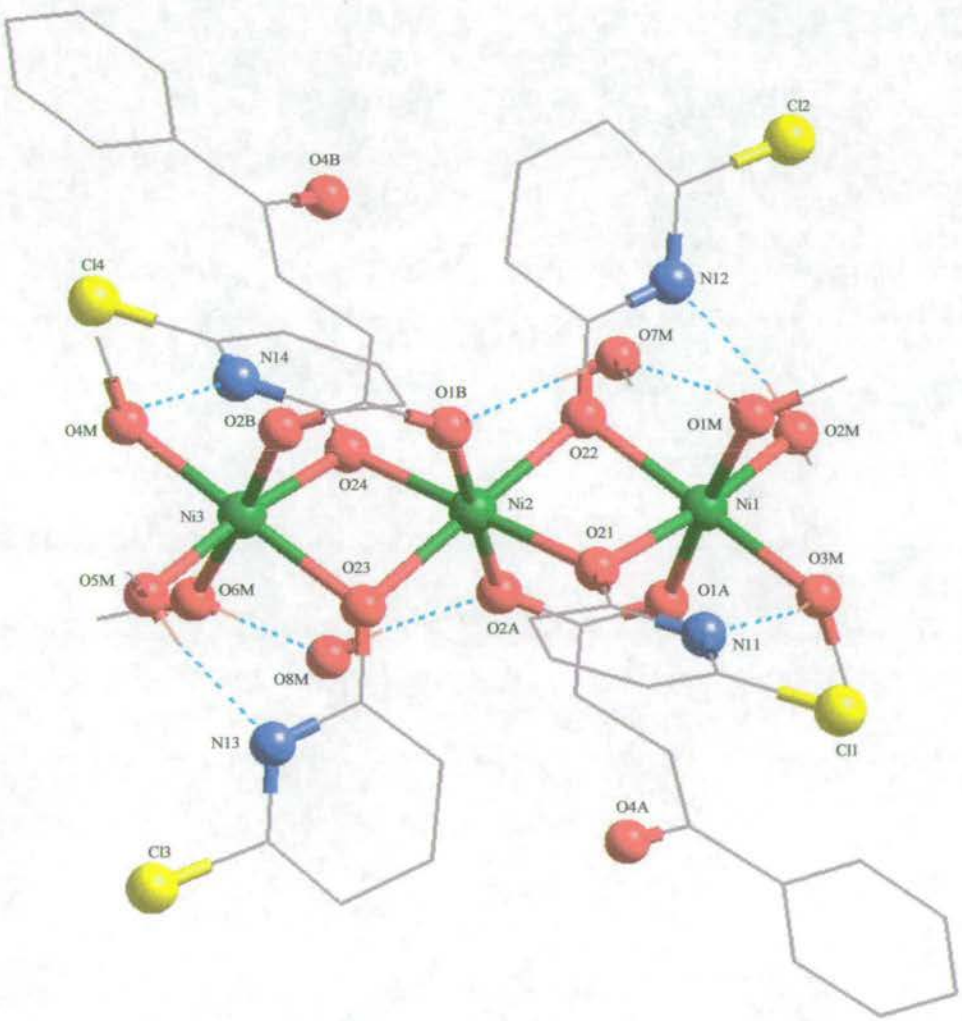

Figure 3.18: Crystal structure of $[Ni_3(chp)_4(bpa)_2(MeOH)_6]$.2MeOH.

Reaction of nickel(II) chloride hexahydrate with the sodium salts of 6-chloro-2-hydroxypyridonate (Hchp) and 3-benzoyl-propionic acid (Hbpa) in methanol, followed by evaporation to dryness gave a green powder. This powder was redissolved in fresh methanol producing a green solution, from which pale green crystals began to grow after two days. Crystallisation was complete after one week, yield 17.6%. X-ray analysis revealed a complex of formula $[Ni_3(chp)_4(bpa)_2(MeOH)_6].2MeOH$ (Figure 3.18). Crystallographic data (Table 19) and selected bond lengths and angles (Table 20) for $[Ni_3(chp)_4(bpa)_2(MeOH)_6].2MeOH$ are given in the appendix. The mixed ligand complex is a linear trimer, (Ni...Ni...Ni angle 179.3°), containing two 1,3-bridging bpa ligands, four deprotonated chp ligands and six terminally coordinated methanols. Each nickel centre is crystallographically unique. The central nickel, Ni(2), is bridged to the external nickels, Ni(1) and Ni(3), by two μ_2 oxygen atoms from two chp ligands and one 1,3-bridging bpa ligand. Ni(1) and Ni(3) are further ligated by three methanol molecules, preventing further oligomerisation. All of the nickel sites therefore have six oxygen donors in a distorted octahedral array. The Ni...Ni distances of 3.101 and 3.104 Å are consistent with previously reported examples.[29,30,31,32] A represention of the core of $[Ni_3(chp)_4(bpa)_2(MeOH)_6].2MeOH$ is shown (Figure 3.19). This core is common to all linear nickel pyridonate/carboxylate trimers for which the structure had been determined.

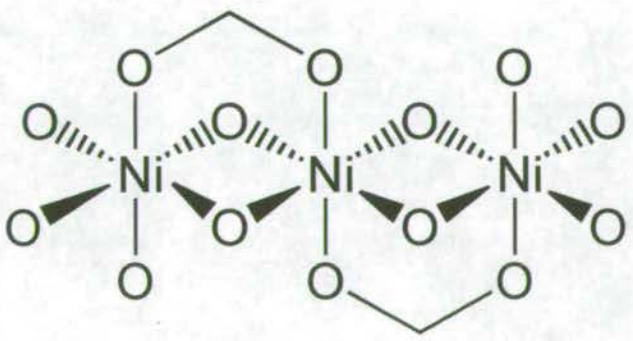

Figure 3.19: Representation of the metal oxide core common to all linear nickel pyridonate/carboxylate trimers.

The oxygen donor atoms of the four pyridonate ligands lie in a "plane" with the two bpa ligands *trans* to each other. The Ni-O(chp) bond lengths are in the range 2.064(4) - 2.082(4) Å whilst the Ni-O(bpa) lengths are generally shorter, 1.998(4) - 2.066(4) Å. The four chp ligands are involved in strong hydrogen bonding to four of the six terminal methanols, average OH...N(chp) 2.680 Å. The remaining terminal methanols hydrogen bond to a solvent methanol molecule which in turn forms a further hydrogen bond to one carboxylate oxygen of the bridging bpa ligand. A list of all hydrogen bond contacts and distances in the complex are given (Table 3.4)

Bond type	Donor atom	Acceptor atom	Bond length
O-H...N	O(2M)	N(12)	2.699
O-H...N	O(3M)	N(11)	2.692
O-H...N	O(4M)	N(14)	2.661
O-H...N	O(5M)	N(13)	2.697
O-H...O	O(1M)	O(7M)	2.607
O-H...O	O(7M)	O(1B)	2.714
O-H...O	O(6M)	O(8M)	2.597
O-H...O	O(8M)	O(2A)	2.725

Table 3.4: Hydrogen bond contacts in $[Ni_3(chp)_4(bpa)_2(MeOH)_6].2MeOH$.

While the carbonyl groups of the two 3-bpa ligands are not involved in the hydrogen bonding of the complex, they do find close contacts with hydrogens of the chp ligands [O(4A)...H(33) 2.769 Å, O(4A)...H(43) 2.586 Å and O(4B)...H(32) 2.630 Å, O(4B)...H(42) 2.712 Å].

The closest contacts between molecules in the crystal involve a Cl...Cl contact of 3.498 Å and a Cl...O(MeOH) contact of 3.354 Å.

3.3.2 Magnetic Studies of $[Ni_3(chp)_4(bpa)_2(MeOH)_6].2MeOH$.

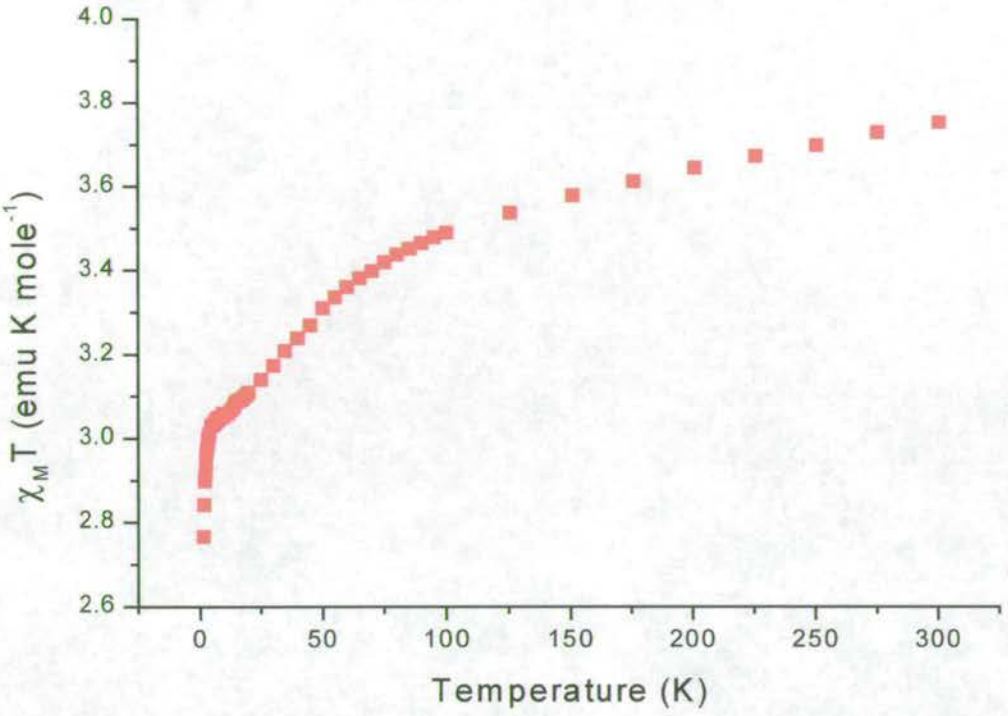

Figure 3.20: The variation of $\chi_M T$ with temperature of $[Ni_3(chp)_4(bpa)_2(MeOH)_6].2MeOH$.

Magnetic studies reveal weak *anti*-ferromagnetic coupling within the trimer. The room temperature value of $\chi_M T$ (Figure 3.21) (where χ_M is the molar susceptibility) is ca 3.75 emu K mol^{-1}, which compares well with a calculated value of 3.63 emu K mol^{-1} for g = 2.2. The decline in $\chi_M T$ as the temperature is lowered indicates the cage has a S = 1 ground state i.e. with the spins on the exterior Ni centres aligned anti-parallel with the spin on the central nickel. This behaviour is consistent with that observed for other linear nickel carboxylate/pyridonate trimers.[29,30,31]

$$\chi_M T = \frac{g^2}{8} nS(S+1)$$

Figure 3.21: Equation for calculating molar susceptibility, where g = the Lande g-factor, S = spin of atom and n = the number of equivalent paramagnetic centres within the complex.

3.3.3 Synthesis and Structure of $[Ni_6Na_2Cl_2(OH)_6(Hmhp)_6(bpa)_6]$. 3.7THF.

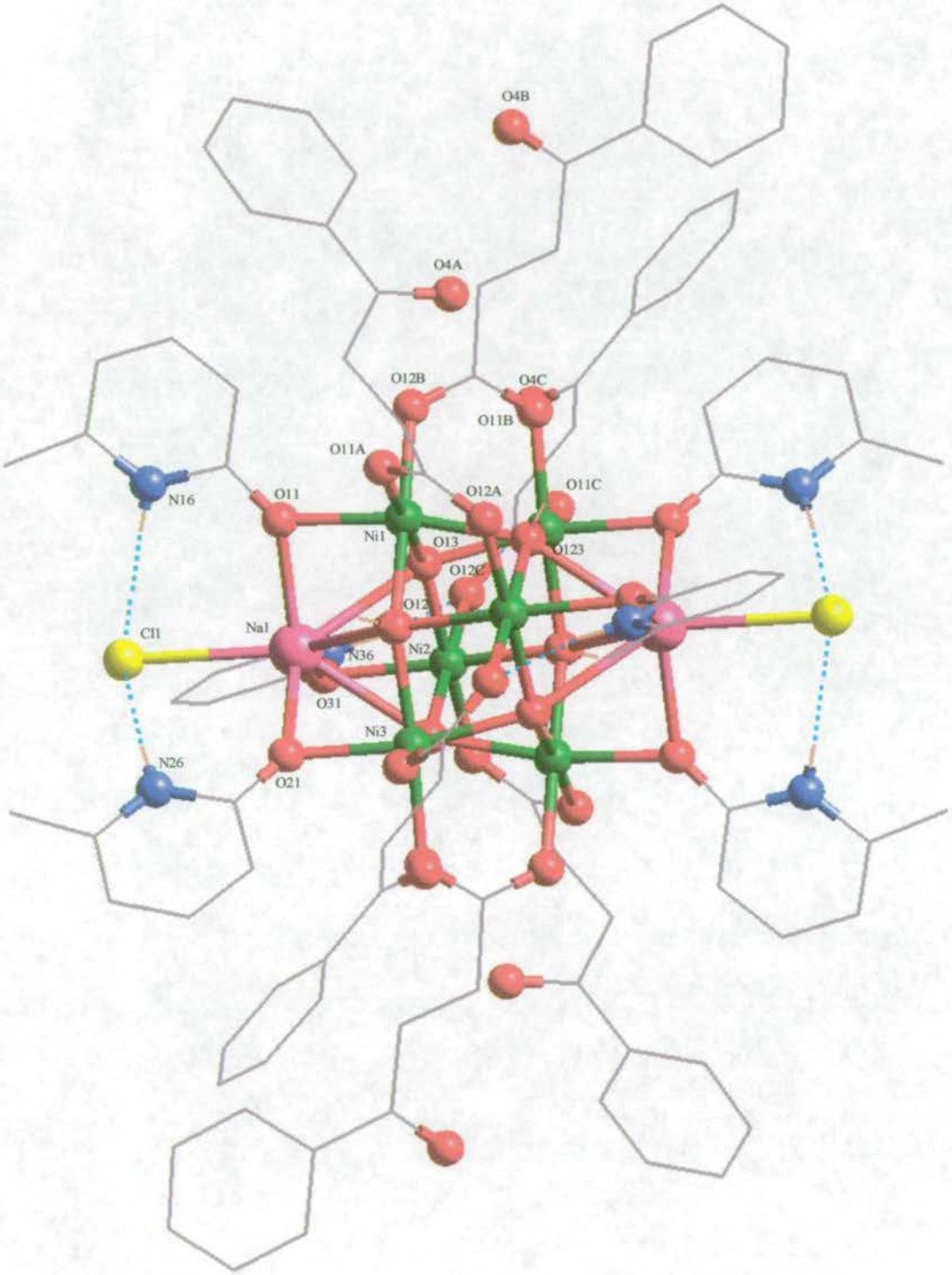

Figure 3.22: Crystal structure of $[Ni_6Na_2Cl_2(OH)_6(Hmhp)_6(bpa)_6]$. 3.7THF.

In a similar reaction to that described previously, nickel(II) chloride hexahydrate, Na(bpa) and the sodium salt of 6-methyl-2-hydroxypyridonate (Hmhp) were stirred in methanol, evaporated to dryness and the resulting green powder extracted with THF. Very pale green, almost colourless, crystals of $[Ni_6Na_2Cl_2(OH)_6(Hmhp)_6(bpa)_6]$. 3.7THF grew after two months in very low yield. During this time it was necessary to filter the solution several times to remove a white precipitate of Hmhp which separated. The structure of $[Ni_6Na_2Cl_2(OH)_6(Hmhp)_6(bpa)_6]$. 3.7THF (Figure 3.22) was determined and a view of the metal oxide core is shown (Figure 3.23). Crystallographic data (Table 21) and selected bond lengths and angles (Table 22) are given in the appendix.

The metal core is very similar to a previously published[33] cage synthesised with trimethylacetic acid, but in this case the sodium is encapsulated by hydrogen bonds from all three Hmhp ligands.

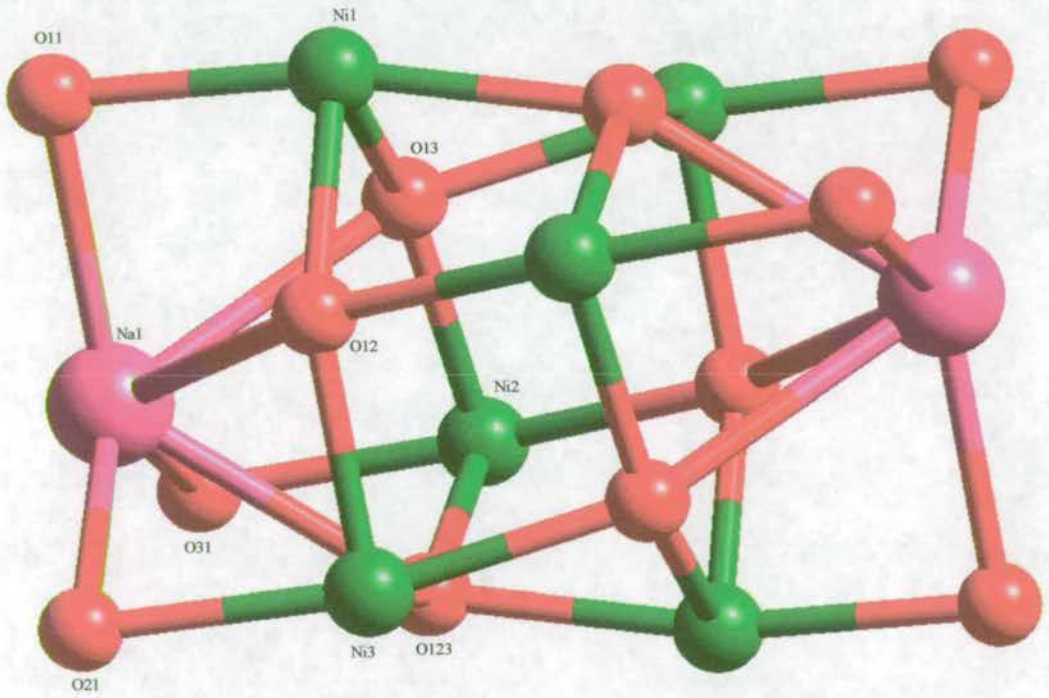

Figure 3.23: Metal oxide core of $[Ni_6Na_2Cl_2(OH)_6(Hmhp)_6(bpa)_6]$. 3.7THF.

The Ni_6Na_2 metal core can be described as a cube (Figure 3.24) with the two sodium sites at opposite ends of a body diagonal. The six Ni...Ni edges of the cube are spanned by 1,3-bridging bpa units, and the Ni...Na edges by μ-O-donors from

Hmhp ligands. The Ni-O (bpa) bond lengths range from 2.019(2) – 2.056(2) Å, while the Ni-O (Hmhp) bond lengths range from 2.080(2) – 2.107(2) Å. The nickel sites have a pseudo-octahedral geometry and are bound to six oxygen donors.

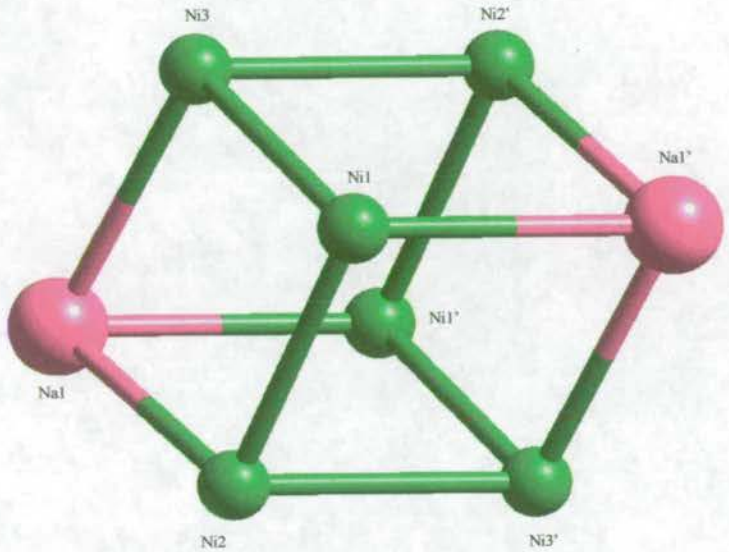

Figure 3.24: Ni_6Na_2 metal core of $[Ni_6Na_2Cl_2(OH)_6(Hmhp)_6(bpa)_6]$. 3.7THF.

The seven coordinate sodium is unusual. Its geometry can probably best be described as an elongated tetrahedron consisting of three hydroxide oxygens and the chloride, capped on the O_2Cl faces by three further oxygen donors derived from Hmhp units. An alternative description is a capped octahedron with the sodium sitting in the centre of a plane defined by the three hydroxide oxygens and the chloride as the capping atom. The Cl-Na-$O_{(Hmhp)}$ angles range from 88.48(7) - 92.91(8)°, the $O_{(Hmhp)}$-Na-$O_{(Hmhp)}$ from 119.26(9) - 120.37(10)°, and the $O_{(OH)}$-Na-$O_{(OH)}$ from 68.34(9) to 69.47(8)°.

The chloride ion in the sodium coordination sphere, [Na(1)-Cl(1) 2.8705(19) Å] forms hydrogen bonds with the protonated nitrogen on two Hmhp ligands, N(26)...Cl(1) 3.113 Å and N(26)...Cl 3.128 Å. The third Hmhp ligand is facing the other direction, forming a hydrogen bond to a carboxylate oxygen of a bpa ligand, N(136)...O(12C) 2.708 Å.

An unusual feature of the complex is the six μ_4-hydroxides at the centre of each face of the cube. The Ni-$O_{(OH)}$ bond lengths are in the range 2.057(2) – 2.091(2) Å and the Na-$O_{(OH)}$ 2.641(3) – 2.668(3) Å. Several examples of μ_4-hydroxide bridges

have been reported for barium,[34] molybdenum,[35] and alkali metals.[36] For 3d metals the two previous cases[37,38] involve tetranuclear nickel or copper complexes encapsulated in macrocycles.

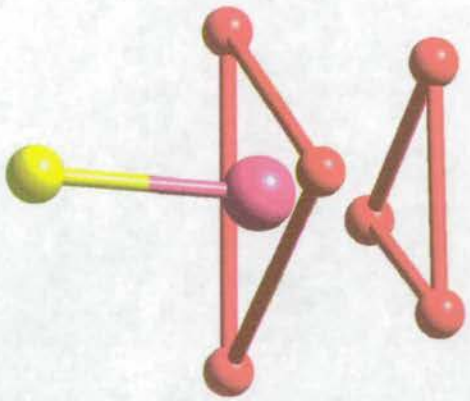

Figure 3. 25: Coordination of the sodium in $[Ni_6Na_2Cl_2(OH)_6(Hmhp)_6(bpa)_6]$. 3.7THF.

Four of the six 3-bpa carbonyls find close contacts O(4A) with a methylene hydrogen [O(4A)...H(2B2) 2.832 Å] and O(4B) with a phenyl hydrogen [O(4B)...H(56A) 2.655 Å].

It is interesting to note that in contrast to the iron chemistry described previously, the carbonyl functionality of the 3-ketocarboxylates in both nickel complexes play no role in either intra- or intermolecular hydrogen bonding. Close contacts are found in both complexes but these are probably as a result of packing restraints.

3.4 Isotherm Studies.

Data for the calibration and isotherm experiments in this section are given in the appendix, Tables 35-40.

The UV/vis spectra of Irg-419, Irg-78 and benzoic acid were recorded in 95/5 % methanol/water and their extinction coefficients determined (Table 3.5) using the Beer-Lambert Law.

Compound	UV/vis bands, λ (nm)	Extinction coefficient ε
3-(4-methylbenzoyl)-propionic acid (Irg-419)	204, 252	14910(230), (λ = 252)
4-p-tolyl-butyric acid (Irg-78)	213, 218	8000(280), (λ = 210)
benzoic acid	224	10400(70)

Table 3.5: Electronic spectra for ligands in 95 % methanol/water (standard deviations in parenthesis).

The adsorption isotherms were determined as described in Section 3.6.3 and are plotted (Figure 3.26).

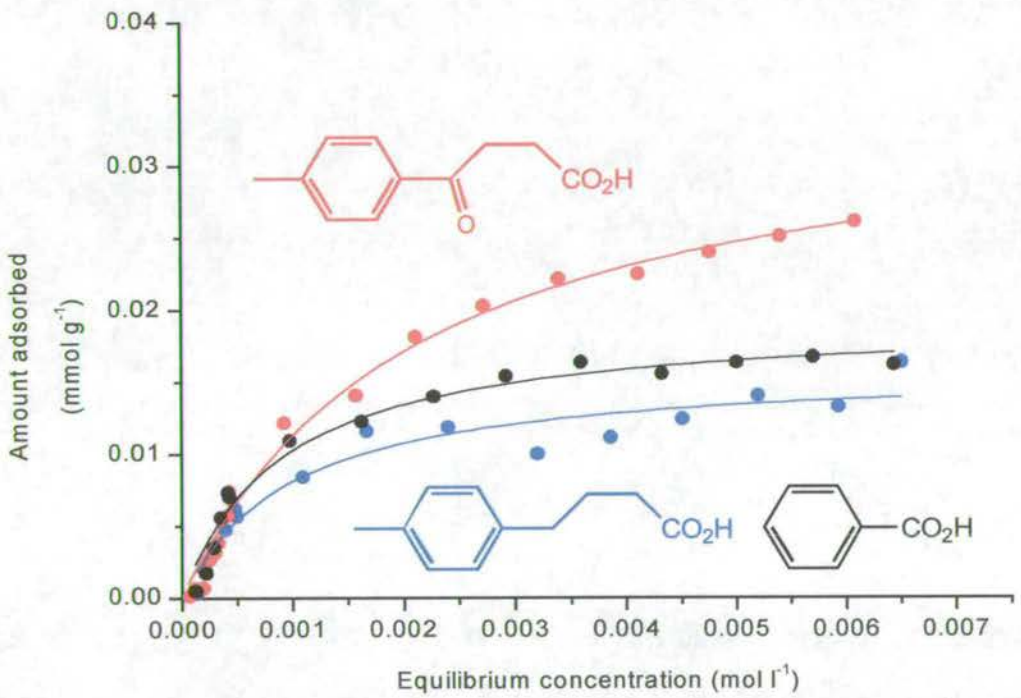

Figure 3.26: Adsorption isotherms for Irg-419 (red), Irg-78 (blue) and benzoic acid (black).

Examination of the low concentration region (<0.5 × 10^{-3} mol l^{-1}) of the isotherms (Figure 3.26) reveals that the initial slope and thus the binding strength of all three compounds are very similar. This is in contrast to goethite [FeO(OH)] where Irg-419 was found[17] to have a markedly steeper initial slope and therefore greater binding strength than Irg-78. This indicates that unlike on goethite, the carbonyl functionality has little or no effect on the binding of carboxylic acids to $Al(OH)_3$ at

low concentrations. Both Irg-419 and Irg-78 also show evidence of initial cooperative binding effects as evidenced by the slight *S* curve shape of the isotherm at very low concentrations. This behaviour has also been observed for benzoate on δ-Al_2O_3, but was not commented on by the authors other than to say that agreement with the Langmuir isotherm model was poor at low concentrations.[39]

This situation changes as the concentration is increased, with the three compounds displaying very different adsorption characteristics and surface coverage values (Table 3.6). Both benzoic acid and Irg-78 reach the "plateau" region of the graph much earlier than Irg-419, which within the concentration range of the isotherm experiment is still rising. It is this difference which leads to the lower equilibrium constant value of Irg-419 compared to benzoic acid and Irg-78, whose value is comparable with that measured on goethite [$1.4(1) \times 10^3$]. The equilibrium adsorption constants (Table 3.6) are obtained from curve fitting the isotherms to the Langmuir adsorption model and the apparent discrepancy is due to the limitations of the model.

The differences in the surface coverage values between Irg-78 and benzoic acid are not large and, if statistically significant, could be due to the relative size of the molecules. Irg-78 is larger than benzoic acid and has a flexible "tail" which could both inhibit the formation of ordered arrays on the surface and obscure potential adsorption sites from other molecules. This is reflected in the required surface area values of 33(2), 73(5) and 61(3) $Å^2$ $molecule^{-1}$ for Irg-419, Irg-78 and benzoic acid respectively, calculated from the surface area of the $Al(OH)_3$ used which is known[40] to be 7 m^2 g^{-1}. These figures show that the ligands are packing more efficiently and covering a larger proportion of the $Al(OH)_3$ surface than was observed for goethite, where the required surface area for a single molecule of Irg-419 obtained from the isotherm experiment was found to be approximately five times larger than the theoretical maximum value. Indeed if the theoretical maximum value of the area occupied by a single molecule of Irg-419 on goethite of 50 $Å^2$ $molecule^{-1}$ also applied for $Al(OH)_3$, a higher surface area of $Al(OH)_3$ would need to be generated.

The higher surface coverage of Irg-419 is less easily explained but is also observed on goethite. A possible explanation for this phenomenon is that while the carbonyl does not increase the binding strength at low concentrations, at higher

concentrations it could improve the ability of the ligand to form organised arrays on the surface as the additional hydrogen bonded anchoring point will fix the conformation of the molecule on the surface.

Molecular modelling work,[41] while restricted due to lack of crystallographic evidence, has shown that in theory Irg-419 can bind to an aluminium oxide surface in a similar fashion to that found within the iron cluster (Figure 3.11).

Compound	Amount of ligand adsorbed at monolayer coverage (n_M) 10^5 [mol g^{-1}]	Equilibrium adsorption constant (K) 10^{-3} [L mol^{-1}]
3-(4-methylbenzoyl)-propionic acid (Irg-419)	3.5(2)	0.5(50)
4-*p*-tolyl-butyric acid (Irg-78)	1.6(1)	1.0(220)
benzoic acid	1.9(1)	1.1(160)

Table 3.6: Adsorption isotherm data (standard deviations in parenthesis).

3.5 Conclusions.

The carboxylates 3-(4-methylbenzoyl)-propionic acid (Irg-419) and 4-*p*-tolyl-butyric acid (Irg-78) were found to have different binding properties to $Al(OH)_3$ than those previously reported for goethite. The binding strength of the ketocarboxylate Irg-419 was not higher than the non-keto derivative Irg-78 but the observed increase in surface coverage could be attributed to the carbonyl group forming a hydrogen bond to a hydroxyl group on the surface as was found on goethite. However, no structural information could be obtained to support this supposition and as a result the utility of molecular modelling was limited.

The preparation of crystalline polynuclear aluminium species which could be used as models proved to be very difficult; aluminium carboxylates are known gelling agents and reactions often lead to uncharacterisable powders or gels. The

literature reveals that unlike iron there are relatively few structurally characterised aluminium carboxylates and there is no standard method for their synthesis. Of those that are reported, several were the result of serendipitous hydrolysis through undesired water in the reaction.

Two nickel complexes were prepared with the ketocarboxylate 3-bpa but in neither case were the carbonyls found to participate in hydrogen bonding, though close contacts with other hydrogen atoms were found in both complexes.

3.6 Experimental.

3.6.1 Chemicals and Instrumentation.

All reagents were used as obtained from Aldrich, Acros or Lancaster, except 3-(4-methylbenzoyl)-propionic acid and 4-*p*-tolyl-butyric acid which were obtained from Ciba Speciality Chemicals. Solvents were used as received. High surface area "superfine $Al(OH)_3$" was supplied by Alcan. Water was distilled before use.

Analytical data were obtained on a Perkin-Elmer 2400 Elemental analyser by the University of Edinburgh Microanalytical Service.

^1H and ^{13}C NMR were obtained using Bruker WP200 and AC250 spectrometers at ambient temperature. Chemical shifts (δ) are reported in parts per million (ppm) relative to residual solvent protons as internal standards.

Electron impact mass spectrometry (EIMS) was carried out on a Kratos MS50TC spectrometer. Fast atom bombardment mass spectrometry (FABMS) was carried out using a Kratos MS50TC spectrometer a 3-nitrobenzyl alcohol (NOBA) or thioglycerol matrix.

The infra-red spectra were obtained as potassium bromide discs using a Perkin Elmer Paragon 1000 FT-IR spectrometer.

Electronic spectra were measured on an ATI UNICAM UV/Vis spectrometer with 1cm path length quartz cuvettes.

Variable temperature magnetic measurements in the region 1.8-325 K were made using a SQUID magnetometer (Quantum Design) with samples sealed in

gelatin capsules. Diamagnetic corrections for sample holders and samples were applied to the data.

Curve fitting were performed using the programs Origin 5.0 © Microcal Software Inc and SigmaPlot 2000 (demo version) © 1986-2000 SPSS Inc.

Single crystal X-raydiffraction data were collected on either a Stoe Stadi-4 diffractometer or a Bruker Smart APEX CCD area detector. Both were equipped with an Oxford Cryosystems low-temperature device. Full listings of atomic positions and thermal parameters are provided electronically on the CD accompanying this thesis.

3.6.2 Synthesis.

Aluminium alkoxide/carboxylate dimers.

The attempted preparation of all compounds in this series was carried out by the same method which is described for $[Al(O^iPr)(PhCO_2)_2]_2$.

Attempted preparation of $[Al(O^iPr)(PhCO_2)_2]_2$.

Triphenylacetic acid (1.4 g, 4.9 mmol) was slowly added to a stirred solution of $Al(O\text{-}^iPr)_3$ (0.5 g, 2.5 mmol) in toluene (10 ml). The reaction was stirred for one hour at room temperature then heated to 100°C for three and a half hours. The solution was cooled to room temperature and the volatiles removed under vacuum to give a white solid (1.6 g).

(Found: C, 72.2; H, 5.6; $C_{86}H_{74}O_{10}Al_2$ requires C, 78.2; H, 5.6 %). Attempts to purify this material by recrystallisation were unsuccessful.

Similar results were obtained in the attempted synthesis of related compounds and these are shown (Table 3.7).

$Al(OR)_3$	$R'CO_2H$	Found	Required
$Al(O^iPr)_3$	benzoic acid	C, 61.2; H, 5.4 %	C, 62.2; H, 5.2 %
$Al(O^iPr)_3$	trimethylacetic acid	C, 58,8; H, 8.2 %	C, 54.2; H, 8.7 %

$Al(O^iPr)_3$	diphenylacetic acid	C, 67.9; H, 6.0 %	C, 73.2; H, 5.7 %
$Al(O^iPr)_3$	3-benzylpropionic acid	C, 60.3; H, 5.7 %	C, 62.7; H, 5.7 %
$Al(O^tBu)_3$	benzoic acid	C, 54.9; H, 5.3 %	C, 73.6; H, 5.9 %
$Al(O^tBu)_3$	trimethylacetic acid	C, 47.2; H, 8.2 %	C, 55.6; H, 8.9 %
$Al(O^tBu)_3$	diphenylacetic acid	C, 69.3; H, 5.5 %	C, 73.6; H, 5.9 %
$Al(O^tBu)_3$	triphenylacetic acid	C, 76.8; H, 5.7 %	C, 78.3; H, 5.8 %

Table 3.7: Attempted preparation of Aluminium alkoxide/carboxylate dimers of formula $[Al(OR)(R'CO_2)_2]_2$.

$[Al_3O(PhCO_2)_6(H_2O)_3].½(PhCO_2).½(NO_3)$.

Benzoic acid (5.74 g, 47.0 mmol) was added to a solution of KOH (2.63 g, 46.9 mmol) in distilled water (75 ml) and the solution heated to 80°C. Aluminium nitrate nonahydrate (5.01 g, 13.4 mmol) in water (50 ml) was added slowly and a white precipitate formed. The suspension was cooled to room temperature and the precipitate filtered off and washed with distilled water. The product was then dried under vacuum to give a white powder (3.7 g, 86 %).

(Found: C, 56.5; H, 3.7; N, 0.6 %; $C_{45.5}H_{38.5}N_{0.5}O_{18.5}Al_3$ requires C, 56.4; H, 4.0; N, 0.7 %); IR (cm^{-1}, KBr disc) ν 3676w, 3436(br)w (OH), 3067w (CH Ar), 1696m, 1605s & 1567s (CO_2^-), 1497m, 1436s (CO_2^-), 1384m (NO_3^-), 1318w, 1287w, 1180w, 1070w, 1027w, 1002m, 825w, 722s, 685m, 548m, 525w.

$[Al_3O((CH_3)_3CCO_2)_6(H_2O)_3](NO_3)$.

Trimethylacetic acid (4.80 g, 47.0 mmol) was added to a solution of KOH (2.67 g, 47.6 mmol) in distilled water (75 ml) and the solution heated to 80°C. Aluminium nitrate nonahydrate (5.00 g, 13.3 mmol) in water (50 ml) was added slowly and a white precipitate formed. The suspension was cooled to room temperature and the precipitate filtered off and washed with distilled water. The product was then dried under vacuum to give a white powder (3.54 g, 98 %).

(Found: C, 43.3; H, 6.9; N, 1.5 %; $C_{30}H_{60}NO_{19}Al_3$ requires C, 43.9; H, 7.3; N, 1.7 %); IR (cm^{-1}, KBr disc) ν 3701w, 3436(br)w (OH), 2966m & 2930w (CH), 1588s, 1492s & 1445s (CO_2^-, bridging benzoate), 1384m (NO_3^-), 1364m, 1236m, 987m, 794w, 628m, 525w.

Sodium Salts.

The sodium salts of 6-chloro-2-hydroxypyridonate (Hchp) and 6-methyl-2-hydroxypyridonate (Hmhp) were formed by reaction with one equivalent of Na(OMe) in methanol for one hour, followed by evaporation to dryness.

$[Ni_3(chp)_4(bpa)_2(MeOH)_6].2MeOH$.

3-Benzoylpropionic acid (1.50 g, 8.4 mmol) was deprotonated by reaction with Na(OMe) (0.45 g, 8.4 mmol) in methanol for one hour, with stirring. Nickel chloride hexahydrate (1.00 g, 4.2 mmol) and Na(chp) (1.27 g, 8.4 mmol) were added and the resultant green solution stirred overnight. The solution was evaporated to dryness to give a green powder. This powder was redissolved in fresh methanol and from the solution, green crystals began to form after two days. Crystallisation was complete after one week (0.32 g, 18 %).

(Found: C, 44.3; H, 4.3; N, 4.2 %; $C_{48}H_{62}Cl_4N_4O_{18}Ni_3$ requires C, 44.3; H, 4.8; N, 4.3 %); IR (cm^{-1}, KBr disc) ν 3368(br)m (OH), 1684m (C=O, carbonyl), 1652m (C=O, chp), 1594s (CO_2^-, bridging carboxylate), 1540m, 1507w, 1444s (CO_2^-, bridging carboxylate), 1342m, 1247w, 1205w, 1167m, 1070w, 994m, 923m, 860w, 788m, 750w, 701w, 615w, 560w.

$[Ni_6Na_2Cl_2(OH)_6(Hmhp)_6(bpa)_6].3.7THF$.

3-Benzoylpropionic acid (1.50 g, 8.4 mmol) was deprotonated by reaction with Na(OMe) (0.45 g, 8.4 mmol) in methanol for one hour, with stirring. Nickel chloride hexahydrate (1.00 g, 4.2 mmol) and Na(mhp) (1.10 g, 8.4 mmol) were added and the resultant green solution stirred overnight. The solution was evaporated to dryness to give a green powder. Very pale green crystals grew in very low yield after two months and were characterised by X-ray diffraction.

3.6.3 Adsorption isotherm measurements.

Preweighed quantities of $Al(OH)_3$ (0.40 g) in polycarbonate centrifuge tubes were stirred with the desired concentration of ligand in methanol/water (10ml, 95:5 v/v) for two hours at 25 °C. The suspensions were centrifuged and filtered, and the supernatant diluted if necessary, for absorbance measurement by UV spectrometry. The measured absorbance was related to the concentration of the ligand remaining in solution by reference to calibration curves. The amount of ligand adsorbed was then calculated from the difference between initial and final concentration. From this plots of amount of ligand adsorbed versus equilibrium concentration were obtained.

3.7 References.

1 Industrial Inorganic Chemistry: Production and Uses by R. Thompson, Published by The Royal Society of Chemistry, 1995.

2 Y. Koide, S. G. Bott and A. R. Barron, *Organometallics*, 1996, **15**, 2213.

3 Y. Koide and A. R. Barron, *Organometallics*, 1995, **14**, 4026.

4 S. G. Bott, A. W. Coleman and J. L. Atwood, *J. Am. Chem. Soc.*, 1986, **108**, 1709.

5 J. Ondracek, A. Jegorov, Z. Kovarova, M. Husak and F. Jursik, *Chem. Commun.*, 1997, 915.

6 A. Muller, H. Reuter, S. Dillinger, Angew. *Chem., Int. Ed. Engl.*, 1995, **34**, 2328.

7 P. Sobota, M. O. Mustafa, J. Utko and T. Lis. *J. Chem. Soc. Dalton Trans.*, 1990, 1809.

8 A. K. Powell and S. L. Heath, *Coord. Chem. Rev.*, 1996, **149**, 59.

9 A. Pandey, V. D. Gupta, H. Noth, *Eur. J. Inorg. Chem.*, 1999, 1291.

10 S. L. Heath, P. A. Jordan, I. D. Johnson, G. R. Moore, A. K. Powell and M. Helliwell. *Journal of Inorganic Biochemistry*. 1995, **59**, 785.

11 T. L. Feng, P. L. Gurian, M. D. Healy and A. R. Barron. *Inorg. Chem.*, 1990, **29**, 408.

12 W. Seichter, H. Mogel, P. Brand and D. Salah, *Eur. J. Inorg. Chem.*, 1998,

795.

13 G. T. Hefter, N. A. North and S. H. Tan. *Corrosion*, 1997, **53**, 657.

14 Y. G. Aronoff, B. Chen, G. Lu, C. Seto, J. Schwartz and S. L. Bernasek. *J. Am. Chem Soc.*, **1997**, 119, 259.

15 Ciba Speciality Chemicals, unpublished work.

16 M. Frey, S. G. Harris, J. M. Holmes, D. A. Nation, S. Parsons, P. A. Tasker, S. J. Teat and R. E. P. Winpenny, *Angew. Chem. Int. Ed.*, **37**, 1998, 3246.

17 M. Frey, S. G. Harris, J. M. Holmes, D. A. Nation, S. Parsons, P. A. Tasker and R. E. P. Winpenny, *Chem. Eur. J.*, 2000, **6**, 1407.

18 S. G. Harris, University of Edinburgh, PhD thesis, 1999.

19 J. H. Wengrovius, M. F. Garbauskes, E. A. Williams, R. C. Going, P. E. Donahue and J. F. Smith. *J. Am. Chem. Soc.*, 1986, **108**, 982.

20 J. T. Leman, J. Graddock-Wilking, A. J. Coolong and A. R. Barron. *Inorg. Chem.*, 1993, **32**, 4324.

21 U. Abraham, D. Belli Dell' Amico, F. Calderazzo, S. Kaskel, L. Labella, F. Marchetti, R. Rovai and J. Strahle, *J. Chem. Soc. Chem. Commun.*, 1997, 1941.

22 D. Belli Dell' Amico, F. Calderazzo, M. Dell' Innocenti, B. Guldenpfennig, S. Ianelli, G. Pelizzi and P. Robino, *Gazzetta Chimica Italiana*, 1993, 283.

23 R. D. Cannon and R. P. White, *Progress in Inorganic Chemistry*, ed. K. D. Karlin, Wiley 1988, **36**, 195-298 and references within.

24 A. T. Casey and K. Starke, *Anal. Chem.*, 1959, **31**, 1060.

25 F. E. Mabbs, E. J. L. McInnes, S. Parsons, G. M. Smith, C. C. Wilson and R. E. P. Winpenny, *J. Chem. Soc. Chem. Commun.*, 1999, 643.

26 I. M. Atkinson, C. Benelli, M. Murrie, S. Parsons, and R. E. P. Winpenny, *J. Chem. Soc. Chem. Commun.*, 1999, 285.

27 S. Batsanov, G. A. Timko, Y. T. Struchkov, N. V. Gerbeleu and K. M. Indrichen, *Koord. Khim*, 1991, **17**, 662.

28 S. Parsons, A. A. Smith and R. E. P. Winpenny, *J. Chem. Soc. Chem. Commun.*, 2000, **7**, 579.

29 A. J. Blake, E. K. Brechin, A. Codron, R. O. Gould, C. M. Grant, S. Parsons, J. M. Rawson and R. E. P. Winpenny, *J. Chem. Soc. Chem. Commun.*, 1995, 1983.

30 E. K. Brechin, University of Edinburgh, PhD thesis, 1997.

31 C. M. Grant, University of Edinburgh, PhD thesis, 1995.

32 A. Sneddon and R. E. P. Winpenny, unpublished work.

33 E. K. Brechin, A. Graham, S. G. Harris, S. Parsons and R. E. P. Winpenny, *J. Chem. Soc. Dalton Trans.*, 1997, 3405.

34 H. Vincent, F. Labrize and L. G. Hubert-Pfalzgraf, *Polyhedron*, 1994, **13**, 3232 and references therein.

35 K. M. Barkigia, L. M. Rajkovic, M. T. Pope, E. Prince and C. O. Quicksall, *Inorg. Chem.*, 1980, **19**, 2531.

36 W. J. Evans, M. S. Sollberger and J. W. Ziller, *J. Am. Chem. Soc.*, 1993, **115**, 4120.

37 M. Bell, A. J. Edwards, B. F. Hoskins, E. H. Kachab and R. Robson, *J. Am. Chem. Soc.*, 1989, **111**, 3603.

38 V. McKee and S. S. Tandon, *J. Chem. Soc. Dalton Trans.*, 1991, 221.

39 P. Benoit, J. G. Hering and W. Stumm, *Applied Geochemistry*, 1993, **8**, 127.

40 Surface area of $Al(OH)_3$ determined by Alcan for a particular batch of "superfine $Al(OH)_3$", S. Ingham, private communication, 1997.

41 A. Parkin, *Using Crystallographic and Molecular Modelling techniques to Investigate Modes-of-Interaction of Organic Ligands with Metal Systems*, 1st Year PhD Report, The University of Edinburgh, 1999.

Chapter 4:

Phosphorus Acids.

Contents.

4.1 Introduction.

4.1.1 Background.

The chemistry of aluminium compounds with phosphorus containing acids (Figure 4.1) has been much studied recently in the context of porous materials.

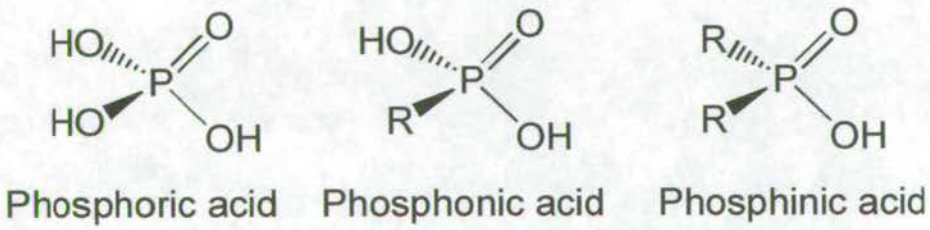

Phosphoric acid Phosphonic acid Phosphinic acid

Figure 4.1: Structures of the common phosphorus (V) acids.

The chemistry of zeolites is well established and their synthesis, properties and applications have been extensively studied.[1] In contrast to zeolites, which have been known since the 18th century, (discovered in 1756 by Swedish mineralogist Grondtedt), the first nanoporous aluminium phosphate was only discovered[2] in 1982 and the first aluminium phosphonate synthesised[3] in 1994, making this a relatively immature area of chemistry. Although, unlike zeolites, aluminium phosphonate materials have yet to find commercial applications there is interest surrounding their potential catalytic and adsorption abilities.

Aluminium phosphinates and phosphonates have been studied extensively both as novel materials in their own right and as models[4] for aluminium phosphate systems, and there have been a number of significant developments within the last few years. A brief review of the current literature in these areas is presented in sections 4.1.2 – 4.1.3.

4.1.2 Aluminium Phosphinates.

Aluminium phosphinates were first synthesised by Coates and Mukherjee in 1964[5] by reaction of trimethyl aluminium with phosphinic acids. From cryoscopic

measurements they were found to be dimeric in solution and IR studies indicated that the phosphinates act as three atom bridges between the aluminium atoms. The data were consistent with the formation of cyclic dimers with C_{2h} symmetry. This structure was confirmed later[6] by detailed IR and Raman spectroscopy and NMR characterisation. There have been only three structurally characterised aluminium phosphinates of this type, $[^tBu_2AlO_2PPh_2]_2$,[7] $[(CH_3)_2AlO_2PPh_2]$[8] and $[(Cl_2AlO_2PPh_2]$.[9] Two of these are shown (Figure 4.2). The structures confirm the predictions of Coates and Mukherjee as all three compounds are cyclic dimers containing eight membered $Al_2P_2O_4$ rings, with the phosphinates adopting a 1,3-bridging mode.

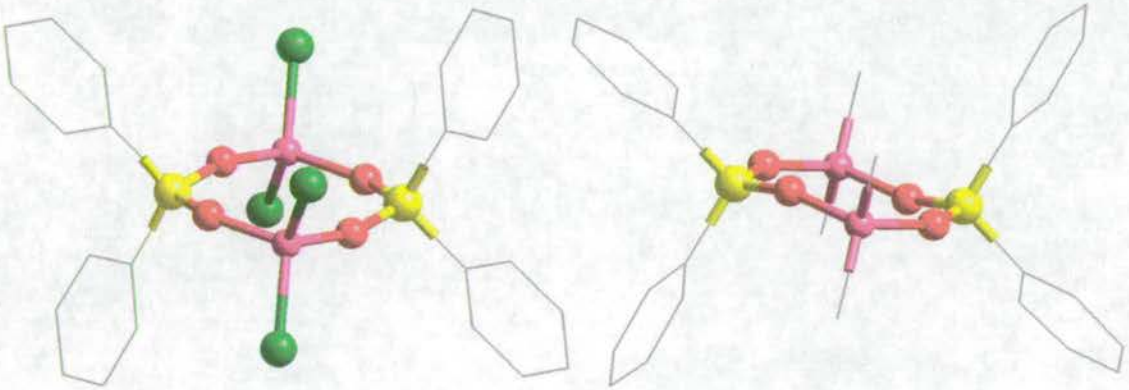

Figure 4.2: Crystal structures of $[(Cl_2AlO_2PPh_2]_2$ and $[(CH_3)_2AlO_2PPh_2]_2$.
Al-pink, O-red, P-yellow, Cl-green, C-grey.

Recently, the first aluminium phosphinate complexes, containing six coordinate aluminium, $[(^tBu_4salpen)Al\{O_2P(H)Ph\}]_2$ (Figure 4.2) and $[(^tBu_4salen)Al\{O_2P(H)Ph\}]_\infty$ have been synthesised[10] by Atwood *et al.* The structures of the ligands $^tBu_4salen$ and $^tBu_4salpen$ are given (Figure 4.4). $[(^tBu_4salpen)Al\{O_2P(H)Ph\}]_2$ is dimeric in the solid state with two phenylphosphinate ligands bridging the two aluminium centers, while $[(^tBu_4salen)Al\{O_2P(H)Ph\}]_\infty$ is polymeric with only one phenylphosphinate bridging two aluminium atoms. In this case the salen unit provides an approximately planar $N_2O_2^{2-}$ donor set and the bridging phosphinate groups occupy the axial sites.

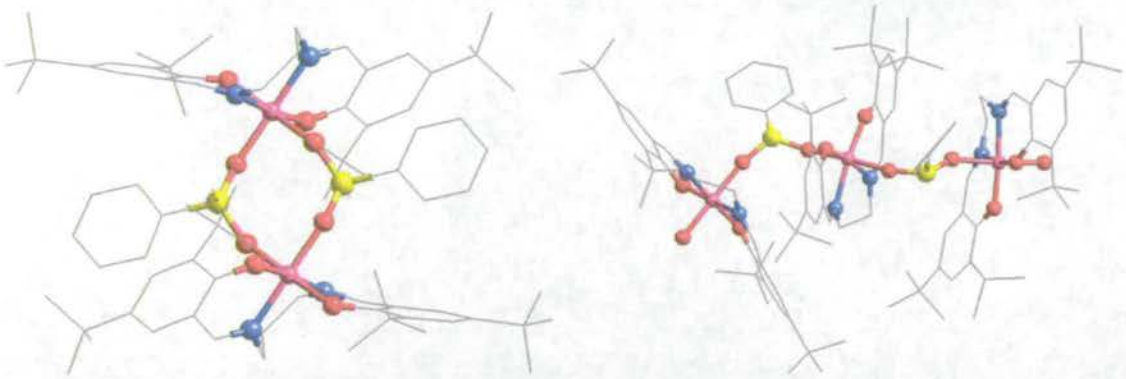

Figure 4.3: Crystal structures of $[(^tBu_4salpen)Al\{O_2P(H)Ph\}]_2$ and $[(^tBu_4salen)Al\{O_2P(H)Ph\}]_\infty$. Al-pink, O-red, P-yellow, N-blue, C-grey.

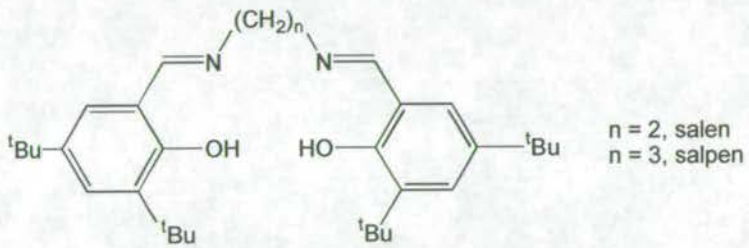

Figure 4.4: Structure of $^tBu_4$salen and $^tBu_4$salpen.

The structures described in this section all contain phosphinate ligands binding in a 1,3 bridging fashion indicating that this is the preferred coordination mode to aluminium.

4.1.3 Aluminium Phosphonates.

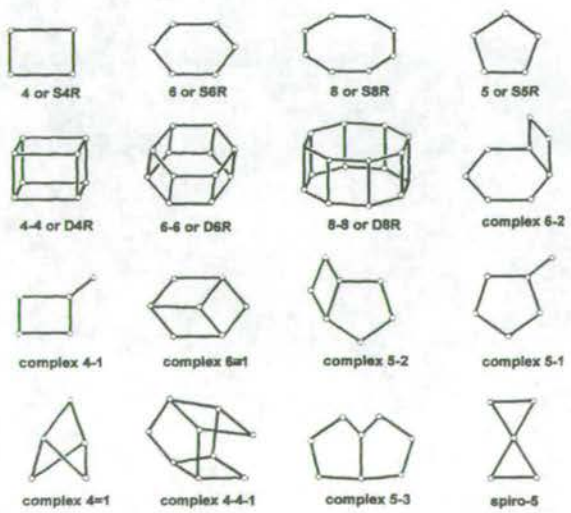

Figure 4.5: Guide to the nomenclature of secondary building units (SBUs).[4]

There are two main routes to aluminium phosphonates. Reaction of alkyl aluminium with phosphonic acids under an inert atmosphere and totally anhydrous conditions leads to discrete, organic solvent-soluble clusters, while hydrothermal synthesis using various aluminium oxides/hydroxides gives two or three dimensional polymeric arrays which are insoluble in common solvents. Two other less common preparative methods are simple melt and reflux reactions, both of which also lead to polmeric materials.

Several complexes have been synthesised via the organometallic route. The most common structural motif found is a tetrameric cage complex of general formula $[RAlO_3PR']_4$. Two of these have been crystallised and their structures solved, $[^tBuPO_3Al^iBu]_4$[11] (Figure 4.6) and $[^tBuAlO_3PMe]_4$[7] and many others have been proposed from mass spectrometric and other evidence. The compounds contain an $Al_4O_{12}P_4$ core made up of six eight membered $Al_2O_4P_2$ rings, constituting the faces of an approximate cube defined by the four aluminium and four phosphorus atoms. This core is similar to the D4R secondary building units (SBUs) (Figure 4.5) found in some phosphate molecular sieves.

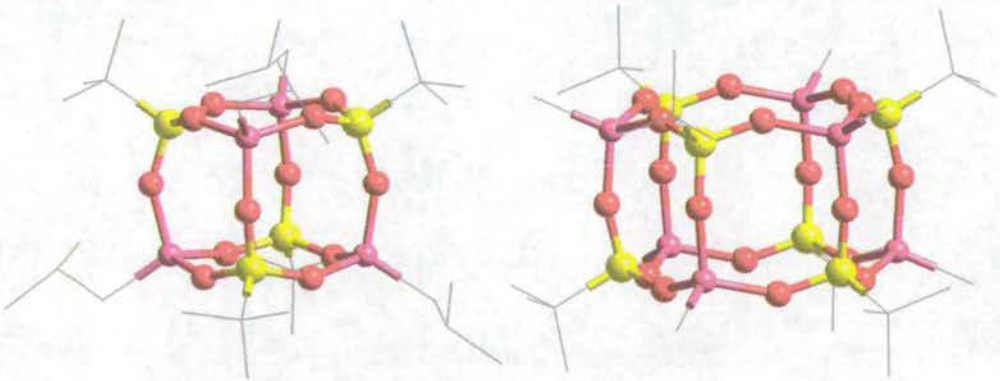

Figure 4.6: Crystal structures of $[^tBuPO_3Al^iBu]_4$ and $[MeAlO_3P^tBu]_6$. Al-pink, O-red, P-yellow, C-grey.

The reaction of *t*-butylphosphonic acid with trimethyl aluminium gives a mixture of tetrameric $[MeAlO_3P^tBu]_4$ and hexameric $[MeAlO_3P^tBu]_6$[12] (Figure 4.6). The central $Al_6O_{18}P_6$ core is based on a hexgonal prism defined by the six aluminium and six phosphorus atoms. Eight membered $Al_2O_4P_2$ rings define the square faces

and the hexagonal faces consist of twelve membered $Al_3O_6P_3$ rings. Again the core resembles the D6R SBUs found in phosphate materials.

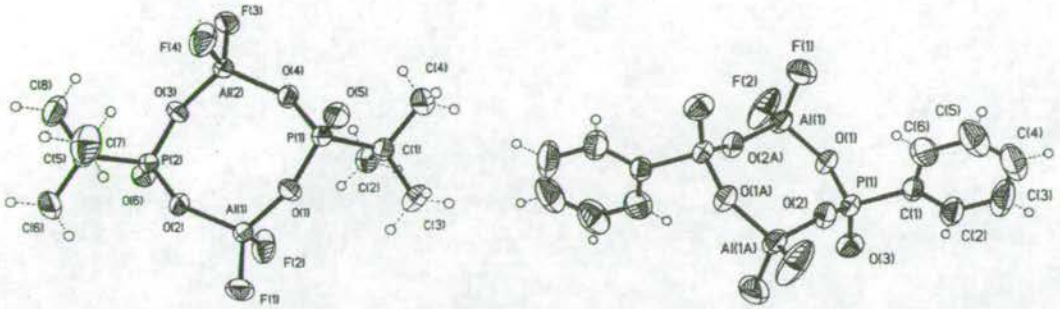

Figure 4.7: Crystal structures of $[^tBuPO_3AlF_2]_2^{2-}$ and $[PhPO_3AlF_2]_2^{2-}$.[13]

While aluminium phosphonate dimers analogous to the aluminium phosphinates have been proposed,[7] it is only recently that two[13] $[^nBu_4N]_2[^tBuPO_3AlF_2]_2$ (Figure 4.7) and $[^nBu_4N]_2[PhPO_3AlF_2]_2$ (Figure 4.7) have been structurally characterised. As with aluminium phosphinates, both contain eight membered $Al_2P_2O_4$ rings. The rings adopt a chair configuration.

$[ClAl(^tBuPO_3)]_{10}$[14] (Figure 4.8) was synthesised as a by-product of the reaction between *t*-butylphosphonic acid, aluminium trichloride and $(Ph_3PMe)[VO_2Cl_2]$. The $Al_{10}O_{30}P_{10}$ core contains six eight membered and six twelve membered rings.

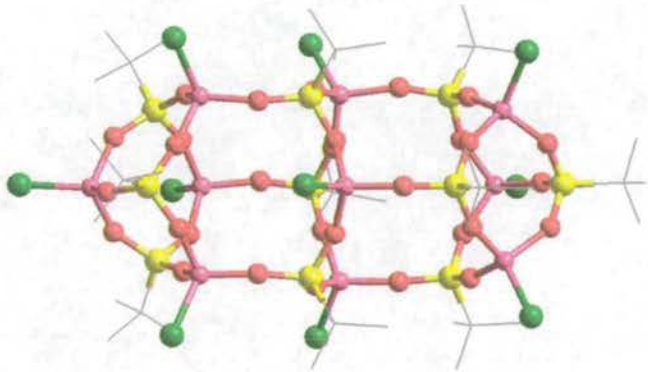

Figure 4.8: Crystal structure of $[ClAl(^tBuPO_3)]_{10}$.
Al-pink, O-red, P-yellow, Cl-green, C-grey.

Reaction of $NaAlEt_2H_2$ with *t*-butylphosphonic acid gave the mixed aluminium/sodium cluster $[Na_3(THF)(^tBuPO_3AlEt_2)_3]_2$[15] (Figure 4.9). The complex

consists of two cyclic aluminophosphonates connected by four sodium ions coordinated to the terminal phosphonate oxygens and one ring oxygen. The remaining two sodium atoms cap the $Al_3O_6P_3$ rings and are coordinated to the oxygen atoms of the ring in a crown-ether fashion. The $Al_3O_6P_3$ rings in this complex are the first structural model for the single six ring (S6R) structural feature in zeolites.

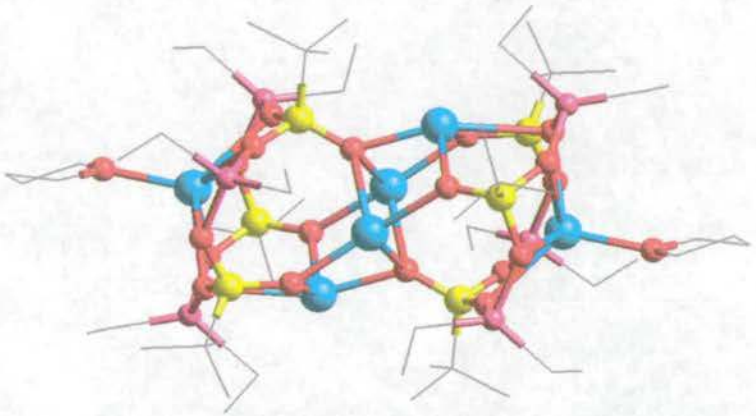

Figure 4.9: Crystal structure of $[Na_3(THF)(^tBuPO_3AlEt_2)_3]_2$. Al-pink, O-red, P-yellow, Na-pale blue, C-grey.

A mixed aluminium/caesium complex $[Cs_3(THF)F(^iBuAl)_3(^tBuPO_3)_4]_2[(^iBuAl)_2Al_2(\mu\text{-}F)_2(^tBuPO_3)_4]$[16] (Figure 4.10) was crystallised from the reaction of $Cs(^iBu_3AlF)$ with *t*-butylphosphonic acid. The complex can be described as having a $Al_4O_{12}P_4(\mu\text{-}F)_2F_2$ cube-like core connected by the six caesium ions to two peripheral $Al_3O_{12}P_4$ units.

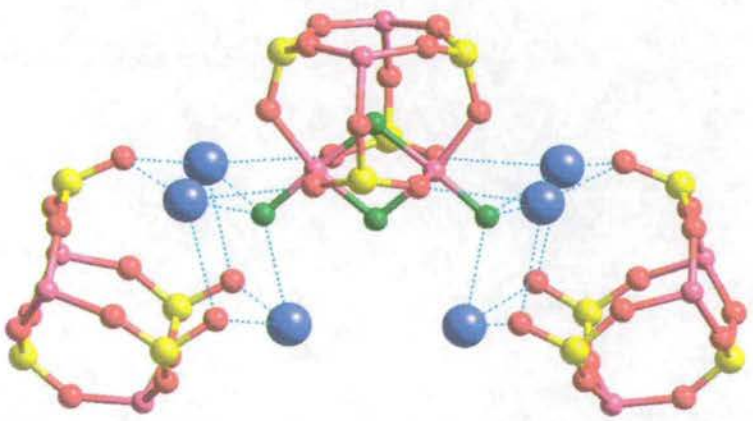

Figure 4.10: Crystal structure of $[Cs_3(THF)F(^iBuAl)_3(^tBuPO_3)_4]_2[(^iBuAl)_2Al_2(\mu\text{-}F)_2(^tBuPO_3)_4]$. All carbon atoms have been removed for clarity. Al-pink, O-red, P-yellow, Cs-blue, F-green.

As can be seen the organometallic aluminium phosphonates contain mainly four coordinate aluminium, making them unsuitable as models for surface interactions as all known aluminium oxide/hydroxide phases consist of six coordinate aluminium ions.

Under hydrothermal conditions the solvent, usually water, is heated in a sealed vessel and as a result is superheated past its normal boiling point. This results in increased solubility of many materials, allowing reactions to take place more efficiently and making possible reactions that would previously have been impossible. This method has proved successful in aluminium phosphate chemistry and has opened the door to number of new novel aluminium phosphonate phases.

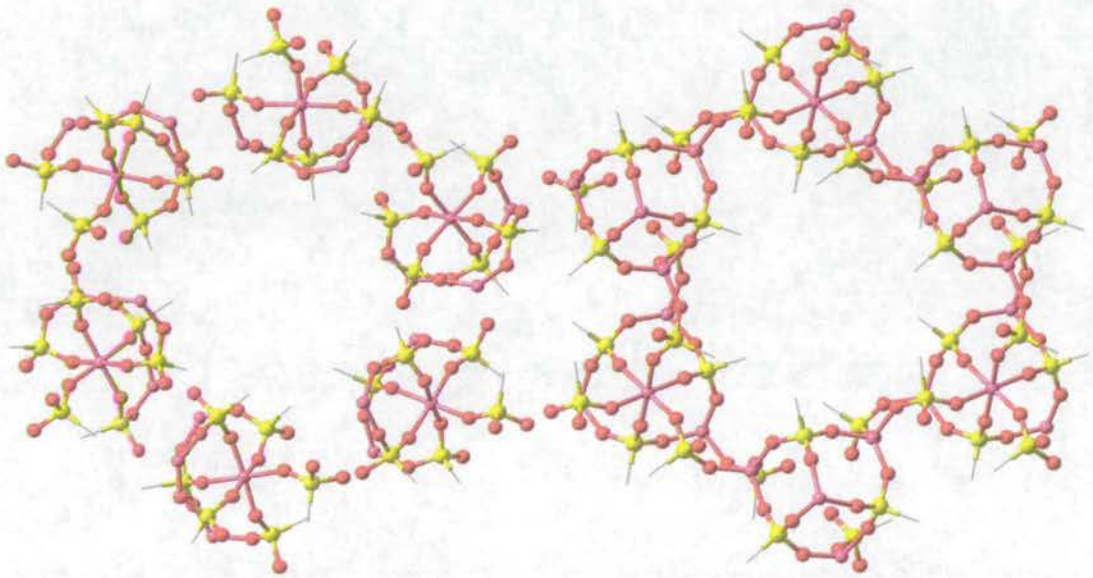

Figure 4.11: Crystal structures of AlMepO-β and AlMepO-α.
Al-pink, O-red, P-yellow, C-grey.

The first microporous aluminium phosphonates AlMepO-β[3,17] (Figure 4.11) and AlMepO-α[18] (Figure 4.11) were described in 1994 and 1995 respectively by Maeda *et al.* The materials share the same composition, ($Al_2(CH_3PO_3)_3.H_2O$), and both have been characterised by single crystal X-ray diffraction. Both polymorphs have structures consisting of hexagonal arrays of one dimensional pores with free diameters of around 6.5 Å which are partly lined with methyl groups from the phosphonic acid. The removal of the structure-directing agent, dioxane, from

AlMepO-β and its topotactic conversion to AlMepO-α on heating has been studied.[19] A third aluminium methyl phosphonate, AlMepO-ξ, has been synthesised[20,21] and has the composition $Al(OH)(O_3PCH_3).H_2O$. The structure of this compound has been determined separately by *ab initio* calculations from powder diffraction data[21] and single crystal X-ray analysis.[20] The structure is shown (Figure 4.12). This and $Al(HO_3PCH_3)(O_3PCH_3).H_2O$ (Figure 4.12) synthesised[22] by a simple melt reaction between aluminium hydroxide and methylphosphonic acid are lamellar structures in contrast to AlMepO-α and AlMepO-β which are open three dimensional frameworks.

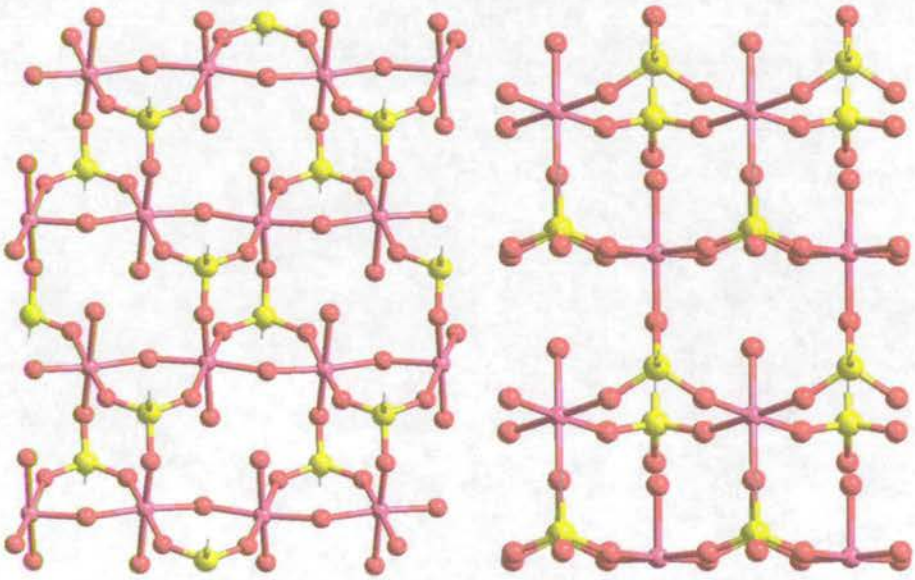

Figure 4.12: Crystal structure of AlMepO-ξ and $Al(HO_3PCH_3)(O_3PCH_3).H_2O$. Al-pink, O-red, P-yellow, C-grey.

Several aluminium phenylphosphonates have been identified including $Al_2(O_3PPh)_3.4H_2O$,[23] $AlH(PhPO_3)_2.H_2O$[24], $Al_2(O_3PPh)_3.H_2O$[25] and six by Bruque *et al*,[26] $Al_2(O_3PPh)_3.2H_2O$, $Al_2(O_3PPh)_3$, α-$Al(HO_3PPh)(O_3PPh).H_2O$, β-$Al(HO_3PPh)(O_3PPh).H_2O$, $Al(HO_3PPh).H_2O$ and $Al(OH)(O_3PPh)$. The compounds were prepared either under reflux conditions or by hydrothermal methods. Of the compounds isolated, the crystal structure has only been determined for α-$Al(HO_3PPh)(O_3PPh).H_2O$ (Figure 4.13) through the use of high resolution powder synchrotron diffraction data.

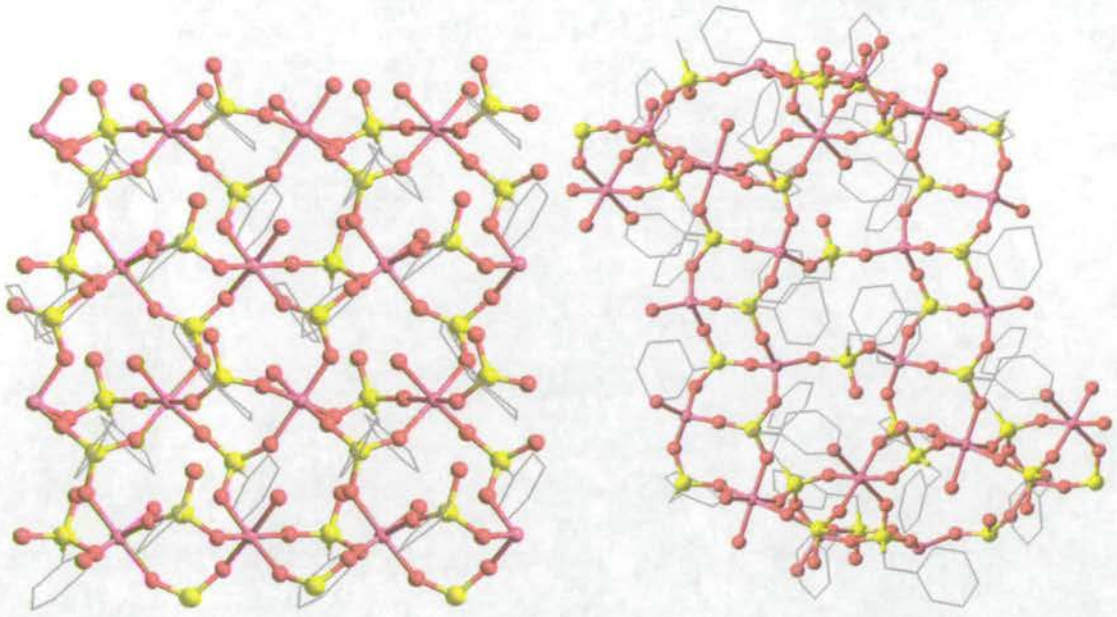

Figure 4.13: Crystal structures of for α-$Al(HO_3PPh)(O_3PPh).H_2O$ and $Al_3H(PO_3CH_2Ph)_5.H_2O$. Al-pink, O-red, P-yellow, C-grey.

Recently, efforts have focused on benzyl phosphonic acid and its 4-bromo-derivative. This has led to the discovery of a new family of aluminium phosphonates including, $Al(OH)(O_3PCH_2C_6H_4Br).H_2O$,[25] $Al(OH)(O_3PCH_2Ph).H_2O$[27] and $Al_3H(PO_3CH_2Ph)_5.H_2O$[27] (Figure 4.13), The latter two have been structurally characterised by powder and single crystal X-ray diffraction respectively. It should be noted that a compound of the same formula, $Al(OH)(O_3PCH_2Ph).H_2O$, has been synthesised[25] by Le Bideau *et al.* However, as its structure was not determined, and given the fact that aluminium phosphonates can exist in more than one polymorph it is impossible to say whether it is the same as that found[27] by Morris *et al.*

The carboxymethylphosphonate $Al(O_3PCH_2CO_2).3H_2O$ was synthesised[28] hydrothermally. Its structure (Figure 4.14) consists of layers made up from square sub-units formed by coordination of two aluminium atoms by two oxygens from each of two PO_3^{2-} units.

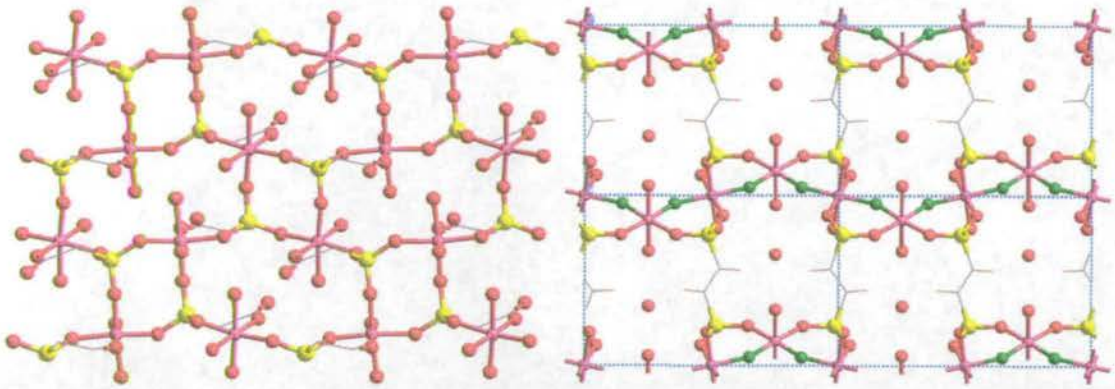

Figure 4.14: Crystal structures of $Al(O_3PCH_2CO_2).3H_2O$ and $Al_2[O_3PC_2H_4PO_3](H_2O)_2F_2.H_2O$ as viewed along the [100] direction. Al-pink, O-red, P-yellow, F-green, C-grey, H-beige.

During the course of writing this thesis Attfield *et al*[29] reported the synthesis and structure of the first aluminium bisphosphonate. $Al_2[O_3PC_2H_4PO_3](H_2O)_2F_2.H_2O$ which was synthesised hydrothermally from a mixture of $Al_2(SO_4)_3.18H_2O$, ethylenediphosphonic acid, HF/pyridine, pyridine and de-ionised water in the molar ratio 1:2.16:8.7:54:144. Its structure (Figure 4.14) consists of chains of corner sharing AlO_4F_2 octahedra linked by bridging fluorine atoms. There are two types of AlO_4F_2 octahedra, the first where the fluorines are in a *trans* configuration, and the second in which they are *cis*.

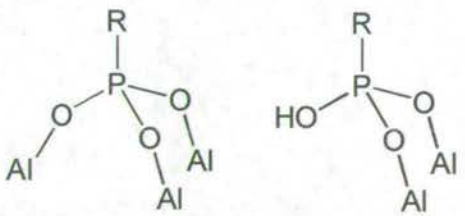

Figure 4.15: Binding modes of phosphonic acids found in aluminium complexes.

Despite the diverse range of structures described in this section, it is clear that there are two predominant binding modes (Figure 4.15) for phosphonates to aluminium. The first involves bonding of all three oxygen atoms to three separate aluminium atoms and occurs when the phosphonate is fully deprotonated (RPO_3^{2-}). In the second mode, the phosphonate is singly deprotonated (RPO_3H^-) and only two oxygen atoms find two separate aluminium atoms forming a 1,3 bridge similar to that found in aluminium phosphinate chemistry. Both of these modes are common in metal phosphonate chemistry.[30]

The only exceptions are the μ_2-O and μ_3-O bridging modes found in the mixed aluminium/alkali metal complexes $[Na_3(THF)(^tBuPO_3AlEt_2)_3]_2$ (Figure 4.9). and $[Cs_3(THF)F(^iBuAl)_3(^tBuPO_3)_4]_2[(^iBuAl)_2Al_2(\mu\text{-}F)_2(^tBuPO_3)_4]$ (Figure 4.10).

4.1.4 Phosphinic and Phosphonic Acids as Surface Ligands.

As previously described (Chapter 1, Section 1.5) phosphoric acid is used extensively in the surface treatment of aluminium. Phosphinic and phosphonic acids have also been studied as corrosion inhibitors/adhesion promoters[31,32] for metal/metal oxide surfaces and there are a number of patents[33] in these areas.

Adler *et al* studied[34,35] a number of compounds of type $C_{18}H_{37}X$ adsorbed on aluminium powder, where X = Br, OH, SH, NH_2, CO_2H, SO_4Na, SO_3Na, $SiOMe(Me)_3$, $Si(OMe)_3$, $N(CH_2PO_3H_2)$, PR_3Br, PO_3H_2 and OPO_3H_2 groups with the aim of replacing the current procedure of pre-treatment of aluminium by chromic acid in order to improve corrosion inhibition and adhesion properties. The compounds were all subjected to three initial screening tests.

The flotation test gives an idea of the adsorption abilities of the ligands and the wetting behaviour of the coated aluminium powder. It is carried out by adding a small amount of aluminium powder to solutions, at different pH, containing the ligand. The behaviour of the powder after 24 hrs is recorded. If the powder has risen to the surface then adsorption has taken place, as the powder has been hydrophobised by the long alkyl chains causing it to try to "escape" the water by floating. If no adsorption has occurred then the powder remains on the bottom. Compounds which are relatively poor adsorbers can also show this effect partly, with some powder floating and the rest remaining on the bottom.

Dynamic contact angle measurements provide information on the wettability of ligand coated aluminium plates. Both advancing and receding angles were measured. For a good surface ligand advancing and receding angles will be the same, however in practice the advancing angle is always higher than the receding angle due to the roughness and inhomogenity of the surface. The best ligand is then the one that displays the smallest difference between the two angles.

Constant humidity climate test measures the corrosion inhibition capability of the ligands. Ligand coated aluminium plates are exposed to a constant humidity climate of 100 % of relative atmospheric humidity for 96 hrs at 40 °C. As the plates corrode they discolour from glossy to grey/black and at the end of the test they are rated by percentage of protected area.

From the initial screening, the two phosphorus head groups, PO_3H_2 and OPO_3H_2 showed the best results, complete flotation, highest hydrophobicity, smallest difference between advancing and receding angle and 90 % protected area and as a result were chosen for further investigation.

The phosphorus compounds were then studied by grazing angle FT-IR spectroscopy, angle dependent XPS and Auger spectroscopy with the results showing that the molecules can form a structured layer on the surface.

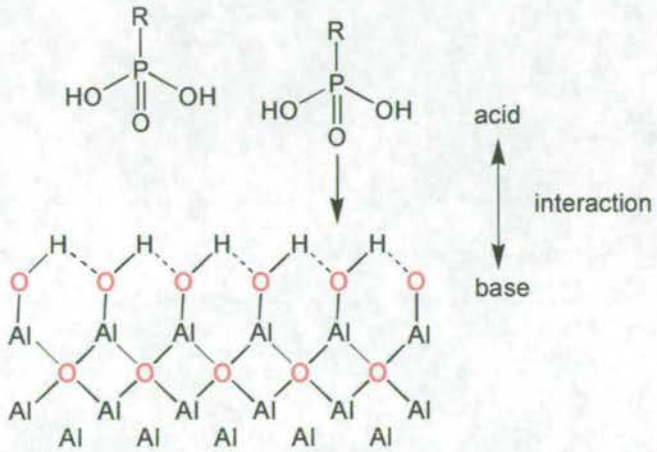

Figure 4.16: Model for the acid base interactions on an aluminium surface as proposed by Adler *et al.*

A model (Figure 4.16) for the adsorption of alkyl-phosphonic and phosphoric acid monoalkyl esters on aluminium surfaces involving an acid-base reaction is proposed. The driving force being the formation of an insoluble surface salt. This implies complex formation. A tridentate binding mode is also proposed based on the absence of P=O and P-OH stretching frequencies.

Previous work[36] within the group at Edinburgh has shown that certain phenolic-phosphonic acids are effective at inhibiting the dissolution of aluminium electrodes under electrochemically oxidative conditions.

4.2 Synthesis of 1st Row Transition metal Phosphinates/Phosphonates.

4.2.1 Melt Reactions Involving Transition Metal Salts.

Melt reactions, where a metal salt is dissolved in molten ligand have proved successful in the past for the synthesis of high nuclearity clusters.[37] This method was used in this work because in their deprotonated (sodium salt) forms, the phosphonic acids tend to be very insoluble in common organic solvents and this rules out use of the simple solution method of forming high nuclearity clusters employed in Chapters 2 and 3.

A series of reactions using cobalt and nickel hydroxide, simple phosphonic acids together with the 6-chloro-2-hydroxypyridonate (Hchp) were carried out both by myself, Dr E. K. Brechin and a project student, P. Marshall. Pyridonates were added to the reactions because they are proven to favour the formation of high nuclearity complexes and would hopefully solubilise the products as, once formed, metal phosphonates are very insoluble. In all cases two equivalents of pyridonate with respect to cobalt were added. The amount of phosphonic acid used was varied between one third and two equivalents. A summary of these reactions is given (Table 4.1).

Metal hydroxide ($M(OH)_2$)	Phosphonic acid (RPO_3H_2)	Amount of phosphonic acid (molar equivalents)
$Co(OH)_2$	$PhPO_3H_2$	$^1/_3$, ½, 1, 2
$Co(OH)_2$	$PhCH_2PO_3H_2$	$^1/_3$, ½, 1
$Co(OH)_2$	$MePO_3H_2$	$^1/_3$
$Co(OH)_2$	$EtPO_3H_2$	$^1/_3$
$Co(OH)_2$	$PrPO_3H_2$	$^1/_3$
$Co(OH)_2$	$^tBuPO_3H_2$	$^1/_3$
$Ni(OH)_2$	$PhPO_3H_2$	$^1/_3$
$Ni(OH)_2$	$PhCH_2PO_3H_2$	$^1/_3$
$Ni(OH)_2$	$MePO_3H_2$	$^1/_3$
$Ni(OH)_2$	$EtPO_3H_2$	$^1/_3$

$Ni(OH)_2$	$PrPO_3H_2$	$^1/_3$
$Ni(OH)_2$	$^tBuPO_3H_2$	$^1/_3$

Table 4.1: Summary of melt reactions carried out (All reactions performed with two equivalents of Hchp).

In general it was found that reactions involving nickel hydroxide formed powders that proved to be almost totally insoluble in common organic solvents.

Products of reactions between cobalt hydroxide and alkyl phosphonic acids were found to be similarly insoluble, whilst for phenyl- and benzylphosphonic acid use of less than half an equivalent of acid with respect to cobalt gave materials that were extractable into solvents such as acetonitrile, THF and ethyl acetate. Use of more than half an equivalent once again gave insoluble material.

Of these reactions, only one produced crystals of X-ray quality giving the tridecanuclear complex $[Co_{13}(OH)_3(H_2O)_2(chp)_{19}(PhPO_3)_2(CH_3C(O)OCH_2CH_3)_2]$ $.2(CH_3C(O)OCH_2CH_3)$. This is discussed further in Section 4.2.3.

4.2.2 Melt Reactions Involving Aluminium Salts.

After the report of Hix *et al*[22] that crystals of $[Al(O_3PCH_3)(HO_3PCH_3).H_2O$ were formed *in situ* from the melt reaction of $Al(OH)_3$ and methylphosphonic acid, a series of melt reaction involving $Al(OH)_3$ and simple phosphinic/phosphonic acids was carried out. However, we were unable to obtain any crystalline material under these conditions and the products from the reactions were insoluble in common organic solvents and therefore could not be recrystallised.

Due to the numerous reports in the literature of organic substituted Keggin and Keggin-like complexes in polyoxometallate chemistry,[38] the aluminium analogue $Na[Al_{13}O(OH)_{24}(H_2O)_{12}](SO_4)_4$, "$Al_{13}$", was prepared via a modified literature method (see Section 4.5.2 for details) and melted with the same series of phosphinic and phosphonic acids. Again the products of the reaction were found to be insoluble. The idea of using Al_{13} Keggin complexes precursors for polynuclear complexes has not been reported before and more success may be gained by using hydrothermal methods, or by carrying out reactions in ionic liquids which may be capable of dissolving the highly cationic Al_{13}, allowing it then to react with the ligands.

4.2.3 Synthesis and Structure of $[Co_{13}(OH)_3(H_2O)_2(chp)_{19}(PhPO_3)_2(CH_3C(O)OCH_2CH_3)_2].2(CH_3C(O)OCH_2CH_3)$.

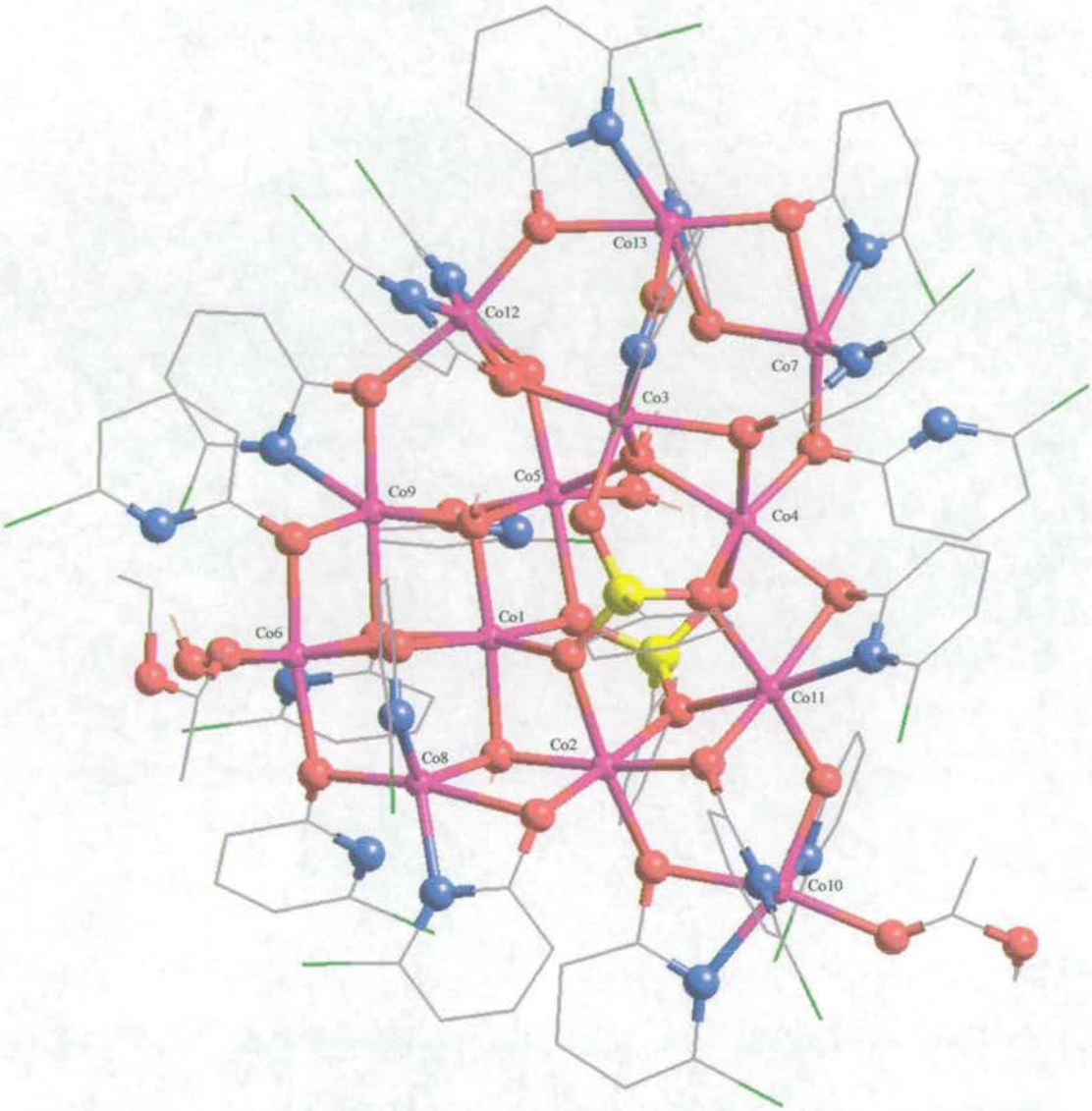

Figure 4.17: Crystal structure of $[Co_{13}(OH)_3(H_2O)_2(chp)_{19}(PhPO_3)_2(CH_3C(O)OCH_2CH_3)_2].2(CH_3C(O)OCH_2CH_3)$

The melt reaction between cobalt hydroxide, two equivalents of 6-chloro-2-hydroxypyridonate (Hchp) and one third equivalent of phenylphosphonic acid gave a purple powder which when extracted with ethyl acetate gave magenta crystals in 10 % yield after a few weeks.

The crystals were found by X-ray analysis to be the tridecanuclear complex $[Co_{13}(OH)_3(H_2O)_2(chp)_{19}(PhPO_3)_2(CH_3C(O)OCH_2CH_3)_2].2(CH_3C(O)OCH_2CH_3)$

whose structure is shown (Figure 4.17). Crystallographic data (Table 23) and significant bond lengths and angles (Table 24) are given in the appendix.

The complex is overall charge neutral with the thirteen cobalt(II) sites balanced by nineteen deprotonated chp ligands, two fully deprotonated phenylphosphonate ligands and three μ_3-hydroxides. Two water molecules and two ethyl acetates complete the coordination around the complex. A summary of the range of values of various types of bond lengths and angles in the coordination sphere of the cobalt atoms are presented (Table 4.2).

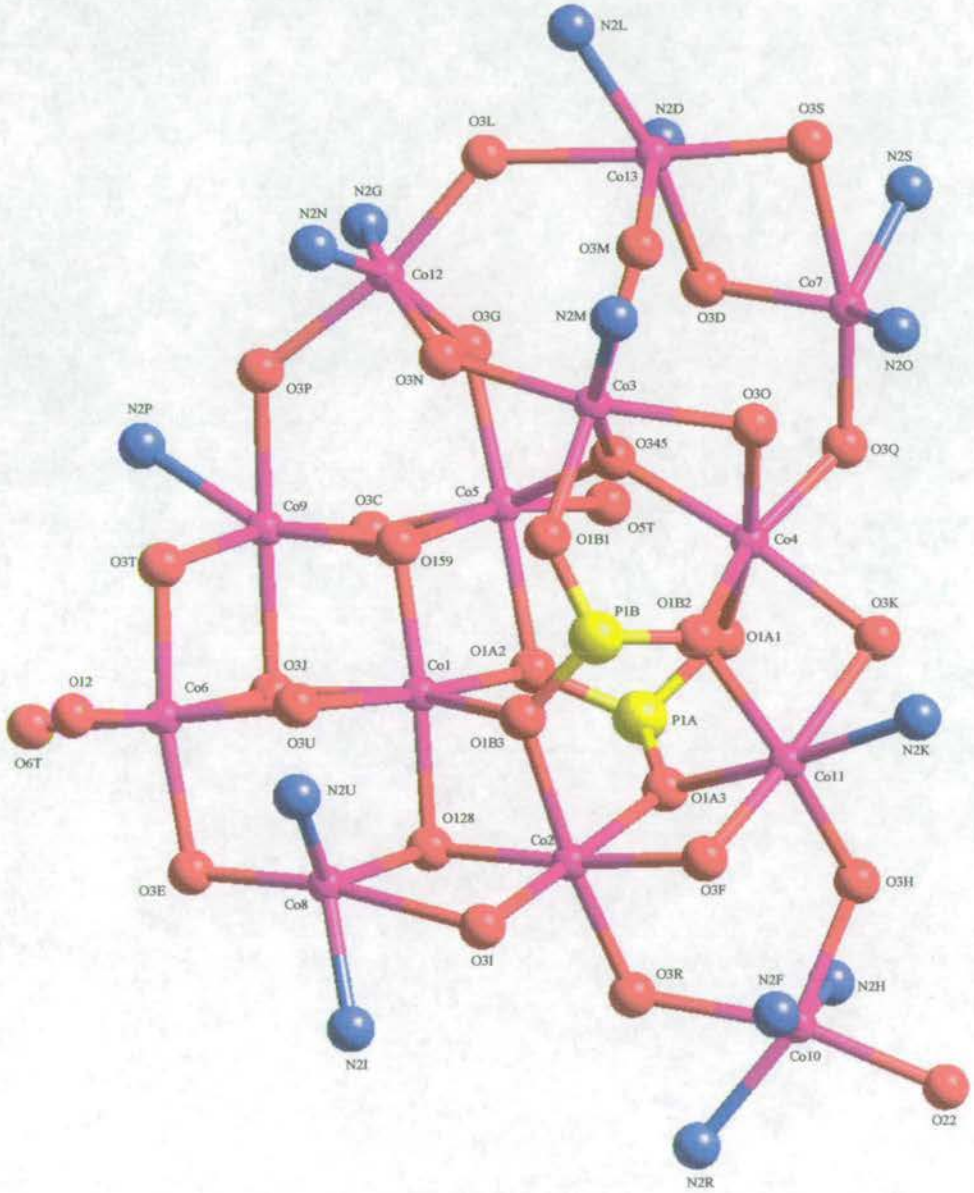

Figure 4.18: Core of $[Co_{13}(OH)_3(H_2O)_2(chp)_{19}(PhPO_3)_2(CH_3C(O)OCH_2CH_3)_2]$. $2(CH_3C(O)OCH_2CH_3)$.

Bond length/angle type	Bond length/angle range, average (Å/°)
Co-N	2.050(15)-2.241(16), 2.138
$Co\text{-}O_{(OH)}$	1.998(10)-2.109(11), 2.054
$Co\text{-}O_{(P)}$	1.988(10)-2.259(11), 2.106
O-Co-N (chelating chp)	59.5(5)-62.9(6), 61.5
$Co\text{-}O_{(P)}\text{-}Co$	95.6(7)-97.0(5), 96.2
$Co\text{-}O_{(OH)}\text{-}Co$	98.8(5)-127.3(5), 106.9
Co-O-Co (μ_2-chp ,chelating)	94.2(4)-131.1(6), 114.6
Co-O-Co (μ_2-chp, non-chelating)	95.1(5)-110.3(6), 102.6
Co-O-Co (μ_3-chp, non-chelating)	91.0(4) 95.5(5) and 98.7(5)

Table 4.2: Significant bond lengths and angles within $[Co_{13}(OH)_3(H_2O)_2(chp)_{19}(PhPO_3)_2(CH_3C(O)OCH_2CH_3)_2]$. $2(CH_3C(O)OCH_2CH_3)$.

The overall structure of the complex is irregular. However there are sections of the core (Figure 4.18) which show some order and can be described more easily. The six cobalt atoms [Co(1), Co(2), Co(5), Co(6), Co(8) and Co(9)] form four face-sharing distorted defective cubanes, each missing one vertex (Figure 4.19). In addition the defective cubane defined by Co(1), Co(6) and Co(8) is missing an edge, the distance between Co(8) and O(3U) at 2.430 Å being to long to be considered a bond. The six cobalt atoms in this portion of the structure are approximately coplanar, with maximum deviation from the least squares plane defined by Co(1), Co(2), Co(5), Co(6), Co(8) and Co(9) being 0.0789 Å and –0.0436 Å for atoms Co(1) and Co(6). The average deviation from the least squares plane is 0.0558 Å. These six cobalt atoms define four tessellated approximately equilateral triangles (Figure 4.20). Attached to this section by a shared vertex, Co(5), is a pentagon defined by Co(4), Co(5), Co(7), Co(12) and Co(13) which is capped by Co(3). The core is completed by a triangle, defined by Co(2), Co(10) and Co(11) attached to the "central" section by the shared vertex, Co(2). This triangle is inclined with respect to the approximately planar "central" section at an angle of 37.2°.

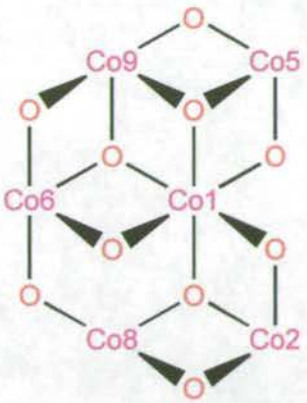

Figure 4.19: Schematic representation of the four face sharing distorted defective cubanes formed by the six cobalt centres (Cobalts 1, 2, 5, 6, 8 and 9).

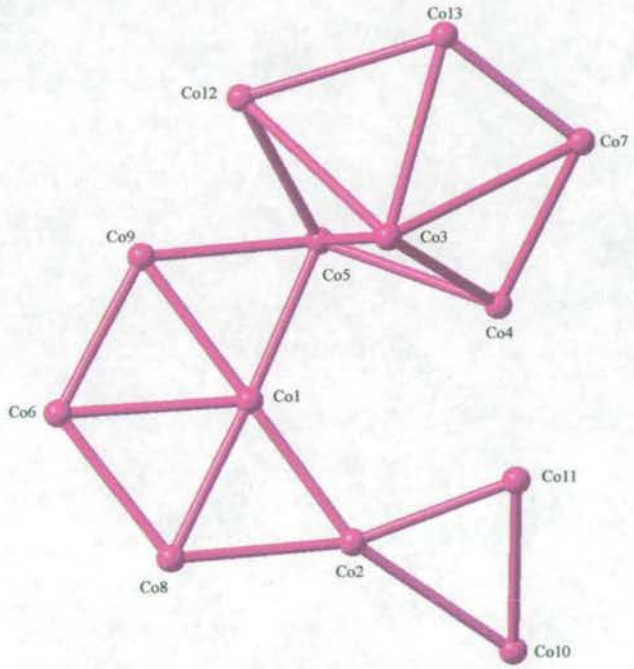

Figure 4.20: View of the metal vertices within $[Co_{13}(OH)_3(H_2O)_2(chp)_{19}(PhPO_3)_2(CH_3C(O)OCH_2CH_3)_2].2(CH_3C(O)OCH_2CH_3)$.

The cobalt sites display five different coordination environments (Figure 4.21), eleven are distorted octahedral and two are trigonal bipyramidal. The octahedral centres with mixed oxygen/nitrogen donor sets are more distorted than those with an all oxygen donor set due to the strain imposed by chelating chp groups. The two trigonal bipyramidal sites both have two nitrogen and three oxygen donors, with the nitrogens in two of the three equatorial positions.

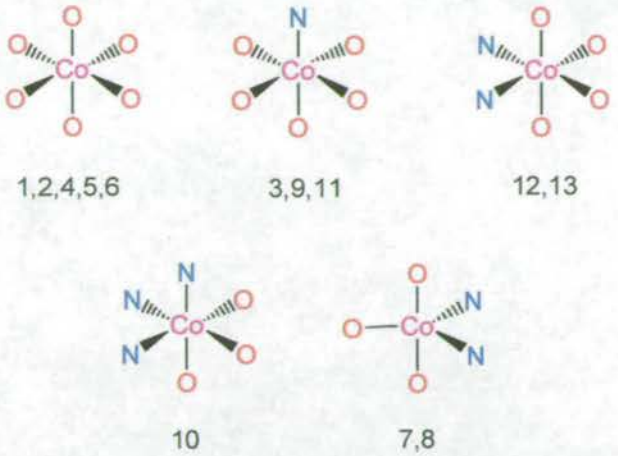

Figure 4.21: Cobalt coordination environments in $[Co_{13}(OH)_3(H_2O)_2(chp)_{19}(PhPO_3)_2(CH_3C(O)OCH_2CH_3)_2].\ 2(CH_3C(O)OCH_2CH_3)$.

The nineteen chp ligands adopt four different coordination modes (Figure 4.22). Two of these involve coordination through the oxygen donor only, bridging two (2.20) and three (3.30) cobalt atoms respectively. The third (3.21) involves the oxygen bridging to two cobalt atoms and the nitrogen is bound to a third cobalt atom. The remaining mode of binding has the oxygen terminally coordinated to one cobalt and, with the nitrogen, chelating a second. This last chelating mode, is the most common in the cluster with eleven of the nineteen chp ligands adopting this arrangement.

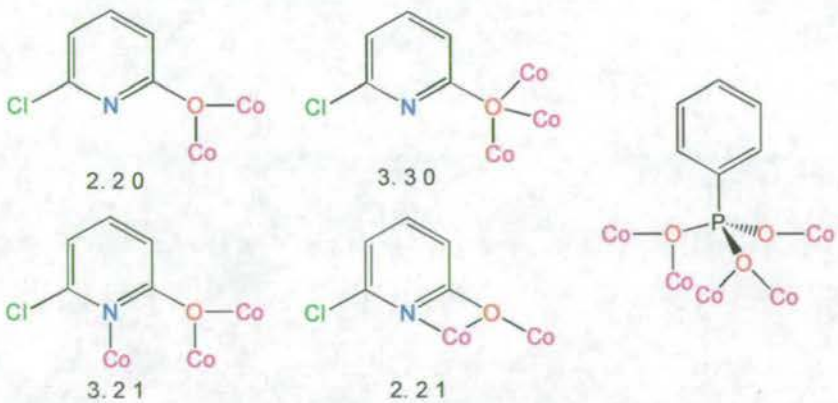

Figure 4.22: Binding modes of chp and phenylphosphonate ligands in $[Co_{13}(OH)_3(H_2O)_2(chp)_{19}(PhPO_3)_2(CH_3C(O)OCH_2CH_3)_2].2(CH_3C(O)OCH_2CH_3)$.

Both phenylphosphonate ligands adopt the same configuration (Figure 4.22), with two oxygens each bridging two cobalts and the remaining oxygen bound to one

cobalt. Thus each phenylphosphonate ligand addresses five cobalt atoms in the core. This is the first example of this coordination mode for cobalt phosphates/phosphonates. There are only seven examples known for other 1st row transition metal phosphonates, four for zinc[39,40,41,42] and three for copper.[43,44]

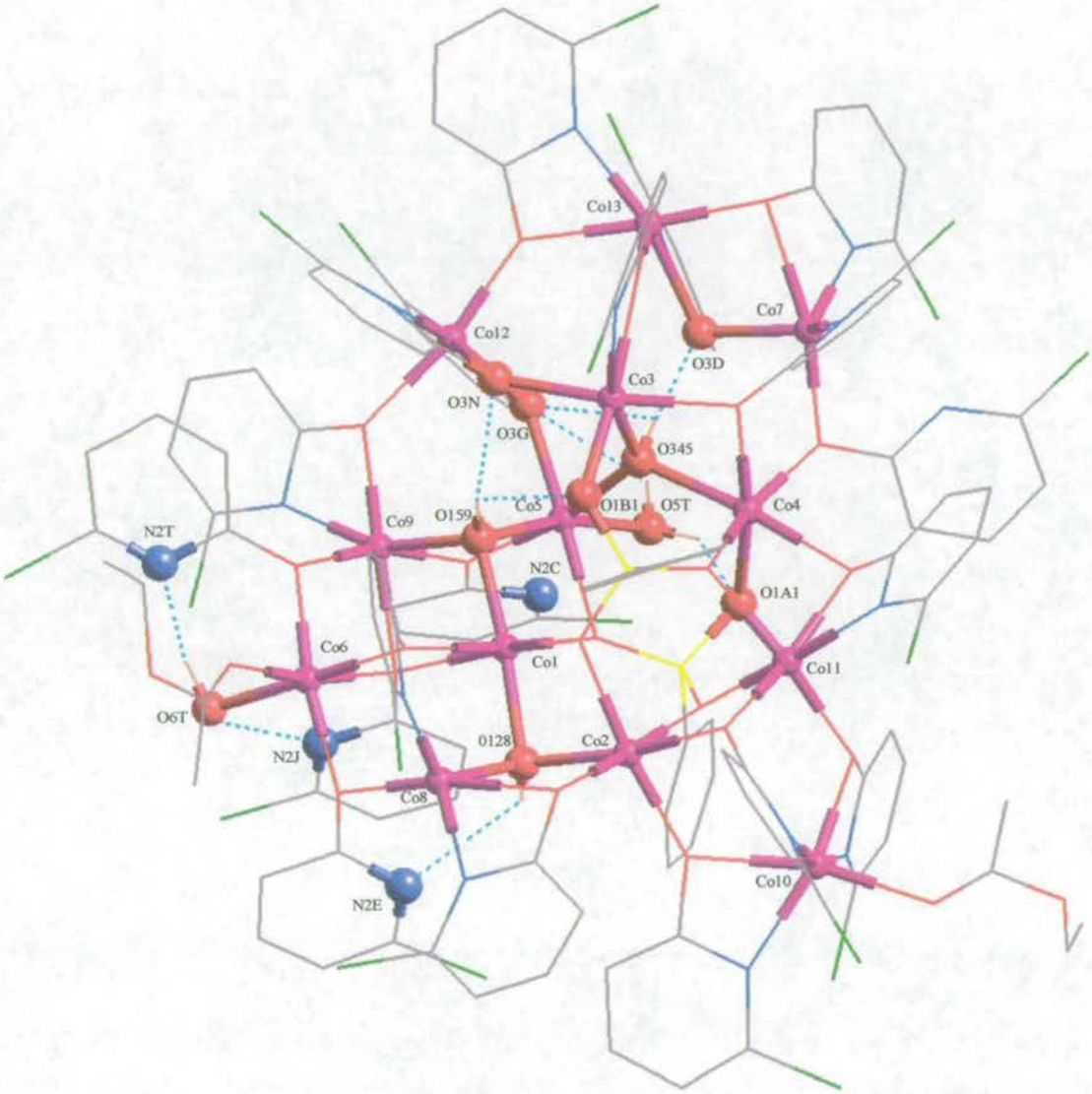

Figure 4.23: Hydrogen bonding in $[Co_{13}(OH)_3(H_2O)_2(chp)_{19}(PhPO_3)_2(CH_3C(O)OCH_2CH_3)_2]$. $2(CH_3C(O)OCH_2CH_3)$.

The hydrogen bonding (Figure 4.23) within the complex is centred around the three hydroxides and the two coordinated water molecules. Hydrogen bond types and distances are listed (Table 4.3).

Of the hydroxides, O(128) forms a bond with a chp nitrogen, N(2E), O(345) has two bonds to chp oxygens, O(3D) and O(3G), and O(159) forms two bonds, one to a chp oxygen, O(3N), and one to a phosphonate oxygen, O(1B1).

The water molecule, O(6T), forms hydrogen bonds with the nitrogens from two neighbouring chp ligands [O(6T)...N(2J) and N(2T)]. The second water molecule, O(5T), sits in a "pocket" where it can form two of three possible hydrogen bonds. The phosphonate oxygen, O(1A1), the chp oxygen, O(3G), and the chp nitrogen, N(2C), are all within hydrogen bonding distance. Analysis of the distances suggests that O(1A1) and N(2C) are the likeliest acceptors however in the crystal the water is probably disordered over the three possible combinations.

Bond type	Donor atom	Acceptor atom	Bond length (Å)
O-H...O	O(128)	N(2E)	3.053
O-H...O	O(159)	O(1B1)	3.060
O-H...O	O(159)	O(3N)	2.891
O-H...O	O(345)	O(3D)	2.735
O-H...O	O(345)	O(3G)	2.857
O-H...O	O(5T)	O(1A1)	2.768
O-H...O	O(5T)	O(3G)	3.050
O-H...N	O(5T)	N(2C)	2.619
O-H...N	O(6T)	N(2J)	2.747
O-H...N	O(6T)	N(2T)	2.706

Table 4.3: Hydrogen bonding in $[Co_{13}(OH)_3(H_2O)_2(chp)_{19}(PhPO_3)_2(CH_3C(O)OCH_2CH_3)_2]$. $2(CH_3C(O)OCH_2CH_3)$.

4.2.4 Preparation of 1st Row Transition Metal Phosphinate/Phosphonate Complexes in the Presence of Urea.

An alternative route to transition metal phosphinates/phosphonates is to utilise the hydrolysis of urea, on heating, in solution to form ammonia thereby slowly raising the pH of a solution containing a metal salt and a phosphinic or phosphonic acid. If the rate of raising pH is controlled the product may crystallise as opposed to simply precipitating out of solution. This method has been used previously to form several transition metal(II) phosphonates with copper[45] chromium[46] and recently iron.[47] A series of reactions was carried out using this general methodology (Figure 4.24) and a summary of these is given (Table 4.4). Full experimental details are given in Section 4.5.2.

$$MX_2.nH_2O + RPO_3H_2 + H_2NC(O)NH_2 \xrightarrow[H_2O,\ 65°C]{NaOH} M(RPO_3).H_2O + 2NH_4X + CO_2\uparrow + (n-1)H_2O$$

Figure 4.24: Preparation of phosphonate complexes in the presence of urea.

Metal Salt	Phosphinic/phosphonic acid ($RPHO_2H/RPO_3H_2$)	Product
$Co(NO_3)_2.6H_2O$	$PhPHO_2H$	Pale pink plate-like crystals, $Co(PhPHO_2)_2.2H_2O$.
$Co(ClO_4)_2.6H_2O$	$PhPHO_2H$	Pale pink plate-like crystals, $Co(PhPHO_2)_2.2H_2O$.
$Ni(NO_3).6H_2O$	$PhPHO_2H$	No precipitate formed.
$Cu(SO_4).5H_2O$	$PhPHO_2H$	Pale blue plate-like crystals and pale blue powder, $Cu(PhPHO_2)_2.3H_2O$.
$Co(SO_4).7H_2O$	$PhCH_2PO_3H_2$	Purple microcrystals, $Co(PhCH_2PO_3).H_2O$.
$Co(NO_3)_2.6H_2O$	$PhCH_2PO_3H_2$	Purple microcrystals, $Co(PhCH_2PO_3).H_2O$.
$Ni(SO_4).6H_2O$	$PhCH_2PO_3H_2$	Yellow powder, $Ni(PhCH_2PO_3).H_2O$.
$Cu(SO_4).5H_2O$	$PhCH_2PO_3H_2$	Pale blue microcrystals, $Cu(PhCH_2PO_3).H_2O$.

$Cr(NO_3)_3.9H_2O$	$PhPO_3H_2$	Immediate insoluble white precipitate on mixing.
$Fe(NO_3)_3.9H_2O$	$PhPO_3H_2$	Immediate insoluble white precipitate on mixing.
$Al_2(SO_4)_3.18H_2O$	$PhPO_3H_2$	White microcrystals, $Al_2(PhPO_3)_3.H_2O$.

Table 4.4: Summary of urea reactions carried out.

Diphenylphosphinic acid proved to be too insoluble for the conditions used therefore only phenylphosphinic acid was used in this type of experiment. Only five structures have so far been reported for 1st row transition metal complexes containing phenylphosphinic acid, two manganese,[48] one mixed manganese/cadmium,[49] one mixed cobalt/cadmium[49] and one vanadium.[50]

For the reactions involving phenylphosphinic acid, very thin plate-like crystals were obtained for copper and cobalt. Unfortunately these diffracted poorly and therefore no structure could be obtained. Infra-red spectroscopy confirmed that the phosphinic acid P-H group (lit. $\nu_{P\text{-}H} \sim 2440 - 2350$ cm^{-1})[51] had been retained in both compounds and not hydrolysed to phosphonic acid. $Cu(PhPHO_2).3H_2O$ gave one sharp peak ($\nu_{P\text{-}H}$ 2421(m) cm^{-1}) consistent with one phosphinic acid environment while $Co(PhPHO_2).2H_2O$ revealed two sharp peaks ($\nu_{P\text{-}H}$ 2391(m) and 2370(m) cm^{-1}) suggesting that two different phosphinic acid environments are present in the compound. No crystals were obtained from reactions with nickel(II) sulfate and precipitation could only be induced by the addition of excess sodium hydroxide, leading to an uncharacterisable green powder in this case.

Benzylphosphonic acid was chosen, as in contrast to other simple phosphonic acids such as phenyl, methyl, and ethyl, there are currently no reported structures with 1st row transition metals. In fact with the exception of the aluminium benzylphosphonates reported in Section 4.1.3, there are no crystal structures of metal complexes of benzylphosphonic acid reported at this time.

The reactions involving benzylphosphonic acid gave compounds of formula $M(PhCH_2PO_3).H_2O$, where M = Co, Ni and Cu. This is consistent with other reported 1st row transition metal phosphonates of general formula $M(II)(RPO_3).H_2O$, where M = Cr, Mn, Fe, Co, Zn and Cu.[46,52]

Preliminary powder diffraction studies were performed on the three benzylphosphonate samples. However, these provided little extra information.

Attempts to extend this chemistry to other metals were generally unsuccessful, iron(III) and chromium(III) salts both giving immediate insoluble white precipitates on contact with phenylphosphonic acid.

An aluminium phosphonate, $Al_2(PhPO_3)_3.H_2O$ was synthesised. However as this is the same composition as a known compound,[25] no further analysis was carried out.

4.3 Isotherm Studies.

Data for the calibration and isotherm experiments in this section are given in the appendix, Tables 41-50.

The UV/vis spectra of all ligands were recorded in 95/5 % methanol/water and their extinction coefficients determined (Table 4.5) using the Beer-Lambert Law.

Compound	UV/vis bands, λ (nm)	Extinction coefficient ε
phenylphosphinic acid	212	8290(150)
diphenylphosphinic acid	202, 223	14840(120), (λ = 223)
phenylphosphonic acid	210 258, 264, 270	8540(120), (λ = 210)
benzylphosphonic acid	210	8480(140)
4-nitrobenzylphosphonic acid	203, 216, 283	10090(50), (λ = 283)

Table 4.5: Electronic spectra for ligands in 95 % methanol/water (standard deviations in parenthesis).

The adsorption isotherms were determined as described in Section 4.5.3 and are plotted in (Figure 4.25) and (Figure 4.26)

Examination of the isotherms (Figure 4.25) for phenylphosphinic and diphenylphosphinic acid reveals that, as expected, both have similar equilibrium adsorption constants (Table 4.6) and therefore binding strength. As for the carboxylic acids Irg-419 and Irg-78 (see Chapter 3) the *S* curve shape of the isotherms for both

of the phosphinic acids at low concentrations are consistent with cooperative binding on the $Al(OH)_3$ surface. The effect is more pronounced than was the case for the carboxylic acids. Phenylphosphinic acid has a required surface area of 31(2) $Å^2$ $molecule^{-1}$, calculated from the monolayer coverage (Table 4.6), determined by the Langmuir isotherm model. This is approximately equivalent to that of Irg-419 (33 $Å^2$ $molecule^{-1}$, Chapter 3), while the value for the bulkier diphenylphosphinic acid is lower at 38(2) $Å^2$ $molecule^{-1}$. Examination of the graphs show that these figures may be on the low side as the isotherms appear to be reaching a plateau at packing densities of 3×10^{-5} mol g^{-1} and 2.5×10^{-5} mol g^{-1} respectively. Using these numbers gives occupied surface area values for phenlyphosphinic and diphenylphosphinic acid of 39 and 47 $Å^2$ $molecule^{-1}$ respectively.

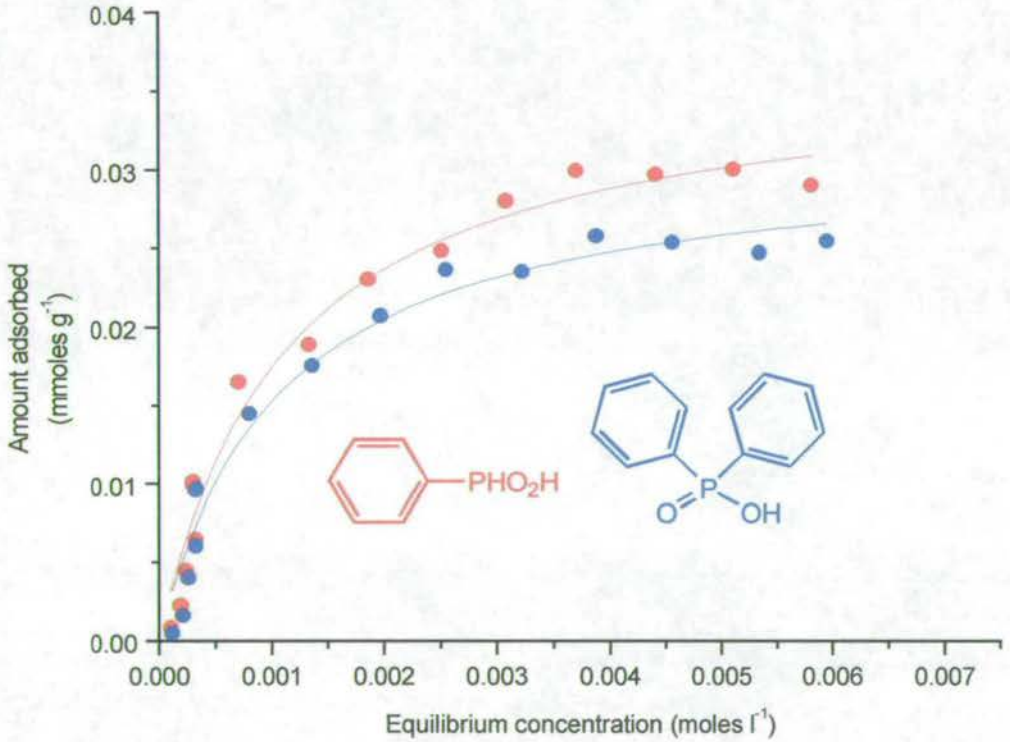

Figure 4.25: Adsorption isotherms for phenylphosphinic (red) and diphenylphosphinic acid (blue).

The isotherm (Figure 4.26) for phenylphosphonic acid gives a calculated occupied surface area of 35(1) $Å^2$ $molecule^{-1}$. Molecular modelling work[53] has indicated that this is close to the maximum possible loading of the $Al(OH)_3$ used. The steepness of the early part of this isotherm and the equilibrium constant obtained

suggest that phosphonic acids have a much stronger binding than both carboxylic and phosphinic acids while retaining comparable surface coverage.

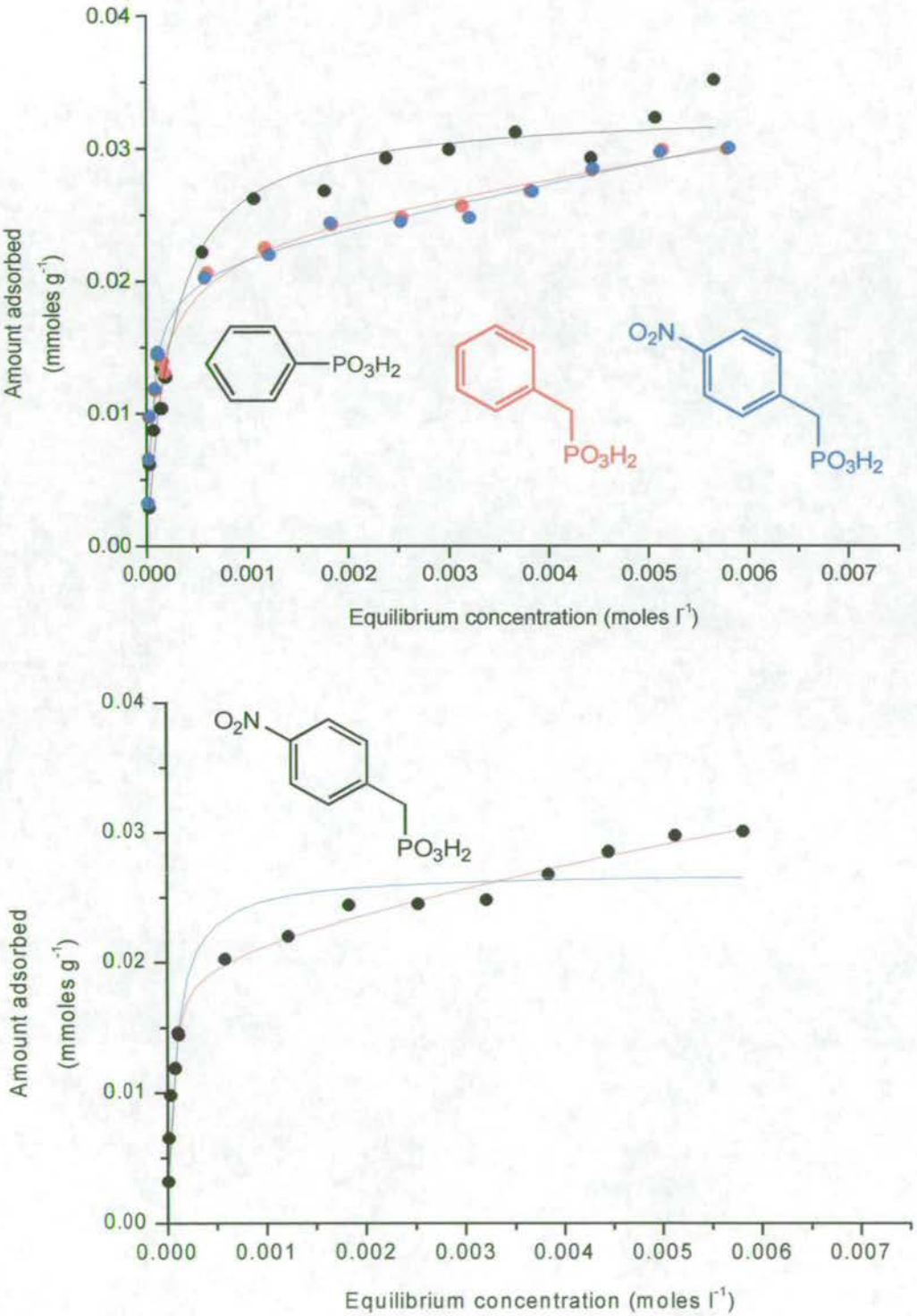

Figure 4.26: Top - Adsorption isotherms for phenylphosphonic (black), benzylphosphonic (red) and 4-nitrobenzylphosphonic acid (blue). Bottom - Adsorption isotherm for 4-nitrobenzylphosphonic as fitted to the simple Langmuir model (blue) and the double Langmuir model (red)

The two isotherms (Figure 4.26) for benzyl and 4-nitrobenzylphosphonic acid are very similar within experimental error, indicating that the electron withdrawing *para*-nitro group has no appreciable effect on the binding strength or surface coverage of the ligand. The shapes of the isotherms indicate that two different binding modes are occurring at different concentrations. Indeed the data does not fit the simple Langmuir model. Instead both curves can be fitted to the double Langmuir function which is a "two site" model. Due to their nature it is difficult to compare equilibrium constant values between the two models. Examination of the low concentration region of the isotherms ($<0.5 \times 10^{-3}$ moles l^{-1}) reveals a similar slope to phenylphosphonic acid indicating comparable binding strength. Estimation of the surface coverage of the two ligands is difficult because within the concentration range of the experiment the curves appear to be extending to infinity. Previously for this type of curve, limiting values of adsorption have been obtained by extrapolating the isotherm to the limit of solubility for the system.[54] However this method was not deemed appropriate for these systems.

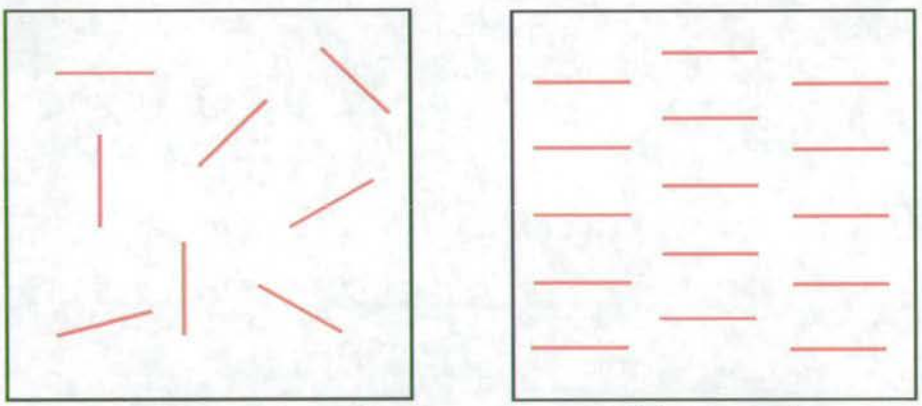

Figure 4.27: Schematic representation of disordered nature of the benzyl groups arranged on the $Al(OH)_3$ surface at low concentration, becoming more ordered at higher concentrations.

One possible explanation for the shape of the graphs is the creation of an ordered monolayer at higher concentrations. At low concentrations the free rotation of the benzyl group means that it can adopt any conformation, while at higher concentrations the need to pack more molecules onto the surface forces the arrangement of the benzyl groups to become more ordered (Figure 4.27) due to the

restrictions of neighbouring molecules. This may also be accompanied by a rearrangement of the phosphonate groups on the surface to maximise the surface coverage of the ligand. This rearrangement would explain the gentle slope seen after the steep initial phase. Curve fitting gives the surface coverages for this initial binding mode of 1.4(2) × 10^{-5} mol g^{-1} and 2.0(1) × 10^{-5} mol g^{-1} for benzyl and 4-nitrobenzylphosphonic acid respectively. These give required surface areas of 83(12) and 58(3) $Å^2$ $molecule^{-1}$, approximately two to three times that of phenylphosphonic acid. Monolayer coverage for the second binding mode has not been reached under the experimental conditions used here but appears likely to be comparable with that of phenylphosphonic acid. Some evidence for this theory can be gained from the crystal structure of $Al_3H(PO_3CH_2Ph)_5.H_2O$, (Figure 4.13, Section 4.1.3) in which the benzyl groups are found to be severely disordered.

Compound	Amount of ligand adsorbed at monolayer coverage (n_M) 10^5 [mol g^{-1}]		Equilibrium adsorption constant (K) 10^{-3} [L mol^{-1}]	
	Langmuir	Double Langmuir	Langmuir	Double Langmuir
phenylphosphinic acid	3.7(2)	-	0.9(1)	-
diphenylphosphinic acid	3.1(2)	-	1.0(1)	-
phenylphosphonic acid	3.3(1)	-	3.9(5)	-
benzylphosphonic acid	-	n_1 1.4(2) n_2 1.9(2)	-	K_1 40(15) K_2 0.6(3)
4-nitrobenzylphosphonic acid	-	n_1 2.0(1) n_2 4(4)	-	K_1 25(5) K_2 0.06(6)

Table 4.6: Adsorption isotherm data (standard deviations in parenthesis).

4.4 Conclusions.

The review of the literature surrounding aluminium(III) phosphinates/phosphonates revealed that while this branch of chemistry is attracting much interest it is still a relatively young and developing area. Complexes with well-defined structures are still rare and in general are made by specialist methods. The defined structures of aluminium(III) phosphonates confirm that the ligands are polynucleating, showing two binding modes. Many of the structures are layered, suggesting that similar complexes could be formed at the surface and that simple phosphonic acids are likely to be good surface ligands.

We were unable to crystallise any aluminium phosphinates/phosphonates but the novel cobalt cluster $[Co_{13}(OH)_3(H_2O)_2(chp)_{19}(PhPO_3)_2(CH_3C(O)OCH_2CH_3)_2]$ $.2(CH_3C(O)OCH_2CH_3)$ was prepared and its structure determined. The coordination mode of the phosphonic acids in the cluster does not match known phosphonate coordination modes in aluminium complexes.

The proposition that phosphinic and phosphonic acids will act as strong surface ligands is supported by isotherm studies which revealed that both classes of compound bind more strongly to $Al(OH)_3$ than the other ligands (pyridonates and carboxylates) studied so far. Phosphonic acids in particular appear to be excellent ligand candidates for aluminium oxide surfaces and should be capable of improvement by further development. This theme is considered in Chapter 5.

4.5 Experimental.

4.5.1 Chemicals and Instrumentation.

All reagents were used as obtained from Aldrich, Acros or Lancaster except 4-nitrobenzylphosphonic acid, which was prepared by Dr D. Nation. Solvents were used as received. High surface area "superfine $Al(OH)_3$" was supplied by Alcan. Water was distilled before use.

Analytical data were obtained on a Perkin-Elmer 2400 Elemental analyser by the University of Edinburgh Microanalytical Service.

Fast atom bombardment mass spectrometry (FABMS) was carried out using a Kratos MS50TC spectrometer a 3-nitrobenzyl alcohol (NOBA) or thioglycerol matrix.

The infra-red spectra were obtained as potassium bromide discs using a Perkin Elmer Paragon 1000 FT-IR spectrometer.

Electronic spectra were measured on an ATI UNICAM UV/vis spectrometer with 1cm path length quartz cuvettes.

Curve fitting were performed using the programs Origin 5.0 © Microcal Software Inc and SigmaPlot 2000 (demo version) © 1986-2000 SPSS Inc.

Crystal data were collected on a Bruker Smart APEX CCD area detector equipped with an Oxford Cryosystems low-temperature device. Full listings of atomic positions and thermal parameters are provided electronically on the CD accompanying this thesis.

4.5.2 Synthesis.

$[Co_{13}(OH)_3(H_2O)_2(chp)_{19}(PhPO_3)_2(CH_3C(O)OCH_2CH_3)_2]$. $2(CH_3C(O)OCH_2CH_3)$.

$Co(OH)_2$ (0.50 g, 5.4 mmol), phenylphosphonic acid (0.28 g, 1.8 mmol) and 6-chloro-2-hydroxypyridonate (1.40 g, 10.8 mmol) were mixed thoroughly and added to a Schlenk tube. The tube was placed under vacuum, filled with nitrogen and heated under a constant flow of nitrogen to 140 °C. Upon heating, the mixture changed colour from pale pink to purple. The reaction was heated at 140 °C for a further hour to ensure completion then cooled to room temperature. The purple powder formed was extracted with ethyl acetate, filtered to remove insoluble material and the resultant solution left to stand at room temperature. The solution gave magenta crystals after a few weeks which were determined by X-ray analysis to be $[Co_{13}(OH)_3(H_2O)_2(chp)_{19}(PhPO_3)_2(CH_3C(O)OCH_2CH_3)_2].2(CH_3C(O)OCH_2CH_3)$. Yield (10 %).

(Found: C, 36.0; H, 2.2; N, 7.6; $C_{111}H_{82}Cl_{19}Co_{13}N_{19}O_{32}P_2$ (Corresponds to complex minus two ethyl acetates.) requires C, 36.0; H, 2.2; N, 7.2 %); IR (cm^{-1}, KBr disc) ν 3423(br)w (OH), 3081w (CH), 1736w, 1649w, 1597s, 1442s (PPh), 1404m, 1340m, 1238w, 1169m, 1140w, 1120w, 1004m, 933m, 859w, 786m, 755w, 731w, 718w, 699w, 571w, 541w.

$Na[Al_{13}O_4(OH)_{24}(H_2O)_{12}](SO_4)_4$.

$AlCl_3.6H_2O$ (25 ml of a 0.5M solution) was heated to 80 °C. NaOH (60 ml of a 0.5M solution) was added dropwise with stirring, allowing the solution to clarify after each addition and maintaining the temperature at around 80 °C. The reaction was stirred for a further 30 min, then allowed to cool to room temperature. The clear solution was added to a Na_2SO_4 solution (175 ml of a 0.5M solution). If necessary at this stage the solution was filtered through glass fibre microfilter paper to clarify it. The solution was then transferred to a crystallising dish, covered with a watch glass and left to stand. Crystallisation was generally complete after 2-3 days and the small colourless tetrahedral crystals that formed were filtered and washed with distilled water. Typical yield for the reaction was around 1 g.

IR (cm^{-1}, KBr disc) ν 3402(br)s (OH), 1647m, 1088s (S=O), 726s (Al-O tetrahedral), 624s (Al-O octahedral), 487s (Al-OH_2 octahedral).

$Co(PhPHO_2)_2.2H_2O$.

$PhPHO_2H$ (0.80 g, 5.6 mmol) was dissolved in distilled water (20 ml) using NaOH (2 ml of a 1M solution). This was added to a solution of $Co(ClO_4)_2.6H_2O$ (1.03 g 2.8 mmol) in distilled waster (20 ml) and NaOH (4 ml of a 1M solution) added portionwise until the precipitate which formed did not redissolve. A few drops of dilute HCl (~ 1M solution) was added to clarify the solution and it was filtered into a thick walled test tube. Urea (0.50 g, 8.3 mmol) was added and the tube sealed and heated to 65 °C. Pink plate-like crystals were formed overnight (0.65 g, 30.8 %).

(Found: C, 37.7; H, 4.2; $C_{12}H_6CoO_6P_2$ requires C, 38.2; H, 4.2 %); IR (cm^{-1}, KBr disc) ν 3306s (OH), 3053m (CH), 2391m (PH), 2370m (PH), 1973w, 1920w,

1883w, 1706m, 1590m, 1484m, 1437s (PPh), 1325w, 1140s & 1057s (P-O), 1031m, 1024s, 980s, 763m, 753m, 743s, 707m, 692s, 555s, 482m.

$Cu(PhPHO_2)_2.3H_2O$.

$Cu(SO_4).5H_2O$ (1.00 g, 4.0 mmol) and $PhPHO_2H$ (1.14 g, 8.0 mmol) were dissolved in distilled water (40 ml) and NaOH (8 ml of a 1M solution) added portionwise. The solution was filtered into a thick walled test tube, urea (0.50 g, 8.3 mmol) added and the tube sealed and heated to 65 °C. The product was obtained as a mixture of pale blue plate-like crystals and pale blue powder after a few days (0.32 g, 20 %).

(Found: C, 35.2; H, 4.6; $C_{12}H_{18}CuO_7P_2$ requires C, 36.0; H, 4.5 %); IR (cm^{-1}, KBr disc) ν 3425s (OH), 3126s (CH), 2421m (PH), 1963w, 1901w, 1830w, 1700w, 1645m, 1593w, 1560w, 1487w, 1436m (PPh), 1313w, 1142s & 1044s (P-O), 1024m, 1004m, 986s, 854w, 749m, 708m, 695s, 565s, 473m.

$Co(PhCH_2PO_3).H_2O$.

$Co(SO_4).7H_2O$ (1.46 g, 5.2 mmol) and $PhCH_2PO_3H_2$ (0.90 g, 5.2 mmol) were dissolved in distilled water (50ml) and the solution filtered into a Schlenk tube. Urea (0.48 g, 8 mmol) was added and the solution heated to 65°C. No change was observed after five days at 65°C, therefore NaOH (8 ml of a 1M solution) was added portionwise to the solution and additional urea (0.48 g, 8 mmol) added. The product formed overnight as purple microcrystals (0.31 g, 24 %).

(Found: C, 34.0; H, 3.6; $C_7H_9CoO_4P$ requires C, 34.0; H, 3.6 %); IR (cm^{-1}, KBr disc) ν 3458s (OH), 3086w (CH), 3059w (CH), 3026w (CH), 1602m, 1495m, 1452w, 1419w, 1262w, 1095s, 1007m, 962s, 834w, 788m, 730w, 702s, 670w, 614, 551m, 534m, 496m.

$Cu(PhCH_2PO_3).H_2O$.

$Cu(SO_4).5H_2O$ (1.30g, 5.2 mmol) and $PhCH_2PO_3H_2$ (0.90g, 5.2 mmol) were dissolved in distilled water (50ml) and the solution filtered into a Shlenk tube. Urea

(0.48 g, 8.0 mmol) was added and the solution heated to 65°C. The product formed overnight as blue microcrystals (0.35 g, 27 %).

(Found: C, 33.4; H, 3.5; $C_7H_9CuO_4P$ requires C, 33.4; H, 3.6 %); IR (cm^{-1}, KBr disc) ν 3212m (OH), 3059m (CH), 1574w, 1496w, 1453w, 1409w, 1259w, 1142w, 1077s, 1061s, 1033s, 876w, 786w, 723w, 704w, 619w, 554w, 513w.

$Ni(PhCH_2PO_3).H_2O$.

$Ni(SO_4).6H_2O$ (1.37 g, 5.2 mmol) and $PhCH_2PO_3H_2$ (0.90 g, 5.2 mmol) were dissolved in distilled water (50 ml) and the solution filtered into a Shlenk tube. Urea (0.48 g, 8.0 mmol) was added and the solution heated to 65 °C. No change was observed after five days at 65 °C, therefore NaOH (10 ml of a 1M solution) was added portionwise to the solution and additional urea (0.48 g, 8 mmol) added. The product formed overnight as a yellow powder (0.28 g, 22 %).

(Found: C, 34.0; H, 3.6; $C_7H_9NiO_4P$ requires C, 34.0; H, 3.6 %); IR (cm^{-1}, KBr disc) ν 3450s (OH), 3086w (CH), 3059w (CH), 3026w (CH), 1624w, 1496w, 1453w, 1420w, 1265w, 1089s, 994s, 971s, 831w, 786w, 703m, 617w, 554m, 543m.

4.5.3 Adsorption isotherm measurements.

Preweighed quantities of $Al(OH)_3$ (0.40 g) in polycarbonate centrifuge tubes were stirred with the desired concentration of ligand in methanol/water (10ml, 95:5 v/v) for 2 h at 25 °C. The suspensions were centrifuged and filtered, and the supernatant diluted if necessary, for absorbance measurement by UV spectrometry. The measured absorbance was related to the concentration of the ligand remaining in solution by reference to calibration curves. The amount of ligand adsorbed was then calculated from the difference between initial and final concentration. From this plots of amount of ligand adsorbed versus equilibrium concentration were obtained.

4.6 References.

1 An Introduction to Zeolite Molecular Sieves by A. Dyer, published by John Wiley & Sons, 1988

2 S. T. Wilson, B. M. Lok, C. A. Messina, T. R. Cannan and E. M. Flanigen, *J. Am. Chem. Soc.*, 1982, **104**, 1146.

3 K. Maeda, Y. Kiyozumi and F. Mizukami, *Angew. Chem. Int. Ed. Engl.*, 1994, **33**, 2335.

4 M. G. Walawalker, H. W. Roesky and R. Murgugavel, *Acc. Chem. Res.*, 1999, **32**, 117.

5 G. E. Coates and R. N. Mukherjee, *J. Chem. Soc.*, 1964, 1295.

6 H. Olapinski, B. Schaible and J. Weidlein. *J. Organomet. Chem.*, 1972, **43**, 107.

7 M. R. Mason, *J. Cluster. Sci.*, 1998, **9**, 1.

8 J. M. Corker, D. J. Browning and M. Webster, *Acta Crystallogr., Sect. C (Cr. Str. Comm.)*, 1996, **52**, 583.

9 S. A. Sangokoya, W. T. Pennington, G. H. Robinson and D. C. Hrncir, *J. Organomet. Chem.*, 1990, **385**, 23.

10 Y. Wang, S. Parkin and D. Atwood, *Chem. Commun.*, 2000, 1799.

11 Y. Yang, H. Schmidt, M. Noltemeyer, J. Pinkas and H. W. Roesky, *J. Chem. Soc., Dalton Trans.*, 1996, 3609.

12 Y. Yang, M. G. Walawalkar, J. Pinkas, H. W. Roesky and H. Schmidt, *Angew. Chem., Int. Ed. Engl.*, 1998, **37**, 96.

13 D. Chakraborty, S. Horchler, H. W. Roesky, M. Noltemeyer and H-G. Schmidt, *Inorg. Chem.*, 2000, **39**, 3995.

14 D. Wulff-Molder and T. Meisel, *Z. Kristallogr.-New Crystal Structures*, 1998, **213**, 353.

15 Y. Yang, J. Pinkas, M. Noltemeyer and H. W. Roesky, *Inorg.Chem.*, 1998, **37**, 6404.

16 Y. Yang, J. Pinkas, M. Schafer and H. W. Roesky, *Angew. Chem., Int. Ed. Engl.*, 1998, **37**, 2650.

17 K. Maeda, J. Akimoto, Y. Kiyozumi and F. Mizukami, *Chem. Commun.*, 1995, 1033.

18 K. Maeda, J. Akimoto, Y. Kiyozumi and F. Mizukami, *Angew. Chem., Int. Ed. Engl.*, 1995, **34**, 1199.

19 V. J. Carter, P. A. Wright, J. D. Gale, R. E. Morris, E. Saestre and J. Perez-Pariente, *J. Mater. Chem.*, 1997, **7**, 2287.

20 K. Maeda, Y. Hashiguchi, Y. Kiyozumi and F. Mizukami, *Bull. Chem. Soc. Jpn.*, 1997, **70**, 345.

21 L-J. Sawers, V. J. Carter, A. R. Armstrong, P. G. Bruce, P. A. Wright and B. E. Gore, *J. Chem. Soc., Dalton Trans.*, 1996, 3159.

22 G. B. Hix, V. J. Carter, D. S. Wragg, R. E. Morris and P. A. Wright, *J. Mater. Chem.*, 1999, **9**, 179.

23 L. Raki and C. Detellier, *Chem. Commun.*, 1996, 2475.

24 J. E. Haky, J. B. Brady, N. Dando and D. Weaver, *Mater. Res. Bull.*, 1997, **32**, 297.

25 G. Chaplais, J. Le Bideau, D. Leclercq, H. Mutin and A. Vioux, *J. Mater. Chem.*, 2000, **10**, 1593.

26 A. Cabeza, M. A. G. Aranda, S. Bruque, D. M. Poojary, A. Clearfield and J. Sanz, *Inorg. Chem.*, 1998, **37**, 4168.

27 N. Zakowsky, G. B. Hix, and R. E. Morris, *J. Mater. Chem.*, 2000, **10**, 2375.

28 G. B. Hix, D. S. Wragg, P. A. Wright and R. E. Morris, *J. Chem. Soc., Dalton Trans.*, 1998, 3359.

29 H. G. Harvey, S. J. Teat and M. P. Attfield, *J. Mater, Chem.*, 2000, **10**, 2632.

30 A. Clearfield, in *Progress in Inorganic Chemistry*, ed. K. D. Karlin, Wiley, 1998, **47**, 371.

31 A. N. Rider and D. R. Arnot, *Surface and Interface Analysis*, 1996, **24**, 583.

32 G. D. Davies, J. S. Ahearn, L. J. Matienzo, J. D. Venables, *Journal of Materials Science*, 1985, **20**, 975.

33 a) K. Wefers, G. A. Nitowski and L. F. Wieserman, *US Patent* 5,132,181, Aluminum Company of America, 1992. b) S. M. Opalka, *US Patent* 6,120,618, Alcoa Inc, 2000. c) Z. Vachlas and S. J. Thorne, *US Patent* 4,916,176, Imperial Chemical Industries, 1990. d) P. H. Lamers, A. Park, K. G. Olson, J.

E. Poole and D. W. Maier, *US Patent* 5,429,674, PPG Industries, 1995. e) C. F. Kahle, *US Patent* 5,034,556, PPG Industries, 1991. f) L. F. Wieserman, J. W. Novak, C. M. Conroy and K. Wefers. *US Patent* 478,6,628, Aluminum Company of America, 1988. g) J. D. Venables, M. E. Tadros, B. M. Ditchek, *US Patent* 4,308,079, Martin Marietta Corporation, 1980.

34 I. Maege, E. Jaehne, A. Henke, H-J. P. Adler, C. Bram, C. Jung and M. Stratmann, *Macromol. Symp*, 1997, **126**, 7.

35 I. Maege, E. Jaehne, A. Henke, H-J. P. Adler, C. Bram, C. Jung and M. Stratmann, *Progress in Organic Coatings*, 1998, **34**, 13.

36 P. A. Lovatt, *Synthesis of Novel Polynucleating Ligands for Lightly Oxidised Aluminium Surfaces*, Project Report, The University of Edinburgh, 1998.

37 S. Parsons and R. E. P. Winpenny. *Acc. Chem. Res.*, 1997, **30**, 89 and references within.

38 M. I. Khan, J. Zubieta, in *Progress in Inorganic Chemistry*, ed. K. D. Karlin, Wiley, 1995, **43**, 1.

39 Y. Yang, J. Pinkas, M. Noltemeyer, H-G. Schmidt and H. W. Roesky, *Angew. Chem., Int. Ed. Engl.*, 1999, **38**, 664.

40 C. Bhardwaj, H. Hu and A. Clearfield, *Inorg. Chem.*, 1993, **32**, 4294.

41 D. M. Poojary, B. Zhang, P. Bellinghausen and A. Clearfield, *Inorg. Chem.*, 1996, **35**, 5254.

42 S. Drumel, P. Janvier, P. Barboux, M. Bujoli-Doeuff and B. Bujoli, *Inorg. Chem.*, 1995, **34**, 148.

43 J. Le Bideau, B. Bujoli, A. Jouanneaux, C. Payen, P. Palvadeau and J. Rouxel, *Inorg. Chem.*, 1993, **32**, 4617.

44 J. Le Bideau, C. Payen, P. Palvadeau and B. Bujoli, *Inorg. Chem.*, 1994, **33**, 4885.

45 Y. Zhang and A. Clearfield, *Inorg. Chem.*, 1992, **31**, 2821.

46 C. Bellitto, F. Federici and S. A. Ibrahim, *Chem. Mater.*, 1998, **10**, 1076.

47 A. Altmore, C. Bellitto, S. A. Ibrahim, M. R. Mahmoud and R. Rizzi, , *J. Chem. Soc., Dalton Trans.*, 2000, 3913.

48 J-L. Du, S. J. Rettig, R. C. Thompson, J. Trotter, P. Betz and A. Bino, *Can. J. Chem.*, 1992, **70**, 732.

[49] P. Betz, A. Bino, J-L. Du, L. S-M. Lo and R. C. Thompson, *Inorg. Chim. Acta*, 1990, **170**, 45.

[50] N. S. Dean, M. R. Bond, C. J. O'Conner and C. J. Carrano, *Inorg. Chem*, 1996, **35**, 7643.

[51] Spectroscopic Methods in Organic Chemistry, 5th Ed, by D. H. Williams, and I. Fleming, published by McGRAW-HILL Book Company Europe, 1995.

[52] G. Alberti, In *Comprehensive Supramolecular Chemistry*, J. L. Atwood, J. E. D. Davies, D. D. Macnicol, F. Vogel, Eds, Permagon Press, 1996, **7**, 151.

[53] A. Parkin, *Using Crystallographic and Molecular Modelling techniques to Investigate Modes-of-Interaction of Organic Ligands with Metal Systems*, 1st Year PhD Report, The University of Edinburgh, 1999.

[54] J. J. Kipling and E. H. M. Wright, *J. Chem. Soc.*, 1964, 3535.

Chapter 5:

Development of Phosphonic Acids.

Contents.

5.1 Introduction.

A review of aluminium phosphonates and the use of phosphonic acids as surface ligands are included in Chapter 4, Sections 4.1.3 and 4.1.4.

5.2 Synthesis of Phosphonic Acid Derivatives.

The phosphonic acids prepared in this chapter and any abbreviations used in the text are shown (Table 5.1). Full experimental details and characterisations for all compounds are given in Section 5.6.2.

Structure	Name	Abbreviations (where used)
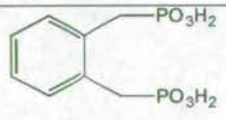	(2-phosphonomethyl-benzyl)-phosphonic acid	2-pmbpa
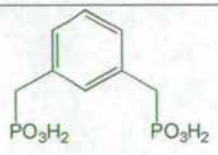	(3-phosphonomethyl-benzyl)-phosphonic acid	3-pmbpa
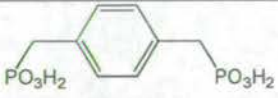	(4-phosphonomethyl-benzyl)-phosphonic acid	4-pmbpa
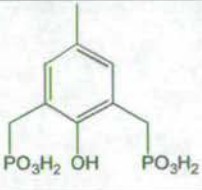	4-methyl-2,6-bis (phosphonomethyl)phenol	H_5mbpp
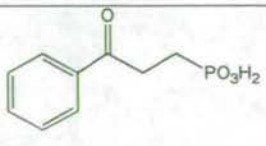	(3-oxo-3-phenyl-propyl)-phosphonic acid	P-bpa
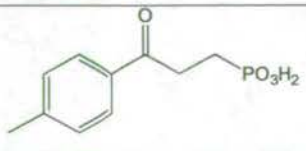	(3-oxo-3-*p*-tolyl-propyl)-phosphonic acid	P-419

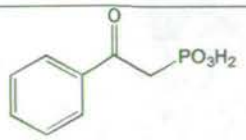	(2-oxo-2-phenyl-ethyl)-phosphonic acid	2-opepa
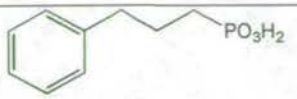	(3-phenyl-propyl)-phosphonic acid	3-pppa
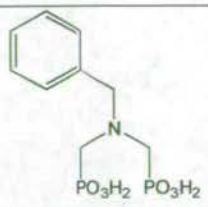	[(benzyl-phosphonomethyl-amino)-methyl]-phosphonic acid	-

Table 5.1: Phosphonic acids synthesised within this chapter.

The preparation of the bispphosphonic acids (n-pmbpa, where n = 2, 3 or 4) was carried out by Dr P. A. Lovatt at the University of Edinburgh, using a modified literature[1,2] method (Scheme 5.1), the first step of which is synthesis of the n-(diethoxy-phosphorylmethyl)-benzyl]-phosphonic acid diethyl ester from the appropriate bischloride via the Arbutzov reaction, with triethyl phosphite [$P(OEt)_3$]. The general mechanism[3,4] of the Arbutzov reaction is given (Figure 5.1). The first step is attack of the alkyl group of the alkyl halide (R'X) by the lone pair of electrons on the phosphite, forming the new phosphorus carbon bond. In the second step an alkyl group of the phosphite dissociates from the intermediate, resulting in the formation of a P=O bond and the elimination of the alkyl group as a new alkyl halide (RX). Formation of the bisphosphonic acid is completed by hydrolysis with concentrated hydrochloric acid.

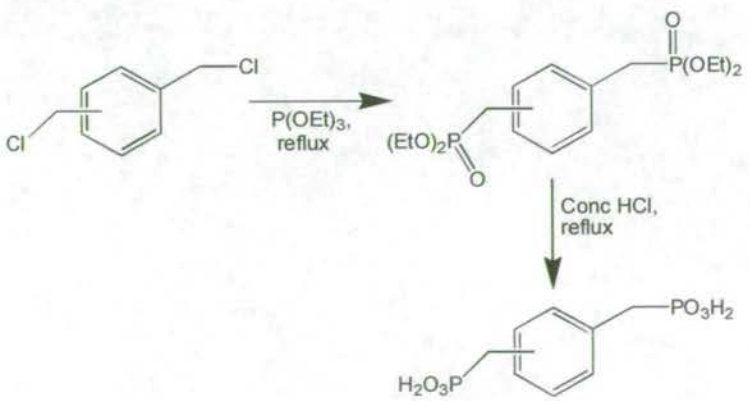

Scheme 5.1: General synthetic route to (n-phosphonmethyl-benzyl)-phosphonic acids (n-pmbpa), where n = 2, 3 or 4.

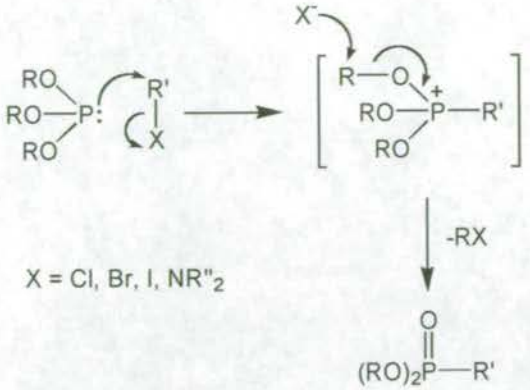

Figure 5.1: Mechanism of the Arbutzov reaction.

H_5mbpp was prepared by a slightly different method[1] (Scheme 5.2). Trimethyl phosphite was used to form the ester and the hydrolysis carried out under milder conditions by heating under reflux in a water/methanol solution. This is in contrast to all other phosphonic acids synthesised, which require the more forcing conditions of concentrated hydrochloric acid in order to hydrolyse the ester. Care has to be taken when drying H_5mbpp as it is known[1] that above 100 °C it can lose water through a chemical reaction, probably between the acidic and phenolic OH groups.

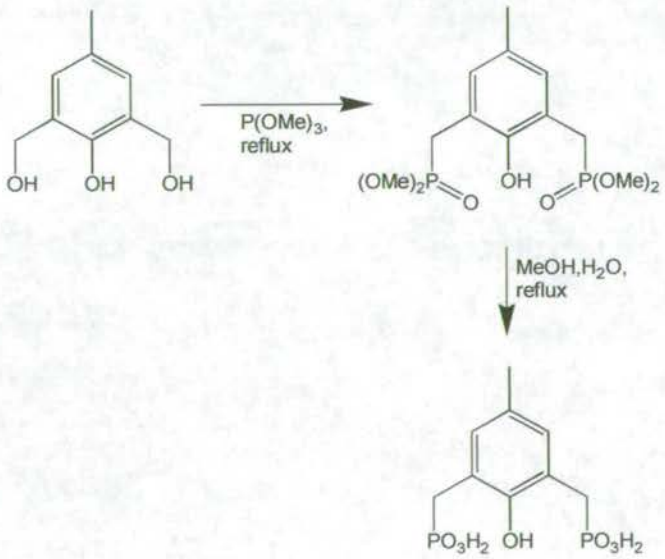

Scheme 5.2: Synthetic route to 4-methyl-2,6-bis(phosphonomethyl)phenol (H_5mbpp).

The crystal structure of H_5mbpp (Figure 5.2) was determined[5] in 1993. It was crystallised as a dihydrate and the structure reveals that the ligand adopts a *trans*

conformation of the methylene phosphonic acid arms. There is an extensive three dimensional hydrogen bond network involving the phenolic and phosphonic acid groups in the compound and the two water molecules present in the lattice.

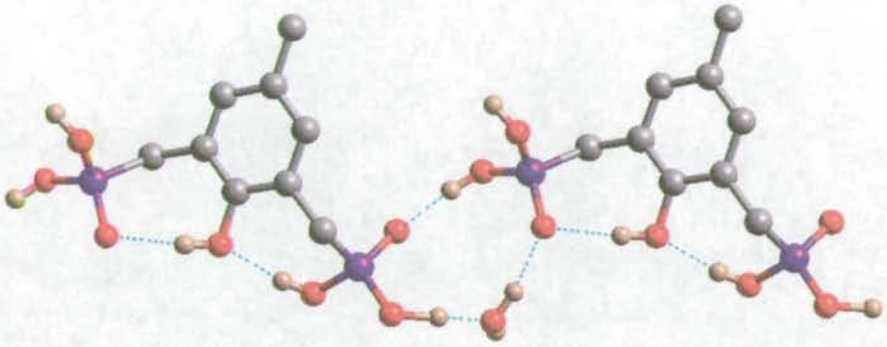

Figure 5.2: Crystal structure of 4-methyl-2,6-bis(phosphonomethyl)phenol dihydrate (H_5bmpp).

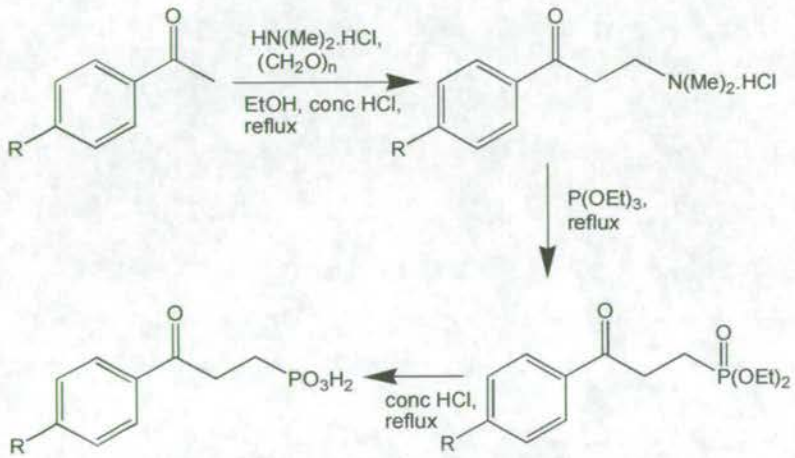

Scheme 5.3: General reaction scheme for the synthesis of γ-ketophosphonic acids.

γ-Ketophosphonic acids can be synthesised in three steps via the route shown (Scheme 5.3). The first step[6] is conversion of the appropriate acetophenone derivative to the amine hydrochloride by means of the acid catalysed Mannich reaction. The general mechanism[4] of this reaction is shown (Figure 5.3). The Arbutzov reaction (Figure 5.1), with triethyl phosphite as the reagent, is used to synthesise[7] the γ-ketophosphonate esters. The phosphonic acids are then obtained by simple hydrolysis with concentrated hydrochloric acid. Two phosphonic acids, P-bpa, where R = H, and P-419, where R = Me, were synthesised using this route. The overall yield for the three steps was 37 % and 42 % for P-419 and P-bpa respectively.

An attempt to synthesise [3-(4-nitro-phenyl)-3-oxo-propyl]-phosphonic acid failed as the triethyl phosphite appeared to react with the *p*-nitro group of 3-dimethylamino-1-(4-nitro-phenyl)-propan-1-one.hydrochloride, giving an uncharacterisable brown material.

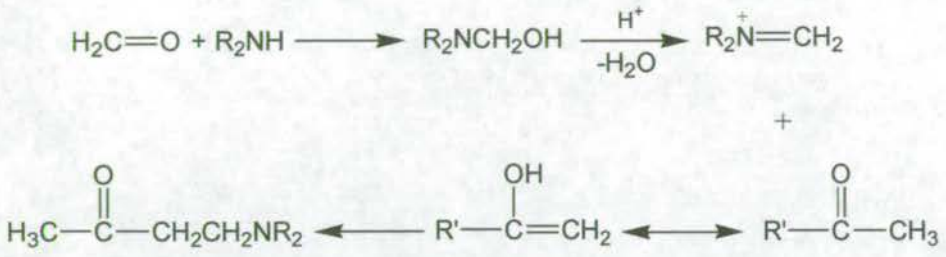

Figure 5.3: Mechanism of the acid catalysed Mannich reaction.

Crystals of X-ray quality were obtained for both of the γ-ketophosphonic acids, through slow evaporation of the filtrate from the reaction solutions.

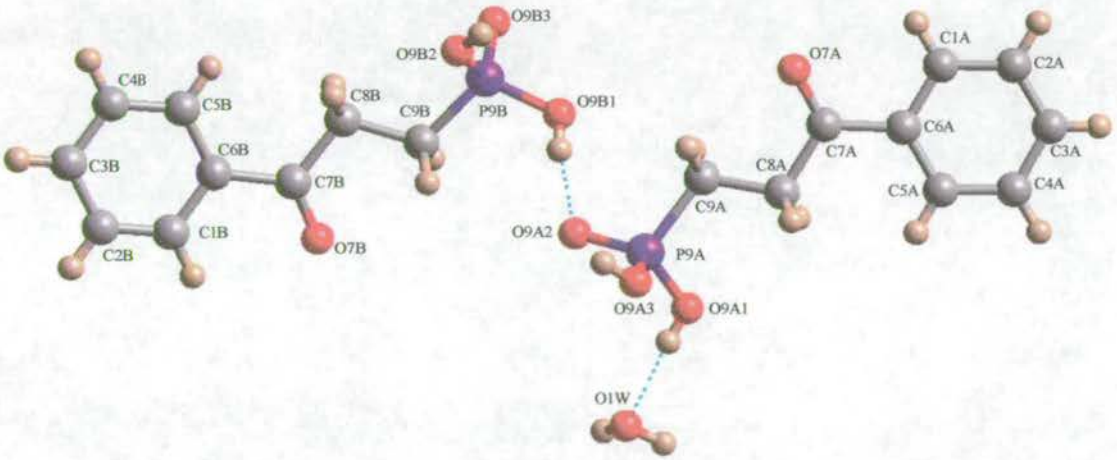

Figure 5.4: Crystal structure of (3-oxo-3-phenyl-propyl)-phosphonic acid (P-bpa).

(3-Oxo-3-phenyl-propyl)-phosphonic acid (Figure 5.4) crystallises as a hydrate with one water molecule for every two acid molecules. The packing (Figure 5.5) reveals that it forms two dimensional hydrogen bonded arrays through the phosphonate groups and the water molecules. A list of hydrogen bond contacts is given (Table 5.2). The carbonyl groups form close contacts [O(7B)...H(8B1) 2.534 Å and [0(7A)...H(8A2) 2.784 Å] with methylene hydrogens of neighbouring molecules within the hydrogen bonded sheets. The "tails" of the molecules within

these sheets interlock with neighbouring layers but there are no hydrogen bonds or close contacts between the layers. Crystallographic data (Table 25) and significant bond lengths and angles (Table 26) are given in the appendix.

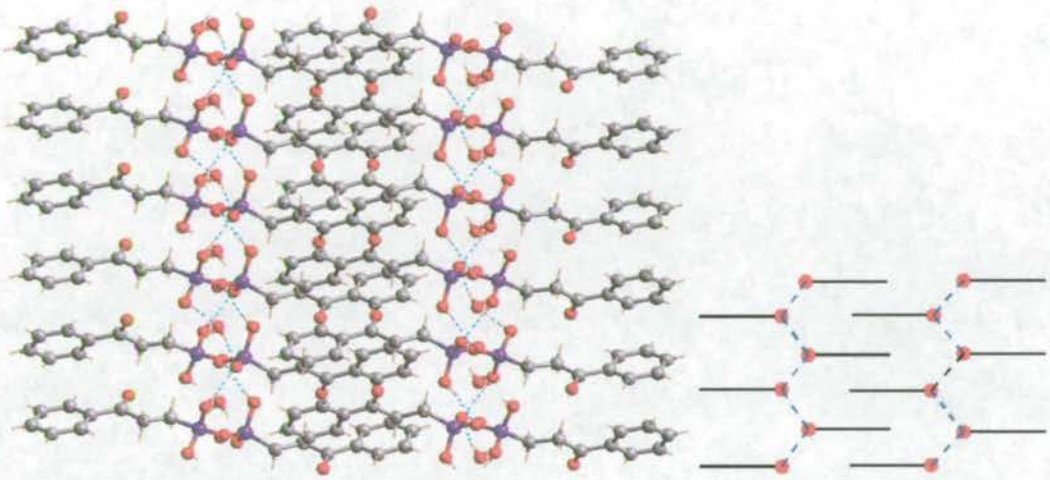

Figure 5.5: Crystal packing of (3-oxo-3-phenyl-propyl)-phosphonic acid (P-bpa) as viewed down the b axis and schematic showing the interlocking of the molecule "tails".

Bond type	Donor atom	Acceptor atom	Bond length (Å)
O-H...O	O(9A1)	O(1W)	2.522
O-H...O	O(9A3)	O(9B3)	2.516
O-H...O	O(9B1)	O(9A2)	2.599
O-H...O	O(9B2)	O(9A2)	2.585
O-H...O	O(1W)	O(9B3)	2.754

Table 5.2: Table of hydrogen bond contacts in (3-oxo-3-phenyl-propyl)-phosphonic acid (P-bpa).

Despite their similarities and almost identical crystal growth conditions P-419 (Figure 5.6) does not crystallise as a hydrate and has a very different packing structure (Figure 5.7) from that of P-bpa. The molecule again forms two dimensional hydrogen bonded arrays through the phosphonate groups and a list of hydrogen bond contacts is given (Table 5.3). The carbonyl group this time finds a close contact [O(4)...H(10A) 2.559 Å] with a methyl hydrogen of a neighbouring molecule. Crystallographic data (Table 27) and significant bond lengths and angles (Table 28) are given in Appendix II.

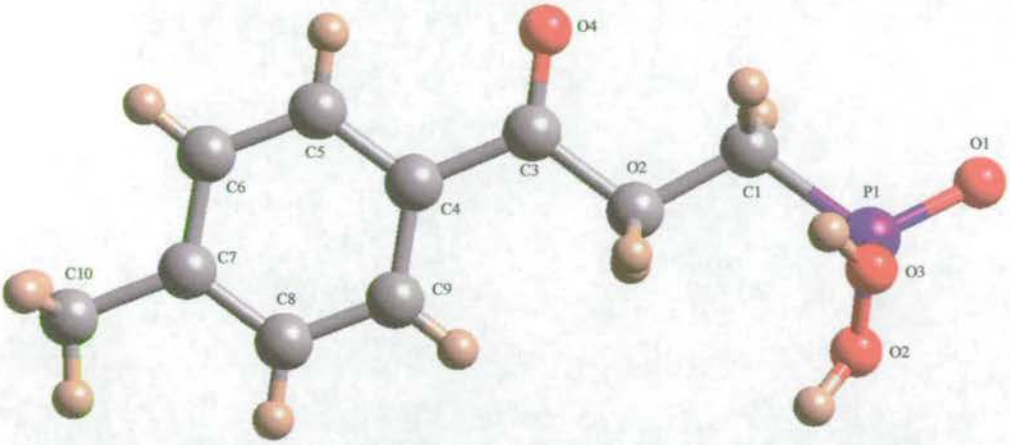

Figure 5.6: Crystal structure of (3-oxo-3-*p*-tolyl-propyl)-phosphonic acid (P-419).

Bond type	Donor atom	Acceptor atom	Bond length (Å)
O-H...O	O(2)	O(1)	2.541
O-H...O	O(3)	O(1)	2.556

Table 5.3: Table of hydrogen bond contacts in (3-oxo-3-*p*-tolyl-propyl)-phosphonic acid (P-419).

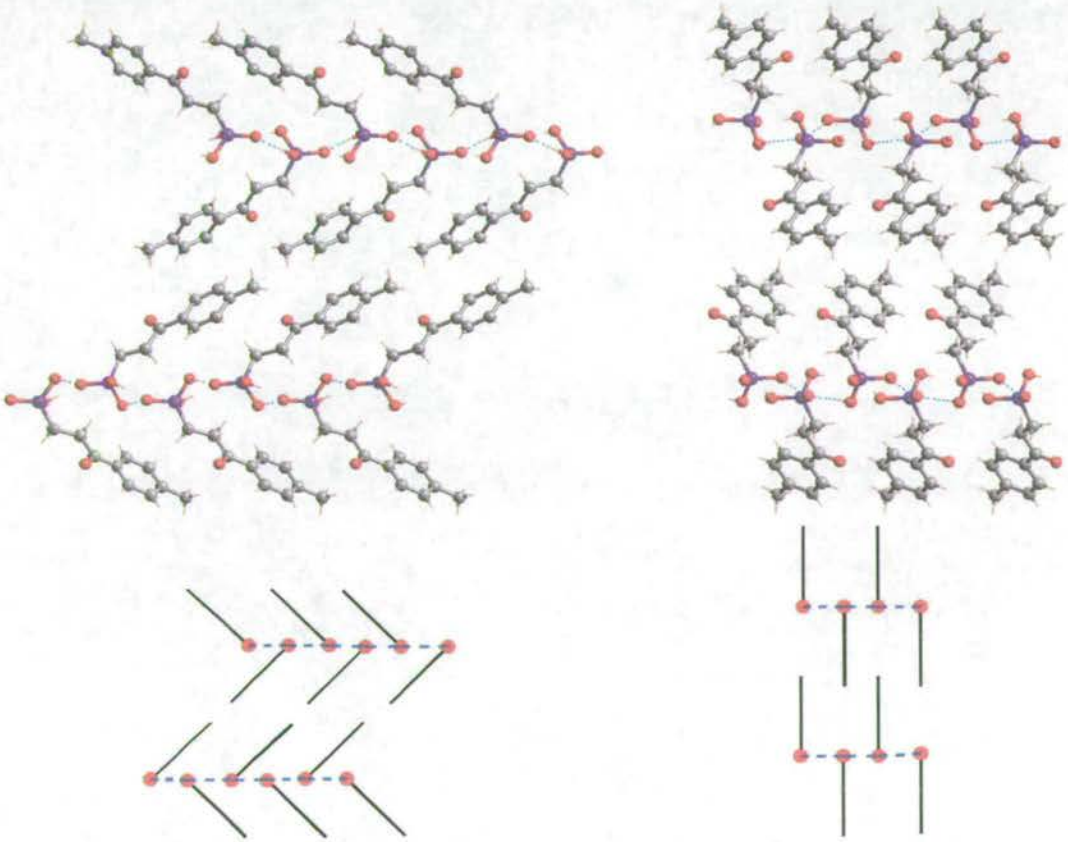

Figure 5.7: Crystal packing of (3-oxo-3-*p*-tolyl-propyl)-phosphonic acid (P-419) as viewed down the a axis (left) and the b axis (right).

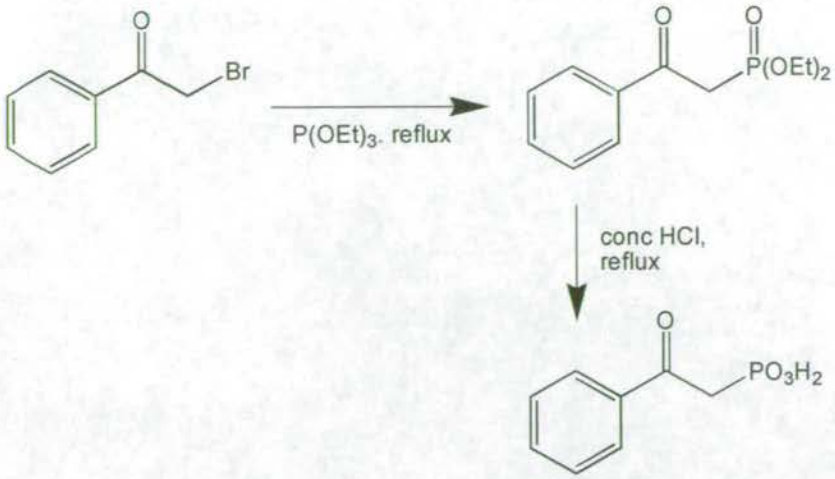

Scheme 5.4: Reaction scheme for the synthesis of (2-oxo-2-phenyl-ethyl)-phosphonic acid (2-opepa).

2-opepa was synthesised (Scheme 5.4) in two steps from α-bromoacetophenone. After recrystallisation from ethyl acetate it was obtained in 42 % overall yield as a pale yellow crystalline solid. It was subsequently discovered that although 2-opepa-diethylester has been made previously from α-bromoacetophenone, this is not the optimum starting material to use, as in addition to the Arbutzov reaction it can also undergo the Perkow[3] reaction. This reaction gives phosphoric acid diethyl ester 1-phenyl-vinyl ester (Figure 5.8) as the product. The first step of the Perkow reaction is the same as for the Arbutzov reaction, nucleophillic attack by the lone pairs of the phosphorus on the carbon atom. This is followed by nucleophillic attack of the carbonyl on the phosphorus forming a new phosphorus oxygen bond. The final step is normal Arbutzov elimination of the alkyl halide forming the phosphate. Although aprotic solvents generally favour the Perkow reaction, it can also occur under other conditions. I. J. Borowitz *et al*[8] found that the reaction of triethyl phosphite with α-bromoacetophenone in 1,2-dimethoxyethane at 120 °C gave yields of 65 % 2-opepa-diethylester and 23 % phosphoric acid diethyl ester 1-phenyl-vinyl ester by NMR. This may be the reason for the low overall yield observed for the reaction. The use of α-iodoacetophenone would have reduced this side reaction as iodine is less electronegative and exerts a smaller polarisation effect as well as being more reactive to simple displacement. Higher reaction temperatures also favour the formation of phosphonates over phosphates.[3]

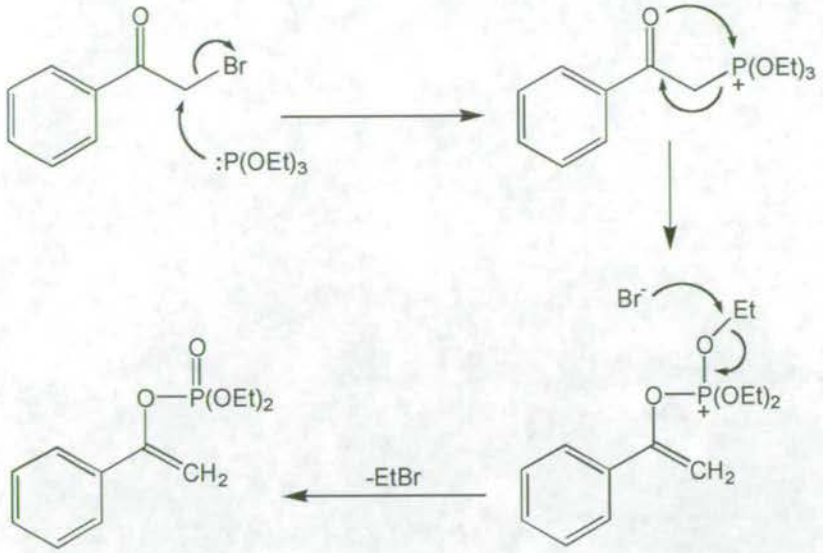

Figure 5.8: Mechanism of the Perkow reaction to form phosphoric acid diethyl ester 1-phenyl-vinyl ester.

3-pppa was prepared via a modified literature[9,10] method (Scheme 5.5) from 1-bromo-3-phenylpropane. The crude ester [(3-phenyl-propyl)-phosphonic acid diethyl ester] was obtained as a colourless oil in excellent yield (95 %) and was used without further purification. However, problems were encountered during the hydrolysis, due to the immiscibility of the ester in concentrated hydrochloric acid. Even after refluxing in concentrated hydrochloric acid overnight, only unreacted ester was recovered from the reaction. Ethanol was added to the reaction mixture to aid dissolution but the yield of the final product was still relatively low (53 %) and a considerable amount of starting ester was recovered from the reaction.

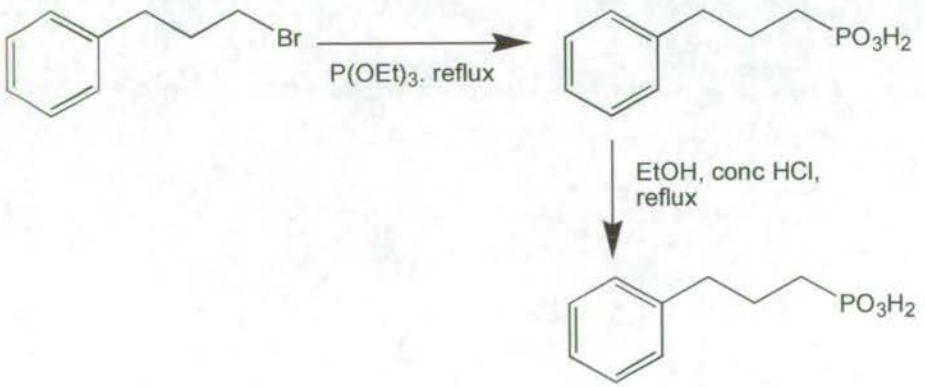

Scheme 5.5: Reaction scheme for the synthesis of (3-phenyl-propyl)-phosphonic acid (3-pppa).

[(Benzyl-phosphonomethyl-amino)-methyl)]-phosphonic acid was synthesised in one step from benzylamine hydrochloride by the method[11] shown (Scheme 5.6). The product crystallised as a white powder from the reaction mixture, on cooling and after drying was obtained in high yield (87 %) with no further purification necessary.

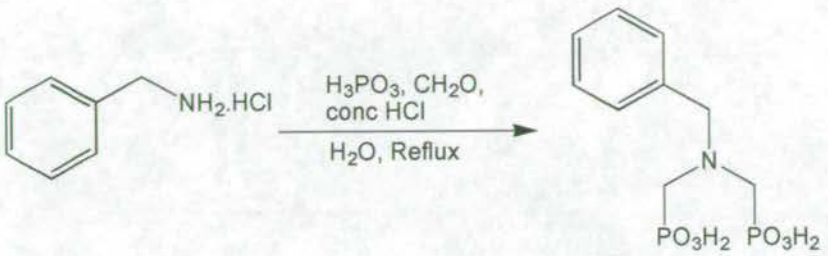

Scheme 5.6: Reaction scheme for the synthesis of [(benzyl-phosphonomethyl-amino)-methyl)]-phosphonic acid.

5.3 Preparation of 1st Row Transition Metal Phosphonate Complexes in the Presence of Urea.

As in Chapter 4, Section 4.2.4 a series of reactions were carried out with the phosphonic acids and copper, cobalt and nickel salts in the presence of urea. In general these reactions gave powders of ambiguous composition and their purity was difficult to discern. The bisphosphonates 2-pmbpa and 3-pmbpa gave pale blue microcrystals with copper salts that, unfortunately, were too small and did not diffract strongly enough for a structure to be determined. H_5mbpp produced X-ray quality crystals with copper salts and the product of these reactions is discussed below.

5.3.1 Synthesis and Structure of $[Cu_4(Hmbpp)_2(H_2NC(O)NH_2)_2(H_2O)_8].4H_2O$

Slowly raising the pH of an aqueous solution of copper perchlorate hexahydrate, H_5mbpp and sodium hydroxide using urea, on standing gave brown crystals that were identified by a combination of X-ray and elemental analysis as the tetranuclear copper complex $[Cu_4(Hmbpp)_2(H_2NC(O)NH_2)_2(H_2O)_8].4H_2O$ (Figure

5.9). Due to the poor quality of the crystals the assignment of terminal coordinating urea groups was made on the basis of elemental analysis data as the crystallographic data set obtained was not sufficiently good to distinguish between carbon, oxygen and nitrogen. A second reaction using copper sulfate pentahydrate in place of copper perchlorate hexahydrate resulted in a lower yield of higher quality crystals of the same type that provided a better data set enabling the structure to be definitively assigned (R-factor 0.0237). Full experimental details and characterisations are given in section 5.6.2 and crystallographic data (Table 29) and selected bond lengths and angles (Table 30) are given in the appendix.

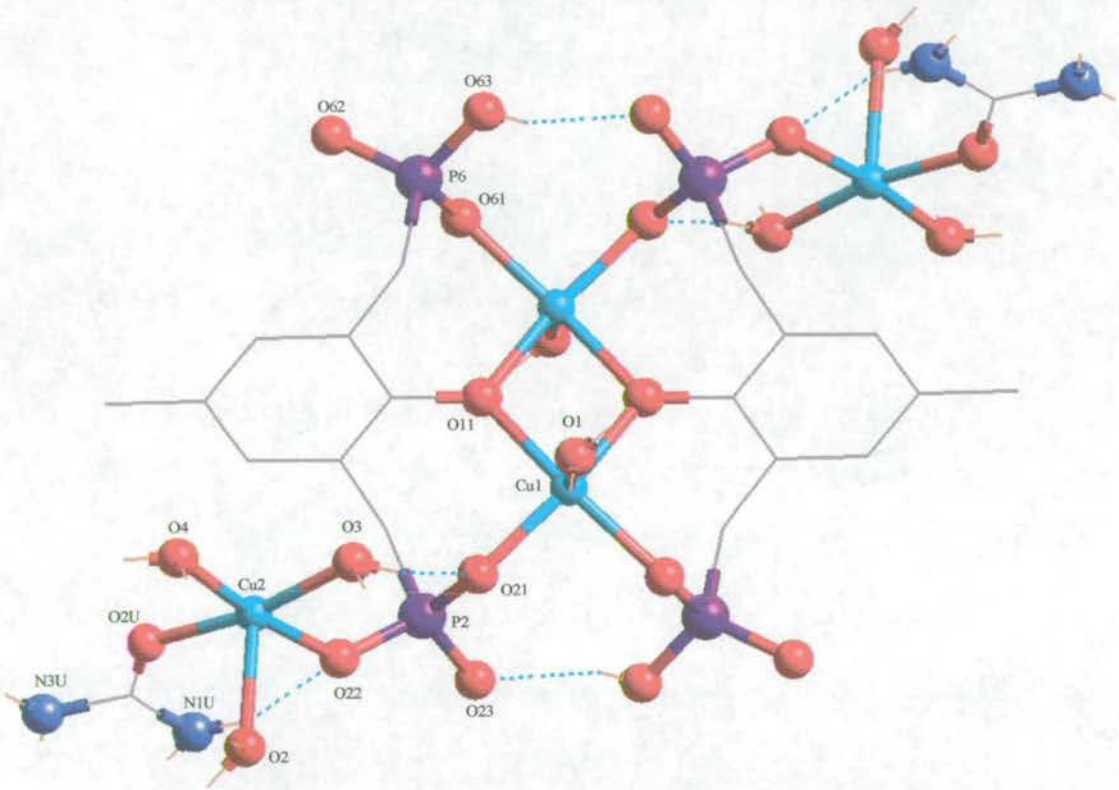

Figure 5.9: Crystal structure of $[Cu_4(Hmbpp)_2(H_2NC(O)NH_2)_2(H_2O)_8].4H_2O$.

The structure contains four, distorted square pyramidal copper atoms with all oxygen donor sets. The equatorial Cu-O bond lengths range from 1.9369(13)–1.9919(15) Å and the axial bonds which are longer due to Jahn-Teller distortion are Cu(1)-O(1) 2.2036(16) Å and Cu(2)-O(2) 2.3681(18) Å. The angles between the axial oxygen and the equatorial oxygens range from $O_{(ax)}$-Cu-$O_{(eq)}$ 89.54(6)–101.65(7)°. The distance between the central Cu(1) centres is 3.089 Å while that

between Cu(1) and the outer copper, Cu(2), is 5.234 Å. The central core of the complex can be described as a Cu_2O_2 dimer, in which the two Cu(1) centres are bridged [Cu(1)-O(11)-Cu(1) 103.75(6)°] by the phenolate oxygens of two Hmbpp ligands. Two phosphonate oxygens, one from each Hmbpp ligand and a water molecule in the axial position complete the coordination of the copper sites, which are crystallographically identical.

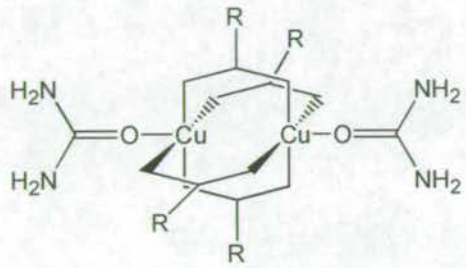

Figure 5.10: Copper carboxylate dimers with terminally coordinated urea.

The second copper atom, Cu(2), is coordinated by one phosphonate oxygen, three water molecules, one of which is in the axial coordination site, and a urea molecule coordinating via its carbonyl oxygen. The presence of coordinated urea is interesting as this feature has not occurred in other complexes which have been prepared, using urea as a base. Coordinated urea is however not uncommon in copper complexes,[12] particularly in copper carboxylate dimers[13] where it occupies the terminal sites (Figure 5.10). The involvement of the urea in both intra- and intermolecular hydrogen bonding within the complex may explain its presence in this case.

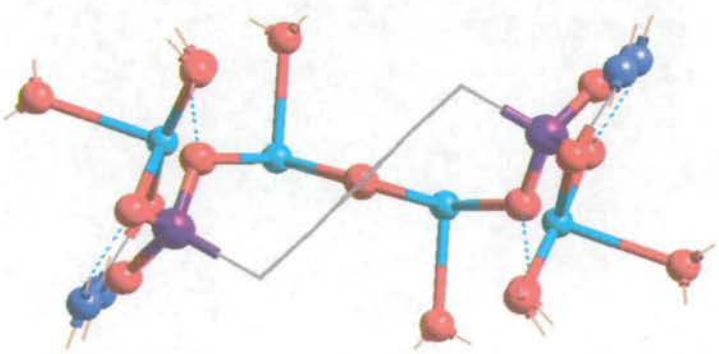

Figure 5.11: View of the angle formed by the plane of the Cu_2O_2 core and the phenyl rings of the Hmbpp ligands.

The Hmbpp ligands are not fully deprotonated and as a result are unsymmetrical with one phosphonate group doubly deprotonated and the second only mono deprotonated. The phenolic oxygen is deprotonated. As might be expected it is the doubly deprotonated phosphonate which performs the bridging function between Cu(1) and Cu(2). The phenyl rings of the Hmbpp ligands are twisted out of the plane formed by the Cu_2O_2 core by an angle of 62.8 ° (Figure 5.11). Interestingly the ligands adopt the same *trans* conformation of the methylene phosphonic acid arms as the free ligand (Figure 5.2).

Within the molecule there are six intramolecular hydrogen bonds (Figure 5.9). The terminal phosphonate oxygens form hydrogen bonds O(63)-H...O(23) 2.497 Å, enclosing the central copper dimer in a pseudo macrocycle. This effect may have implications in the solvent extraction of copper. In addition there are two other interactions. The first between an equatorial water molecule coordinated to Cu(2) and a phosphonate oxygen coordinated to Cu(1), O(3)-H...O(21) 2.616 Å. The second is between a nitrogen donor from the coordinated urea and a phosphonate oxygen coordinated to Cu(1), N(1U)-H...O(22) 2.797 Å. A full list of all intra- and intermolecular hydrogen bonds in the complex is given (Table 5.4).

Bond Type	Donor Atom	Acceptor atom	Bond Length (Å)	Intra-/ Intermolecular
O-H...O	O(63)	O(23)	2.497	Intra
O-H...O	O(3)	O(21)	2.616	Intra
N-H...O	N(1U)	O(22)	2.797	Intra
N-H...O	N(1U)	O(3)	3.041	Inter (c-c)
N-H...O	N(3U)	O(4)	3.332	Inter (c-c)
N-H...O	N(3U)	O(1W)	2.905	Inter (c-w)
O-H...O	O(1)	O(23)	2.724	Inter (c-c)
O-H...O	O(1)	O(2W)	2.808	Inter (c-w)
O-H...O	O(2)	O(61)	3.090	Inter (c-c)
O-H...O	O(2)	O(63)	3.017	Inter (c-c)
O-H...O	O(3)	O(62)	2.558	Inter (c-c)

O-H...O	O(4)	O(61)	2.780	Inter (c-c)
O-H...O	O(4)	O(2W)	2.680	Inter (c-w)
O-H...O	O(1W)	O(2)	2.839	Inter (w-c)
O-H...O	O(1W)	O(22)	2.850	Inter (w-c)
O-H...O	O(2W)	O(62)	2.698	Inter (w-c)
O-H...O	O(2W)	O(1W)	2.780	Inter (w-w)

Table 5.4: Table of hydrogen bond contacts in $[Cu_4(Hmbpp)_2(H_2NC(O)NH_2)_2(H_2O)_8].4H_2O$. (Key: C = complex, w = water molecule)

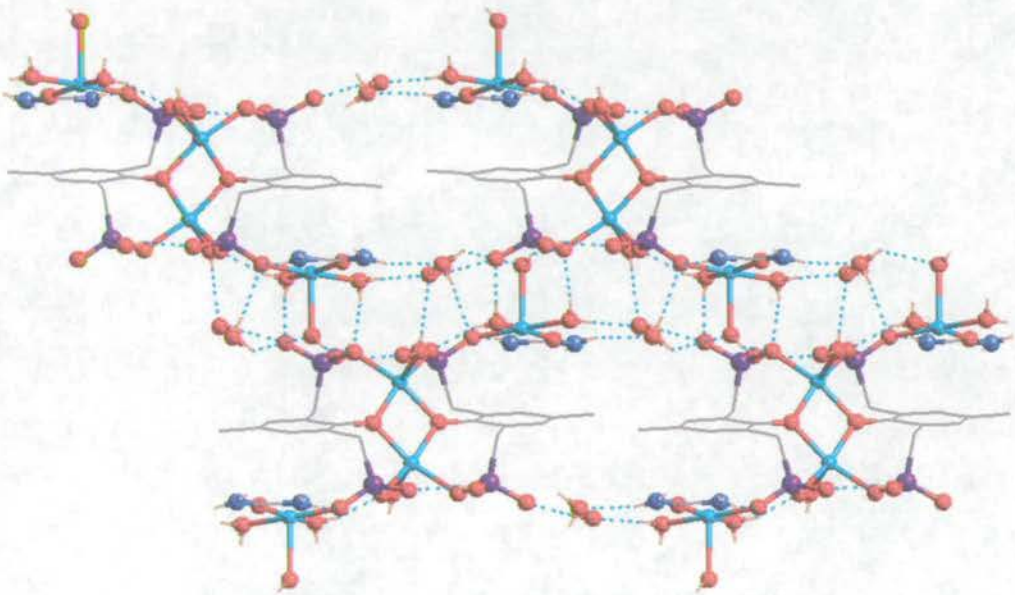

Figure 5.12: Crystal packing of $[Cu_4(Hmbpp)_2(H_2NC(O)NH_2)_2(H_2O)_8].4H_2O$ as viewed down the a axis.

The crystal structure also reveals a very complicated intermolecular hydrogen bond network involving hydrogen bond acceptors/donors in the complex and the four water molecules within the unit cell. The packing of the complex in the crystal is shown (Figure 5.12).

Within the crystal the molecules of $[Cu_4(Hmbpp)_2(H_2NC(O)NH_2)_2(H_2O)_8]$ are linked both via direct hydrogen bonds (Figure 5.13) and through the water molecules (Figure 5.14) within the crystal lattice. Each water molecule is situated at the hub of four hydrogen bonds, one of which is to the other water and the remaining three to oxygens or nitrogens on the complex.

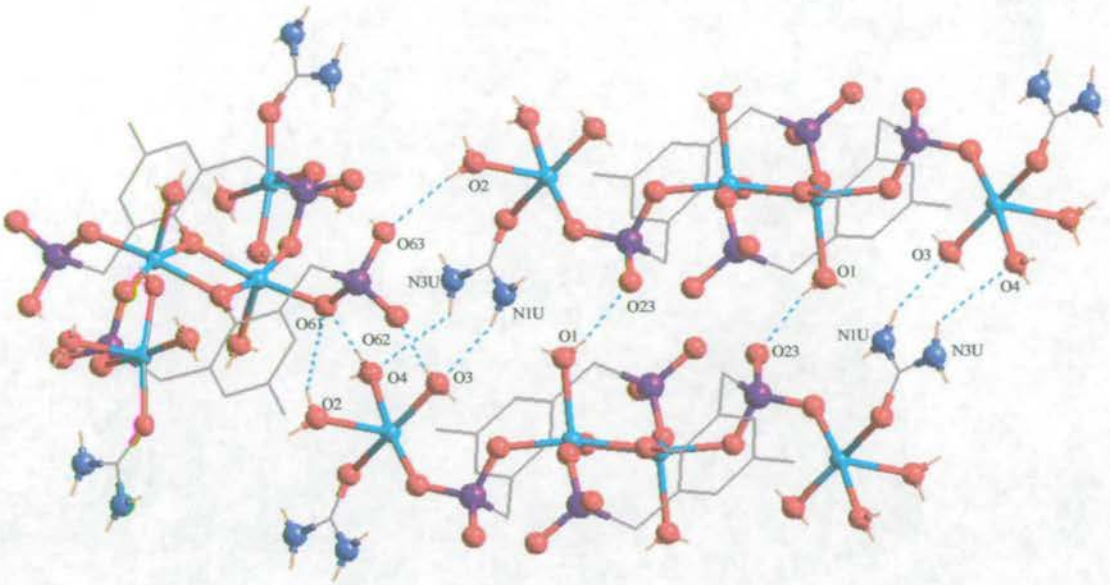

Figure 5.13: Direct hydrogen bond contacts between $[Cu_4(Hmbpp)_2(H_2NC(O)NH_2)_2(H_2O)_8]$ molecules.

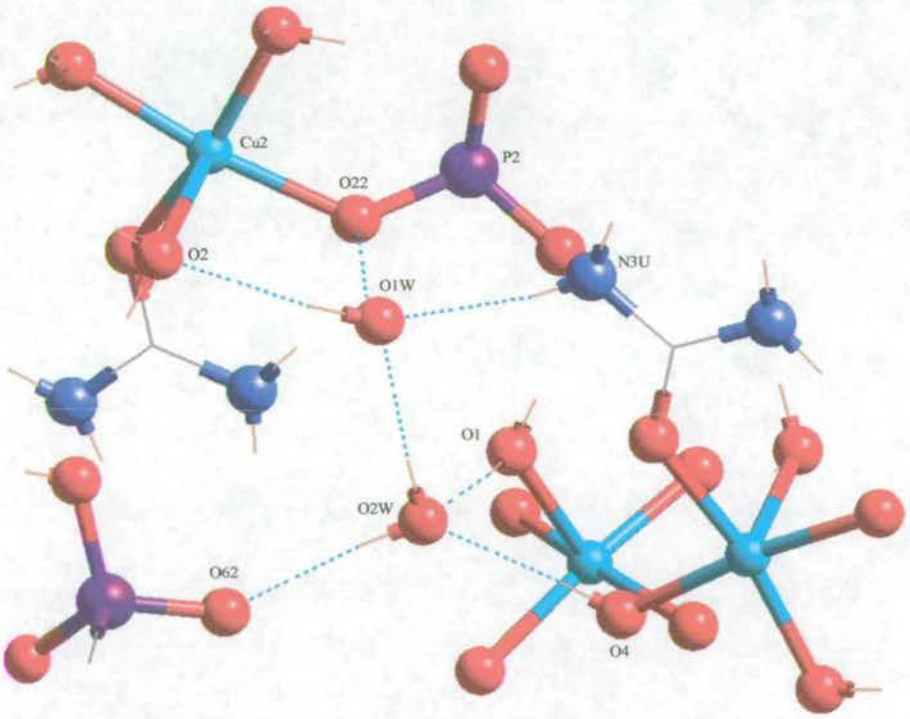

Figure 5.14: Hydrogen bonding through water molecules in $[Cu_4(Hmbpp)_2(H_2NC(O)NH_2)_2(H_2O)_8].4H_2O$.

It is interesting to note that so far this is the only discreet molecular complex that has been synthesised using urea as a base. All other phosphonate complexes made previously have been polymeric.

5.3.2 Magnetic Studies of $[Cu_4(Hmbpp)_2(H_2NC(O)NH_2)_2(H_2O)_8].4H_2O$.

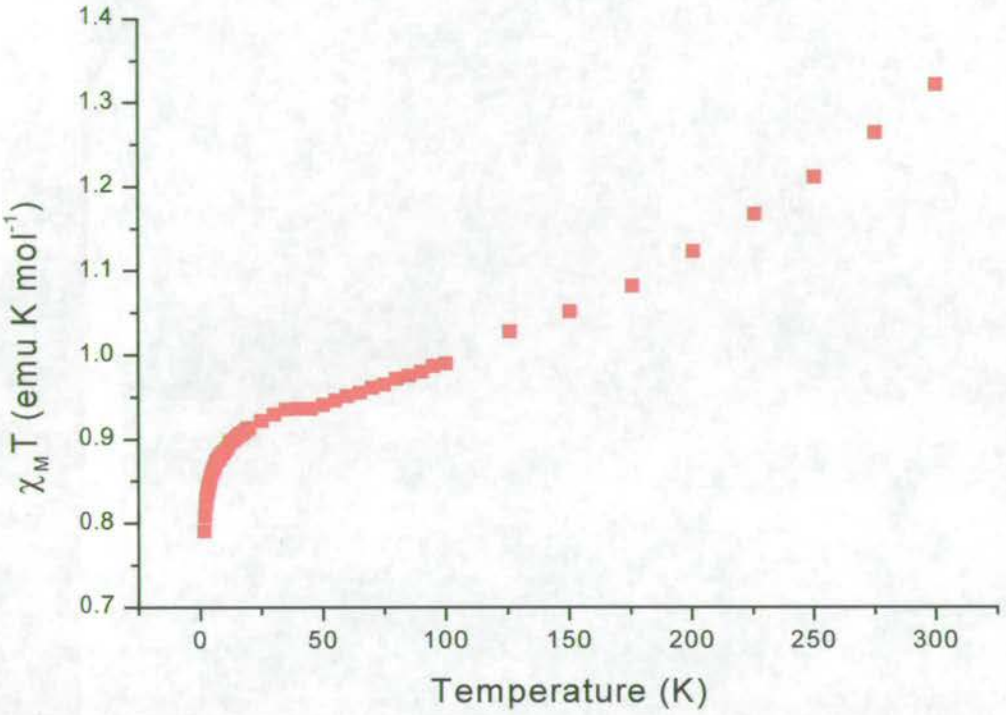

Figure 5.15: The variation of $\chi_M T$ with temperature of $[Cu_4(Hmbpp)_2(H_2NC(O)NH_2)_2(H_2O)_8].4H_2O$.

The magnetic behaviour of $[Cu_4(Hmbpp)_2(H_2NC(O)NH_2)_2(H_2O)_8].4H_2O$ was studied in the range 1.8 to 300 K. Several problems were found with the reproducibility of this data, which may be related to loss of solvate molecules from the sample leading to a changing, and unreliable molecular mass. The data reported (Figure 5.15) are those that appear to be the most reliable.

The room temperature value of $\chi_M T$ (where χ_M is the molar susceptibility) is *ca.* 1.35 emu K mol^{-1}. This compares with a calculated value for $\chi_M T$ of 1.68 emu K mol^{-1} for four non-interacting S = ½ centres (calculated for g = 2.121 as observed by EPR spectroscopy, see Section 5.3.3 below). This indicates the presence of anti-ferromagnetic exchange between the metal centres. The steady decline in $\chi_M T$ with temperature confirms this anti-ferromagnetic exchange. There is a slowing of the decline below 100 K, and at 50 K $\chi_M T$ reaches a plateau at *ca.* 0.95 emu K mol^{-1} before falling rapidly below 15 K. The value for the plateau is a little above that calculated for two non-interacting copper(II) centres (0.84 emu K mol^{-1}).

Although the unreliability of the data makes fitting the behaviour of dubious worth, the result seems clear when compared with the crystal structure. There is strong anti-ferromagnetic exchange between two copper centres at the centre of the molecule. This leads to the steady decline between 300 and 50 K. Between 50 K and 15 K $\chi_M T$ is due to the spins on the external, weakly coupled copper centres, and below 15 K the steep decline is due to the weak exchange involving these two centres. This picture is also consistent with the EPR spectroscopy of the cage.

5.3.3 EPR Studies of $[Cu_4(Hmbpp)_2(H_2NC(O)NH_2)_2(H_2O)_8].4H_2O$.

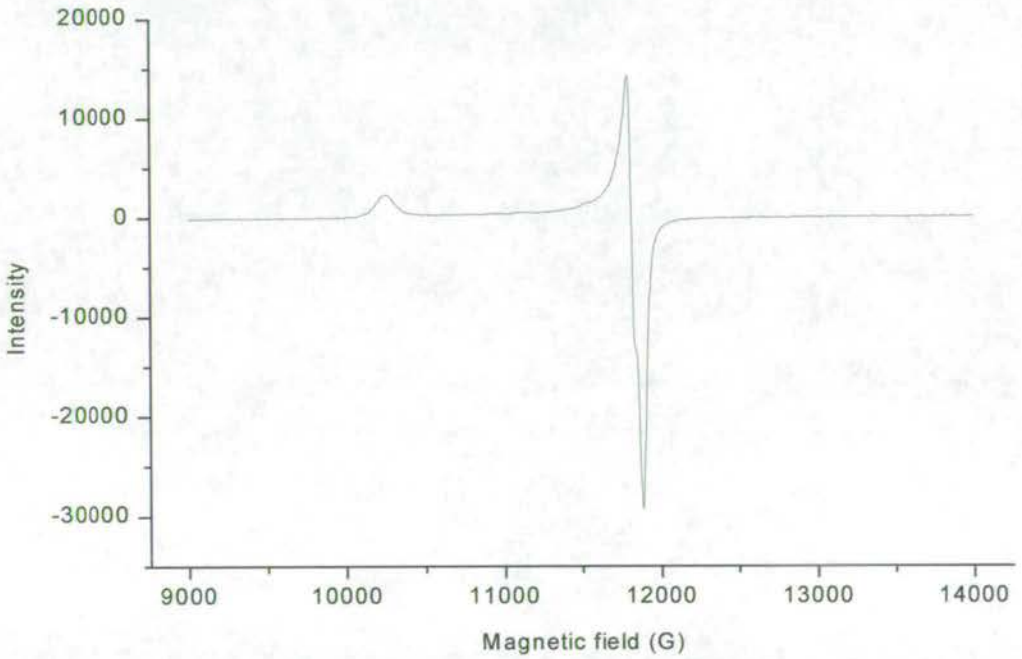

Figure 5.16: EPR spectra of $[Cu_4(Hmbpp)_2(H_2NC(O)NH_2)_2(H_2O)_8].4H_2O$.

The EPR spectrum of a solid sample at room temperature is broad and is typical of a spectrum due to an S = ½ spin state. At 115 K the powder spectrum is much sharper, with three g-values resolved at g = 2.335, 2.020 and 2.009. This is therefore typical for a Cu(II) centre with an unpaired electron in the dx^2-y^2 orbital. No copper hyperfine is resolved. The EPR behaviour indicates that there is very strong anti-ferromagnetic exchange within the central Cu_2O_2 ring of the complex,

causing this part of the compound to be EPR silent. The two external Cu(II) centres are non-interacting, and the EPR signal is presumably due to these copper sites.

5.4 Isotherm Studies.

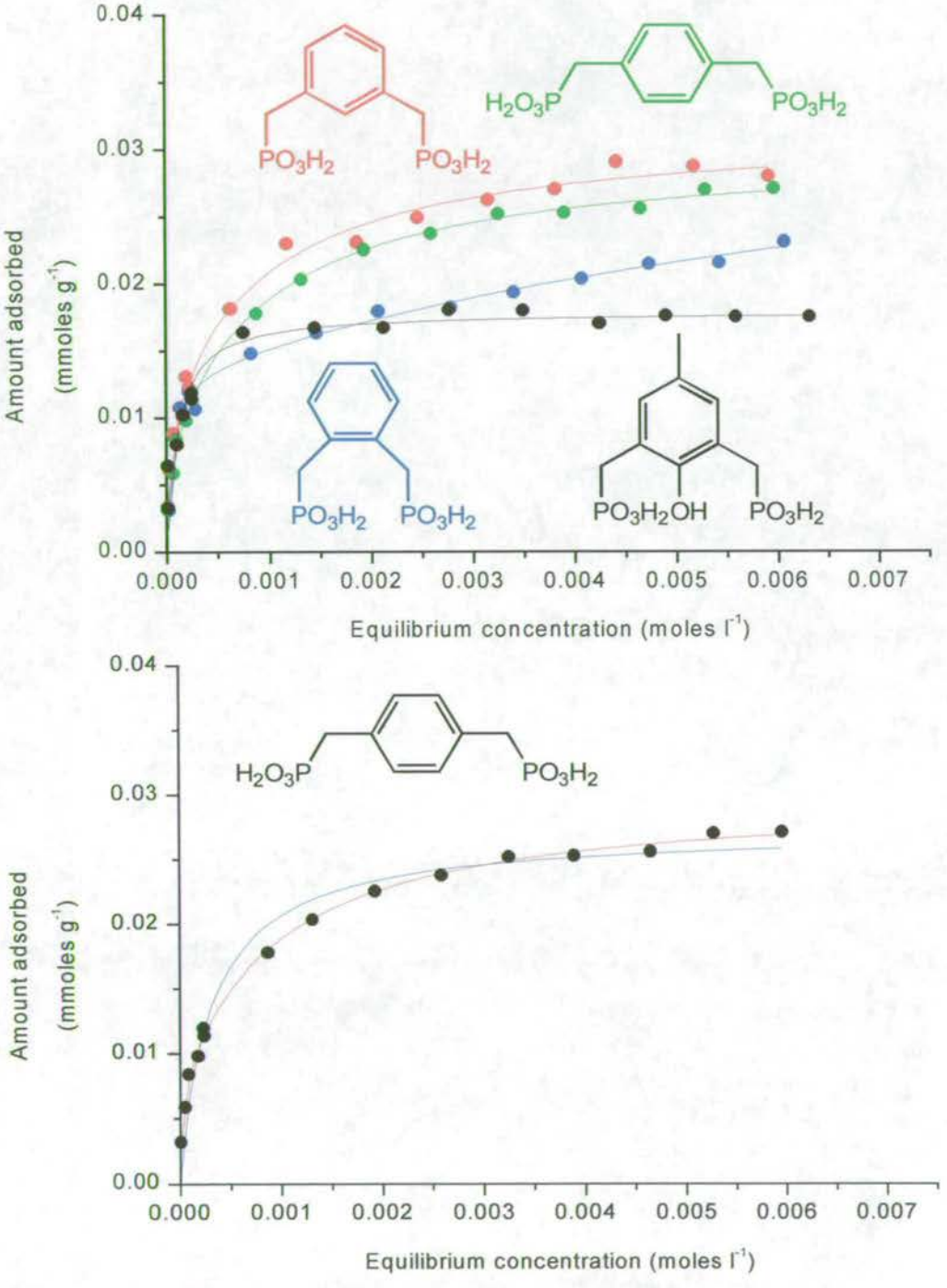

Figure 5.17: Top-Adsorption isotherms for 2-pmbpa (blue), 3-pmbpa (red), 4-pmbpa (green) and H_5mbpp (black). Bottom-Adsorption isotherm for 4-pmbpa as fitted to the simple Langmuir model (blue) and the double Langmuir model (red)

Data for the calibration and isotherm experiments in this section are given in the appendix, Tables 51-66.

The UV/vis spectra of all ligands were recorded in 95/5 % methanol/water and their extinction coefficients determined (Table 5.5) using the Beer-Lambert Law. [(Benzyl-phosphonomethyl-amino)-methyl)]-phosphonic acid was insoluble in the methanol/water solvent system and was therefore not used in the isotherm experiments.

Compound	UV/vis bands, λ (nm)	Extinction coefficient, ε
2-pmbpa	214	9960(50)
3-pmbpa	213	9920(170)
4-pmbpa	222	12060(140)
H_5mbpp	285	2600(10)
P-bpa	243	13050(70)
P-419	259	15960(90)
2-opepa	245	13160(70)
3-pppa	208	8100(90)

Table 5.5: Electronic spectra for ligands in 95% methanol/water (standard deviations in parenthesis).

The adsorption isotherms were determined as described in Section 5.6.3 and are plotted (Figure 5.17) and (Figure 5.19).

The isotherm (Figure 5.17) for 2-pmbpa shows a steep initial slope at low concentrations, followed by a change to a gentler, almost linear, slope. The shape of the graph suggests that two different binding modes are operating at different concentrations (Figure 5.18). This can be explained if in the initial steep section of the graph, the ligand binds through both phosphonic acid groups, then as the concentration increases this changes to binding through a single acid group in order to pack more molecules onto the surface. Curve fitting to the double Langmuir model gives the surface coverage of this "bidentate" binding mode as $1.3(1) \times 10^{-5}$ mol g^{-1} corresponding to the "kink" in the curve. This gives a required surface area value of 89(7) $Å^2$ $molecule^{-1}$. Monolayer coverage of the "monodentate" binding mode cannot

be calculated but it appears that the curve will reach a maximum comparable with the other two bisphosphonic acids.

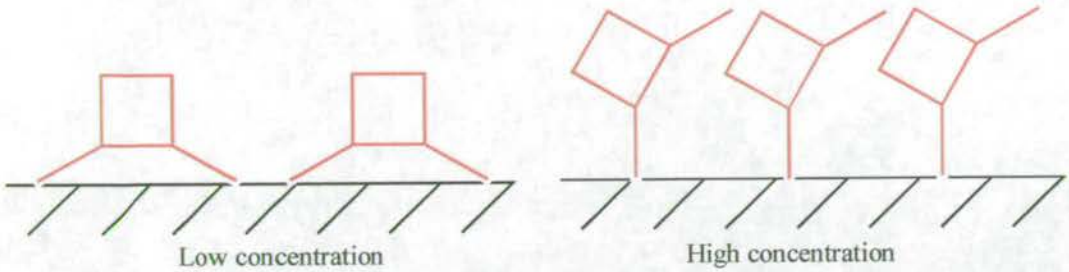

Figure 5.18: Schematic of the bidentate and monodentate binding modes proposed for 2-pmbpa at different concentrations.

The isotherms (Figure 5.17) for 3-pmbpa and 4-pmbpa can be fitted using the simple Langmuir function but the "goodness of fit" is poor. The values (Table 5.6) obtained for the equilibrium adsorption constants are comparable with phenylphosphonic acid [3.9(5) × 10^3 L mol^{-1}]. Calculated values for required surface area are 43(2) $Å^2$ $molecule^{-1}$ for 3-pmbpa and 43(2) $Å^2$ $molecule^{-1}$ for 4-pmbpa. The double Langmuir model gives a much better fit to the data. The reason for this is that there are again two competing binding modes. In this case, however the "bidentate" binding mode is expected to be less favourable, in particular for 4-pmbpa as the hydrophobic phenyl ring would inhibit the binding of the second phosphonic acid group. This results in a much earlier changeover from the "bidentate" to the "monodentate" binding mode as indicated by the lower surface coverage values for this mode of 0.9(2) × 10^{-5} and 0.7(1) × 10^{-5} mol g^{-1} for 3-pmbpa and 4-pmbpa respectively.

By contrast, the data for H_5mbpp fits the simple Langmuir model very well giving an equilibrium constant approximately two and a half to three times that for the bisphosphonates and phenylphosphonic acid. The required surface area is calculated at 65(4) $Å^2$ $molecule^{-1}$ which is approximately twice that for phenylphosphonic acid [35(1) $Å^2$ $molecule^{-1}$] and shows clearly that the ligand is binding onto the surface through both phosphonic acid groups. The phenol group can be deprotonated (pKa = 11.88)[1] to form an additional bond/bonds to the surface, thus providing additional stabilisation for this binding mode. The copper cluster $[Cu_4(Hmbpp)_2(H_2NC(O)NH_2)_2(H_2O)_8]$ (Figure 5.9, Section 5.3.1) provides evidence

for this additional interaction and shows how the ligand could address an array of surface metals.

Compound	Amount of ligand adsorbed at monolayer coverage (n_M) 10^5 [mol g^{-1}]		Equilibrium adsorption constant (K) 10^{-3} [L mol^{-1}]	
	Langmuir	Double Langmuir	Langmuir	Double Langmuir
2-pmbpa	-	n_1 1.3(1) n_2 2.5(1.0)	-	K_1 21(4) K_2 0.1(1)
3-pmbpa	2.8(1)	n_1 0.9(2) n_2 2.2(1)	4.2(6)	K_1 55(25) K_2 1.1(3)
4-pmbpa	2.7(1)	n_1 0.7(1) n_2 2.3(1)	3.2(4)	K_1 75(30) K_2 1.1(1)
H_5mbpp	1.8(1)	-	10(2)	-
P-bpa	3.0(1)	n_1 1.3(1) n_2 2.2(1)	10(2)	K_1 120(30) K_2 1.1(2)
P-419	3.0(1)	n_1 1.3(1) n_2 2.1(1)	10(3)	K_1 140(50) K_2 1.1(4)
2-opepa	2.6(1)	n_1 1.2(3) n_2 1.5(3)	21(5)	K_1 160(80) K_2 4(2)
3-pppa	2.7(1)	-	6.8(6)	-

Table 5.6: Adsorption isotherm data (standard deviations in parenthesis).

The isotherms (Figure 5.19) for P-bpa and P-419 both fit the double Langmuir model. The slope of the graphs in the low concentration region (<0.5 × 10^{-3} mol l^{-1}) and the equilibrium constants obtained from the simple Langmuir model are comparable with that of H_5mbpp, indicating a very high binding strength. Monolayer coverage for both compounds can be estimated at ~3 × 10^{-5} mol g^{-1} giving a required surface area of ~39 $Å^2$ $molecule^{-1}$. No structural evidence could be obtained for the involvement of the keto function in binding to the surface.

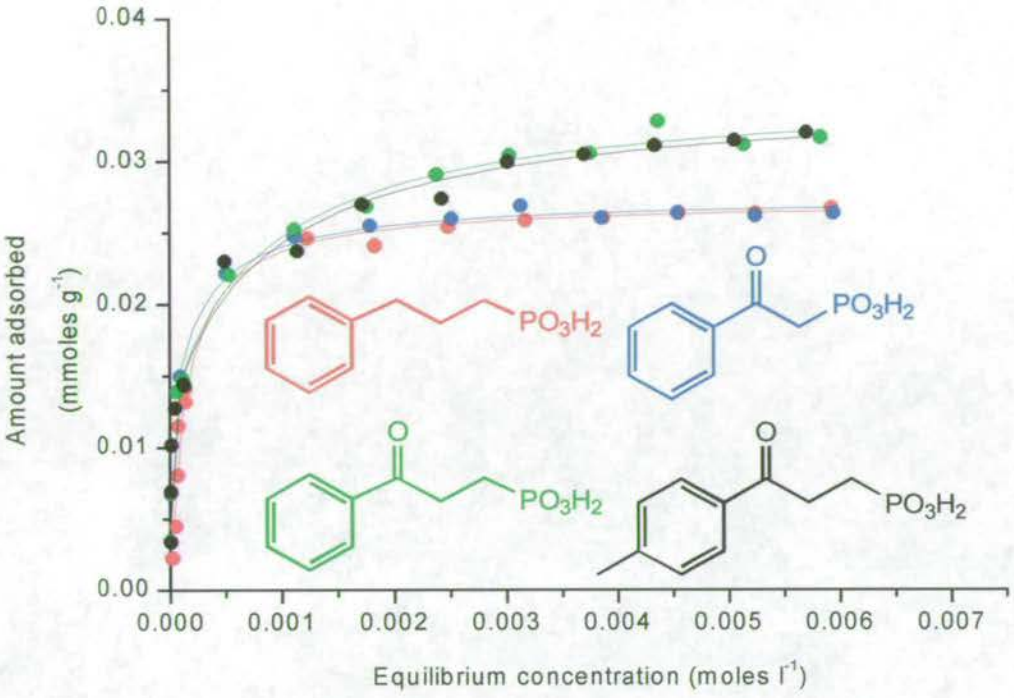

Figure 5.19: Adsorption isotherms for P-bpa (green), P-419 (black), 2-opepa (blue) and 3-pppa (red).

A concern over using the ligand 2-opepa in the isotherm experiment was its structural analogy to acetylacetonate (acac). This means that it could potentially bind to aluminium in the same chelating (Figure 5.20) fashion as acac, via deprotonation of the α carbon, thus sequestering aluminium ions into solution in preference to adsorbing onto the surface. The esters of 2-ketophosphonic acids are known to adopt this binding mode to other metals[14] and the carboxymethylphosphonate in $Al(O_3PCH_2CO_2).3H_2O$[15] (Chapter 4, Section 4.1.3) shows this mode in addition to binding two other aluminium atoms. Complexation during the isotherm experiment should be recognisable by a shift in the absorption band after equilibrating and/or a high degree of scattering of the isotherm. This was not found to be the case and the isotherm (Figure 5.19) fitted well to the double Langmuir model. The required surface area of 45(2) $Å^2$ molecule^{-1} is larger than that for the 3-ketophosphonic acids.

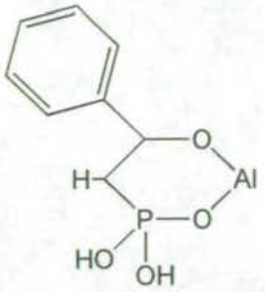

Figure 5.20: Potential chelating mode of the ligand 2-opepa.

Although not immediately apparent from the isotherms, the equilibrium constants obtained from curve fitting to the double Langmuir model show that the three carbonyl containing compounds, P-bpa, P-419 and 2-opepa receive a considerable boost to their initial binding strength over the bisphosphonates 2-, 3- and 4-pmbpa.

The isotherm (Figure 5.19) for 3-pppa gives a monolayer coverage of 2.7×10^{-5} mol g^{-1} leading to a required surface area of 43(2) $Å^2$ $molecule^{-1}$ which is larger than that found for phenylphosphonic acid and the 3-ketophosphonic acids. The reason for this may lie in the compounds relatively flexible tail which means that it obscures potential binding sites on the surface and also is less likely to form ordered arrays on the surface, leading to a lower surface coverage. A similar phenomenon occurs between the carboxylic acids Irg-419 and Irg-78 on both goethite and $Al(OH)_3$ (Chapter 3, Sections 3.1.4 and 3.4).

5.5 Conclusions.

Under the experimental conditions used here, the adsorption isotherms for the bisphosphonic acids (n-pmbpa, where n = 2, 3, 4), demonstrate that there is little benefit in the use of compounds with two phosphonic acid groups over simple benzyl phosphonic acids. While at low concentrations they bind in a bidentate fashion, at higher concentrations they appear to revert to binding through one phosphonic acid group to maximise the surface concentration of the ligand. In contrast work[16] at higher pH (8.5) has shown bisphosphonic acids to have higher binding strengths than simple phosphonic acids.

Unlike the other bisphosphonic acids, H_5mbpp appears to bind to the $Al(OH)_3$ using both phosphonic acids, with surface attachment stabilised by the presence of the *o*-phenol group. The feasibility of such a binding mode is supported by the structure of $[Cu_4(Hmbpp)_2(H_2NC(O)NH_2)_2(H_2O)_8].4H_2O$ which shows the deprotonated phenolate oxygen of H_5mbpp bridging two copper atoms. This difference in binding characteristics between H_5mbpp and other phosphonic acids explains previous observations[17] in which under electrochemical testing H_5mbpp was found to be the superior corrosion inhibitor for aluminium.

The isotherms also show that carbonyl containing phosphonic acids, as with carboxylic acids, display very different adsorption properties.

5.6 Experimental.

5.6.1 Chemicals and Instrumentation.

All reagents were used as obtained from Aldrich, Acros or Lancaster. Solvents were used as received. High surface area "superfine $Al(OH)_3$" was supplied by Alcan. Water was distilled before use.

Analytical data were obtained on a Perkin-Elmer 2400 Elemental analyser by the University of Edinburgh Microanalytical Service.

Melting points were determined using a Gallenkamp melting point apparatus and are uncorrected.

^1H, ^{13}C and ^{31}P NMR were obtained using Bruker WP200 and AC250 spectrometers at ambient temperature. Chemical shifts (δ) are reported in parts per million (ppm) relative to residual solvent protons as internal standards. NMR spectra were interpreted with the aid of gNMR 4.1.0 (demo version) © 1995-1999 IvorySoft.

Electron impact mass spectrometry (EIMS) was carried out on a Kratos MS50TC spectrometer. Fast atom bombardment mass spectrometry (FABMS) was carried out using a Kratos MS50TC spectrometer a 3-nitrobenzyl alcohol (NOBA) or thioglycerol matrix.

The infra-red spectra were obtained as potassium bromide discs using a Perkin Elmer Paragon 1000 FT-IR spectrometer.

Electronic spectra were measured on an ATI UNICAM UV/vis spectrometer with 1cm path length quartz cuvettes.

Variable temperature magnetic measurements in the region 1.8-325 K were made using a SQUID magnetometer (Quantum Design) with samples sealed in gelatin capsules. Diamagnetic corrections for sample holders and samples were applied to the data.

EPR spectra were recorded by Dr Eric McInnes (University of Manchester) on a Bruker ESP300E spectrometer at Q-band (ca. 34 GHz) between 115 K and 300 K.

Curve fitting were performed using the programs Origin 5.0 © Microcal Software Inc and SigmaPlot 2000 (demo version) © 1986-2000 SPSS Inc.

Crystal data were collected on either a Stoe Stadi-4 diffractometer or a Bruker Smart APEX CCD area detector. Both were equipped with an Oxford Cryosystems low-temperature device. Full listings of atomic positions and thermal parameters are provided electronically on the CD accompanying this thesis.

5.6.2 Synthesis.

(2-Phosphonomethyl-benzyl)-phosphonic acid (2-pmbpa).

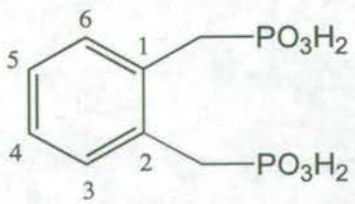

α,α'-Dichloro-*o*-xylene (8.8 g, 50.2 mmol) and triethyl phosphite (18.3 g, 110.2 mmol) were heated under reflux (140 °C) for four hours, then the reaction cooled to room temperature. Excess triethyl phosphite was removed on a rotary evaporator to give a colourless oil. Concentrated hydrochloric acid (100 ml) was added and the solution heated under reflux (100 °C) overnight. The solution was cooled to room temperature. Spontaneous precipitation occurred on placing the

solution under vacuum. The precipitate formed was filtered, washed with ice cold water then acetone and dried under vacuum to give a white powder (11.1 g, 83 %)

m.p. 252-254 °C (Lit.[18] 252 °C); (Found: C, 35.6; H, 4.7 %; $C_8H_{12}O_6P_2$ requires C, 36.1; H, 4.5 %); ^{1}H NMR (d_6DMSO, 200 MHz) δ 7.22 (m, 2H), δ 7.13 (m, 2H), δ 3.15 (d, 4H, 2 × CH_2); ^{13}C NMR (d_6DMSO, 63 MHz) δ 132.90 (C1 & C2), δ 131.43 (C4 & C5), δ 126.42 (C3 & C6), δ 32.78 (d, 2 × CH_2); ^{31}P NMR (d_6DMSO, 101 MHz) δ 22.80 (2P); FABMS *m/z* 267 (LH); IR (cm^{-1}, KBr disc) ν 2804(br)m, 1498w, 1454w, 1405w, 1258m (P=O), 1215w, 1171m, 1128m, 1069s, 961s, 824m, 778s, 598w, 513s, 471m.

(3-Phosphonomethyl-benzyl)-phosphonic acid (3-pmbpa).

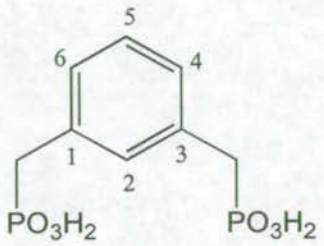

α,α'-Dichloro-*m*-xylene (5.2 g, 29.7 mmol) and triethyl phosphite (10.7 g, 64.5 mmol) were heated under reflux (140 °C) for four hours, then the reaction cooled to room temperature. Excess triethyl phosphite was removed on a rotary evaporator to give a colourless oil. Concentrated hydrochloric acid (100 ml) was added and the solution heated under reflux (100 °C) overnight. The solution was cooled to room temperature. The solvent was removed on a rotary evaporator to give a white solid.. This was recrystallised from ethanol/ether, to give a white powder (6.5 g, 82 %).

m.p. 198-201 °C; (Found: C, 36.2; H, 4.6 %; $C_8H_{12}O_6P_2$ requires C, 36.1; H, 4.5 %); ^{1}H NMR (d_6DMSO, 200 MHz) δ 7.21-7.07 (m, 4H), δ 2.92 (d, 4H, 2 × CH_2); ^{13}C NMR (d_6DMSO, 63 MHz) δ 133.97 (C1 & C3), δ 131.38 (C5), δ 128.13 (C2), δ 127.85 (C4 & C6), δ 35.44 (d, 2 × CH_2); ^{31}P NMR (d_6DMSO, 101 MHz) δ 22.54 (2P); FABMS *m/z* 267 (LH); IR (cm^{-1}, KBr disc) ν 2928m (CH), 2301(br)m, 1604m,

1487m, 1443m, 1404m, 1230m (P=O), 1188m, 1117s, 1028s, 943s, 899m, 807m, 763m, 731w, 702m, 626w, 589w, 503m, 484m.

(4-Phosphonomethyl-benzyl)-phosphonic acid (4-pmbpa).

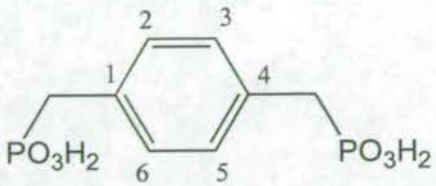

α,α'-Dichloro-*p*-xylene (5.0 g, 28.6 mmol) and triethyl phosphite (10.4 g, 62.7 mmol) were heated under reflux (140 °C) for four hours, then the reaction cooled to room temperature. Excess triethyl phosphite was removed on a rotary evaporator to give a waxy solid. This was dissolved in ether and placed in the freezer overnight. The white crystalline solid formed was filtered and dried under vacuum to give 4-(diethoxy-phosphorylmethyl)-benzyl]-phosphonic acid diethyl ester (8.2 g, 75.9 %), which was dissolved in concentrated hydrochloric acid (70 ml) and distilled water (20 ml) and heated under reflux (100°C) overnight. A white prcipitate formed on cooling to 0 °C that was filtered, washed with ice cold water and dried under vacuum to give a white powder (5.1 g, 88 %).

m.p. 302-305 °C (Lit.[19] 300-302 °C); (Found: C, 36.1; H, 4.4 %; $C_8H_{12}O_6P_2$ requires C, 36.1; H, 4.5 %); ^{1}H NMR (d_6DMSO, 200 MHz) δ 7.17 (s, 4H), δ 2.93 (d, 4H, 2 × CH_2); ^{13}C NMR (d_6DMSO, 63 MHz) δ 140.30 (C1 & C4), δ 127.10 (C2, C3, C5 & C6), δ 27.30 (d, 2 × CH_2); ^{31}P NMR (d_6DMSO, 101 MHz) δ 20.32 (2P); FABMS *m/z* 267 (LH); IR (cm^{-1}, KBr disc) ν 2797(br)s, 2309s, 1928w, 1509m, 1425m, 1402m, 1266s (P=O), 1231s, 1114s, 1090s, 998s, 970s, 942s, 848m, 804m, 749m, 558s, 480m.

4-Methyl-2,6-bis(phosphonomethyl)phenol (H_5mbpp).

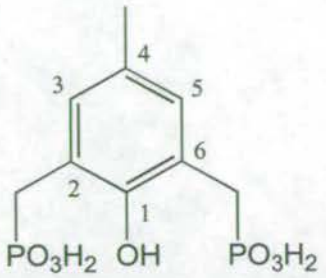

2,6-Bis(hydroxymethyl)-*p*-cresol (8.4 g, 50 mmol) and trimethyl phosphite (13.0 g, 105 mmol) were heated under reflux for four hours. The solution was cooled to room temperature and the excess trimethyl phosphite removed on a rotary evaporator to give a colourless oil. Diethyl ether was added to the flask and the solution placed in the fridge overnight. The white precipitate that formed was filtered and dried under vacuum to give [3-(dimethoxy-phosphorylmethyl)-2-hydroxy-5-methyl-benzyl]-phosphonic acid dimethyl ester as a white crystalline solid. [3-(Dimethoxy-phosphorylmethyl)-2-hydroxy-5-methyl-benzyl]-phosphonic acid dimethyl ester was dissolved in water (100 ml) and methanol (100 ml) and the solution heated under reflux overnight. The solution was cooled to room temperature and the solvent removed on a rotary evaporator to give a white solid which was recrystallised from methanol/ethyl acetate, washed with ethyl acetate then ether and dried under vacuum to give 4-methyl-2,6-bis(phosphonomethyl)phenol as a white solid (9.1 g, 61 %).

m.p. ~250 °C (Decomposition); (Found: C, 36.7; H, 4.6 %; $C_9H_{14}O_7P_2$ requires C, 36.5; H, 4.7 %); ^{1}H NMR (D_2O, 200 MHz) δ 6.88-6.85 (m, 2H), 3.07 (d, 4H, 2 × CH_2), δ 2.10 (d, 3H, CH_3); ^{13}C NMR (D_2O, 63 MHz) δ 149.45 (C1), δ 131.24 (C4), δ 130.54 (C2 & C6), δ 121.64 (C3 & C5), δ 29.36 (2 × CH_2), δ 19.41 (CH_3); ^{31}P NMR (D_2O, 101 MHz) δ 26.92 (2P); FABMS *m/z* 297 (LH); IR (cm^{-1}, KBr disc) ν 2926m (CH), 1636w, 1485s, 1398w, 1377w, 1310m, 1264m (P=O), 1229s, 1159s, 1116s, 1013s, 952s, 927s, 868w, 845w, 731m, 688w, 606w, 541w, 510m, 464w.

3-Dimethylamino-1-phenyl-propan-1-one.hydrochloride.

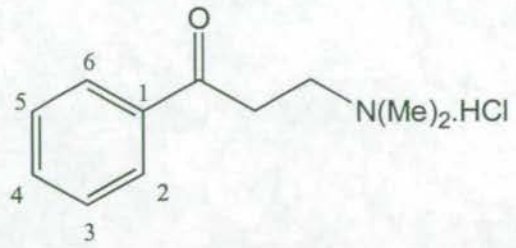

Concentrated hydrochloric acid (1 ml) was added to a stirred suspension of acetophenone (22.2 g, 185.0 mmol), dimethylamine hydrochloride (19.8 g, 242.9 mmol) and paraformaldehyde (7.5 g, 250.0 mmol). The reaction was heated under reflux (100 °C) for 2 hours, then hot filtered, diluted with acetone (150 ml) and the solution placed in the fridge overnight. The precipitate that formed was filtered, washed with cold acetone (100 ml) and dried under vacuum to give a white crystalline solid (27.3 g, 69 %).

m.p. 143-145 °C (Lit.[20] 156 °C); (Found: C, 61.2; H, 7.6; N, 6.4 %; $C_{11}H_{16}NOCl$ requires C, 61.8; H, 7.5; N, 6.6 %); ^{1}H NMR ($CDCl_3$, 200 MHz) δ 7,92 (m, 2H, H2 & H6), δ 7.54 (m, 1H, H4), δ 7.43 (m, 2H, H3 & H5), δ 3.67 (m, 2H, CH_2), δ 3.48 (m, 2H, CH_2) δ 2.82 (s, 6H, $N(CH_3)_2$); ^{13}C NMR ($CDCl_3$, 63 MHz) δ 195.61 (C=O), δ 135.36 (C1), δ 133.96 (C4), δ 128.73 (C2 & C6), δ 128.13 (C3 & C5), δ 52.64 (CH_2N), δ 43.26 ($N(CH_3)_2$) δ 33.67 (CH_2); FABMS *m/z* 178 (L-Cl); IR (cm^{-1}, KBr disc) ν 3434(br)m (NH), 3008m (CH ar), 2958m, 2932m & 2910m (CH alk), 2778m, 2643s, 2567m, 2511m, 2466m, 2439m, 1679s (C=O), 1597m, 1582m, 1468m, 1459m, 1418w, 1405w, 1381m, 1335m, 1315m, 1223m, 1170w, 1134w, 1073w, 1030w, 1002w, 960s, 860w, 755s, 691m, 651w, 616w, 572w.

3-Dimethylamino-1-*p*-tolyl-propan-1-one.hydrochloride

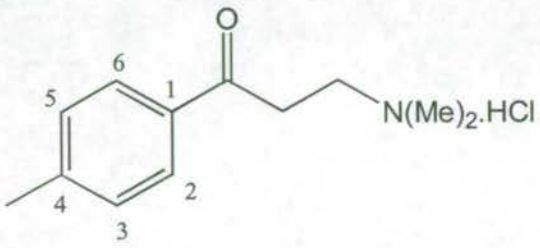

Concentrated hydrochloric acid (1 ml) was added to a stirred suspension of 4-methylacetophenone (22.2 g, 165.6 mmol), dimethylamine hydrochloride (19.8 g, 242.9 mmol) and paraformaldehyde (7.5 g, 250.0 mmol). The reaction was heated under reflux (100 °C) for 2 hours, then hot filtered, diluted with acetone (150 ml) and the solution placed in the fridge overnight. The precipitate that formed was filtered, washed with cold acetone (100 ml) and dried under vacuum to give a white crystalline solid (22.2 g, 59 %).

m.p. 151-154 °C (lit.[21] 152-155 °C); (Found: C, 62.1; H, 8.1; N, 6.4 %; $C_{12}H_{18}NOCl$ requires C, 63.3; H, 7.9; N, 6.2 %); ^{1}H NMR ($CDCl_3$, 200 MHz) δ 7.85 (d, 2H, H2 & H6), δ 7.25 (d, 2H, H3 & H5), δ 3.70 (t, 2H, CH_2), δ 3.50 (t, 2H, CH_2) δ 2.84 (s, 6H, $N(CH_3)_2$), δ 2.39 (s, 3H, CH_3); ^{13}C NMR ($CDCl_3$, 63 MHz) δ 195,74 (C=O), δ 145.68 (C4), δ 133.37 (C1), δ 130.0 (C2 & C6), δ 128.84 (C3 & C5), δ 53.19 (CH_2N), δ 43.79 ($N(CH_3)_2$), δ 34.08 (CH_2), δ 22.18 (CH_3); FABMS *m/z* 192 (L-Cl); IR (cm^{-1}, KBr disc) ν 3433(br)m (NH), 3337m, 3032s (CH ar), 2950s & 2925s (CH alk), 2817s, 2678s, 2520s, 2448s, 1677s (C=O), 1640m, 1610s, 1572m, 1474s, 1468s, 1443s, 1393s, 1380s, 1357s, 1318m, 1305m, 1238s, 1210s, 1188s, 1154s, 1116m, 1068m, 1041m, 1024m, 1012m, 988s, 977s, 958s, 911s, 869m, 830s, 787s, 72w, 710w, 636w, 610w, 561m, 524w, 459m.

3-Dimethylamino-1-(4-nitro-phenyl)-propan-1-one.hydrochloride.

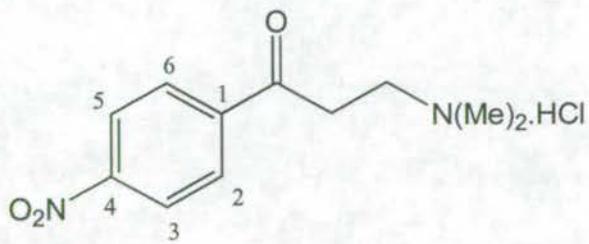

Concentrated hydrochloric acid (3 ml) was added to a stirred suspension of 4-nitroacetophenone (60.1 g, 364.2 mmol), dimethylamine hydrochloride (38.6 g, 473.6 mmol) and paraformaldehyde (14.2 g, 473.3 mmol). The reaction was heated under reflux (100 °C) for two hours, then cooled to room temperature and the solution placed in the fridge overnight. The precipitate that formed was filtered,

washed with cold acetone (100 ml) and dried under vacuum to give a yellow powder (49.2 g, 52.1 %).

m.p. 178-181 °C (decomposition) (lit.[22] 187.5-188.5 °C); (Found: C, 50.7; H, 6.1; N, 11.1 %; $C_{11}H_{16}N_2O_3Cl$ requires C, 50.9; H, 6.2; N, 10.8 %); ^{1}H NMR ($CDCl_3$, 200 MHz) δ 8,33 (d, 2H, H3 & H5), δ 8.16 (d, 2H, H2 & H6), δ 3.57 (s, 2H, CH_2), δ 2.94 (s, 6H, $N(CH_3)_2$) δ 2.69 (s, 2H, CH_2); ^{13}C NMR ($CDCl_3$, 63 MHz) δ 198.47 (C=O), δ 150.55 (C4), δ 139.96 (C1), δ 129.35 (C2 & C6), δ 123.98 (C3 & C5), δ 52.52 (CH_2N), δ 43.04 ($N(CH_3)_2$), δ 34.48 (CH_2), δ 22.18 (CH_3) FABMS *m/z* 224 (L-Cl); IR (cm^{-1}, KBr disc) ν 3101w, 3068w, 3023m & 3009m (CH ar), 2986m, 2964s & 2908m (CH alk), 2847m, 2779m, 2681s, 2609m, 2576m, 2510m, 2473m, 1700s (C=O), 1604w, 1527s (NO_2 anti), 1484w, 1471w, 1400w, 1389w, 1345m, 1330s (NO_2 sym), 1254w, 1214s, 1106w, 1076w, 1001w, 964m, 878, 852m, 807w, 773w, 744m, 691w, 576w, 543w, 509w.

(3-Oxo-3-phenyl-propyl)-phosphonic acid diethyl ester.

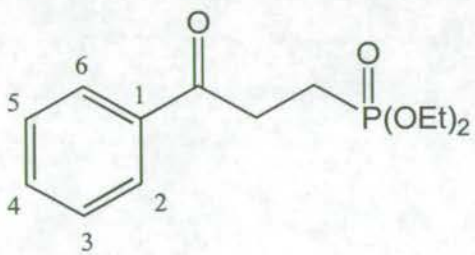

3-Dimethylamino-1-phenyl-propan-1-one.hydrochloride (20.1 g, 94.1 mmol) and triethylphosphite (90.4 g, 484 mmol) were added to a reaction vessel, pre-flushed with nitrogen. The reaction was refluxed (140 °C) under nitrogen for four hours, then cooled to room temperature. The excess triethyl phosphite was removed by distillation under reduced pressure, (70 °C at ~0.05 mmHg), and the product purified by further distillation (162 °C at ~0.05 mmHg (lit.[7] 163-167 °C at 0.08 mmHg) to give a pale yellow oil (22.6 g, 89 %).

(Found: C, 57.1; H, 6.9; N, 0.6* %; $C_{13}H_{19}O_4P$ requires C, 57.8; H, 7.0; N, 0.0 %); ^{1}H NMR ($CDCl_3$), 200 MHz) δ 7.96 (m, 2H, H2 & H6), δ 7.56 (m, 1H, H4), δ 7.45 (m, 2H, H3 & H5), δ 4.09 (m, 4H, 2 × CH_2), δ 3.28 (m, 2H, CH_2), δ 2.17 (m,

2H, CH_2P), δ 1.29 (m, 6H, 2 × CH_3); ^{13}C NMR ($CDCl_3$, 63 MHz) δ 197.33 (d, C=O), δ 136.12 (C1), δ 133.24 (C4), δ 128.54 (C2 & C6), δ 127.90 (C3 & C5), δ 61.60 (d, 2 × OCH_2), δ 31.61 (d, CH_2), δ 19.58 (d, CH_2P), δ 16.31 (d, 2 × CH_3); ^{31}P NMR ($CDCl_3$, 101 MHz) δ 32.53 (1P); FABMS *m/z* 271 (LH).

* Difficult to remove all air from capsule when dealing with liquids, therefore tend to get some trapped N_2.

(3-Oxo-3-phenyl-propyl)-phosphonic acid.½H_2O (P-bpa)

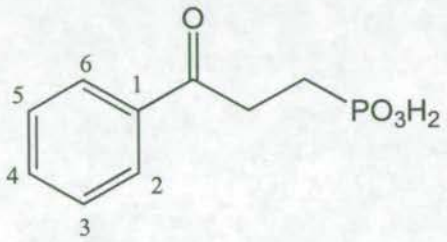

(3-Oxo-3-phenyl-propyl)-phosphonic acid diethyl ester (36.7 g, 135.9 mmol) in concentrated hydrochloric acid (260 ml) was heated under reflux (100°C) for four hours, then cooled to room temperature. Crystallisation was induced by addition of distilled water (5 ml). The precipitate was filtered, washed with distilled water and dried under vacuum to give a white crystalline solid (18.4 g, 61 %).

m.p. 116-118 °C; (Found: C, 48.4; H, 5.4 %; $C_9H_{12}O_{4.5}P$ requires C, 48.4; H, 5.3 %); ^1H NMR (D_2O, 200 MHz) δ 7.93 (m, 2H, H2 & H6), δ 7.63 (m, 1H, H4), δ 7.49 (m, 2H, H3 & H5), δ 3.29 (m, 2H, CH_2), δ 2.06 (m, 2H, CH_2P); ^{13}C NMR (D_2O, 63 MHz) δ 202.49 (d, C=O) δ 135.76 (C1), δ 134.01 (C4), δ 128.79 (C2 & C6), δ 128.14 (C3 & C5) δ 32.06 (d, CH_2), δ 21.11 (d, CH_2P); ^{31}P NMR (D_2O, 101 MHz) δ 29.86; FABMS *m/z* 215 (LH); IR (cm^{-1}, KBr disc) ν 3505m (OH), 2927m (CH), 1684s (C=O), 1594m, 1449m, 1415w, 1358w, 1265s (P=O), 1120m, 1000s, 936s, 728s, 691m, 499m, 458m.

(3-Oxo-3-*p*-tolyl-propyl)-phosphonic acid (P-419).

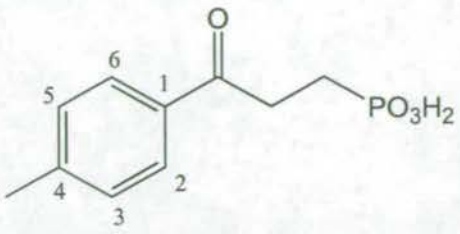

3-Dimethylamino-1-*p*-tolyl-propan-1-one.hydrochloride (19.7 g, 86.6 mmol) and triethylphosphite (96.9 g, 584 mmol) were added to a reaction vessel, pre-flushed with nitrogen. The reaction was refluxed (140 °C) under nitrogen for four hours, then cooled to room temperature. The excess triethyl phosphite was removed by distillation under reduced pressure (70 °C at ~0.05 mmHg), to give (3-oxo-3-*p*-tolyl-propyl)-phosphonate ethyl ester as a pale yellow oil (18.9 g). The ester was converted to the acid without further purification by heating under reflux (100 °C) in concentrated hydrochloric acid (250 ml). The solution was cooled to room temperature and crystallisation induced by addition of distilled water (5 ml). The precipitate was filtered, washed with distilled water and dried under vacuum to give a white crystalline solid (13.9 g, 70 %).

m.p. 157-159 °C; (Found: C, 52.2; H, 5.8 %; $C_{10}H_{13}O_4P$ requires C, 52.4; H, 5.7 %); ^{1}H NMR (d_6DMSO, 200 MHz) δ 7.84 (d, 2H, H2 & H6), δ 7.38-7.30 (m, 2H, H3 & H5), δ 3.16 (m, 2H, CH_2) δ 2.36 (s, 3H, CH_3), δ 1.88 (m, 2H, CH_2P); ^{13}C NMR (d_6DMSO, 63 MHz) δ 197.8 (d, C=O), δ 143.7 (C4), δ 133.95 (C1), δ 129.44 (C2 & C6), δ 128.08 (C3 & C5), δ 38.76 (d, CH_2), δ 21.97 (d, CH_2P), δ 21.28 (CH_3); ^{31}P NMR (d_6DMSO, 101 MHz) δ 27.30; FABMS *m/z* 229 (LH); IR (cm^{-1}, KBr disc) ν 3500(br)w (OH), 3025m (CH ar), 2950m CH alk), 2760(br)m, 2450(br)m, 1681s (C=O), 1604s, 1572w, 1422m, 1361w, 1291w, 1251s (P=O), 1182m, 1126m, 1031s, 959s, 821m, 742m, 596w, 572w, 501m, 464w. Crystals suitable for X-ray analysis were grown by slow evaporation of the filtrate after 2 weeks.

(2-Oxo-2-phenyl-ethyl)-phosphonic acid.

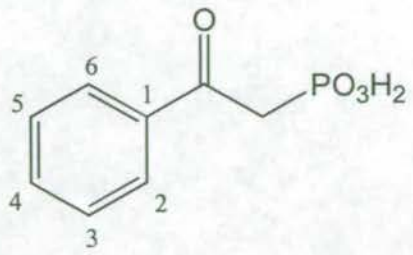

α-Bromoacetophenone (25.1 g, 126.1 mmol) was refluxed in triethyl phosphite (25.2 g, 151.8 mmol), under nitrogen, for three hours and the reaction cooled to room temperature. Excess triethyl phosphite was removed by distillation under reduced pressure (70 °C at ~0.05 mmHg). Concentrated hydrochloric acid (100 ml) was added and the solution heated under reflux overnight, then cooled to room temperature. The solvent was removed on a rotary evaporator and the crude product recrystallised from ethyl acetate to give a pale yellow crystalline solid (10.6 g, 42 %).

m.p. 141-143 °C (lit.[23] 139-140 °C); (Found: C, 47.7; H, 4.7 %; $C_8H_9O_4P$ requires C, 48.0; H, 4.5 %); ^{1}H NMR (d_6DMSO, 200 MHz) δ 8.85 (s, 2H broad, 2 × OH), δ 8.01 (m, 2H, H2 & H6), δ 7.64 (m, 1H, H4), 7.54 (m, 2H, H3 & H5), δ 3.55 (d, 2H, CH_2); ^{13}C NMR (d_6DMSO, 63 MHz); δ 193.63 (d, C=O), 136.87 (C1), δ 133.45 (C4), δ 129.22 (C2 & C6), 128.69 (C3 & C5), (CH_2 underneath D_6DMSO peaks); ^{31}P NMR (d_6DMSO, 101 MHz) δ 15.66; FABMS *m/z* 201 (LH); IR (cm^{-1}, KBr disc) ν 2768(br)m, 1677s (C=O), 1654m, 1594m, 1580m, 1560w, 149m, 1378w, 1368w, 1323m, 1310m, 1204m, 1182m, 1125m, 1016s, 1001s, 966s, 934m, 858m, 772m, 754s, 690s, 537m.

(3-Phenyl-propyl)-phosphonic acid.

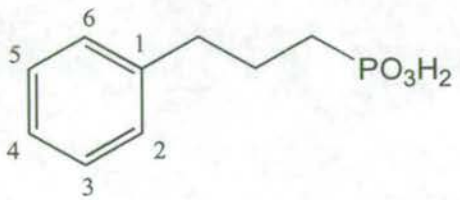

1-Bromo-phenylpropane (26.2 g, 131.7 mmol) was heated under reflux (140 °C) in triethyl phosphite (96.9 g, 583.7 mmol) under nitrogen overnight. The solution

was cooled to room temperature and the excess triethyl phosphite removed by distillation under reduced pressure (70 °C at ~0.05 mmHg). This gave crude (3-phenyl-propyl)-phosphonic acid diethyl ester as a colourless oil (32.0 g, 94.9 %). (3-Phenyl-propyl)-phosphonic acid diethyl ester (10.0 g, 39.1 mmol) was heated under reflux (100 °C) in concentrated hydrochloric acid (50 ml) with ethanol (20 ml) added to aid dissolution. The reaction was cooled to room temperature and the solvent removed on a rotary evaporator to give a colourless oil which on standing gave colourless crystals. These were filtered, washed with hexane and recrystallised from ethylacetate/hexane to give a white crystalline solid (4.1 g, 53 %).

m.p. 121-123 °C (lit.[9,10] 122-125 °C); (Found: C, 53.7; H, 6.3 %; $C_9H_{13}O_3P$ requires C, 54.0; H, 6.5 %); ^{1}H NMR ($CDCl_3$), 200 MHz) δ 11.00 (bs, 2H, 2 × OH), δ 7.38-7.12 (m, 5H), δ 2.70 (t, 2H, CH_2Ph), δ 2.05-1.70 (m, 4H, CH_2CH_2P); ^{13}C NMR ($CDCl_3$, 63 MHz) δ 140.70 (C1), δ 128.40 (C2 & C6), δ 128.30 (C3 & C5),δ 126.00 (C1), δ 36.10 (d, CH_2Ph), 24.50 (d, CH_2), 23.70 (d, CH_2P); ^{31}P NMR ($CDCl_3$, 101 MHz) δ 37.28; FABMS *m/z* 201 (LH); IR (cm^{-1}, KBr disc) ν 3020s CH ar), 2945s (CH alk), 2874s, 1496w, 1463m, 1455m, 1310w, 1251m (P=O), 1222s, 1194s, 1137s, 1118m, 1106w, 1070m, 1051s, 1023s, 1020s, 1009s, 948s, 861w, 833w, 804w, 774m, 720w, 698s, 586s, 531m, 491s.

[(Benzyl-phosphonomethyl-amino)-methyl]-phosphonic acid.

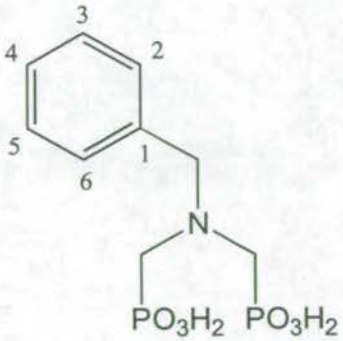

Benzylamine hydrochloride (20.0 g, 139.3 mmol), phosphorus acid (22.8 g, 278.0 mmol) and concentrated hydrochloric acid (30 ml) in distilled water (30 ml) was heated to reflux (100 °C). Formaldehyde (42 ml of a 37 % w/w aqueous solution, 559.4 mmol) was dripped slowly into the reaction mixture over one hour

and the reaction heated under reflux for a further two hours. As the reaction solution cooled to room temperature a white precipitate was formed. The precipitate was filtered, washed with distilled water and dried under vacuum to give a white powder (35.7 g, 87 %).

m.p. 238-240 °C (Lit.[24] 248 °C); (Found: C, 36.3; H, 4.8; N, 4.6 %; $C_9H_{15}NO_6P_2$ requires C, 36.6; H, 5.1; N, 4.8 %); ^{1}H NMR (D_2O + Na_2CO_3, 200 MHz) δ 7.56-7.50 (m, 2H), δ 7.48-7.45 (m, 3H), δ 4.80 (s, 2H, CH_2N), δ 3.37 (d, 4H, 2 × CH_2P); ^{13}C NMR (D_2O + Na_2CO_3, 63 MHz) δ 131.31 (2C), δ 130.14 (1C), δ 129.24 (2C), δ 129.17 (1C), δ 60.12 (CH_2N), δ 50.86 (d, 2C, 2 × CH_2P); ^{31}P NMR (D_2O + Na_2CO_3, 101 MHz) δ 7.78 (2P); FABMS *m/z* 296 (LH); IR (cm^{-1}, KBr disc) ν 2989s & 2940s (CH), 2757s, 1492m, 1458s, 1438m, 1423m, 1384w, 1332m, 1292m, 1231s (P=O), 1156s, 1053s, 1001s, 970s, 939s, 850s, 828s, 766w, 752s, 712s, 699s, 611m, 578s, 531w, 503m, 487m.

$[Cu_4(Hmbpp)_2(H_2NC(O)NH_2)_2(H_2O)_8].4H_2O$.

Copper perchlorate hexahydrate (1.0 g, 2.7 mmol) and 4-methyl-2,6-bis(phosphonomethyl)phenol (H_5mbpp) (0.40 g, mmol) were dissolved in distilled water (40 ml). Sodium hydroxide (2.75 ml of a 1M solution) was added potionwise. During addition the solution changed colour from blue through yellow to brown. The solution was filtered into a 100 ml thick walled test tube and urea (0.40 g) added. The sealed test tube was heated (65 °C) overnight and a small quantity of brown precipitate filtered off. Urea (0.40 g) was added to the solution and the sealed tube left to stand at room temperature where brown crystals of $[Cu_4(H_2mbpp)_2(H_2NC(O)NH_2)_2(H_2O)_8].4H_2O$ formed after a few days (0.23 g, 29 %).

(Found: C, 20.5; H, 4.4; N, 4.8 %; $C_{20}H_{52}N_4O_{28}P_2Cu_4$ requires C, 20.4; H, 4.4; N, 4.8 %). IR (cm^{-1}, KBr disc) ν 3456s (OH), 3325s (NH), 3246s, 2922m (CH), 1657s (C=O), 1578m, 1503w, 1460m, 1409w, 1310w, 1240m (P=O), 1218w, 1207w, 1141s, 1110s, 1083s, 1026s, 984s, 941m, 866w, 860w, 782w, 751m, 627w, 581m, 557m, 502m. Crystals suitable for X-ray analysis were grown from a similar reaction but with copper sulfate pentahydrate in place of copper perchlorate hexahydrate.

5.6.3 Adsorption isotherm measurements.

Preweighed quantities of $Al(OH)_3$ (0.40 g) in polycarbonate centrifuge tubes were stirred with the desired concentration of ligand in methanol/water (10ml, 95:5 v/v) for 2 h at 25 °C. The suspensions were centrifuged and filtered, and the supernatant diluted if necessary, for absorbance measurement by UV spectrometry. The measured absorbance was related to the concentration of the ligand remaining in solution by reference to calibration curves. The amount of ligand adsorbed was then calculated from the difference between initial and final concentration. From this plots of amount of ligand adsorbed versus equilibrium concentration were obtained.

5.7 References.

1 V. Bohmer and W. Vogt, *Helvitica Chimica Acta*, 1993, **76**, 139.

2 C. N. Robertson and R. C. Lewis, *J. Heterocyclic. Chem.*, 1973, **10**, 395.

3 A. K. Bhattacharya and G. Thyagarajan, *Chem. Rev.*, 1981, **81**, 415 and references within.

4 J. March, Advanced Organic Chemistry, 4th Ed, published by John Wiley & Sons, Inc, 1992.

5 G. Ferguson and J. F. Gallagher, *Acta. Cryst. Sect. C*, 1993, **49**, 1024.

6 C. E. Maxwell, *Org. Synth.*, 1943, 30.

7 T. C. Meyers, R. G. Harvey and E. V. Jensen, *J. Am. Chem. Soc.*, 1955, **77**, 3101.

8 I. J. Borowitz, M. Anschel and S. Firstenberg, *J. Org. Chem.*, 1967, **32**, 1723.

9 E. R. Lynch, *J. Chem. Soc.*, 1962, 3729.

10 F. Kagan, R. D. Birkenmyer and R. E. Strube, *J. Am. Chem. Soc.*, 1959, 3026.

11 K. Moedritzer and R. R. Irani, *J. Org. Chem.*, 1966, **31**, 1603.

12 For examples see: a) K. K. Palkina, N. E. Kuz'mina and V. T. Orlova, *Zh. Neorg. Khim.*, 1994, **39**, 1133. b) R. Cuesta, J. Ruiz, J. M. Moreno and E. Colacio, *Inorg. Chim. Acta.*, 1994, **227**, 43. c) M. Koman, E. Jona and D. Nagy, *Z. Kristallogr.*, 1995, **210**, 873.

13 For examples see: H. Uekusa, S. Ohba, Y. Saito, M. Kato, T. Tokii and Y. Muto, Acta Crystallogr., Sect. C (Cr. Str. Comm.), 1989, **45**, 377.

14 For examples see: a) F. A. Cotton, R. Hugel and R. Eiss, *Inorg. Chem.*, 1968, **7**, 18. b) J. Macicek, O. Angelova, G. Petrov and M. Kirilov, *Acta Crystallogr., Sect. C(Cr. Str. Comm.)*, 1998, **44**, 626. c) O. Angelova, J. Macicek and G. Petrov, *J. Coord. Chem.*, 1992, **24**, 305. d) J. Petrova, Z. Zdravkova, O. Angelova and J. Macicek, *J. Coord. Chem.*, 1994, **33**, 161.

15 G. B. Hix, D. S. Wragg, P. A. Wright and R. E. Morris, *J. Chem. Soc., Dalton Trans.*, 1998, 3359.

16 D. A. Nation, *Synthesis and Evaluation of Surface Passivating Agents for Aluminium Flake*, Project Report, The University of Edinburgh, 2000.

17 P. A. Lovatt, *Synthesis of Novel Polynucleating Ligands for Lightly Oxidised Aluminium Surfaces*, Project Report, The University of Edinburgh, 1998.

18 Maier, Crutchfield, *Phosphorus Sulfur*, 1978, **5**, 45.

19 G. M. Kosolapoff, *Chem. Abst.*, 1950, **44**, 7256.

20 H. R. Snyder and J. H. Brewster, *J. Am. Chem. Soc.*, 1948, **70**, 4230.

21 K. Kitsuta, *Chem. Abstr.*, 1956, **50**, 13029.

22 W. B. Wheatly, W. E. Fitzgibbon and L. C. Cheeny, *J. Am. Chem. Soc.*, 1954, **76**, 4490.

23 G. K. Fedorova, L. G. Anan'eva, O. A. Yakovchuk, *Zh. Obshch. Khim.*, 1984, **54**, 1481.

24 K. Moedritzer and R. R. Irani, *J. Org. Chem.*, 1966, 1603.

Chapter 6:

Hydrogen Evolution Tests on Aluminium Flake.

Contents.

6.1 Introduction.

As part of an overlap with a separate project being carried out by Dr D. Nation at the University of Edinburgh, in collaboration with Avecia, samples of several of the phosphonic acid based ligands described in Chapters 4 and 5 were evaluated for their effectiveness in the surface passivation of aluminium flake for water-borne paint systems.

6.1.1 Aluminium Flake.[1]

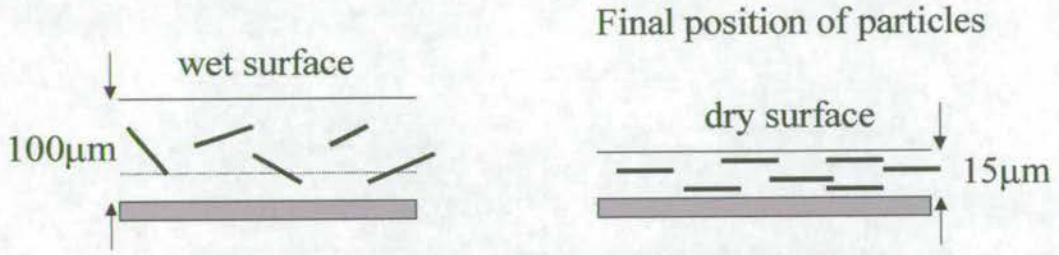

Figure 6.1: Ordering of aluminium flake particles as paint dries.

Aluminium flakes, typically 0.1-1 μm thick and 7-45 μm in length are used, primarily in the automobile industry, to impart desirable optical properties to metallic paints. As the paint dries, the flakes order (Figure 6.1) giving a "flip-flop" or "two-tone" effect which makes the paint change colour on changing the angle of viewing (Figure 6.3). The colour viewed from directly above the paint is described as the "face" and the sideways or grazing angle view is known as the "flop". Dispersants are needed to prevent the agglomeration of the flakes, which leads to seeding and precipitation. A further requirement is passivation of the aluminium surface, as oxidation of aluminium (Figure 6.2) by reaction with water leads to the formation of $Al(OH)_3$ and the evolution of hydrogen gas. This process degrades the appearance of the flakes and as a result the paint. The build up of hydrogen gas can also lead to a dangerous pressure build up within the containers. Studies have shown that moisture levels in excess of 0.15 % in the finished coating can generate sufficient gas to bulge or pop the end of the can.[2] With legislation requiring a move to water-borne paints

from solvent-borne paints (90 % by 2003 in Europe) this has obvious safety implications for the storage of these paints.

$$2\,Al + 6\,H_2O \longrightarrow 2\,Al(OH)_3 + 3\,H_2$$

Figure 6.2: Oxidation of surface aluminium.

Figure 6.3: BASF Variocrom®.[3]

Traditionally, effective passivating treatments for aluminium flake have involved chromating processes.[4] However, there is a concern that chromium(VI) compounds may be carcinogenic. There is now great financial and legislative pressure to replace these chromium-based treatments with more benign alternatives.[5] Various organic ligands have been studied as possible replacements in this regard, including phosphoric and phosphonic acids and their esters.[6]

6.1.2 Hydrogen Evolution Testing Procedures.

The mixture used in the experiment as a model for an aqueous paint formulation is shown below (Table 6.1) and is similar to that used in other hydrogen evolution experiments with aluminium[7] and zinc[8] pigments. The aluminium paste consists of 65 wt % of > 99.9 % pure aluminium and 35 wt % hydrocarbon solvent. Lower purity grades of aluminium are vulnerable to colour change through attack by acid in both the wet paint and after drying.[1] Butoxyethanol (butyl glycol) is the most common organic co-solvent used in water-borne paint systems,[8] while Synperionic NP8 is a non-ionic surfactant added to improve the wetting of the hydrophobic

aluminium paste. Dimethylethanolamine (DMEA) is used as the base as it is known to improve the stability of aqueous aluminum paste dispersions, whereas other bases such as ammonia and triethylamine have been shown to have an adverse effect on the stability.[7] Two mmol of the passivating ligand is used in the formulation. This is considerably in excess of the theoretical amount required to provide monolayer coverage of the aluminium flakes. For example from the isotherm studies (see Chapter 5) 2-opepa has a required surface area of 45(2) $Å^2$ $molecule^{-1}$, therefore two mmol can potentially cover an area of 540(20) m^2. The estimated surface area of aluminium flakes obtained[7] from the BET method is 5 m^2 g^{-1}. Therefore, 3.25 g of aluminium flake (5 g of aluminium paste with 65 % wt of aluminium) has a surface area of only 16.25 m^2.

Component	Mass (g)
Water	90
Butoxyethanol (butyl glycol)	10
Synperonic NP8	2
Aluminium Paste (65 wt %)	5
Passivator	2 mmol
Dimethylethanolamine (DMEA)	sufficient added to adjust to pH 8

Table 6.1: Model aqueous paint formulation.

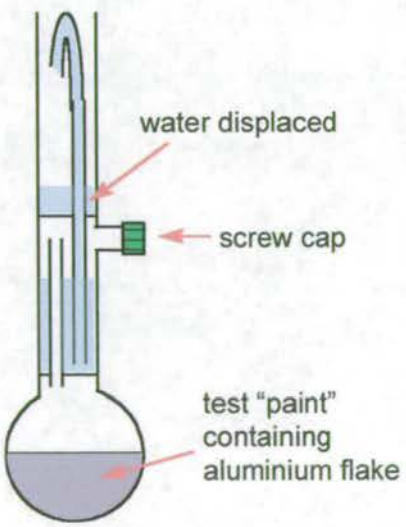

Figure 6.4: Hydrogen evolution apparatus.

The experiments are carried out using special gas volume measuring glassware (Figure 6.4). The round-bottomed flask containing the test mixture is completely immersed in a thermosatted water bath (52 °C), with the screw cap open. The mixture is allowed to equilibrate for one hour before the closing the cap. The apparatus is then monitored periodically to see if water has been displaced from the lower to the upper chamber through generation of hydrogen gas. The volume of water available to be displaced is 80 cm^3; complete reaction of the paste would generate 4.3 litres of hydrogen gas. The onset time is defined as the time at which hydrogen gas evolution is first observed from the sample. Control samples containing no passivating additive, bubble strongly before the end of the one hour equilibration period and once the screw cap is closed, rapidly displace 80 cm^3 of water in less than one minute.

6.2 Results and Discussion.

Compound	Name	mmol	% W/W	Onset time (Hrs)	24 hr Volume (mls)	72 hr Volume (mls)
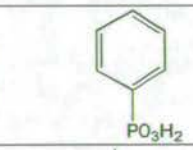	phenylphosphonic acid (ppa)	2	9.7	<16	13-46	64-131
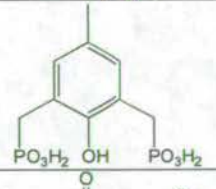	4-methyl-2,6-bis (phosphonomethyl) phenol (H_5mbpp)	2	9.1	1-2.5	>50	>80
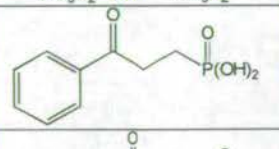	(3-oxo-3-phenyl-propyl)-phosphonic acid (p-bpa)	2	N/A*	94-104	0	0
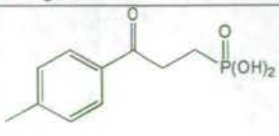	(3-oxo-3-*p*-tolyl-propyl)-phosphonic acid (p-419)	2	7.6	120-126	0	0
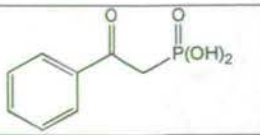	(2-oxo-2-phenyl-ethyl)-phosphonic acid (2-opepa)	2	N/A*	576-648	0	0

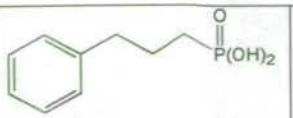	(3-phenyl-propyl)-phosphonic acid (3-pppa)	2	N/A*	22-29	0-2	7.5-8.5
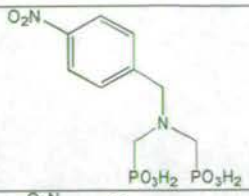	[(4-nitro-benzyl-phosphonomethyl-amino)-methyl]-phosphonic acid (4-nbpampa)	2	11.3	1-2.5	>80	>>80
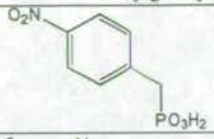	4-nitrobenzyl phosphonic acid (4-nbpa)	2	6.8	<18	N/D	N/D
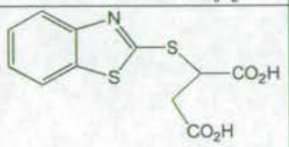	2-(benzothiazol-2-ylsulfanyl)-succinic acid (Irgacor-252)	2	8.8	1min	>80	>>80
-	"Unpassivated"	0	0	1min	>80	>>80
-	"Du-Pont"	N/A	22	>720	0	0

Table 6.2: Results from hydrogen evolution tests measured at Avecia. * Data not available at time of writing.

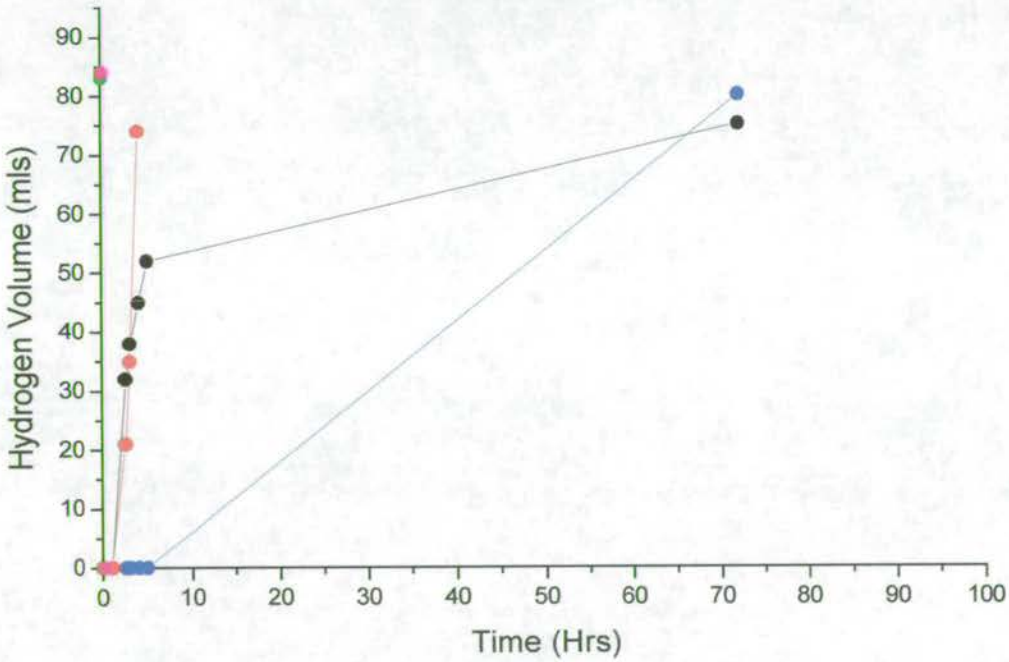

Figure 6.5: Hydrogen evolution results for H_5mbpp (black), 4-nbpampa (red), 4-nbpa (blue), Irgacor-252 (green), and an unpassivated sample (magenta).

The results (Table 6.2) from the hydrogen evolution tests show that the compounds can be broadly split into two groups, those which showed significant

hydrogen evolution within one day ppa, H_5mbpp, 4-nbpampa, 4-nbpa and Irgacor-252 (Figure 6.5) and those which provided good protection over a longer timescale, 3-pppa, p-bpa, p-419 and 2-opepa (Figure 6.6). Full data for ppa were not available and therefore are not plotted.

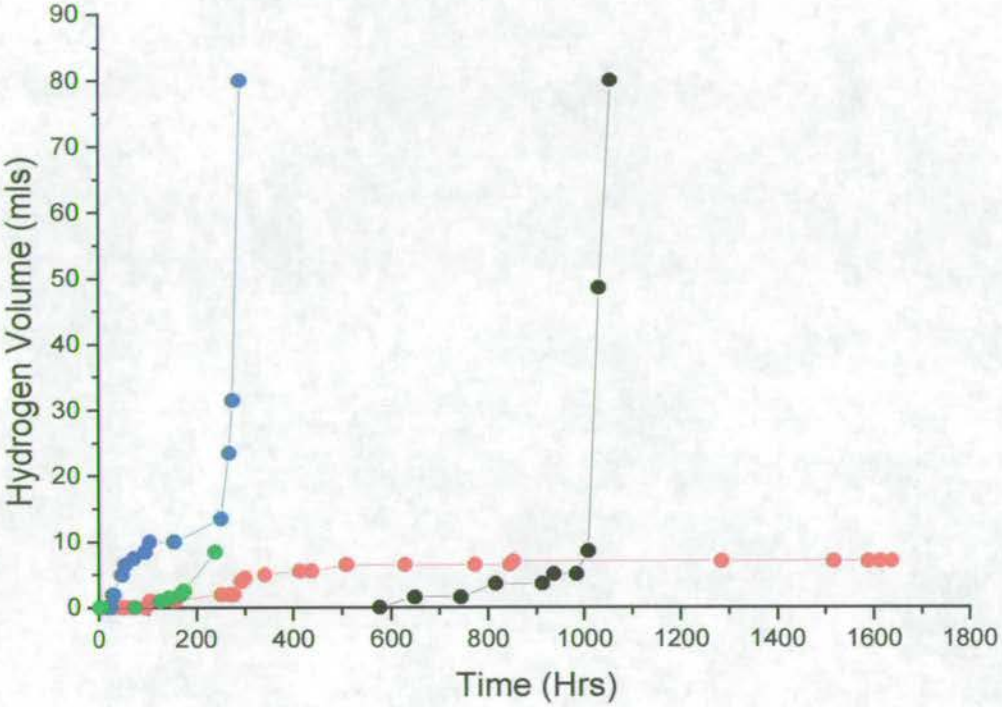

Figure 6.6: Hydrogen evolution results for p-bpa (red), p-419 (green), 2-opepa (black) and 3-pppa (blue)

The fact that ppa and 4-nbpa provide only short term passivation of the surface is not surprising as they are relatively small, simple molecules, which while we have shown to be strongly adsorbing to aluminium oxide/hydroxides, would provide little physical barrier to the hydration of aluminium by water. The relatively poor performance of the other three compounds, H_5mbpp, 4-nbpampa, and Irgacor-252 are of more interest.

Irgacor-252, while not otherwise studied within this thesis, is claimed to be an effective corrosion inhibitor for aluminium in water-borne coatings[9] and as such its performance in these tests was expected to have been much better. The compound in fact provided no surface protection under the experimental conditions used, as with hydrogen evolution commencing almost immediately, it was found to show no improvement over the unpassivated control samples. During the milling of the

aluminium flakes, fatty acids (usually stearic or oleic) are often added as a lubricant to prevent cold welding (formation of three-dimensional flakes or "seeds") of the metal.[1,2] The fatty acids provide a coating for the flakes which is carried through to the paste formulation. We have shown through adsorption isotherms (Chapter 3) that carboxylic acids have moderate binding strength to $Al(OH)_3$ and as Irgacor-252 is also a carboxylic acid based ligand, it may be unable to fully displace these fatty acids from the flakes, explaining why it did not provide any significant degree of surface protection.

The results for H_5mbpp were disappointing, as in previous work[10] done at Edinburgh on electrochemical corrosion testing, this compound was found to afford excellent protection to the surface of an aluminium electrode under highly corrosive conditions. However, in contrast to the hydrogen evolution tests which are done at pH 8, these tests were carried out under highly acidic conditions at pH 2.4 and this may explain the apparent discrepancy in the results. Nevertheless repeating the hydrogen evolution test for this compound is probably worthwhile to determine whether there was a problem with the particular sample used.

4-Nbpampa was found by adsorption isotherm studies[11] to be the most strongly binding compound of the group at pH 8.5, i.e. under conditions similar to that of the hydrogen evolution experiments. The fact that it gives little surface protection again demonstrates that binding strength alone is not the only criteria required for a compound to be considered a good surface ligand.

The onset of hydrogen evolution from the p-bpa sample begins between 94 and 104 hours, then rises to a maximum of 7 ml over a period of ~ 32 days. The sample then remains stable at 7 ml for ~ 32 days until the end of the data collection, after ~ 68 days. No data were available for p-419 over 240 hours but as the performance of the two compounds is similar over this initial period, it is likely that the overall behaviour of the two compounds will be comparable. The improved performance of the 3-keto compounds over 3-pppa again implies that the carbonyl group plays an important role in surface binding. 3-Pppa was nevertheless established to be a better passivator than all bar the carbonyl containing phosphonic acids, with an onset time of between 22 and 29 hours and significant degradation only occurring after ~ 200 hours, when there is a rapid increase in the rate of hydrogen evolution.

Of the compounds tested, 2-opepa had the longest onset time, between 576 and 648 hours. The rate of hydrogen evolution then remains low over a period of ~ 18 days, rising gradually to 8.6 ml, before increasing rapidly over two days to over 80 ml. This sudden increase is similar to that observed for 3-pppa. Adsorption/desorption is an equilibrium process and so molecules are continuously being displaced from and replaced on the surface of the flakes. This process will create "holes" through which water molecules can penetrate and hydrate the aluminium, therefore some evolution of hydrogen over time is to be expected, but the reason for the apparent rapid loss of surface protection of the aluminium flakes in the case of 2-opepa and 3-pppa is unknown and will require further study to determine.

Putting the performance of these compounds in context, the "Du-Pont" sample is a commercially available passivator for aluminium flake, described as a large, polymeric "phosphate ester". The exact composition of the compound is unknown. The "Du-Pont" sample gives complete surface passivation of the aluminium flake (i.e. no hydrogen was evolved) for over 720 hours under the test conditions (performance beyond this timescale is unknown). The polymer probably binds to the flakes via the phosphate groups, while surface passivation is obtained simply by its bulky nature blocking approach by water.

6.3 Conclusions.

Probably the most important point revealed by the hydrogen evolution tests is that binding strength, while important in ranking classes of functional groups, is not the only criterion in determining whether compounds will be effective surface ligands for a particular application. The rest of the molecule also has to be tailored to meet the needs of that application. This is demonstrated by the relatively poor performance of a number of the compounds tested, which from adsorption isotherm studies and other tests we had believed would have been good passivating agents.

The one class of compounds that did stand out in the testing, were the carbonyl functionalised, phosphonic acid based ligands. These provided a comparable level of surface passivation, over a period of ~ one month, to that of a

commercially available polymeric, phosphate ester based passivation agent. Significantly, for a commercial application, the weight of compound required to give this level of passivation was less, which could lead to a reduction in costs. Although further work will be required to determine the optimum position for the carbonyl in relation to the phosphonic acid group, this class of compound shows considerable promise for the development of a commercially viable product, either as a "small molecule" passivator or by incorporation of the combined phosphonic acid/carbonyl functionality into a polymer based system.

6.4 Experimental.

For details of the synthesis and characterisation of the compounds 4-methyl-2,6-bis(phosphonomethyl)phenol, (3-oxo-3-phenyl-propyl)-phosphonic acid, (3-oxo-3-*p*-tolyl-propyl)-phosphonic acid, (2-oxo-2-phenyl-ethyl)-phosphonic acid and (3-phenyl-propyl)-phosphonic acid see Chapter 5, Sections 5.6.1 and 5.6.2. 4-Nitrobenzylphosphonic acid and [(4-nitro-benzyl-phosphonomethyl-amino)-methyl]-phosphonic acid were prepared by Dr D. Nation at the University of Edinburgh. High surface area "superfine $Al(OH)_3$" was supplied by Alcan. Irgacor-252 [2-(benzothiazol-2-ylsulfanyl)-succinic acid] was obtained from Ciba Speciality Chemicals.

Hydrogen evolution measurements were performed by Mr Paul Snelson at Avecia in Blackley, Manchester.

6.5 References.

1 R. Knowles, *Aluminium pigments in vehicle finishing and refinishing paints*, *Polymers Paint Colour Journal*, December 11/25, 1991.

2 http://www.silberline.com

3 http://www.basf.de/en/forschung/innovations/pigmente.htm

4 J. D. Venables, D. K. McNamara, J. M. Chen, T. S. Sun and R. Hopping, *Applications of Surface Science 3*, 1979, 88 and references within.

[5] Y. I. Kuznetsov, *Organic Inhibitors of Corrosion of Metals*, Plenum, New York, 1996.

[6] For examples see: a) Z. Vachlas and S. J. Thorne, *US Patent* 4,916,176, Imperial Chemical Industries, 1990. b) P. H. Lamers, A. Park, K. G. Olson, J. E. Poole and D. W. Maier, *US Patent* 5,429,674, PPG Industries, 1995.

[7] B. Muller, *British Corrosion Journal*, 1996, **4**, 315 and references within.

[8] B. Muller and I. Forster, *Corrosion Science*, **38**, 1103.

[9] Ciba Speciality Chemicals, private communication.

[10] P. A. Lovatt, *Synthesis of Novel Polynucleating Ligands for Lightly Oxidised Aluminium Surfaces*, Project Report, The University of Edinburgh, 1998.

[11] D. A. Nation, *Synthesis and Evaluation of Surface Passivating Agents for Aluminium Flake*, Project Report, The University of Edinburgh, 2000.

Chapter 7:

Conclusions and Further Work.

The objectives at the outset of this project fell into two broad headings. (1) To screen and identify functional head groups which bind strongly to lightly oxidised aluminium surfaces. These could then be developed for a number of applications such as surface passivation, corrosion inhibition and be used as alternatives to existing pre-treatments that are required before aluminium can be welded or adhesively bonded. Current pre-treatments are hazardous and generate large volumes of waste material. (2) To improve our understanding of the ligand design features which are required for strong binding at metal oxide surfaces.

The approach taken was to use polynucleating ligands that could address arrays of metals on surface oxide structures and to optimise the thermodynamic stability of the "surface complexes" formed by choosing ligands with a high density of donor functions which maximised the number of ligand-to-surface metal interactions. It was also believed that the use of rigid ligands would improve the stability of the complexes and suppress sequestering of the metal into solution. While the major interaction with the surface was expected to be replacement of surface hydroxides by the donor atoms of the ligand, other factors such as secondary hydrogen bonding were considered to be important in determining the binding characteristics of the ligands.

Measurement of adsorption isotherms for uptake of ligands on high surface area $Al(OH)_3$, although time consuming, proved to be a very effective screening process to achieve objective 1. A ranking order of head groups has been established based on work in this thesis and other parallel research* in the Edinburgh Centre for Surface Coordination Chemistry (ECSCC): amine-substituted 1,3,5-triazines < alcohols/polyphenols* ≤ pyridonates (oxygen substituted 1,3,5-triazines) << carboxylic acids ≅ 3-ketocarboxylic acids < phosphinic acids << phosphonic acids ≅ bisphosphonic acids < ketophosphonic acids ≅ gallates* was established. In addition, the shapes of the graphs gave information on the mode/modes of binding of the compounds.

1,3,5-Triazine derivatives were quickly rejected as candidate head groups due to their unpredictable behaviour and the poor binding strength shown by the

* Data on polyphenols and gallates, not presented within this thesis, have been obtained by the author, P. A. Lovatt and J. H. Robertson, unpublished work Edinburgh.

structurally related ligands, 2-hydroxypyridine and uracil. Investigation of the coordination chemistry of 1,3,5-triazine derivatives, whilst leading to some very interesting polynuclear complexes, confirmed that the ligands readily undergo rearrangement and condensation reactions making them poor candidates for the rational design of surface ligands.

While the binding strength of a compound is a useful indicator of its likely effectiveness as a surface ligand, it has been established within this thesis and from other work within the ECSCC that binding strength is not the only criterion. Binding studies have provided "structure-activity" relationships which have contributed significantly to objective 2, defining factors which are important in the design of a successful ligand. An example of this is that while the 3-ketocarboxylic acid (Irg-419) does not show an increased binding strength over the non-keto derivative (Irg-78), the carbonyl functionality does help it to achieve a much higher surface coverage at higher ligand concentrations. This may be due[†] to improved packing efficiency, brought about by a hydrogen bond between the carbonyl and a surface hydroxide, fixing the conformation of the molecule on the surface and thus improving the chances of an ordered monolayer being built up. This carbonyl-induced increase in surface coverage is also observed for these compounds on high surface area goethite [$(Fe(O)(OH)_2$] and in the phosphonic acid containing analogues. Further evidence for the effect of secondary bonding comes from the hydrogen evolution tests in which the carbonyl containing phosphonic acids performed significantly better than the other compounds tested. This is significant as isotherms carried out at the same pH as the hydrogen evolution tests revealed that bisphosphonic acids bind more strongly than the 3-ketophosphonic acids. These observations open up the interesting possibility that secondary bonding interactions may prove to be very important in enhancing the kinetic stability of surface complexes.

Although structural evidence exists to corroborate the involvement of the carbonyl functionality in the binding of carboxylic acids to goethite, the synthesis and crystallisation of similar aluminium complexes proved difficult. The synthesis of

[†] Work of this kind on the uptake at iron(III) oxide surfaces at Edinburgh has been published (see also chapter 3).

crystalline, characterisable, aluminium complexes was a persistent problem throughout this project, with established methods for the synthesis of high nuclearity clusters proving to be inapplicable to aluminium chemistry. Aluminium phosphonates have been synthesised by hydrothermal methods and this may be an avenue which can be explored in the future.

In broad terms the results obtained support the hypothesis that good surface ligands should contain donor functionalities which cannot form 5- or 6-membered metal chelates because these may will favour transport of metal ions from the surface into the adjacent phase.

Appendix

Contents.

Crystallographic Data.

Table 1: Crystal data and structure refinement for 6-(diethylamino)-2,4-dichloro-1,3,5-triazine.

Empirical formula	$C_7H_{10}Cl_2N_4$
Formula weight	221.09
Wavelength	0.71073 Å
Temperature	220(2) K
Crystal system	Monoclinic
Space group	C2/c
Unit cell dimensions	a = 11.1867(12) Å α = 90 °. b = 11.5877(13) Å β = 103.249(11) °. c = 7.8852(9) Å γ = 90 °.
Volume	994.94(19) $Å^3$
Number of reflections for cell	48 (15 < θ < 16 °.)
Z	4
Density (calculated)	1.476 Mg/m^3
Absorption coefficient	0.612 mm^{-1}
F(000)	456
Crystal description	Colourless block
Crystal size	0.78 x 0.43 x 0.43 mm
θ range for data collection	2.57 to 32.52 °.
Index ranges	-16<=h<=16, -2<=k<=17, 0<=l<=11
Reflections collected	2033
Independent reflections	1804 [R(int) = 0.0127]
Scan type	ω - θ
Solution	direct (SHELXS-97 (Sheldrick, 1990))
Refinement type	Full-matrix least-squares on F^2
Program used for refinement	SHELXL-97
Hydrogen atom placement	geometric
Hydrogen atom treatment	mixed
Data / restraints / parameters	1804/0/62
Goodness-of-fit on F^2	1.034
Conventional R [F>4σ(F)]	R1 = 0.0323 [1406 data]
Weighted R (F^2 and all data)	wR2 = 0.0847
Extinction coefficient	0.034(2)
Final maximum Δ/σ	0.001
Weighting scheme	calc w=1/[\σ²(Fo²)+(0.0407P)²+0.2880P] where P=(Fo²+2Fc²)/3
Largest diff. peak and hole	0.302 and -0.274 e.$Å^{-3}$

Table 2: Bond lengths [Å] and angles [°] for 6-(diethylamino)-2,4-dichloro-1,3,5-triazine.

Cl(1)-C(2)	1.7366(11)	N(3)-C(2)-N(1)	129.56(11)
N(1)-C(2)	1.3305(14)	N(3)-C(2)-Cl(1)	116.05(9)
N(1)-C(2)#1	1.3305(14)	N(1)-C(2)-Cl(1)	114.39(9)
C(2)-N(3)	1.3063(15)	C(2)-N(3)-C(4)	113.28(10)
N(3)-C(4)	1.3681(11)	N(5)-C(4)-N(3)	118.19(7)
C(4)-N(5)	1.329(2)	N(5)-C(4)-N(3)#1	118.19(7)
C(4)-N(3)#1	1.3681(11)	N(3)-C(4)-N(3)#1	123.62(14)
N(5)-C(6)	1.4703(13)	C(4)-N(5)-C(6)	121.06(6)
N(5)-C(6)#1	1.4703(13)	C(4)-N(5)-C(6)#1	121.06(6)
C(6)-C(7)	1.5134(17)	C(6)-N(5)-C(6)#1	117.87(13)
		N(5)-C(6)-C(7)	112.11(9)
C(2)-N(1)-C(2)#1	110.66(14)		

Symmetry transformations used to generate equivalent atoms: #1 -x+1,y,-z+1/2

Table 3: Crystal data and structure refinement for 6-(diethylamino)-1,3,5-triazine-2-thione-4-one.

Empirical formula	$C_7H_{12}N_4OS$
Formula weight	200.27
Wavelength	1.54178 Å
Temperature	220(2) K
Crystal system	Monoclinic
Space group	$P2_1/c$
Unit cell dimensions	a = 7.789(3) Å α = 90 °. b = 7.043(2) Å β = 93.36(4) °. c = 17.452(8) Å γ = 90 °.
Volume	955.7(7) $Å^3$
Number of reflections for cell	32 (20 < θ < 22 °.)
Z	4
Density (calculated)	1.392 Mg/m^3
Absorption coefficient	2.764 mm^{-1}
F(000)	424
Crystal description	Colourless block
Crystal size	0.60 x 0.60 x 0.40 mm
θ range for data collection	5.08 to 70.13 °.
Index ranges	-9<=h<=9, -8<=k<=7, -19<=l<=21
Reflections collected	2683
Independent reflections	1647 [R(int) = 0.0313]
Scan type	ω - θ
Absorption correction	Psi-scans (Tmin= 0.101, Tmax=0.319)
Solution	direct (SHELXS-97)
Refinement type	Full-matrix least-squares on F^2
Program used for refinement	SHELXL-97
Hydrogen atom placement	geometric
Hydrogen atom treatment	riding
Data / restraints / parameters	1647/19/156
Goodness-of-fit on F^2	1.082
Conventional R [F>4σ(F)]	R1 = 0.0758 [1446 data]
Weighted R (F^2 and all data)	wR2 = 0.2224
Extinction coefficient	0.0031(17)
Final maximum Δ/σ	0.002
Weighting scheme	calc $w=1/[\sigma^2(Fo^2)+(0.1475P)^2+1.3044P]$ where $P=(Fo^2+2Fc^2)/3$
Largest diff. peak and hole	0.552 and -0.450 e. $Å^{-3}$

Table 4: Bond lengths [Å] and angles [°] for 6-(diethylamino)-1,3,5-triazine-2-thione-4-one.

N(1)-C(2)	1.364(5)	C(2)-N(3)-C(4)	121.6(3)
N(1)-C(6)	1.377(5)	N(41)-C(4)-N(5)	118.9(4)
C(2)-O(2)	1.215(5)	N(41)-C(4)-N(3)	119.3(4)
C(2)-N(3)	1.365(5)	N(5)-C(4)-N(3)	121.8(3)
N(3)-C(4)	1.368(5)	C(4)-N(41)-C(44)	118.5(4)
C(4)-N(41)	1.318(6)	C(4)-N(41)-C(42)	123.7(4)
C(4)-N(5)	1.332(5)	C(44)-N(41)-C(42)	110.2(4)
N(41)-C(44)	1.519(7)	C(4)-N(41)-C(42')	120.6(5)
N(41)-C(42)	1.521(7)	C(44)-N(41)-C(42')	120.1(5)
N(41)-C(42')	1.540(8)	C(42)-N(41)-C(42')	36.1(5)
N(41)-C(44')	1.559(8)	C(4)-N(41)-C(44')	116.1(5)
C(42)-C(43)	1.501(9)	C(44)-N(41)-C(44')	40.3(5)
C(44)-C(45)	1.503(8)	C(42)-N(41)-C(44')	119.1(6)
C(42')-C(43')	1.504(9)	C(42')-N(41)-C(44')	102.7(6)
C(44')-C(45')	1.502(10)	C(43)-C(42)-N(41)	106.1(6)
N(5)-C(6)	1.337(5)	C(45)-C(44)-N(41)	104.5(6)
C(6)-S(6)	1.679(4)	C(43')-C(42')-N(41)	105.3(8)
		C(45')-C(44')-N(41)	104.6(9)
C(2)-N(1)-C(6)	123.4(3)	C(4)-N(5)-C(6)	118.8(3)
O(2)-C(2)-N(1)	122.1(3)	N(5)-C(6)-N(1)	119.4(3)
O(2)-C(2)-N(3)	123.0(3)	N(5)-C(6)-S(6)	118.4(3)
N(1)-C(2)-N(3)	114.9(3)		

Table 5: Crystal data and structure refinement for 6-(diethylamino)-1,3,5-triazine-2,4-dithione.

Empirical formula	$C_7H_{12}N_4S_2$
Formula weight	216.33
Wavelength	1.54178 Å
Temperature	295(2) K
Crystal system	Monoclinic
Space group	P21/c
Unit cell dimensions	a = 9.030(2) Å α = 90 °. b = 13.949(4) Å β = 111.079(13) °. c = 9.394(2) Å γ = 90 °.
Volume	1104.1(5) $Å^3$
Number of reflections for cell	32 (20 < θ < 22 °.)
Z	4
Density (calculated)	1.301 Mg/m^3
Absorption coefficient	4.083 mm^{-1}
F(000)	456
Crystal description	Colourless block
Crystal size	0.60 x 0.60 x 0.50 mm
θ range for data collection	5.25 to 69.99 °.
Index ranges	-11<=h<=10, -15<=k<=14, -9<=l<=11
Reflections collected	2950
Independent reflections	1925 [R(int) = 0.0150]
Scan type	ω - θ
Absorption correction	Shelxa (Tmin= 0.054, Tmax=0.483)
Solution	direct (SHELXS-97 (Sheldrick, 1990))
Refinement type	Full-matrix least-squares on F^2
Program used for refinement	SHELXL-97
Hydrogen atom placement	geom
Hydrogen atom treatment	riding
Data / restraints / parameters	1925/54/116
Goodness-of-fit on F^2	1.088
Conventional R [F>4σ(F)]	R1 = 0.0989 [1568 data]
Weighted R (F^2 and all data)	wR2 = 0.3011
Extinction coefficient	0.011(3)
Final maximum Δ/σ	0.024
Weighting scheme	Calc $w=1/[\sigma^2(Fo^2)+(0.1783P)^2+2.4654P]$ where $P=(Fo^2+2Fc^2)/3$
Largest diff. peak and hole	0.557 and -0.588 e. $Å^{-3}$

Table 6: Bond lengths [Å] and angles [°] for 6-(diethylamino)-1,3,5-triazine-2,4-dithione.

N(1)-C(2)	1.332(8)	C(4)-N(3)-C(2)	121.1(6)
N(1)-C(6)	1.370(7)	N(41)-C(4)-N(5)	119.1(6)
C(2)-N(3)	1.380(8)	N(41)-C(4)-N(3)	118.8(6)
C(2)-S(2)	1.656(6)	N(5)-C(4)-N(3)	122.1(6)
N(3)-C(4)	1.370(8)	C(4)-N(41)-C(44)	123.6(7)
C(4)-N(41)	1.321(8)	C(4)-N(41)-C(42')	118.3(10)
C(4)-N(5)	1.339(9)	C(44)-N(41)-C(42')	116.5(11)
N(41)-C(44)	1.497(9)	C(4)-N(41)-C(42)	118.3(7)
N(41)-C(42')	1.524(10)	C(44)-N(41)-C(42)	112.9(8)
N(41)-C(42)	1.533(8)	C(42')-N(41)-C(42)	37.5(7)
N(41)-C(44')	1.536(9)	C(4)-N(41)-C(44')	121.5(7)
C(42)-C(43)	1.489(13)	C(44)-N(41)-C(44')	20.7(6)
C(44)-C(45)	1.496(14)	C(42')-N(41)-C(44')	109.2(9)
C(42')-C(43')	1.492(14)	C(42)-N(41)-C(44')	120.1(8)
C(44')-C(45')	1.479(14)	C(43)-C(42)-N(41)	107.4(8)
N(5)-C(6)	1.342(7)	C(45)-C(44)-N(41)	105.3(10)
C(6)-S(6)	1.664(6)	C(43')-C(42')-N(41)	103.9(11)
		C(45')-C(44')-N(41)	111.9(11)
C(2)-N(1)-C(6)	125.9(5)	C(4)-N(5)-C(6)	118.2(5)
N(1)-C(2)-N(3)	114.0(5)	N(5)-C(6)-N(1)	118.5(5)
N(1)-C(2)-S(2)	123.9(4)	N(5)-C(6)-S(6)	121.5(4)
N(3)-C(2)-S(2)	122.1(5)	N(1)-C(6)-S(6)	119.9(4)

Table 7: Crystal data and structure refinement for 6-(diethylamino)-1,3,5-triazine-2,4-dione.

Empirical formula	$C_7H_{12}N_4O_2$
Formula weight	184.21
Wavelength	0.71073 Å
Temperature	220(2) K
Crystal system	Triclinic
Space group	P-1
Unit cell dimensions	a = 7.928(3) Å α = 98.48(3) °. b = 9.304(4) Å β = 90.51(4) °. c = 12.767(6) Å γ = 104.50(3) °.
Volume	900.7(6) $Å^3$
Number of reflections for cell	24 (14.5 < θ < 15 °.)
Z	4
Density (calculated)	1.358 Mg/m^3
Absorption coefficient	0.103 mm^{-1}
F(000)	392
Crystal description	Colourless block
Crystal size	0.58 x 0.31 x 0.23 mm
θ range for data collection	2.59 to 25.11 °.
Index ranges	-9<=h<=9, -11<=k<=10, 0<=l<=15
Reflections collected	3983
Independent reflections	3182 [R(int) = 0.0367]
Scan type	ω - θ
Solution	direct (SHELXS-97 (Sheldrick, 1990))
Refinement type	Full-matrix least-squares on F^2
Program used for refinement	SHELXL-97
Hydrogen atom placement	geometric/difference map (NH)
Hydrogen atom treatment	Riding or refall (NH)
Data / restraints / parameters	3182/9/260
Goodness-of-fit on F^2	1.042
Conventional R [F>4σ(F)]	R1 = 0.0551 [2281 data]
Weighted R (F^2 and all data)	wR2 = 0.1583
Extinction coefficient	0.015(4)
Final maximum Δ/σ	0.000
Weighting scheme	calc w=1/[\σ²(Fo²)+(0.0889P)²+0.2615P] where P=(Fo²+2Fc²)/3
Largest diff. peak and hole	0.491 and -0.346 e. $Å^{-3}$ Major peaks near Et groups => a small amount of further disorder

Table 8: Bond lengths [Å] and angles [°] for 6-(diethylamino)-1,3,5-triazine-2,4-dione.

N(1)-C(2)	1.362(3)	C(44')-C(45')	1.506(4)
N(1)-C(6)	1.390(3)		
O(2)-C(2)	1.220(3)	C(2)-N(1)-C(6)	124.1(2)
C(2)-N(3)	1.373(3)	O(2)-C(2)-N(1)	123.0(2)
N(3)-C(4)	1.371(3)	O(2)-C(2)-N(3)	122.9(2)
C(4)-N(5)	1.324(3)	N(1)-C(2)-N(3)	114.1(2)
C(4)-N(41)	1.334(3)	C(4)-N(3)-C(2)	121.8(2)
N(5)-C(6)	1.350(3)	N(5)-C(4)-N(41)	119.2(2)
O(6)-C(6)	1.234(3)	N(5)-C(4)-N(3)	122.6(2)
N(41)-C(44)	1.475(3)	N(41)-C(4)-N(3)	118.2(2)
N(41)-C(42)	1.485(4)	C(4)-N(5)-C(6)	118.4(2)
C(42)-C(43)	1.478(5)	O(6)-C(6)-N(5)	122.7(2)
C(44)-C(45)	1.508(4)	O(6)-C(6)-N(1)	118.3(2)
N(1')-C(2')	1.352(3)	N(5)-C(6)-N(1)	119.0(2)
N(1')-C(6')	1.389(3)	C(4)-N(41)-C(44)	122.6(2)
O(2')-C(2')	1.224(3)	C(4)-N(41)-C(42)	119.2(2)
C(2')-N(3')	1.369(3)	C(44)-N(41)-C(42)	118.2(2)
N(3')-C(4')	1.369(3)	C(43)-C(42)-N(41)	111.6(3)
C(4')-N(5')	1.325(3)	N(41)-C(44)-C(45)	114.4(2)
C(4')-N(41')	1.331(3)	C(2')-N(1')-C(6')	124.0(2)
N(5')-C(6')	1.352(3)	O(2')-C(2')-N(1')	123.2(2)
O(6')-C(6')	1.226(3)	O(2')-C(2')-N(3')	122.0(2)
N(41')-C(44')	1.462(3)	N(1')-C(2')-N(3')	114.7(2)
N(41')-C(42')	1.483(4)	C(4')-N(3')-C(2')	121.9(2)
N(41')-C(42")	1.588(12)	N(5')-C(4')-N(41')	119.0(2)
C(42')-C(43')	1.495(5)	N(5')-C(4')-N(3')	121.8(2)
C(42")-C(43")	1.520(13)	N(41')-C(4')-N(3')	119.2(2)

C(4')-N(5')-C(6')	119.1(2)	C(4')-N(41')-C(42")	113.1(5)
O(6')-C(6')-N(5')	122.3(2)	C(44')-N(41')-C(42")	116.0(5)
O(6')-C(6')-N(1')	119.2(2)	C(42')-N(41')-C(42")	33.5(4)
N(5')-C(6')-N(1')	118.4(2)	N(41')-C(42')-C(43')	108.8(3)
C(4')-N(41')-C(44')	124.5(2)	C(43")-C(42")-N(41')	101.9(10)
C(4')-N(41')-C(42')	118.8(2)	N(41')-C(44')-C(45')	114.6(2)
C(44')-N(41')-C(42')	116.3(2)		

Table 9: Crystal data and structure refinement for [Ni{(Sta)S(S_2ta)}].

Empirical formula	$C_{14}H_{20}N_8NiS_4$
Formula weight	487.33
Wavelength	1.54178 Å
Temperature	220(2) K
Crystal system	Monoclinic
Space group	$P2_1/n$
Unit cell dimensions	a = 7.5234(15) Å α = 90 °. b = 16.689(3) Å β = 101.145(17) °. c = 16.472(3) Å γ = 90 °.
Volume	2029.2(7) $Å^3$
Number of reflections for cell	48 (20 < θ < 22 °.)
Z	4
Density (calculated)	1.595 Mg/m^3
Absorption coefficient	5.381 mm^{-1}
F(000)	1008
Crystal description	Pale-yellow block
Crystal size	0.58 x 0.16 x 0.08 mm
θ range for data collection	3.81 to 70.01 °.
Index ranges	-8<=h<=7, -14<=k<=20, -14<=l<=20
Reflections collected	6005
Independent reflections	3575 [R(int) = 0.0438]
Scan type	ω - θ
Absorption correction	Optimised numerical (Tmin= 0.425, Tmax=0.769)
Solution	Patterson (DIRDIF)
Refinement type	Full-matrix least-squares on F^2
Program used for refinement	SHELXL-97
Hydrogen atom placement	geometric
Hydrogen atom treatment	riding
Data / restraints / parameters	3575/82/326
Goodness-of-fit on F^2	1.006
Conventional R [F>4σ(F)]	R1 = 0.0740 [2542 data]
Weighted R (F^2 and all data)	wR2 = 0.2095
Final maximum Δ/σ	0.063
Weighting scheme	calc w=1/[$\sigma^2(Fo^2)$+(0.1471P)^2+0.0000P] where P=(Fo^2+2Fc^2)/3
Largest diff. peak and hole	1.148 and -0.658 e. $Å^{-3}$

Table 10: Bond lengths [Å] and angles [°] for [Ni{(Sta)S(S_2ta)}].

Ni(1)-N(1A)	1.841(5)	C(2B)-N(3B)	1.300(8)
Ni(1)-N(1B)	1.913(5)	C(2B)-S(2B)	1.733(6)
Ni(1)-S(3B)	2.1307(18)	S(2B)-S(3B)	2.049(3)
Ni(1)-S(2A)	2.240(2)	N(3B)-C(4B)	1.372(8)
N(1A)-C(6A)	1.323(8)	C(4B)-N(41B)	1.316(8)
N(1A)-C(2A)	1.345(8)	C(4B)-N(5B)	1.362(7)
C(2A)-N(3A)	1.323(7)	N(41B)-C(44B)	1.469(9)
C(2A)-S(2A)	1.730(6)	N(41B)-C(42B)	1.470(8)
N(3A)-C(4A)	1.367(8)	C(42B)-C(43B)	1.517(10)
C(4A)-N(41A)	1.344(7)	C(44B)-C(45B)	1.538(10)
C(4A)-N(5A)	1.350(8)	N(5B)-C(6B)	1.282(8)
N(41A)-C(44A)	1.459(9)	C(6B)-S(6AB)	1.775(6)
N(41A)-C(42A)	1.473(9)		
C(42A)-C(43A)	1.489(12)	N(1A)-Ni(1)-N(1B)	96.0(2)
C(44A)-C(46A)	1.496(16)	N(1A)-Ni(1)-S(3B)	168.27(19)
C(44A)-C(45A)	1.512(16)	N(1B)-Ni(1)-S(3B)	95.68(15)
N(5A)-C(6A)	1.325(7)	N(1A)-Ni(1)-S(2A)	73.47(18)
C(6A)-S(6AB)	1.751(7)	N(1B)-Ni(1)-S(2A)	169.46(15)
N(1B)-C(6B)	1.378(8)	S(3B)-Ni(1)-S(2A)	94.86(8)
N(1B)-C(2B)	1.378(7)	C(6A)-N(1A)-C(2A)	116.7(5)

C(6A)-N(1A)-Ni(1)	139.7(5)	N(5A)-C(6A)-S(6AB)	115.7(5)
C(2A)-N(1A)-Ni(1)	103.3(4)	C(6B)-N(1B)-C(2B)	111.2(5)
N(3A)-C(2A)-N(1A)	125.4(6)	C(6B)-N(1B)-Ni(1)	128.0(4)
N(3A)-C(2A)-S(2A)	129.0(5)	C(2B)-N(1B)-Ni(1)	120.8(4)
N(1A)-C(2A)-S(2A)	105.7(4)	N(3B)-C(2B)-N(1B)	127.6(6)
N(3A)-C(2A)-Ni(1)	170.7(5)	N(3B)-C(2B)-S(2B)	113.1(4)
N(1A)-C(2A)-Ni(1)	45.4(3)	N(1B)-C(2B)-S(2B)	119.3(5)
S(2A)-C(2A)-Ni(1)	60.30(19)	C(2B)-S(2B)-S(3B)	103.8(2)
C(2A)-S(2A)-Ni(1)	77.5(2)	S(2B)-S(3B)-Ni(1)	100.21(9)
C(2A)-N(3A)-C(4A)	112.7(5)	C(2B)-N(3B)-C(4B)	115.3(5)
N(41A)-C(4A)-N(5A)	118.4(6)	N(41B)-C(4B)-N(5B)	120.0(6)
N(41A)-C(4A)-N(3A)	115.5(6)	N(41B)-C(4B)-N(3B)	118.2(5)
N(5A)-C(4A)-N(3A)	126.1(5)	N(5B)-C(4B)-N(3B)	121.9(6)
C(4A)-N(41A)-C(44A)	122.1(6)	C(4B)-N(41B)-C(44B)	121.7(5)
C(4A)-N(41A)-C(42A)	120.6(6)	C(4B)-N(41B)-C(42B)	120.7(5)
C(44A)-N(41A)-C(42A)	117.2(5)	C(44B)-N(41B)-C(42B)	117.0(6)
N(41A)-C(42A)-C(43A)	112.2(7)	N(41B)-C(42B)-C(43B)	110.9(5)
N(41A)-C(44A)-C(46A)	113.7(9)	N(41B)-C(44B)-C(45B)	109.7(6)
N(41A)-C(44A)-C(45A)	111.0(9)	C(6B)-N(5B)-C(4B)	117.5(5)
C(46A)-C(44A)-C(45A)	109.5(12)	N(5B)-C(6B)-N(1B)	126.4(5)
C(6A)-N(5A)-C(4A)	114.5(5)	N(5B)-C(6B)-S(6AB)	107.0(4)
N(1A)-C(6A)-N(5A)	124.3(6)	N(1B)-C(6B)-S(6AB)	126.6(5)
N(1A)-C(6A)-S(6AB)	120.0(4)	C(6A)-S(6AB)-C(6B)	109.3(3)

Table 11: Crystal data and structure refinement for $[Co_6NaO(OStaH)_7\{S(Ota)_2\}_2(O_2CPh)_2(H_2O)_2]$.

Empirical formula	$C_{107}H_{155}Co_6N_{52}NaO_{18}S_9$
Formula weight	3122.94
Wavelength	0.71073 Å
Temperature	150(2) K
Crystal system	Monoclinic
Space group	$P2_1/n$
Unit cell dimensions	a = 19.6882(8) Å α = 90 °. b = 19.7229(8) Å β = 94.844(2) °. c = 39.7227(18) Å γ = 90 °.
Volume	15369.6(11) $Å^3$
Number of reflections for cell	124909
Z	4
Density (calculated)	1.350 Mg/m^3
Absorption coefficient	0.830 mm^{-1}
F(000)	6488
Crystal description	Blue flake
Crystal size	0.10 x 0.025 x 0.01 mm
θ range for data collection	2.30 to 22.50 °.
Index ranges	-21<=h<=21, -21<=k<=21, -42<=l<=42
Reflections collected	124909
Independent reflections	19775 [R(int) = 0.3291]
Scan type	ω - ϕ
Absorption correction	Sortav (Tmin= 0.994, Tmax=0.922)
Solution	direct (SHELXS-97 (Sheldrick, 1990))
Refinement type	Full-matrix least-squares on F^2
Program used for refinement	SHELXL-97
Hydrogen atom placement	geometric.NH and OH based on H-bonding
Hydrogen atom treatment	riding
Data / restraints / parameters	19775/877/979
Goodness-of-fit on F^2	0.961
Conventional R [F>4σ(F)]	R1 = 0.0998 [6930 data]
Weighted R (F^2 and all data)	wR2 = 0.3073
Final maximum Δ/σ	0.040
Weighting scheme	calc $w=1/[\sigma^2(Fo^2)+(0.1371P)^2+0.0000P]$ where $P=(Fo^2+2Fc^2)/3$
Largest diff. peak and hole	0.977 and -0.523 e. $Å^{-3}$

Table 12: Selected bond lengths [Å] and angles [°] for $[Co_6NaO(OStaH)_7\{S(Ota)_2\}_2(O_2CPh)_2(H_2O)_2]$.

Co(1)-O(6A)	2.039(10)	O(6B)-Co(3)-O(6D)	88.4(4)
Co(1)-O(11)	2.066(9)	O(2W)-Co(3)-O(6D)	178.5(4)
Co(1)-O(6J)	2.069(9)	O(6F)-Co(3)-O(1W)	94.1(4)
Co(1)-O(6K)	2.096(9)	O(6B)-Co(3)-O(1W)	92.9(4)
Co(1)-O(124)	2.132(9)	O(2W)-Co(3)-O(1W)	87.3(4)
Co(1)-O(6C)	2.152(9)	O(6D)-Co(3)-O(1W)	93.3(4)
Co(2)-O(21)	1.954(10)	O(6F)-Co(3)-O(6H)	86.9(4)
Co(2)-O(124)	1.977(9)	O(6B)-Co(3)-O(6H)	86.1(4)
Co(2)-N(1B)	2.006(11)	O(2W)-Co(3)-O(6H)	92.1(3)
Co(2)-N(1A)	2.009(11)	O(6D)-Co(3)-O(6H)	87.3(3)
Co(3)-O(6F)	2.058(9)	O(1W)-Co(3)-O(6H)	178.9(4)
Co(3)-O(6B)	2.080(9)	O(22)-Co(4)-O(124)	100.5(4)
Co(3)-O(2W)	2.080(9)	O(22)-Co(4)-N(1D)	132.6(4)
Co(3)-O(6D)	2.101(9)	O(124)-Co(4)-N(1D)	104.4(4)
Co(3)-O(1W)	2.109(9)	O(22)-Co(4)-N(1C)	120.8(4)
Co(3)-O(6H)	2.136(9)	O(124)-Co(4)-N(1C)	101.3(4)
Co(3)-Na(1)	3.336(6)	N(1D)-Co(4)-N(1C)	93.0(4)
Co(4)-O(22)	2.010(9)	N(1I)-Co(5)-N(1K)	96.2(4)
Co(4)-O(124)	2.021(9)	N(1I)-Co(5)-S(2H)	96.0(3)
Co(4)-N(1D)	2.023(11)	N(1K)-Co(5)-S(2H)	108.7(3)
Co(4)-N(1C)	2.035(11)	N(1I)-Co(5)-S(2J)	168.3(3)
Co(5)-N(1I)	1.956(10)	N(1K)-Co(5)-S(2J)	95.4(3)
Co(5)-N(1K)	1.960(10)	S(2H)-Co(5)-S(2J)	82.04(16)
Co(5)-S(2H)	2.277(5)	N(1I)-Co(5)-S(2I)	71.4(3)
Co(5)-S(2J)	2.286(4)	N(1K)-Co(5)-S(2I)	159.2(3)
Co(5)-S(2I)	2.296(5)	S(2H)-Co(5)-S(2I)	89.62(17)
Co(5)-S(2K)	2.320(4)	S(2J)-Co(5)-S(2I)	96.99(16)
Co(6)-N(1G)	1.929(10)	N(1I)-Co(5)-S(2K)	93.0(3)
Co(6)-N(1F)	1.939(10)	N(1K)-Co(5)-S(2K)	70.6(3)
Co(6)-N(1E)	1.945(10)	S(2H)-Co(5)-S(2K)	171.01(17)
Co(6)-S(2F)	2.280(4)	S(2J)-Co(5)-S(2K)	89.08(16)
Co(6)-S(2G)	2.283(4)	S(2I)-Co(5)-S(2K)	92.85(17)
Co(6)-S(2E)	2.302(5)	N(1G)-Co(6)-N(1F)	98.2(4)
Na(1)-O(6E)	2.333(10)	N(1G)-Co(6)-N(1E)	95.3(4)
Na(1)-O(6I)	2.339(10)	N(1F)-Co(6)-N(1E)	101.2(4)
Na(1)-O(6F)	2.468(10)	N(1G)-Co(6)-S(2F)	93.9(3)
Na(1)-O(6H)	2.488(10)	N(1F)-Co(6)-S(2F)	72.0(3)
Na(1)-O(22)	2.560(10)	N(1E)-Co(6)-S(2F)	169.3(3)
Na(1)-O(6G)	2.652(11)	N(1G)-Co(6)-S(2G)	71.6(3)
Na(1)-O(6D)	2.995(11)	N(1F)-Co(6)-S(2G)	162.0(3)
Na(1)-C(6E)	3.098(14)	N(1E)-Co(6)-S(2G)	94.6(3)
		S(2F)-Co(6)-S(2G)	93.46(16)
O(6A)-Co(1)-O(11)	97.5(4)	N(1G)-Co(6)-S(2E)	161.0(3)
O(6A)-Co(1)-O(6J)	91.4(4)	N(1F)-Co(6)-S(2E)	97.4(4)
O(11)-Co(1)-O(6J)	89.5(4)	N(1E)-Co(6)-S(2E)	71.0(3)
O(6A)-Co(1)-O(6K)	175.4(4)	S(2F)-Co(6)-S(2E)	101.22(16)
O(11)-Co(1)-O(6K)	87.1(4)	S(2G)-Co(6)-S(2E)	95.76(17)
O(6J)-Co(1)-O(6K)	87.9(4)	O(6E)-Na(1)-O(6I)	125.8(4)
O(6A)-Co(1)-O(124)	89.7(3)	O(6E)-Na(1)-O(6F)	92.7(4)
O(11)-Co(1)-O(124)	88.1(3)	O(6I)-Na(1)-O(6F)	132.1(4)
O(6J)-Co(1)-O(124)	177.5(4)	O(6E)-Na(1)-O(6H)	147.7(4)
O(6K)-Co(1)-O(124)	91.2(3)	O(6I)-Na(1)-O(6H)	83.7(3)
O(6A)-Co(1)-O(6C)	85.7(4)	O(6F)-Na(1)-O(6H)	71.2(3)
O(11)-Co(1)-O(6C)	176.4(4)	O(6E)-Na(1)-O(22)	76.2(3)
O(6J)-Co(1)-O(6C)	88.8(4)	O(6I)-Na(1)-O(22)	86.7(3)
O(6K)-Co(1)-O(6C)	89.7(3)	O(6F)-Na(1)-O(22)	134.2(4)
O(124)-Co(1)-O(6C)	93.6(3)	O(6H)-Na(1)-O(22)	94.9(3)
O(21)-Co(2)-O(124)	106.2(4)	O(6E)-Na(1)-O(6G)	77.8(3)
O(21)-Co(2)-N(1B)	111.4(4)	O(6I)-Na(1)-O(6G)	79.6(3)
O(124)-Co(2)-N(1B)	122.7(4)	O(6F)-Na(1)-O(6G)	82.8(3)
O(21)-Co(2)-N(1A)	112.8(4)	O(6H)-Na(1)-O(6G)	125.4(4)
O(124)-Co(2)-N(1A)	109.6(4)	O(22)-Na(1)-O(6G)	135.0(4)
N(1B)-Co(2)-N(1A)	93.7(4)	O(6E)-Na(1)-O(6D)	84.0(3)
O(6F)-Co(3)-O(6B)	170.4(4)	O(6I)-Na(1)-O(6D)	139.6(4)
O(6F)-Co(3)-O(2W)	94.0(4)	O(6F)-Na(1)-O(6D)	60.7(3)
O(6B)-Co(3)-O(2W)	92.9(4)	O(6H)-Na(1)-O(6D)	63.7(3)
O(6F)-Co(3)-O(6D)	84.6(4)	O(22)-Na(1)-O(6D)	73.9(3)

O(6G)-Na(1)-O(6D)	138.2(3)	O(6H)-Na(1)-C(6E)	128.1(4)
O(6E)-Na(1)-C(6E)	21.2(3)	O(22)-Na(1)-C(6E)	82.5(3)
O(6I)-Na(1)-C(6E)	147.0(4)	O(6G)-Na(1)-C(6E)	86.3(3)
O(6F)-Na(1)-C(6E)	74.3(3)	O(6D)-Na(1)-C(6E)	65.9(3)

Table 13: Crystal data and structure refinement for $[Co(OSta)_3]$.

Empirical formula	$C_{193}H_{308}Co_8N_{107}O_{32}S_{24}$
Formula weight	5880.34
Wavelength	1.54187 Å
Temperature	293(2) K
Crystal system	Orthorhombic
Space group	Pbcn
Unit cell dimensions	a = 53.242(11) Å α = 90 °. b = 33.671(7) Å β = 90 °. c = 33.537(7) Å γ = 90 °.
Volume	60122(21) $Å^3$
Number of reflections for cell	34 (20 < θ < 22 °.)
Z	8
Density (calculated)	1.299 Mg/m^3
Absorption coefficient	5.539 mm^{-1}
F(000)	24568
Crystal description	Green block
Crystal size	0.86 x 0.58 x 0.51 mm
θ range for data collection	2.62 to 40.00 °.
Index ranges	0<=h<=44, -28<=k<=0, 0<=l<=27
Reflections collected	23565
Independent reflections	18245 [R(int) = 0.0630]
Scan type	ω
Absorption correction	Face-indexed (Tmin= 0.062, Tmax=0.157)
Solution	direct (SHELXS-97 (Sheldrick, 1990))
Refinement type	Full-matrix least-squares on F^2
Program used for refinement	SHELXL-97
Hydrogen atom placement	geometric
Hydrogen atom treatment	riding
Data / restraints / parameters	18245/20/1762
Goodness-of-fit on F^2	1.127
Conventional R [F>4σ(F)]	R1 = 0.1373 [7035 data]
Weighted R (F^2 and all data)	wR2 = 0.4236
Extinction coefficient	0.000031(5)
Final maximum Δ/σ	0.000
Weighting scheme	calc $w=1/[\sigma^2(Fo^2)+(0.2000P)^2+0.0000P]$ where $P=(Fo^2+2Fc^2)/3$
Largest diff. peak and hole	1.594 and -0.468 $e.Å^{-3}$

Table 14: Selected bond lengths [Å] and angles [°] for $[Co(OSta)_3]$.

Co(1)-N(3A)	1.92(3)	Co(4)-S(10)	2.268(12)
Co(1)-N(1A)	1.95(3)	Co(4)-S(11)	2.280(11)
Co(1)-N(2A)	1.96(3)	Co(4)-C(10A)	2.46(4)
Co(1)-S(1)	2.263(11)	Co(4)-C(11A)	2.49(4)
Co(1)-S(3)	2.277(11)	Co(5)-N(13A)	1.92(3)
Co(1)-S(2)	2.289(11)	Co(5)-N(15A)	1.92(3)
Co(2)-N(4A)	1.94(3)	Co(5)-N(14A)	1.99(3)
Co(2)-N(6A)	1.94(2)	Co(5)-S(15)	2.277(11)
Co(2)-N(5A)	1.98(3)	Co(5)-S(13)	2.283(11)
Co(2)-S(5)	2.280(11)	Co(5)-S(14)	2.293(12)
Co(2)-S(6)	2.292(11)	Co(5)-C(14A)	2.47(4)
Co(2)-S(4)	2.311(11)	Co(5)-C(13A)	2.49(5)
Co(3)-N(9A)	1.89(3)	Co(6)-N(16A)	1.91(3)
Co(3)-N(7A)	1.95(3)	Co(6)-N(17A)	1.93(3)
Co(3)-N(8A)	1.96(3)	Co(6)-N(18A)	1.95(3)
Co(3)-S(7)	2.284(11)	Co(6)-S(16)	2.269(13)
Co(3)-S(8)	2.296(12)	Co(6)-S(17)	2.276(13)
Co(3)-S(9)	2.300(11)	Co(6)-S(18)	2.286(12)
Co(4)-N(10A)	1.84(3)	Co(7)-N(19A)	1.89(3)
Co(4)-N(12A)	1.94(3)	Co(7)-N(20A)	1.94(3)
Co(4)-N(11A)	1.94(3)	Co(7)-N(21A)	1.95(3)
Co(4)-S(12)	2.267(12)	Co(7)-S(19)	2.270(11)

Co(7)-S(21)	2.276(12)	S(10)-Co(4)-S(11)	95.7(4)
Co(7)-S(20)	2.281(12)	N(10A)-Co(4)-C(10A)	32.2(11)
Co(7)-C(21A)	2.51(4)	N(12A)-Co(4)-C(10A)	130.4(13)
Co(8)-N(23A)	1.93(3)	N(11A)-Co(4)-C(10A)	97.6(12)
Co(8)-N(24A)	1.95(3)	S(12)-Co(4)-C(10A)	95.0(9)
Co(8)-N(22A)	1.96(3)	S(10)-Co(4)-C(10A)	41.5(9)
Co(8)-S(23)	2.249(13)	S(11)-Co(4)-C(10A)	136.0(10)
Co(8)-S(24)	2.272(12)	N(10A)-Co(4)-C(11A)	129.5(13)
Co(8)-S(22)	2.290(14)	N(12A)-Co(4)-C(11A)	97.3(13)
		N(11A)-Co(4)-C(11A)	31.0(10)
N(3A)-Co(1)-N(1A)	99.7(12)	S(12)-Co(4)-C(11A)	139.5(9)
N(3A)-Co(1)-N(2A)	97.0(11)	S(10)-Co(4)-C(11A)	97.8(9)
N(1A)-Co(1)-N(2A)	95.9(10)	S(11)-Co(4)-C(11A)	40.5(9)
N(3A)-Co(1)-S(1)	168.3(9)	C(10A)-Co(4)-C(11A)	120.0(12)
N(1A)-Co(1)-S(1)	72.3(9)	N(13A)-Co(5)-N(15A)	97.3(13)
N(2A)-Co(1)-S(1)	92.4(8)	N(13A)-Co(5)-N(14A)	97.1(13)
N(3A)-Co(1)-S(3)	70.9(9)	N(15A)-Co(5)-N(14A)	97.0(12)
N(1A)-Co(1)-S(3)	92.1(7)	N(13A)-Co(5)-S(15)	91.1(9)
N(2A)-Co(1)-S(3)	166.6(8)	N(15A)-Co(5)-S(15)	71.7(9)
S(1)-Co(1)-S(3)	100.3(4)	N(14A)-Co(5)-S(15)	167.0(10)
N(3A)-Co(1)-S(2)	89.1(8)	N(13A)-Co(5)-S(13)	72.6(10)
N(1A)-Co(1)-S(2)	166.5(8)	N(15A)-Co(5)-S(13)	166.6(10)
N(2A)-Co(1)-S(2)	72.8(9)	N(14A)-Co(5)-S(13)	93.1(9)
S(1)-Co(1)-S(2)	100.3(4)	S(15)-Co(5)-S(13)	99.1(4)
S(3)-Co(1)-S(2)	100.5(4)	N(13A)-Co(5)-S(14)	168.8(10)
N(4A)-Co(2)-N(6A)	97.3(12)	N(15A)-Co(5)-S(14)	91.1(9)
N(4A)-Co(2)-N(5A)	96.0(12)	N(14A)-Co(5)-S(14)	74.5(10)
N(6A)-Co(2)-N(5A)	95.1(10)	S(15)-Co(5)-S(14)	98.6(4)
N(4A)-Co(2)-S(5)	92.0(9)	S(13)-Co(5)-S(14)	100.0(4)
N(6A)-Co(2)-S(5)	166.0(8)	N(13A)-Co(5)-C(14A)	129.9(12)
N(5A)-Co(2)-S(5)	73.5(8)	N(15A)-Co(5)-C(14A)	94.8(12)
N(4A)-Co(2)-S(6)	168.2(10)	N(14A)-Co(5)-C(14A)	33.0(11)
N(6A)-Co(2)-S(6)	72.5(8)	S(15)-Co(5)-C(14A)	138.8(10)
N(5A)-Co(2)-S(6)	90.8(8)	S(13)-Co(5)-C(14A)	98.4(9)
S(5)-Co(2)-S(6)	99.1(4)	S(14)-Co(5)-C(14A)	41.5(9)
N(4A)-Co(2)-S(4)	72.0(10)	N(13A)-Co(5)-C(13A)	32.4(11)
N(6A)-Co(2)-S(4)	94.1(8)	N(15A)-Co(5)-C(13A)	129.6(13)
N(5A)-Co(2)-S(4)	165.8(8)	N(14A)-Co(5)-C(13A)	93.8(13)
S(5)-Co(2)-S(4)	98.7(4)	S(15)-Co(5)-C(13A)	98.5(9)
S(6)-Co(2)-S(4)	102.4(4)	S(13)-Co(5)-C(13A)	40.4(9)
N(9A)-Co(3)-N(7A)	98.5(12)	S(14)-Co(5)-C(13A)	139.0(10)
N(9A)-Co(3)-N(8A)	95.6(11)	C(14A)-Co(5)-C(13A)	118.6(13)
N(7A)-Co(3)-N(8A)	98.2(12)	N(16A)-Co(6)-N(17A)	98.5(13)
N(9A)-Co(3)-S(7)	168.4(9)	N(16A)-Co(6)-N(18A)	100.0(14)
N(7A)-Co(3)-S(7)	72.2(10)	N(17A)-Co(6)-N(18A)	98.3(13)
N(8A)-Co(3)-S(7)	92.6(8)	N(16A)-Co(6)-S(16)	70.9(11)
N(9A)-Co(3)-S(8)	90.7(9)	N(17A)-Co(6)-S(16)	91.6(9)
N(7A)-Co(3)-S(8)	166.5(9)	N(18A)-Co(6)-S(16)	167.5(10)
N(8A)-Co(3)-S(8)	71.0(9)	N(16A)-Co(6)-S(17)	164.6(11)
S(7)-Co(3)-S(8)	99.7(4)	N(17A)-Co(6)-S(17)	70.9(10)
N(9A)-Co(3)-S(9)	72.1(9)	N(18A)-Co(6)-S(17)	92.7(9)
N(7A)-Co(3)-S(9)	93.0(9)	S(16)-Co(6)-S(17)	97.7(5)
N(8A)-Co(3)-S(9)	164.6(9)	N(16A)-Co(6)-S(18)	93.9(9)
S(7)-Co(3)-S(9)	101.0(4)	N(17A)-Co(6)-S(18)	165.2(10)
S(8)-Co(3)-S(9)	99.2(4)	N(18A)-Co(6)-S(18)	71.5(10)
N(10A)-Co(4)-N(12A)	99.1(13)	S(16)-Co(6)-S(18)	100.0(4)
N(10A)-Co(4)-N(11A)	98.9(13)	S(17)-Co(6)-S(18)	98.4(5)
N(12A)-Co(4)-N(11A)	100.1(13)	N(19A)-Co(7)-N(20A)	96.2(13)
N(10A)-Co(4)-S(12)	91.0(10)	N(19A)-Co(7)-N(21A)	101.6(13)
N(12A)-Co(4)-S(12)	70.2(11)	N(20A)-Co(7)-N(21A)	98.9(13)
N(11A)-Co(4)-S(12)	167.3(9)	N(19A)-Co(7)-S(19)	70.9(10)
N(10A)-Co(4)-S(10)	73.6(10)	N(20A)-Co(7)-S(19)	92.4(8)
N(12A)-Co(4)-S(10)	164.5(11)	N(21A)-Co(7)-S(19)	167.2(11)
N(11A)-Co(4)-S(10)	94.5(8)	N(19A)-Co(7)-S(21)	94.4(10)
S(12)-Co(4)-S(10)	95.9(4)	N(20A)-Co(7)-S(21)	166.3(9)
N(10A)-Co(4)-S(11)	165.3(10)	N(21A)-Co(7)-S(21)	70.5(10)
N(12A)-Co(4)-S(11)	93.7(9)	S(19)-Co(7)-S(21)	99.2(4)
N(11A)-Co(4)-S(11)	71.4(9)	N(19A)-Co(7)-S(20)	165.3(10)
S(12)-Co(4)-S(11)	100.4(4)	N(20A)-Co(7)-S(20)	71.7(9)

N(21A)-Co(7)-S(20)	88.8(9)	N(23A)-Co(8)-S(23)	70.6(11)
S(19)-Co(7)-S(20)	100.6(4)	N(24A)-Co(8)-S(23)	92.2(9)
S(21)-Co(7)-S(20)	98.9(4)	N(22A)-Co(8)-S(23)	167.1(10)
N(19A)-Co(7)-C(21A)	98.4(12)	N(23A)-Co(8)-S(24)	164.7(11)
N(20A)-Co(7)-C(21A)	131.1(12)	N(24A)-Co(8)-S(24)	72.2(10)
N(21A)-Co(7)-C(21A)	32.5(11)	N(22A)-Co(8)-S(24)	93.7(9)
S(19)-Co(7)-C(21A)	136.4(10)	S(23)-Co(8)-S(24)	97.9(5)
S(21)-Co(7)-C(21A)	38.1(9)	N(23A)-Co(8)-S(22)	94.4(10)
S(20)-Co(7)-C(21A)	95.9(9)	N(24A)-Co(8)-S(22)	164.6(10)
N(23A)-Co(8)-N(24A)	97.6(13)	N(22A)-Co(8)-S(22)	71.7(11)
N(23A)-Co(8)-N(22A)	99.0(14)	S(23)-Co(8)-S(22)	100.9(5)
N(24A)-Co(8)-N(22A)	96.8(13)	S(24)-Co(8)-S(22)	97.7(5)

Table 15: Crystal data and structure refinement for $[Na_6(HO_2ta)_6(H_2O_2ta)_6(CH_3OH)_8(H_2O)_2].2CH_3OH.H_2O$.

Empirical formula	$C_{82}H_{160}N_{48}Na_6O_{37}$
Formula weight	2548.52
Wavelength	0.71073 Å
Temperature	150(2) K
Crystal system	Triclinic
Space group	P-1
Unit cell dimensions	a = 13.6573(5) Å α = 85.093(2) °. b = 14.4137(5) Å β = 68.858(2) °. c = 17.4583(7) Å γ = 72.767(2) °.
Volume	3060.6(2) $Å^3$
Z	1
Density (calculated)	1.383 Mg/m^3
Absorption coefficient	0.127 mm^{-1}
F(000)	1350
Crystal description	Colourless tablet
Crystal size	0.35 x 0.20 x 0.05 mm
θ range for data collection	2.41 to 30.53 °.
Index ranges	-18<=h<=18, -20<=k<=20, -24<=l<=24
Reflections collected	59339
Independent reflections	17317 [R(int) = 0.1047]
Scan type	ϕ - ω
Absorption correction	Sortav (Tmin= 0.720, Tmax=1.000)
Solution	direct (SIR92)
Refinement type	Full-matrix least-squares on F^2
Program used for refinement	SHELXL-97
Hydrogen atom placement	geometric
Hydrogen atom treatment	riding
Data / restraints / parameters	17317/9/774
Goodness-of-fit on F^2	1.042
Conventional R [F>4σ(F)]	R1 = 0.0781 [8433 data]
Weighted R (F^2 and all data)	wR2 = 0.2436
Extinction coefficient	0.0012(8)
Final maximum Δ/σ	0.083
Weighting scheme	calc w=1/[\σ²(Fo²)+(0.1227P)²+0.0000P] where P=(Fo²+2Fc²)/3
Largest diff. peak and hole	0.781 and -0.532 e. $Å^{-3}$

Table 16: Selected bond lengths [Å] and angles [°] for $[Na_6(HO_2ta)_6(H_2O_2ta)_6(CH_3OH)_8(H_2O)_2].2CH_3OH.H_2O$.

Na(1)-O(1M)	2.318(3)	Na(3)-O(4M)	2.415(4)
Na(1)-O(2D)	2.338(2)	Na(3)-O(3M)	2.480(4)
Na(1)-O(2C)#1	2.366(2)	Na(3)-O(2E)	2.496(2)
Na(1)-O(2A)	2.392(2)	Na(3)-O(2C)	2.773(2)
Na(1)-O(2M)	2.424(2)	O(2A)-Na(3)#1	2.352(2)
Na(1)-O(2B)	2.483(2)	O(2B)-Na(2)#1	2.375(2)
Na(2)-O(2W)	2.288(3)	O(2C)-Na(1)#1	2.366(2)
Na(2)-O(2M)	2.366(2)		
Na(2)-O(2B)#1	2.375(2)	O(1M)-Na(1)-O(2D)	94.00(10)
Na(2)-O(2B)	2.386(2)	O(1M)-Na(1)-O(2C)#1	81.87(9)
Na(2)-O(2C)	2.432(2)	O(2D)-Na(1)-O(2C)#1	173.10(9)
Na(2)-O(2E)	2.531(2)	O(1M)-Na(1)-O(2A)	92.44(10)
Na(3)-O(4M')	2.119(7)	O(2D)-Na(1)-O(2A)	89.21(7)
Na(3)-O(2F)	2.343(3)	O(2C)#1-Na(1)-O(2A)	85.47(7)
Na(3)-O(2A)#1	2.352(2)	O(1M)-Na(1)-O(2M)	96.52(10)

O(2D)-Na(1)-O(2M)	103.94(8)	O(2C)-Na(2)-O(2E)	99.19(7)
O(2C)#1-Na(1)-O(2M)	82.09(7)	O(4M')-Na(3)-O(2F)	100.7(2)
O(2A)-Na(1)-O(2M)	163.46(8)	O(4M')-Na(3)-O(2A)#1	92.8(3)
O(1M)-Na(1)-O(2B)	165.24(10)	O(2F)-Na(3)-O(2A)#1	156.51(11)
O(2D)-Na(1)-O(2B)	100.51(8)	O(4M')-Na(3)-O(4M)	23.9(2)
O(2C)#1-Na(1)-O(2B)	83.43(7)	O(2F)-Na(3)-O(4M)	79.71(12)
O(2A)-Na(1)-O(2B)	85.11(7)	O(2A)#1-Na(3)-O(4M)	116.32(12)
O(2M)-Na(1)-O(2B)	82.68(7)	O(4M')-Na(3)-O(3M)	87.6(2)
O(2W)-Na(2)-O(2M)	96.08(11)	O(2F)-Na(3)-O(3M)	79.68(13)
O(2W)-Na(2)-O(2B)#1	170.33(13)	O(2A)#1-Na(3)-O(3M)	81.84(11)
O(2M)-Na(2)-O(2B)#1	91.18(7)	O(4M)-Na(3)-O(3M)	94.77(14)
O(2W)-Na(2)-O(2B)	99.46(11)	O(4M')-Na(3)-O(2E)	97.2(2)
O(2M)-Na(2)-O(2B)	86.04(7)	O(2F)-Na(3)-O(2E)	110.93(12)
O(2B)#1-Na(2)-O(2B)	87.38(7)	O(2A)#1-Na(3)-O(2E)	86.00(8)
O(2W)-Na(2)-O(2C)	89.01(10)	O(4M)-Na(3)-O(2E)	94.29(11)
O(2M)-Na(2)-O(2C)	172.89(8)	O(3M)-Na(3)-O(2E)	167.16(12)
O(2B)#1-Na(2)-O(2C)	84.34(7)	O(4M')-Na(3)-O(2C)	166.6(3)
O(2B)-Na(2)-O(2C)	88.24(7)	O(2F)-Na(3)-O(2C)	85.50(8)
O(2W)-Na(2)-O(2E)	82.01(11)	O(2A)#1-Na(3)-O(2C)	77.63(7)
O(2M)-Na(2)-O(2E)	86.45(7)	O(4M)-Na(3)-O(2C)	165.19(12)
O(2B)#1-Na(2)-O(2E)	92.11(7)	O(3M)-Na(3)-O(2C)	81.87(11)
O(2B)-Na(2)-O(2E)	172.46(8)	O(2E)-Na(3)-O(2C)	91.55(7)

Symmetry transformations used to generate equivalent atoms: #1 -x+1,-y,-z

Table 17: Crystal data and structure refinement for 6-(diethylamino)-4-methoxy-1,3,5-triazine-2-one.

Empirical formula	$C_8H_{14}N_4O_2$
Formula weight	198.23
Wavelength	1.54178 Å
Temperature	220(2) K
Crystal system	Triclinic
Space group	P-1
Unit cell dimensions	a = 7.565(4) Å α = 75.52(3) °. b = 8.004(4) Å β = 88.62(3) °. c = 8.854(4) Å γ = 72.31(3) °.
Volume	493.7(4) $Å^3$
Number of reflections for cell	56 (20 < θ < 22 °.)
Z	2
Density (calculated)	1.333 Mg/m^3
Absorption coefficient	0.822 mm^{-1}
F(000)	212
Crystal description	Colourless tablet
Crystal size	0.47 x 0.31 x 0.12 mm
Theta range for data collection	5.17 to 69.97 °.
Index ranges	-9<=h<=9, -9<=k<=9, -10<=l<=9
Reflections collected	2653
Independent reflections	1744 [R(int) = 0.0065]
Scan type	ω - θ
Solution	direct (SHELXS-97)
Refinement type	Full-matrix least-squares on F^2
Program used for refinement	SHELXL-97
Hydrogen atom placement	geometric/ diff. map (H1)
Hydrogen atom treatment	Riding/ refall (H1)
Data / restraints / parameters	1744/0/132
Goodness-of-fit on F^2	1.068
Conventional R [F>4σ(F)]	R1 = 0.0395 [1578 data]
Weighted R (F^2 and all data)	wR2 = 0.1084
Extinction coefficient	0.0145(19)
Final maximum Δ/σ	0.000
Weighting scheme	calc $w=1/[\sigma^2(Fo^2)+(0.0610P)^2+0.1242P]$ where $P=(Fo^2+2Fc^2)/3$
Largest diff. peak and hole	0.187 and -0.184 e. $Å^{-3}$

Table 18: Bond lengths [A] and angles [°] for 6-(diethylamino)-4-methoxy-1,3,5-triazine-2-one.

N(1)-C(6)	1.3404(18)	O(21)-C(2)-N(1)	118.41(12)
N(1)-C(2)	1.3966(18)	N(3)-C(2)-N(1)	118.14(12)
C(2)-O(21)	1.2390(16)	C(4)-N(3)-C(2)	117.50(12)
C(2)-N(3)	1.3424(18)	N(3)-C(4)-N(41)	118.83(12)
N(3)-C(4)	1.3353(17)	N(3)-C(4)-N(5)	126.20(12)
C(4)-N(41)	1.3429(18)	N(41)-C(4)-N(5)	114.96(12)
C(4)-N(5)	1.3742(18)	C(4)-N(41)-C(44)	120.44(12)
N(41)-C(44)	1.4659(18)	C(4)-N(41)-C(42)	121.35(12)
N(41)-C(42)	1.4682(19)	C(44)-N(41)-C(42)	118.16(11)
C(42)-C(43)	1.506(2)	N(41)-C(42)-C(43)	113.22(14)
C(44)-C(45)	1.516(2)	N(41)-C(44)-C(45)	113.48(12)
N(5)-C(6)	1.2979(18)	C(6)-N(5)-C(4)	114.05(12)
C(6)-O(61)	1.3204(17)	N(5)-C(6)-O(61)	122.47(12)
O(61)-C(62)	1.4500(17)	N(5)-C(6)-N(1)	124.36(12)
		O(61)-C(6)-N(1)	113.16(12)
C(6)-N(1)-C(2)	119.65(11)	C(6)-O(61)-C(62)	117.19(11)
O(21)-C(2)-N(3)	123.44(12)		

Table 19: Crystal data and structure refinement for $[Ni_3(chp)_4(bpa)_2(MeOH)_6].2MeOH$.

Empirical formula	$C_{48}H_{62}Cl_4N_4Ni_3O_{18}$
Formula weight	1300.95
Wavelength	0.71073 Å
Temperature	150(2) K
Crystal system	Monoclinic
Space group	$P2_1/c$
Unit cell dimensions	a = 15.342(3) Å α = 90 °. b = 15.206(5) Å β = 101.84(2) °. c = 26.079(8) Å γ = 90 °.
Volume	5954(3) $Å^3$
Number of reflections for cell	48 (11 < θ < 12 °.)
Z	4
Density (calculated)	1.451 Mg/m^3
Absorption coefficient	1.187 mm^{-1}
F(000)	2696
Crystal description	Green block
Crystal size	0.64 x 0.38 x 0.20 mm
θ range for data collection	2.66 to 25.09 °.
Index ranges	-18<=h<=17, 0<=k<=18, 0<=l<=31
Reflections collected	10589
Independent reflections	10551 [R(int) = 0.2873]
Scan type	ω - θ
Absorption correction	Psi-scans (Tmin= 0.170, Tmax=0.340)
Solution	direct (SIR97)
Refinement type	Full-matrix least-squares on F^2
Program used for refinement	SHELXL-97
Hydrogen atom placement	geometric/difference map (MeOH)
Hydrogen atom treatment	geometric/rgid group/restr. refxyz
Data / restraints / parameters	10551/15/716
Goodness-of-fit on F^2	1.058
Conventional R [F>4σ(F)]	R1 = 0.0600 [6459 data]
Weighted R (F^2 and all data)	wR2 = 0.1669
Final maximum Δ/σ	0.013
Weighting scheme	calc $w=1/[\sigma^2(Fo^2)+(0.0617P)^2+9.6934P]$ where $P=(Fo^2+2Fc^2)/3$
Largest diff. peak and hole	0.473 and -0.484 $e.Å^{-3}$

Table 20: Selected bond lengths [Å] and angles [°] for $[Ni_3(chp)_4(bpa)_2(MeOH)_6].2MeOH$.

Ni(1)-O(1A)	1.998(4)	Ni(2)-O(1B)	2.066(4)
Ni(1)-O(1M)	2.044(4)	Ni(2)-O(24)	2.067(4)
Ni(1)-O(2M)	2.068(4)	Ni(2)-O(22)	2.073(4)
Ni(1)-O(21)	2.070(4)	Ni(2)-O(23)	2.080(4)
Ni(1)-O(3M)	2.077(4)	Ni(3)-O(2B)	2.001(4)
Ni(1)-O(22)	2.082(4)	Ni(3)-O(6M)	2.038(4)
Ni(2)-O(2A)	2.062(4)	Ni(3)-O(24)	2.059(4)
Ni(2)-O(21)	2.064(4)	Ni(3)-O(5M)	2.069(5)

Ni(3)-O(4M)	2.070(4)	O(2A)-Ni(2)-O(22)	87.32(15)
Ni(3)-O(23)	2.078(4)	O(21)-Ni(2)-O(22)	79.83(15)
		O(1B)-Ni(2)-O(22)	92.24(15)
O(1A)-Ni(1)-O(1M)	175.66(17)	O(24)-Ni(2)-O(22)	100.76(15)
O(1A)-Ni(1)-O(2M)	91.54(17)	O(2A)-Ni(2)-O(23)	91.09(15)
O(1M)-Ni(1)-O(2M)	86.85(18)	O(21)-Ni(2)-O(23)	100.21(15)
O(1A)-Ni(1)-O(21)	89.46(16)	O(1B)-Ni(2)-O(23)	89.36(15)
O(1M)-Ni(1)-O(21)	92.66(17)	O(24)-Ni(2)-O(23)	79.25(15)
O(2M)-Ni(1)-O(21)	172.49(16)	O(22)-Ni(2)-O(23)	178.40(15)
O(1A)-Ni(1)-O(3M)	91.95(17)	O(2B)-Ni(3)-O(6M)	176.21(17)
O(1M)-Ni(1)-O(3M)	84.08(18)	O(2B)-Ni(3)-O(24)	91.00(16)
O(2M)-Ni(1)-O(3M)	92.01(17)	O(6M)-Ni(3)-O(24)	91.23(17)
O(21)-Ni(1)-O(3M)	95.40(16)	O(2B)-Ni(3)-O(5M)	92.01(18)
O(1A)-Ni(1)-O(22)	93.63(15)	O(6M)-Ni(3)-O(5M)	86.11(19)
O(1M)-Ni(1)-O(22)	90.48(16)	O(24)-Ni(3)-O(5M)	173.07(16)
O(2M)-Ni(1)-O(22)	93.01(16)	O(2B)-Ni(3)-O(4M)	91.29(17)
O(21)-Ni(1)-O(22)	79.50(15)	O(6M)-Ni(3)-O(4M)	85.42(17)
O(3M)-Ni(1)-O(22)	172.39(16)	O(24)-Ni(3)-O(4M)	96.15(16)
O(2A)-Ni(2)-O(21)	91.35(15)	O(5M)-Ni(3)-O(4M)	90.02(18)
O(2A)-Ni(2)-O(1B)	179.31(16)	O(2B)-Ni(3)-O(23)	92.52(16)
O(21)-Ni(2)-O(1B)	88.05(15)	O(6M)-Ni(3)-O(23)	90.90(16)
O(2A)-Ni(2)-O(24)	90.25(15)	O(24)-Ni(3)-O(23)	79.47(15)
O(21)-Ni(2)-O(24)	178.32(15)	O(5M)-Ni(3)-O(23)	94.16(16)
O(1B)-Ni(2)-O(24)	90.35(15)	O(4M)-Ni(3)-O(23)	174.24(16)

Table 21: Crystal data and structure refinement for $[Ni_6Na_2Cl_2(OH)_6(Hmhp)_6(bpa)_6]$. 3.7THF.

Empirical formula	$C_{110.80}H_{131.60}Cl_2N_6Na_2Ni_6O_{33.70}$
Formula weight	2555.76
Wavelength	0.71073 Å
Temperature	150(2) K
Crystal system	Triclinic
Space group	P-1
Unit cell dimensions	a = 14.969(8) Å α = 61.556(8) °. b = 15.374(8) Å β = 65.336(9) °. c = 15.579(8) Å γ = 82.202(9) °.
Volume	2856(3) $Å^3$
Number of reflections for cell	6110 (2.5 < θ < 26 °.)
Z	1
Density (calculated)	1.486 Mg/m^3
Absorption coefficient	1.106 mm^{-1}
F(000)	1332
Crystal description	Colourless plate
Crystal size	0.15 x 0.10 x 0.06 mm
θ range for data collection	1.50 to 26.48 °.
Index ranges	-18<=h<=18, -19<=k<=19, -18<=l<=19
Reflections collected	22933
Independent reflections	11460 [R(int) = 0.0339]
Scan type	ϕ and ω scans
Absorption correction	Sadabs (Tmin= 0.771, Tmax=0.862)
Solution	heavy atom method (SHELXS-97 (Sheldrick, 1990))
Refinement type	Full-matrix least-squares on F^2
Program used for refinement	SHELXL-97
Hydrogen atom placement	geometric except hydroxyls, difmap
Hydrogen atom treatment	mixed
Data / restraints / parameters	11460/0/742
Goodness-of-fit on F^2	0.914
Conventional R [F>4σ(F)]	R1 = 0.0438 [7552 data]
Weighted R (F^2 and all data)	wR2 = 0.1056
Extinction coefficient	0
Final maximum Δ/σ	0.007
Weighting scheme	calc $w=1/[\sigma^2(Fo^2)+(0.0566P)^2+0.0000P]$ where $P=(Fo^2+2Fc^2)/3$
Largest diff. peak and hole	0.797 and -0.488 e. $Å^{-3}$

Table 22: Selected bond lengths [Å] and angles [°] for $[Ni_6Na_2Cl_2(OH)_6(Hmhp)_6(bpa)_6]$. 3.7THF.

Ni(1)-O(12B)	2.019(2)	Ni(2)-Ni(1)-Ni(3)	82.80(3)
Ni(1)-O(11A)	2.051(2)	O(12B)-Ni(1)-Na(1)#1	125.08(7)
Ni(1)-O(12)#1	2.060(2)	O(11A)-Ni(1)-Na(1)#1	122.68(7)
Ni(1)-O(13)	2.071(2)	O(12)#1-Ni(1)-Na(1)#1	58.01(6)
Ni(1)-O(11)	2.080(2)	O(13)-Ni(1)-Na(1)#1	58.47(7)
Ni(1)-O(123)	2.091(2)	O(11)-Ni(1)-Na(1)#1	49.42(7)
Ni(1)-Ni(2)	2.9487(14)	O(123)-Ni(1)-Na(1)#1	117.94(8)
Ni(1)-Ni(3)	2.9861(17)	Ni(2)-Ni(1)-Na(1)#1	99.48(4)
Ni(1)-Na(1)#1	3.0840(19)	Ni(3)-Ni(1)-Na(1)#1	99.40(3)
Ni(2)-O(12A)	2.039(2)	O(12A)-Ni(2)-O(123)	91.38(10)
Ni(2)-O(123)	2.042(2)	O(12A)-Ni(2)-O(12C)#1	85.32(9)
Ni(2)-O(12C)#1	2.056(2)	O(123)-Ni(2)-O(12C)#1	176.55(9)
Ni(2)-O(13)#1	2.057(2)	O(12A)-Ni(2)-O(13)#1	175.25(9)
Ni(2)-O(12)#1	2.082(2)	O(123)-Ni(2)-O(13)#1	93.34(10)
Ni(2)-O(31)	2.107(2)	O(12C)#1-Ni(2)-O(13)#1	89.96(10)
Ni(2)-Ni(3)#1	2.9919(15)	O(12A)-Ni(2)-O(12)#1	99.34(10)
Ni(2)-Na(1)	3.105(2)	O(123)-Ni(2)-O(12)#1	83.63(9)
Ni(3)-O(11C)	2.035(2)	O(12C)#1-Ni(2)-O(12)#1	97.87(9)
Ni(3)-O(11B)	2.038(2)	O(13)#1-Ni(2)-O(12)#1	81.83(10)
Ni(3)-O(123)	2.057(2)	O(12A)-Ni(2)-O(31)	89.24(9)
Ni(3)-O(12)	2.057(2)	O(123)-Ni(2)-O(31)	86.64(9)
Ni(3)-O(13)	2.076(2)	O(12C)#1-Ni(2)-O(31)	92.31(8)
Ni(3)-O(21)	2.085(2)	O(13)#1-Ni(2)-O(31)	90.40(10)
Ni(3)-Ni(2)#1	2.9919(15)	O(12)#1-Ni(2)-O(31)	167.15(9)
Ni(3)-Na(1)	3.0738(18)	O(12A)-Ni(2)-Ni(1)	79.71(7)
O(123)-Na(1)	2.641(3)	O(123)-Ni(2)-Ni(1)	45.15(7)
Na(1)-O(11)#1	2.343(3)	O(12C)#1-Ni(2)-Ni(1)	134.78(7)
Na(1)-O(31)	2.344(3)	O(13)#1-Ni(2)-Ni(1)	104.11(8)
Na(1)-O(21)	2.372(3)	O(12)#1-Ni(2)-Ni(1)	44.31(6)
Na(1)-O(12)	2.650(3)	O(31)-Ni(2)-Ni(1)	129.50(6)
Na(1)-O(13)#1	2.668(3)	O(12A)-Ni(2)-Ni(3)#1	135.12(7)
Na(1)-Cl(1)	2.8705(19)	O(123)-Ni(2)-Ni(3)#1	104.49(8)
Na(1)-Ni(1)#1	3.0840(19)	O(12C)#1-Ni(2)-Ni(3)#1	78.62(7)
O(11)-Na(1)#1	2.343(3)	O(13)#1-Ni(2)-Ni(3)#1	43.87(7)
O(13)-Ni(2)#1	2.057(2)	O(12)#1-Ni(2)-Ni(3)#1	43.37(7)
O(13)-Na(1)#1	2.668(3)	O(31)-Ni(2)-Ni(3)#1	132.61(6)
O(12C)-Ni(2)#1	2.056(2)	Ni(1)-Ni(2)-Ni(3)#1	82.60(4)
O(12)-Ni(1)#1	2.060(2)	O(12A)-Ni(2)-Na(1)	124.54(7)
O(12)-Ni(2)#1	2.082(2)	O(123)-Ni(2)-Na(1)	57.36(7)
		O(12C)#1-Ni(2)-Na(1)	124.01(7)
O(12B)-Ni(1)-O(11A)	87.07(9)	O(13)#1-Ni(2)-Na(1)	58.07(7)
O(12B)-Ni(1)-O(12)#1	175.50(9)	O(12)#1-Ni(2)-Na(1)	118.26(7)
O(11A)-Ni(1)-O(12)#1	88.44(9)	O(31)-Ni(2)-Na(1)	48.98(7)
O(12B)-Ni(1)-O(13)	90.22(10)	Ni(1)-Ni(2)-Na(1)	99.21(3)
O(11A)-Ni(1)-O(13)	177.16(9)	Ni(3)#1-Ni(2)-Na(1)	98.79(3)
O(12)#1-Ni(1)-O(13)	94.27(10)	O(11C)-Ni(3)-O(11B)	86.24(10)
O(12B)-Ni(1)-O(11)	90.28(9)	O(11C)-Ni(3)-O(123)	173.76(9)
O(11A)-Ni(1)-O(11)	91.00(10)	O(11B)-Ni(3)-O(123)	87.84(10)
O(12)#1-Ni(1)-O(11)	90.09(9)	O(11C)-Ni(3)-O(12)	91.74(10)
O(13)-Ni(1)-O(11)	88.14(10)	O(11B)-Ni(3)-O(12)	176.53(9)
O(12B)-Ni(1)-O(123)	97.50(9)	O(123)-Ni(3)-O(12)	94.27(11)
O(11A)-Ni(1)-O(123)	99.58(10)	O(11C)-Ni(3)-O(13)	96.87(10)
O(12)#1-Ni(1)-O(123)	82.96(9)	O(11B)-Ni(3)-O(13)	101.04(9)
O(13)-Ni(1)-O(123)	81.63(10)	O(123)-Ni(3)-O(13)	82.33(10)
O(11)-Ni(1)-O(123)	167.14(9)	O(12)-Ni(3)-O(13)	81.99(10)
O(12B)-Ni(1)-Ni(2)	133.49(7)	O(11C)-Ni(3)-O(21)	90.06(9)
O(11A)-Ni(1)-Ni(2)	78.21(7)	O(11B)-Ni(3)-O(21)	89.91(9)
O(12)#1-Ni(1)-Ni(2)	44.91(7)	O(123)-Ni(3)-O(21)	91.90(9)
O(13)-Ni(1)-Ni(2)	104.33(8)	O(12)-Ni(3)-O(21)	87.26(9)
O(11)-Ni(1)-Ni(2)	133.27(6)	O(13)-Ni(3)-O(21)	167.36(9)
O(123)-Ni(1)-Ni(2)	43.82(6)	O(11C)-Ni(3)-Ni(1)	132.01(7)
O(12B)-Ni(1)-Ni(3)	77.85(6)	O(11B)-Ni(3)-Ni(1)	78.61(7)
O(11A)-Ni(1)-Ni(3)	135.91(7)	O(123)-Ni(3)-Ni(1)	44.41(6)
O(12)#1-Ni(1)-Ni(3)	105.29(7)	O(12)-Ni(3)-Ni(1)	104.82(7)
O(13)-Ni(1)-Ni(3)	44.00(6)	O(13)-Ni(3)-Ni(1)	43.86(7)
O(11)-Ni(1)-Ni(3)	129.68(7)	O(21)-Ni(3)-Ni(1)	134.55(7)
O(123)-Ni(1)-Ni(3)	43.49(7)	O(11C)-Ni(3)-Ni(2)#1	79.04(7)

O(11B)-Ni(3)-Ni(2)#1	137.96(6)	O(11)#1-Na(1)-Cl(1)	89.10(7)
O(123)-Ni(3)-Ni(2)#1	104.21(8)	O(31)-Na(1)-Cl(1)	92.91(8)
O(12)-Ni(3)-Ni(2)#1	44.04(6)	O(21)-Na(1)-Cl(1)	88.48(7)
O(13)-Ni(3)-Ni(2)#1	43.38(7)	O(123)-Na(1)-Cl(1)	140.51(8)
O(21)-Ni(3)-Ni(2)#1	128.82(7)	O(12)-Na(1)-Cl(1)	135.83(7)
Ni(1)-Ni(3)-Ni(2)#1	82.57(2)	O(13)#1-Na(1)-Cl(1)	140.90(8)
O(11C)-Ni(3)-Na(1)	127.23(8)	O(11)#1-Na(1)-Ni(3)	112.58(8)
O(11B)-Ni(3)-Na(1)	121.06(8)	O(31)-Na(1)-Ni(3)	109.97(7)
O(123)-Ni(3)-Na(1)	57.97(8)	O(21)-Na(1)-Ni(3)	42.65(6)
O(12)-Ni(3)-Na(1)	58.24(7)	O(123)-Na(1)-Ni(3)	41.32(5)
O(13)-Ni(3)-Na(1)	117.48(8)	O(12)-Na(1)-Ni(3)	41.29(5)
O(21)-Ni(3)-Na(1)	50.42(6)	O(13)#1-Na(1)-Ni(3)	87.90(8)
Ni(1)-Ni(3)-Na(1)	99.11(4)	Cl(1)-Na(1)-Ni(3)	131.12(5)
Ni(2)#1-Ni(3)-Na(1)	98.76(5)	O(11)#1-Na(1)-Ni(1)#1	42.39(6)
Ni(1)-O(123)-Na(1)	154.00(13)	O(31)-Na(1)-Ni(1)#1	112.98(7)
O(11)#1-Na(1)-O(31)	120.37(10)	O(21)-Na(1)-Ni(1)#1	109.74(7)
O(11)#1-Na(1)-O(21)	119.26(9)	O(123)-Na(1)-Ni(1)#1	88.06(7)
O(31)-Na(1)-O(21)	120.37(9)	O(12)-Na(1)-Ni(1)#1	41.25(6)
O(11)#1-Na(1)-O(123)	130.39(9)	O(13)#1-Na(1)-Ni(1)#1	41.41(5)
O(31)-Na(1)-O(123)	69.36(8)	Cl(1)-Na(1)-Ni(1)#1	131.33(5)
O(21)-Na(1)-O(123)	72.64(8)	Ni(3)-Na(1)-Ni(1)#1	79.10(5)
O(11)#1-Na(1)-O(12)	71.55(8)	O(11)#1-Na(1)-Ni(2)	110.28(7)
O(31)-Na(1)-O(12)	131.22(9)	O(31)-Na(1)-Ni(2)	42.70(6)
O(21)-Na(1)-O(12)	69.11(8)	O(21)-Na(1)-Ni(2)	112.98(7)
O(123)-Na(1)-O(12)	69.47(8)	O(123)-Na(1)-Ni(2)	40.63(6)
O(11)#1-Na(1)-O(13)#1	70.01(8)	O(12)-Na(1)-Ni(2)	88.59(6)
O(31)-Na(1)-O(13)#1	71.92(8)	O(13)#1-Na(1)-Ni(2)	40.88(5)
O(21)-Na(1)-O(13)#1	130.45(9)	Cl(1)-Na(1)-Ni(2)	135.58(5)
O(123)-Na(1)-O(13)#1	68.34(9)	Ni(3)-Na(1)-Ni(2)	78.86(4)
O(12)-Na(1)-O(13)#1	69.40(8)	Ni(1)#1-Na(1)-Ni(2)	79.18(3)

Symmetry transformations used to generate equivalent atoms: #1 -x,-y,-z+1

Table 23: Crystal data and structure refinement for $[Co_{13}(OH)_3(H_2O)_2(chp)_{19}(PhPO_3)_2(CH_3C(O)OCH_2CH_3)_2].2(CH_3C(O)OCH_2CH_3)$.

Empirical formula	$C_{119}H_{98}C_{119}Co_{13}N_{19}O_{36}P_2$
Formula weight	3871.74
Wavelength	0.71073 Å
Temperature	220(2) K
Crystal system	Triclinic
Space group	P-1
Unit cell dimensions	a = 16.880(5) Å α = 104.47(2) °. b = 17.978(5) Å β = 102.391(15) °. c = 29.874(10) Å γ = 94.077(18) °.
Volume	8499(4) $Å^3$
Number of reflections for cell	42 (10 < θ < 11 °.)
Z	2
Density (calculated)	1.513 Mg/m^3
Absorption coefficient	1.619 mm^{-1}
F(000)	3874
Crystal description	Magenta plate
Crystal size	0.39 x 0.35 x 0.19 mm
θ range for data collection	2.52 to 20.00 °.
Index ranges	-16<=h<=15, -17<=k<=16, 0<=l<=28
Reflections collected	16170
Independent reflections	15739 [R(int) = 0.0955]
Scan type	ω - θ
Absorption correction	Face-indexed (Tmin= 0.62439, Tmax=0.82854)
Solution	direct (SHELXS-97 (Sheldrick, 1990))
Refinement type	Full-matrix least-squares on F^2
Program used for refinement	SHELXL-97
Hydrogen atom placement	geometric
Hydrogen atom treatment	riding
Data / restraints / parameters	15739/8/995
Goodness-of-fit on F^2	0.867
Conventional R [F>4σ(F)]	R1 = 0.0854 [6002 data]
Weighted R (F^2 and all data)	wR2 = 0.1959
Extinction coefficient	0
Final maximum Δ/σ	0.023
Weighting scheme	calc w=1/[\σ²(Fo²)+(0.0665P)²+0.0000P] where P=(Fo²+2Fc²)/3
Largest diff. peak and hole	0.724 and -0.540 $e.Å^{-3}$

Table 24: Selected bond lengths [Å] and angles [°] for $[Co_{13}(OH)_3(H_2O)_2(chp)_{19}(PhPO_3)_2(CH_3C(O)OCH_2CH_3)_2].2(CH_3C(O)OCH_2CH_3)$.

Co(1)-O(159)	2.027(10)	Co(12)-O(3P)	2.106(12)
Co(1)-O(1A2)	2.055(11)	Co(12)-O(3N)	2.124(11)
Co(1)-O(128)	2.074(11)	Co(12)-N(2G)	2.173(14)
Co(1)-O(1B3)	2.108(11)	Co(12)-N(2N)	2.232(15)
Co(1)-O(3U)	2.145(12)	Co(13)-O(3M)	1.994(12)
Co(1)-O(3J)	2.277(12)	Co(13)-O(3S)	2.044(12)
Co(2)-O(128)	2.060(11)	Co(13)-N(2L)	2.079(16)
Co(2)-O(3R)	2.081(13)	Co(13)-N(2D)	2.095(14)
Co(2)-O(3I)	2.086(12)	Co(13)-O(3D)	2.204(11)
Co(2)-O(3F)	2.089(11)	Co(13)-O(3L)	2.207(12)
Co(2)-O(1A3)	2.093(11)		
Co(2)-O(1B3)	2.129(11)	O(159)-Co(1)-O(1A2)	83.6(4)
Co(3)-O(1B1)	1.988(10)	O(159)-Co(1)-O(128)	173.9(5)
Co(3)-O(345)	2.083(10)	O(1A2)-Co(1)-O(128)	97.1(4)
Co(3)-O(3N)	2.100(11)	O(159)-Co(1)-O(1B3)	107.8(4)
Co(3)-O(3O)	2.121(11)	O(1A2)-Co(1)-O(1B3)	95.2(4)
Co(3)-O(3M)	2.177(11)	O(128)-Co(1)-O(1B3)	78.2(4)
Co(3)-N(2M)	2.241(16)	O(159)-Co(1)-O(3U)	91.5(4)
Co(4)-O(3Q)	2.096(11)	O(1A2)-Co(1)-O(3U)	174.8(5)
Co(4)-O(1A1)	2.103(11)	O(128)-Co(1)-O(3U)	87.6(4)
Co(4)-O(345)	2.109(11)	O(1B3)-Co(1)-O(3U)	87.9(4)
Co(4)-O(3K)	2.145(12)	O(159)-Co(1)-O(3J)	80.6(4)
Co(4)-O(1B2)	2.147(11)	O(1A2)-Co(1)-O(3J)	103.2(4)
Co(4)-O(3O)	2.148(11)	O(128)-Co(1)-O(3J)	93.4(4)
Co(5)-O(345)	2.015(10)	O(1B3)-Co(1)-O(3J)	160.6(4)
Co(5)-O(159)	2.079(10)	O(3U)-Co(1)-O(3J)	74.1(4)
Co(5)-O(5T)	2.094(12)	O(128)-Co(2)-O(3R)	104.9(5)
Co(5)-O(3C)	2.109(12)	O(128)-Co(2)-O(3I)	82.8(4)
Co(5)-O(3G)	2.184(11)	O(3R)-Co(2)-O(3I)	97.5(5)
Co(5)-O(1A2)	2.259(11)	O(128)-Co(2)-O(3F)	170.8(5)
Co(6)-O(3U)	2.021(12)	O(3R)-Co(2)-O(3F)	84.1(5)
Co(6)-O(3T)	2.037(12)	O(3I)-Co(2)-O(3F)	94.1(4)
Co(6)-O(6T)	2.049(15)	O(128)-Co(2)-O(1A3)	100.8(4)
Co(6)-O(3E)	2.107(13)	O(3R)-Co(2)-O(1A3)	85.8(4)
Co(6)-O(3J)	2.142(12)	O(3I)-Co(2)-O(1A3)	174.4(5)
Co(6)-O(12)	2.175(15)	O(3F)-Co(2)-O(1A3)	81.7(4)
Co(7)-O(3Q)	2.028(12)	O(128)-Co(2)-O(1B3)	78.0(4)
Co(7)-O(3D)	2.062(11)	O(3R)-Co(2)-O(1B3)	172.2(5)
Co(7)-N(2O)	2.072(14)	O(3I)-Co(2)-O(1B3)	90.0(4)
Co(7)-N(2S)	2.108(15)	O(3F)-Co(2)-O(1B3)	93.3(4)
Co(7)-O(3S)	2.348(12)	O(1A3)-Co(2)-O(1B3)	86.6(4)
Co(8)-O(3E)	2.021(13)	O(1B1)-Co(3)-O(345)	91.5(4)
Co(8)-O(128)	2.041(11)	O(1B1)-Co(3)-O(3N)	93.0(4)
Co(8)-N(2I)	2.050(15)	O(345)-Co(3)-O(3N)	92.3(4)
Co(8)-N(2U)	2.116(15)	O(1B1)-Co(3)-O(3O)	101.3(4)
Co(8)-O(3I)	2.314(12)	O(345)-Co(3)-O(3O)	76.0(4)
Co(9)-O(159)	1.998(10)	O(3N)-Co(3)-O(3O)	161.7(4)
Co(9)-O(3T)	2.028(12)	O(1B1)-Co(3)-O(3M)	161.9(5)
Co(9)-O(3P)	2.123(12)	O(345)-Co(3)-O(3M)	106.5(4)
Co(9)-O(3C)	2.153(12)	O(3N)-Co(3)-O(3M)	88.4(4)
Co(9)-N(2P)	2.161(15)	O(3O)-Co(3)-O(3M)	81.7(4)
Co(9)-O(3J)	2.223(12)	O(1B1)-Co(3)-N(2M)	102.4(5)
Co(10)-O(3H)	2.084(12)	O(345)-Co(3)-N(2M)	162.4(5)
Co(10)-O(22)	2.120(16)	O(3N)-Co(3)-N(2M)	97.6(5)
Co(10)-N(2F)	2.126(15)	O(3O)-Co(3)-N(2M)	90.6(5)
Co(10)-N(2R)	2.132(17)	O(3M)-Co(3)-N(2M)	59.5(5)
Co(10)-N(2H)	2.183(17)	O(3Q)-Co(4)-O(1A1)	94.0(4)
Co(10)-O(3R)	2.193(13)	O(3Q)-Co(4)-O(345)	96.6(4)
Co(11)-O(3H)	2.051(12)	O(1A1)-Co(4)-O(345)	94.3(4)
Co(11)-O(3F)	2.059(11)	O(3Q)-Co(4)-O(3K)	89.3(4)
Co(11)-O(1B2)	2.094(11)	O(1A1)-Co(4)-O(3K)	83.3(4)
Co(11)-O(1A3)	2.114(11)	O(345)-Co(4)-O(3K)	173.8(4)
Co(11)-N(2K)	2.157(14)	O(3Q)-Co(4)-O(1B2)	160.1(4)
Co(11)-O(3K)	2.159(11)	O(1A1)-Co(4)-O(1B2)	98.0(4)
Co(12)-O(3L)	2.053(12)	O(345)-Co(4)-O(1B2)	98.3(4)
Co(12)-O(3G)	2.059(11)	O(3K)-Co(4)-O(1B2)	76.4(4)

O(3Q)-Co(4)-O(3O)	85.7(4)	O(159)-Co(9)-O(3J)	82.6(4)
O(1A1)-Co(4)-O(3O)	169.1(4)	O(3T)-Co(9)-O(3J)	78.8(4)
O(345)-Co(4)-O(3O)	74.9(4)	O(3P)-Co(9)-O(3J)	174.3(5)
O(3K)-Co(4)-O(3O)	107.6(4)	O(3C)-Co(9)-O(3J)	85.3(4)
O(1B2)-Co(4)-O(3O)	85.5(4)	N(2P)-Co(9)-O(3J)	121.8(5)
O(345)-Co(5)-O(159)	95.5(4)	O(3H)-Co(10)-O(22)	90.4(5)
O(345)-Co(5)-O(5T)	90.6(4)	O(3H)-Co(10)-N(2F)	98.4(5)
O(159)-Co(5)-O(5T)	166.0(5)	O(22)-Co(10)-N(2F)	101.3(6)
O(345)-Co(5)-O(3C)	169.1(5)	O(3H)-Co(10)-N(2R)	153.2(6)
O(159)-Co(5)-O(3C)	79.2(4)	O(22)-Co(10)-N(2R)	104.8(7)
O(5T)-Co(5)-O(3C)	96.6(5)	N(2F)-Co(10)-N(2R)	100.0(6)
O(345)-Co(5)-O(3G)	85.7(4)	O(3H)-Co(10)-N(2H)	62.9(6)
O(159)-Co(5)-O(3G)	102.0(4)	O(22)-Co(10)-N(2H)	82.2(6)
O(5T)-Co(5)-O(3G)	90.9(4)	N(2F)-Co(10)-N(2H)	161.2(6)
O(3C)-Co(5)-O(3G)	86.1(4)	N(2R)-Co(10)-N(2H)	96.9(6)
O(345)-Co(5)-O(1A2)	96.6(4)	O(3H)-Co(10)-O(3R)	101.3(5)
O(159)-Co(5)-O(1A2)	77.6(4)	O(22)-Co(10)-O(3R)	165.4(6)
O(5T)-Co(5)-O(1A2)	89.2(4)	N(2F)-Co(10)-O(3R)	85.7(5)
O(3C)-Co(5)-O(1A2)	91.6(4)	N(2R)-Co(10)-O(3R)	61.1(6)
O(3G)-Co(5)-O(1A2)	177.7(4)	N(2H)-Co(10)-O(3R)	95.3(5)
O(3U)-Co(6)-O(3T)	87.0(5)	O(3H)-Co(11)-O(3F)	89.7(5)
O(3U)-Co(6)-O(6T)	178.9(5)	O(3H)-Co(11)-O(1B2)	167.2(5)
O(3T)-Co(6)-O(6T)	92.0(5)	O(3F)-Co(11)-O(1B2)	94.0(4)
O(3U)-Co(6)-O(3E)	84.0(5)	O(3H)-Co(11)-O(1A3)	85.4(4)
O(3T)-Co(6)-O(3E)	170.6(5)	O(3F)-Co(11)-O(1A3)	81.9(4)
O(6T)-Co(6)-O(3E)	97.0(5)	O(1B2)-Co(11)-O(1A3)	83.0(4)
O(3U)-Co(6)-O(3J)	79.6(5)	O(3H)-Co(11)-N(2K)	95.5(5)
O(3T)-Co(6)-O(3J)	80.5(5)	O(3F)-Co(11)-N(2K)	106.3(5)
O(6T)-Co(6)-O(3J)	100.6(5)	O(1B2)-Co(11)-N(2K)	95.3(5)
O(3E)-Co(6)-O(3J)	95.3(5)	O(1A3)-Co(11)-N(2K)	171.7(5)
O(3U)-Co(6)-O(12)	91.4(5)	O(3H)-Co(11)-O(3K)	101.8(5)
O(3T)-Co(6)-O(12)	90.8(5)	O(3F)-Co(11)-O(3K)	164.3(5)
O(6T)-Co(6)-O(12)	88.3(5)	O(1B2)-Co(11)-O(3K)	77.2(4)
O(3E)-Co(6)-O(12)	92.0(5)	O(1A3)-Co(11)-O(3K)	109.5(4)
O(3J)-Co(6)-O(12)	167.8(5)	N(2K)-Co(11)-O(3K)	62.3(5)
O(3Q)-Co(7)-O(3D)	87.5(5)	O(3L)-Co(12)-O(3G)	97.0(5)
O(3Q)-Co(7)-N(2O)	104.7(5)	O(3L)-Co(12)-O(3P)	168.8(5)
O(3D)-Co(7)-N(2O)	132.6(5)	O(3G)-Co(12)-O(3P)	89.2(5)
O(3Q)-Co(7)-N(2S)	118.5(5)	O(3L)-Co(12)-O(3N)	94.0(4)
O(3D)-Co(7)-N(2S)	91.7(5)	O(3G)-Co(12)-O(3N)	96.3(5)
N(2O)-Co(7)-N(2S)	119.3(6)	O(3P)-Co(12)-O(3N)	94.6(4)
O(3Q)-Co(7)-O(3S)	164.5(5)	O(3L)-Co(12)-N(2G)	89.0(5)
O(3D)-Co(7)-O(3S)	77.1(4)	O(3G)-Co(12)-N(2G)	62.6(5)
N(2O)-Co(7)-O(3S)	87.2(5)	O(3P)-Co(12)-N(2G)	85.5(5)
N(2S)-Co(7)-O(3S)	61.2(5)	O(3N)-Co(12)-N(2G)	158.9(5)
O(3E)-Co(8)-O(128)	101.4(5)	O(3L)-Co(12)-N(2N)	91.4(5)
O(3E)-Co(8)-N(2I)	111.1(6)	O(3G)-Co(12)-N(2N)	157.1(5)
O(128)-Co(8)-N(2I)	110.2(5)	O(3P)-Co(12)-N(2N)	86.4(5)
O(3E)-Co(8)-N(2U)	101.4(6)	O(3N)-Co(12)-N(2N)	61.8(5)
O(128)-Co(8)-N(2U)	124.8(5)	N(2G)-Co(12)-N(2N)	139.1(6)
N(2I)-Co(8)-N(2U)	107.1(6)	O(3M)-Co(13)-O(3S)	92.4(5)
O(3E)-Co(8)-O(3I)	169.9(5)	O(3M)-Co(13)-N(2L)	104.7(5)
O(128)-Co(8)-O(3I)	77.8(4)	O(3S)-Co(13)-N(2L)	114.2(6)
N(2I)-Co(8)-O(3I)	60.5(5)	O(3M)-Co(13)-N(2D)	145.8(5)
N(2U)-Co(8)-O(3I)	87.1(5)	O(3S)-Co(13)-N(2D)	94.6(5)
O(159)-Co(9)-O(3T)	101.0(5)	N(2L)-Co(13)-N(2D)	102.8(6)
O(159)-Co(9)-O(3P)	93.8(5)	O(3M)-Co(13)-O(3D)	87.0(5)
O(3T)-Co(9)-O(3P)	97.8(5)	O(3S)-Co(13)-O(3D)	80.8(4)
O(159)-Co(9)-O(3C)	80.0(4)	N(2L)-Co(13)-O(3D)	160.0(5)
O(3T)-Co(9)-O(3C)	163.7(5)	N(2D)-Co(13)-O(3D)	61.3(5)
O(3P)-Co(9)-O(3C)	98.4(4)	O(3M)-Co(13)-O(3L)	88.1(4)
O(159)-Co(9)-N(2P)	155.4(5)	O(3S)-Co(13)-O(3L)	175.8(5)
O(3T)-Co(9)-N(2P)	87.7(5)	N(2L)-Co(13)-O(3L)	61.7(5)
O(3P)-Co(9)-N(2P)	62.1(5)	N(2D)-Co(13)-O(3L)	87.3(5)
O(3C)-Co(9)-N(2P)	98.0(5)	O(3D)-Co(13)-O(3L)	103.4(4)

Table 25: Crystal data and structure refinement for (3-oxo-3-phenyl-propyl)-phosphonic acid.

Empirical formula	$C_9H_{12}O_{4.50}P$
Formula weight	223.16
Wavelength	0.71073 Å
Temperature	220(2) K
Crystal system	Monoclinic
Space group	P2(1)/c
Unit cell dimensions	a = 24.619(2) Å α = 90 °. b = 11.2527(17) Å β = 90.988(10) °. c = 7.441(2) Å γ = 90 °.
Volume	2061.0(7) $Å^3$
Number of reflections for cell	52 (15 < θ < 16 °.)
Z	8
Density (calculated)	1.438 Mg/m^3
Absorption coefficient	0.259 mm^{-1}
F(000)	936
Crystal description	Colourless block
Crystal size	0.4 x 0.4 x 0.4 mm
θ range for data collection	3.07 to 25.00 °.
Index ranges	0<=h<=29, -13<=k<=0, -8<=l<=8
Reflections collected	3653
Independent reflections	3604 [R(int) = 0.1446]
Scan type	ω - θ
Absorption correction	Psi-scans (Tmin= 0.31039, Tmax=0.40674)
Solution	direct (SHELXS-97 (Sheldrick, 1990))
Refinement type	Full-matrix least-squares on F^2
Program used for refinement	SHELXL-97
Hydrogen atom placement	geometric except phosphonate H-atoms placed on difmap
Hydrogen atom treatment	mixed
Data / restraints / parameters	3604/3/282
Goodness-of-fit on F^2	1.024
Conventional R [F>4σ(F)]	R1 = 0.0413 [2634 data]
Weighted R (F^2 and all data)	wR2 = 0.1015
Extinction coefficient	0.0120(15)
Final maximum Δ/σ	0.022
Weighting scheme	calc $w=1/[\sigma^2(Fo^2)+(0.0512P)^2+0.3692P]$ where $P=(Fo^2+2Fc^2)/3$
Largest diff. peak and hole	0.455 and -0.346 e.$Å^{-3}$

Table 26: Bond lengths [Å] and angles [°] for (3-oxo-3-phenyl-propyl)-phosphonic acid.

C(1A)-C(2A)	1.382(6)	P(9B)-O(9B1)	1.549(3)
C(1A)-C(6A)	1.390(6)		
C(2A)-C(3A)	1.371(7)	C(2A)-C(1A)-C(6A)	120.3(4)
C(3A)-C(4A)	1.376(6)	C(3A)-C(2A)-C(1A)	120.2(4)
C(4A)-C(5A)	1.389(6)	C(2A)-C(3A)-C(4A)	120.4(4)
C(5A)-C(6A)	1.387(6)	C(3A)-C(4A)-C(5A)	119.8(4)
C(6A)-C(7A)	1.495(5)	C(6A)-C(5A)-C(4A)	120.3(4)
C(7A)-O(7A)	1.216(5)	C(5A)-C(6A)-C(1A)	119.0(4)
C(7A)-C(8A)	1.508(5)	C(5A)-C(6A)-C(7A)	122.7(4)
C(8A)-C(9A)	1.518(5)	C(1A)-C(6A)-C(7A)	118.3(4)
C(9A)-P(9A)	1.781(4)	O(7A)-C(7A)-C(6A)	120.3(4)
P(9A)-O(9A2)	1.501(3)	O(7A)-C(7A)-C(8A)	120.8(4)
P(9A)-O(9A1)	1.540(3)	C(6A)-C(7A)-C(8A)	118.9(3)
P(9A)-O(9A3)	1.547(3)	C(7A)-C(8A)-C(9A)	111.5(3)
C(1B)-C(2B)	1.382(6)	C(8A)-C(9A)-P(9A)	116.4(3)
C(1B)-C(6B)	1.388(6)	O(9A2)-P(9A)-O(9A1)	113.58(17)
C(2B)-C(3B)	1.381(7)	O(9A2)-P(9A)-O(9A3)	111.69(16)
C(3B)-C(4B)	1.366(7)	O(9A1)-P(9A)-O(9A3)	105.39(19)
C(4B)-C(5B)	1.389(6)	O(9A2)-P(9A)-C(9A)	109.77(18)
C(5B)-C(6B)	1.383(5)	O(9A1)-P(9A)-C(9A)	105.6(2)
C(6B)-C(7B)	1.496(5)	O(9A3)-P(9A)-C(9A)	110.6(2)
C(7B)-O(7B)	1.212(5)	C(2B)-C(1B)-C(6B)	120.5(4)
C(7B)-C(8B)	1.506(5)	C(3B)-C(2B)-C(1B)	119.7(4)
C(8B)-C(9B)	1.520(5)	C(4B)-C(3B)-C(2B)	120.4(4)
C(9B)-P(9B)	1.771(4)	C(3B)-C(4B)-C(5B)	120.1(4)
P(9B)-O(9B3)	1.490(3)	C(6B)-C(5B)-C(4B)	120.3(4)
P(9B)-O(9B2)	1.538(3)	C(5B)-C(6B)-C(1B)	119.0(4)

C(5B)-C(6B)-C(7B)	122.9(4)	O(9B3)-P(9B)-O(9B2)	112.56(18)
C(1B)-C(6B)-C(7B)	118.1(4)	O(9B3)-P(9B)-O(9B1)	107.38(17)
O(7B)-C(7B)-C(6B)	119.7(4)	O(9B2)-P(9B)-O(9B1)	110.57(19)
O(7B)-C(7B)-C(8B)	120.4(4)	O(9B3)-P(9B)-C(9B)	114.03(19)
C(6B)-C(7B)-C(8B)	119.8(3)	O(9B2)-P(9B)-C(9B)	103.79(19)
C(7B)-C(8B)-C(9B)	110.9(3)	O(9B1)-P(9B)-C(9B)	108.47(19)
C(8B)-C(9B)-P(9B)	15.9(3)		

Table 27: Crystal data and structure refinement for (3-oxo-3-*p*-tolyl-propyl)-phosphonic acid.

Empirical formula	$C_{10}H_{13}O_4P$
Formula weight	228.17
Wavelength	1.54178 Å
Temperature	150(2) K
Crystal system	Orthorhombic
Space group	P2(1)2(1)2(1)
Unit cell dimensions	a = 5.5131(10) Å α = 90 °. b = 7.1358(12) Å β = 90 °. c = 26.724(4) Å γ = 90 °.
Volume	1051.3(3) $Å^3$
Number of reflections for cell	70 (40 < θ < 44 °.)
Z	4
Density (calculated)	1.442 Mg/m^3
Absorption coefficient	2.284 mm^{-1}
F(000)	480
Crystal description	Colourless Plate
Crystal size	0.51 x 0.23 x 0.08 mm
θ range for data collection	3.31 to 70.15°.
Index ranges	-6<=h<=5, -7<=k<=8, -23<=l<=32
Reflections collected	2232
Independent reflections	1116 [R(int) = 0.0112]
Scan type	ω - θ
Absorption correction	Optimised numerical (Tmin= 0.462, Tmax=0.775)
Solution	direct (SHELXS-97 (Sheldrick, 1990))
Refinement type	Full-matrix least-squares on F^2
Program used for refinement	SHELXL-97
Hydrogen atom placement	riding, rotating groups (Me)
Hydrogen atom treatment	mixed
Data / restraints / parameters	1116/0/143
Goodness-of-fit on F^2	1.062
Conventional R [F>4σ(F)]	R1 = 0.0371 [1072 data]
Weighted R (F^2 and all data)	wR2 = 0.0995
Absolute structure parameter	0.00(4)
Extinction coefficient	0.0037(8)
Final maximum Δ/σ	0.000
Weighting scheme	calc w=1/[\σ²(Fo²)+(0.0700P)²+0.4494P] where P=(Fo²+2Fc²)/3
Largest diff. peak and hole	0.481 and -0.524 $e.Å^{-3}$

Table 28: Bond lengths [Å] and angles [°] for (3-oxo-3-*p*-tolyl-propyl)-phosphonic acid.

O(1)-P(1)	1.504(2)	O(3)-P(1)-O(2)	105.76(13)
O(2)-P(1)	1.559(2)	O(1)-P(1)-C(1)	111.12(14)
O(3)-P(1)	1.543(2)	O(3)-P(1)-C(1)	109.38(13)
P(1)-C(1)	1.778(3)	O(2)-P(1)-C(1)	109.55(13)
C(1)-C(2)	1.518(4)	C(2)-C(1)-P(1)	113.3(2)
C(2)-C(3)	1.514(4)	C(3)-C(2)-C(1)	113.2(3)
C(3)-O(4)	1.221(4)	O(4)-C(3)-C(4)	121.1(3)
C(3)-C(4)	1.488(4)	O(4)-C(3)-C(2)	120.2(3)
C(4)-C(5)	1.397(4)	C(4)-C(3)-C(2)	118.7(3)
C(4)-C(9)	1.402(5)	C(5)-C(4)-C(9)	118.4(3)
C(5)-C(6)	1.381(5)	C(5)-C(4)-C(3)	118.8(3)
C(6)-C(7)	1.398(5)	C(9)-C(4)-C(3)	122.7(3)
C(7)-C(8)	1.398(4)	C(6)-C(5)-C(4)	120.5(3)
C(7)-C(10)	1.497(5)	C(5)-C(6)-C(7)	121.3(3)
C(8)-C(9)	1.373(5)	C(8)-C(7)-C(6)	117.6(3)
		C(8)-C(7)-C(10)	121.2(3)
O(1)-P(1)-O(3)	112.83(12)	C(6)-C(7)-C(10)	121.2(3)
O(1)-P(1)-O(2)	108.02(13)	C(9)-C(8)-C(7)	121.7(3)

C(8)-C(9)-C(4)	120.4(3)		

Table 29: Crystal data and structure refinement for $[Cu_4(Hmbpp)_2(H_2NC(O)NH_2)_2(H_2O)_8].4H_2O$.

Empirical formula	$C_{20}H_{52}Cu_4N_4O_{28}P_4Cu_4$
Formula weight	1174.70
Wavelength	0.71073 Å
Temperature	150(2) K
Crystal system	Monoclinic
Space group	P2(1)/c
Unit cell dimensions	a = 7.9478(18) Å α = 90 °. b = 14.715(3) Å β = 99.129(4) °. c = 17.977(4) Å γ = 90 °.
Volume	2075.9(8) $Å^3$
Number of reflections for cell	1020 (2.5 < theta < 27 °.)
Z	2
Density (calculated)	1.879 Mg/m^3
Absorption coefficient	2.275 mm^{-1}
F(000)	1200
Crystal description	Orange rod
Crystal size	0.40 x 0.10 x 0.09 mm
Theta range for data collection	1.80 to 26.38 °.
Index ranges	-8<=h<=9, -18<=k<=17, -22<=l<=17
Reflections collected	11608
Independent reflections	4214 [R(int) = 0.0161]
Scan type	phi and ω scans
Absorption correction	Sadabs (Tmin= 0.735, Tmax=0.928)
Solution	direct (SHELXS-97 (Sheldrick, 1990))
Refinement type	Full-matrix least-squares on F^2
Program used for refinement	SHELXL-97
Hydrogen atom placement	All oxygen H atoms placed on difmap, rest geometric
Hydrogen atom treatment	Disordered around N1U, N3U, C41; mixed
Data / restraints / parameters	4214/0/326
Goodness-of-fit on F^2	1.060
Conventional R [F>4σ(F)]	R1 = 0.0237 [3820 data]
Weighted R (F^2 and all data)	wR2 = 0.0695
Extinction coefficient	0
Final maximum Δ/σ	0.002
Weighting scheme	calc w=1/[\σ²(Fo²)+(0.0483P)²+0.0000P] where P=(Fo²+2Fc²)/3
Largest diff. peak and hole	0.493 and -0.341 e.$Å^{-3}$

Table 30: Selected bond lengths [Å] and angles [°] for $[Cu_4(Hmbpp)_2(H_2NC(O)NH_2)_2(H_2O)_8].4H_2O$.

Cu(1)-O(21)	1.9369(13)	O(21)-Cu(1)-O(11)	94.45(6)
Cu(1)-O(11)#1	1.9434(13)	O(11)#1-Cu(1)-O(11)	76.25(6)
Cu(1)-O(11)	1.9826(13)	O(21)-Cu(1)-O(61)#1	91.22(6)
Cu(1)-O(61)#1	1.9826(13)	O(11)#1-Cu(1)-O(61)#1	95.26(6)
Cu(1)-O(1)	2.2036(16)	O(11)-Cu(1)-O(61)#1	164.87(5)
O(11)-Cu(1)#1	1.9434(13)	O(21)-Cu(1)-O(1)	90.54(7)
P(2)-O(23)	1.5129(14)	O(11)#1-Cu(1)-O(1)	101.65(7)
P(2)-O(21)	1.5357(14)	O(11)-Cu(1)-O(1)	98.38(6)
P(2)-O(22)	1.5401(14)	O(61)#1-Cu(1)-O(1)	95.57(6)
O(22)-Cu(2)	1.9628(14)	Cu(1)#1-O(11)-Cu(1)	103.75(6)
P(6)-O(62)	1.4994(14)	O(2U)-Cu(2)-O(3)	169.27(6)
P(6)-O(61)	1.5319(13)	O(2U)-Cu(2)-O(22)	97.16(6)
P(6)-O(63)	1.5613(16)	O(3)-Cu(2)-O(22)	89.66(6)
O(61)-Cu(1)#1	1.9826(13)	O(2U)-Cu(2)-O(4)	88.86(6)
Cu(2)-O(2U)	1.9420(14)	O(3)-Cu(2)-O(4)	83.91(7)
Cu(2)-O(3)	1.9627(15)	O(22)-Cu(2)-O(4)	173.15(6)
Cu(2)-O(4)	1.9919(15)	O(2U)-Cu(2)-O(2)	89.54(6)
Cu(2)-O(2)	2.3681(18)	O(3)-Cu(2)-O(2)	98.36(6)
		O(22)-Cu(2)-O(2)	93.23(6)
O(21)-Cu(1)-O(11)#1	165.53(5)	O(4)-Cu(2)-O(2)	90.05(6)

Symmetry transformations used to generate equivalent atoms: #1 -x,-y+2,-z+1

Adsorption Isotherm Data.

Table 31: Calibration curve data for 2-hydroxypyridine.

Concentration (10^{-5}) Mole l^{-1}	Absorbance	Concentration (10^{-5}) Mole l^{-1}	Absorbance
1.4310	0.078	8.5860	0.467
2.8620	0.159	10.0170	0.528
4.2930	0.232	11.4480	0.624
5.7240	0.306	12.8790	0.695
7.1550	0.386	14.3100	0.782

Table 32: Adsorption isotherm data for 2-hydroxypyridine.

Initial concentration (10^{-3}) mol l^{-1}	Weight of $Al(OH)_3$ g	Absorbance	Dilution factor	Equilibrium concentration (10^{-3}) mol l^{-1}	Amount of ligand adsorbed (10^{-2}) mmol g^{-1}
0.1430	0.392	0.074	10	0.137	0.015
0.2860	0.418	0.148	10	0.273	0.031
0.4290	0.397	0.224	10	0.413	0.040
0.5720	0.408	0.299	10	0.552	0.049
0.7150	0.391	0.369	10	0.681	0.087
0.7150	0.407	0.361	10	0.666	0.120
1.4300	0.399	0.143	50	1.319	0.278
2.1450	0.398	0.217	50	2.002	0.359
2.8600	0.384	0.291	50	2.685	0.456
3.5750	0.420	0.365	50	3.368	0.493
4.2900	0.400	0.436	50	4.023	0.68
5.0050	0.393	0.510	50	4.706	0.761
5.7200	0.411	0.583	50	3.379	0.830
6.4350	0.404	0.658	50	6.071	0.901
7.1500	0.403	0.728	50	6.717	1.074

Table 33: Calibration curve data for uracil.

Concentration (10^{-5}) Mole l^{-1}	Absorbance	Concentration (10^{-5}) Mole l^{-1}	Absorbance
1.4350	0.108	8.6100	0.689
2.8700	0.221	10.0450	0.807
4.3050	0.341	11.4800	0.934
5.7400	0.457	12.9150	1.040
7.1750	0.565	14.3500	1.159

Table 34: Adsorption isotherm data for uracil.

Initial concentration (10^{-3}) mol l^{-1}	Weight of $Al(OH)_3$ g	Absorbance	Dilution factor	Equilibrium concentration (10^{-3}) mol l^{-1}	Amount of ligand adsorbed (10^{-2}) mmol g^{-1}
0.1435	0.402	1.083	0	0.133	0.026
0.2869	0.392	0.213	10	0.261	0.066
0.4304	0.399	0.321	10	0.393	0.094
0.5738	0.391	0.428	10	0.524	0.127
0.7173	0.396	0.509	10	0.623	0.238
0.7173	0.408	0.499	10	0.611	0.261
1.4366	0.388	0.538	20	1.318	0.300
2.1519	0.386	0.824	20	2.019	0.344
2.8692	0.403	1.081	20	2.648	0.549
3.5865	0.397	0.530	50	3.246	0.858
4.3038	0.393	0.642	50	3.932	0.946
5.0211	0.403	0.743	50	4.550	1.169
5.7384	0.395	0.862	50	5.279	1.163
6.4557	0.416	0.986	50	6.039	1.002
7.1730	0.416	1.089	50	6.670	1.209

Table 35: Calibration curve data for benzoic acid

Concentration (10^{-5}) Mole l^{-1}	Absorbance	Concentration (10^{-5}) Mole l^{-1}	Absorbance
0.7075	0.078	4.2450	0.445
1.4150	0.145	4.9525	0.520
2.1225	0.215	5.6600	0.593
2.8300	0.291	6.3675	0.559
3.5375	0.363	7.0750	0.732

Table 36: Adsorption isotherm data for benzoic acid.

Initial concentration (10^{-3}) mol l^{-1}	Weight of $Al(OH)_3$ g	Absorbance	Dilution factor	Equilibrium concentration (10^{-3}) mol l^{-1}	Amount of ligand adsorbed (10^{-2}) mmol g^{-1}
0.1415	0.405	1.255	0	0.121	0.051
0.2830	0.404	0.221	10	0.212	0.176
0.4245	0.405	0.292	10	0.281	0.354
0.5660	0.404	0.354	10	0.340	0.559
0.7075	0.404	0.439	10	0.422	0.707
0.7075	0.405	0.427	10	0.410	0.735
1.4150	0.405	1.050	10	0.971	1.096
2.1225	0.405	0.845	20	1.625	1.228
2.8300	0.403	1.178	20	2.265	1.402
3.5375	0.398	0.608	50	2.923	1.544
4.2450	0.397	0.748	50	3.595	1.637
4.9525	0.405	0.899	50	4.321	1.559
5.6600	0.401	1.041	50	5.004	1.636
6.3675	0.398	0.593	100	5.701	1.675
7.0750	0.397	0.699	100	6.431	1.622

Table 37: Calibration curve data for 3-(4-methylbenzoyl)-propionic acid (Irg-419).

Concentration (10^{-5}) Mole l^{-1}	Absorbance	Concentration (10^{-5}) Mole l^{-1}	Absorbance
0.7138	0.109	4.2828	0.642
1.4276	0.218	4.9966	0.747
2.1414	0.314	5.7104	0.872
2.8552	0.449	6.4242	0.935
3.5690	0.525	7.1380	1.080

Table 38: Adsorption isotherm data for 3-(4-methylbenzoyl)-propionic acid (Irg-419).

Initial concentration (10^{-3}) mol l^{-1}	Weight of $Al(OH)_3$ g	Absorbance	Dilution factor	Equilibrium concentration (10^{-3}) mol l^{-1}	Amount of ligand adsorbed (10^{-2}) mmol g^{-1}
0.0714	0.401	0.097	10	0.065	0.016
0.1428	0.392	0.175	10	0.117	0.066
0.2141	0.419	0.274	10	0.184	0.072
0.2855	0.410	0.310	10	0.208	0.189
0.3569	0.401	0.369	10	0.248	0.272
0.4283	0.414	0.442	10	0.296	0.320
0.4997	0.410	0.478	10	0.321	0.387
0.5710	0.393	0.528	10	0.354	0.552
0.6424	0.400	0.614	10	0.412	0.576
0.7138	0.397	0.656	10	0.440	0.690
0.7138	0.393	0.629	10	0.422	0.742
1.4276	0.418	0.137	100	0.919	1.218
2.1414	0.404	0.234	100	1.570	1.413
2.8552	0.397	0.315	100	2.113	1.819
3.5690	0.416	0.406	100	2.723	2.033
4.2828	0.404	0.505	100	3.387	2.218
4.9966	0.396	0.612	100	4.105	2.253
5.7104	0.397	0.709	100	4.756	2.403
6.4242	0.408	0.805	100	5.398	2.512
7.1380	0.403	0.907	100	6.084	2.615

Table 39: Calibration curve data for 4-p-tolyl-butyric acid (Irg-78).

Concentration (10^{-5}) Mole l^{-1}	Absorbance	Concentration (10^{-5}) Mole l^{-1}	Absorbance
0.9096	0.044	5.4576	0.489
1.8192	0.147	6.3672	0.502
2.7288	0.226	7.2768	0.562
3.6384	0.290	8.1864	0.650
4.5480	0.369	9.0960	0.716

Table 40: Adsorption isotherm data for 4-p-tolyl-butyric acid (Irg-78).

Initial concentration (10^{-3}) mol l^{-1}	Weight of $Al(OH)_3$ g	Absorbance	Dilution factor	Equilibrium concentration (10^{-3}) mol l^{-1}	Amount of ligand adsorbed (10^{-2}) mmol g^{-1}
0.1436	0.402	0.104	10	0.130	0.034
0.2873	0.402	0.167	10	0.209	0.195
0.4309	0.416	0.227	10	0.284	0.353
0.5746	0.395	0.309	10	0.386	0.477
0.7182	0.392	0.379	10	0.474	0.623
0.7182	0.391	0.396	10	0.495	0.571
1.4364	0.410	0.872	10	1.090	0.845
2.1546	0.418	0.267	50	1.669	1.162
2.8728	0.397	0.384	50	2.400	1.191
3.5910	0.390	0.512	50	3.200	1.003
4.3092	0.405	0.617	50	3.857	1.117
5.0274	0.413	0.722	50	4.513	1.246
5.7456	0.388	0.832	50	5.201	1.404
6.4638	0.405	0.948	50	5.926	1.328
7.1820	0.416	1.040	50	6.501	1.637

Table 41: Calibration curve data for phenylphosphinic acid.

Concentration (10^{-5}) Mole l^{-1}	Absorbance	Concentration (10^{-5}) Mole l^{-1}	Absorbance
1.3970	0.144	8.3820	0.684
2.7940	0.24	9.7790	0.859
4.1910	0.366	11.1760	0.932
5.5880	0.465	12.5730	1.039
6.9850	0.576	13.9700	1.187

Table 42: Adsorption isotherm data for phenylphosphinic acid.

Initial concentration (10^{-3}) mol l^{-1}	Weight of $Al(OH)_3$ g	Absorbance	Dilution factor	Equilibrium concentration (10^{-3}) mol l^{-1}	Amount of ligand adsorbed (10^{-2}) mmol g^{-1}
0.1397	0.404	0.086	10	0.104	0.087
0.2794	0.393	0.157	10	0.190	0.227
0.4192	0.413	0.193	10	0.233	0.451
0.5889	0.409	0.267	10	0.323	0.650
0.6986	0.402	0.247	10	0.298	0.997
0.6986	0.398	0.245	10	0.296	1.016
1.3972	0.418	0.585	10	0.707	1.652
2.0958	0.403	1.104	10	1.334	1.890
2.7944	0.406	0.769	20	1.858	2.306
3.4930	0.394	1.040	20	2.513	2.487
4.1916	0.398	0.509	50	3.075	2.806
4.8902	0.396	0.613	50	3.703	2.998
5.5888	0.386	0.735	50	4.441	2.974
6.2874	0.401	0.841	50	5.081	3.008
6.9860	0.406	0.961	50	5.806	2.906

Table 43: Calibration curve data for diphenylphosphinic acid.

Concentration (10^{-5}) Mole l^{-1}	Absorbance	Concentration (10^{-5}) Mole l^{-1}	Absorbance
0.6990	0.089	4.1940	0.612
1.3980	0.196	4.8930	0.722
2.0970	0.308	5.5920	0.812
2.7960	0.392	6.2910	0.926
3.4950	0.497	6.990	1.020

Table 44: Adsorption isotherm data for diphenylphosphinic acid.

Initial concentration (10^{-3}) mol l^{-1}	Weight of $Al(OH)_3$ g	Absorbance	Dilution factor	Equilibrium concentration (10^{-3}) mol l^{-1}	Amount of ligand adsorbed (10^{-2}) mmol g^{-1}
0.1398	0.408	0.177	10	0.119	0.051
0.2796	0.412	0.314	10	0.212	0.164
0.4195	0.410	0.384	10	0.259	0.405
0.5593	0.395	0.474	10	0.319	0.608
0.6991	0.385	0.484	10	0.326	0.969
0.6991	0.394	0.475	10	0.320	0.962
1.3982	0.413	1.187	10	0.800	1.448
2.0973	0.417	1.005	20	1.355	1.756
2.7964	0.398	0.585	50	1.971	2.074
3.4955	0.398	0.758	50	2.554	2.366
4.1946	0.416	0.954	50	3.215	2.35
4.8937	0.392	0.578	100	3.882	2.581
5.5928	0.406	0.677	100	4.562	2.539
6.2919	0.386	0.792	100	5.337	2.474
6.9910	0.408	0.883	100	5.951	2.549

Table 45: Calibration curve data for phenylphosphonic acid.

Concentration (10^{-5}) Mole l^{-1}	Absorbance	Concentration (10^{-5}) Mole l^{-1}	Absorbance
1.4120	0.127	8.4720	0.724
2.8240	0.218	9.8840	0.845
4.2360	0.387	11.2960	0.96
5.6480	0.473	12.7080	1.083
7.060o	0.576	14.1200	1.207

Table 46: Adsorption isotherm data for phenylphosphonic acid.

Initial concentration (10^{-3}) mol l^{-1}	Weight of $Al(OH)_3$ g	Absorbance	Dilution factor	Equilibrium concentration (10^{-3}) mol l^{-1}	Amount of ligand adsorbed (10^{-2}) mmol g^{-1}
0.1412	0.412	0.193	0	0.023	0.287
0.2824	0.417	0.222	0	0.026	0.615
0.4235	0.404	0.601	0	0.070	0.875
0.5647	0.404	0.123	10	0.144	1.041
0.7059	0.406	0.160	10	0.187	1.278
0.7059	0.417	0.125	10	0.146	1.343
1.4118	0.385	0.095	50	0.556	2.223
2.1177	0.401	0.182	50	1.065	2.625
2.8236	0.391	0.303	50	1.773	2.687
3.5295	0.393	0.406	50	2.376	2.935
4.2554	0.414	0.515	50	3.014	2.999
4.9413	0.405	0.628	50	3.675	3.127
5.6472	0.415	0.757	50	4.430	2.933
6.3531	0.395	0.867	50	5.074	3.238
7.0590	0.397	0.967	50	5.660	3.524

Table 47: Calibration curve data for benzylphosphonic acid.

Concentration (10^{-5}) Mole l^{-1}	Absorbance	Concentration (10^{-5}) Mole l^{-1}	Absorbance
1.4050	0.098	8.4300	0.666
2.8100	0.232	9.8350	0.786
4.2150	0.326	1.1240	0.925
5.6200	0.443	12.6450	1.081
7.0250	0.560	14.0500	1.162

Table 48: Adsorption isotherm data for benzylphosphonic acid.

Initial concentration (10^{-3}) mol l^{-1}	Weight of $Al(OH)_3$ g	Absorbance	Dilution factor	Equilibrium concentration (10^{-3}) mol l^{-1}	Amount of ligand adsorbed (10^{-2}) mmol g^{-1}
0.1405	0.394	0.116	0	0.014	0.321
0.2809	0.399	0.156	0	0.018	0.659
0.4214	0.405	0.224	0	0.026	0.976
05618	0.403	0.744	0	0.088	1.176
0.7023	0.394	0.131	10	0.155	1.389
0.7023	0.401	0.150	10	0.177	1.310
1.4096	0.391	0.511	10	0.603	2.063
2.1064	0.411	1.001	10	1.181	2.252
2.8092	0.400	0.778	20	1.836	2.433
3.5115	0.390	0.431	50	2.542	2.486
4.2138	0.416	0.533	50	3.144	2.572
4.9161	0.409	0.647	50	3.817	2.687
5.6184	0.416	0.752	50	4.436	2.842
6.3207	0.395	0.871	50	5.138	2.994
7.0230	0.410	0.982	50	5.793	3.000

Table 49: Calibration curve data for 4-nitrobenzylphosphonic acid.

Concentration (10^{-5}) Mole l^{-1}	Absorbance	Concentration (10^{-5}) Mole l^{-1}	Absorbance
0.7010	0.074	4.2030	0.433
1.4010	0.150	4.9040	0.500
2.1020	0.219	5.6040	0.571
2.8020	0.292	6.3050	0.648
3.5030	0.360	7.0050	0.709

Table 50: Adsorption isotherm data for 4-nitrobenzylphosphonic acid.

Initial concentration (10^{-3}) mol l^{-1}	Weight of $Al(OH)_3$ g	Absorbance	Dilution factor	Equilibrium concentration (10^{-3}) mol l^{-1}	Amount of ligand adsorbed (10^{-2}) mmol g^{-1}
0.1401	0.399	0.101	0	0.010	0.321
0.2802	0.405	0.166	0	0.016	0.653
0.4203	0.398	0.305	0	0.030	0.981
0.5604	0.404	0.803	0	0.080	1.189
0.7005	0.404	1.097	0	0.109	1.464
0.7005	0.405	1.158	0	0.115	1.445
1.4010	0.403	0.588	10	0.583	2.029
2.1015	0.399	1.233	10	1.222	2.204
2.8020	0.398	0.923	20	1.829	2.445
3.5025	0.395	0.510	50	2.526	2.454
4.2030	0.400	0.698	50	3.210	2.483
4.9035	0.397	0.775	50	3.839	2.681
5.6040	0.405	0.898	50	4.448	2.854
6.3045	0.397	1.034	50	5.122	2.979
7.0050	0.397	1.173	50	5.810	3.010

Table 51: Calibration curve data for (2-phosphonomethyl-benzyl)-phosphonic acid.

Concentration (10^{-5}) Mole l^{-1}	Absorbance	Concentration (10^{-5}) Mole l^{-1}	Absorbance
1.0488	0.108	6.2928	0.633
2.0976	0.209	7.3416	0.736
3.1479	0.316	8.3904	0.836
4.1952	0.427	9.4392	0.942
5.2440	0.536	10.4880	1.050

Table 52: Adsorption isotherm data for (2-phosphonomethyl-benzyl)-phosphonic acid.

Initial concentration (10^{-3}) mol l^{-1}	Weight of $Al(OH)_3$ g	Absorbance	Dilution factor	Equilibrium concentration (10^{-3}) mol l^{-1}	Amount of ligand adsorbed (10^{-2}) mmol g^{-1}
0.1398	0.394	0.182	0	0.018	0.309
0.2797	0.392	0.458	0	0.046	0.596
0.4195	0.411	0.569	0	0.057	0.882
0.5514	0.395	0.125	10	0.126	1.077
0.6992	0.404	0.214	10	0.215	1.199
0.6992	0.397	0.275	10	0.276	1.066
1.3984	0.390	0.818	10	0.821	1.481
2.0976	0.393	0.725	20	1.456	1.633
2.7968	0.405	1.030	20	2.069	1.797
3.4980	0.395	0.553	50	2.777	1.825
4.1952	0.408	0.678	50	3.404	1.939
4.8944	0.406	0.810	50	4.067	2.038
5.5936	0.404	0.941	50	4.725	2.150
6.2928	0.403	0.540	100	5.423	2.158
6.9920	0.403	1.207	50	6.060	2.313

Table 53: Calibration curve data for (3-phosphonomethyl-benzyl)-phosphonic acid.

Concentration (10^{-5}) Mole l^{-1}	Absorbance	Concentration (10^{-5}) Mole l^{-1}	Absorbance
0.7023	0.076	4.2138	0.439
1.4046	0.141	4.9161	0.488
2.1069	0.202	5.6184	0.564
2.8092	0.297	6.3207	0.643
3.5115	0.364	7.0230	0.690

Table 54: Adsorption isotherm data for (3-phosphonomethyl-benzyl)-phosphonic acid.

Initial concentration (10^{-3}) mol l^{-1}	Weight of $Al(OH)_3$ g	Absorbance	Dilution factor	Equilibrium concentration (10^{-3}) mol l^{-1}	Amount of ligand adsorbed (10^{-2}) mmol g^{-1}
0.1405	0.384	0.111	0	0.011	0.337
0.2809	0.419	0.258	0	0.026	0.608
0.4214	0.410	0.580	0	0.058	0.886
0.5618	0.403	0.152	10	0.153	1.014
0.7023	0.400	0.207	10	0.207	1.233
0.7023	0.396	0.182	10	0.183	1.311
1.4046	0.393	0.686	10	0.691	1.816
2.1069	0.409	0.578	20	1.165	2.303
2.8092	0.409	0.924	20	1.863	2.313
3.5115	0.421	1.221	20	2.461	2.495
4.2138	0.403	0.626	50	3.155	2.627
4.9161	0.407	0.757	50	3.815	2.705
5.6184	0.414	0.876	50	4.414	2.909
6.3207	0.402	1.025	50	5.165	2.875
7.0230	0.397	1.173	50	5.911	2.801

Table 55: Calibration curve data for (4-phosphonomethyl-benzyl)-phosphonic acid.

Concentration (10^{-5}) Mole l^{-1}	Absorbance	Concentration (10^{-5}) Mole l^{-1}	Absorbance
0.7083	0.078	4.2498	0.495
1.4166	0.171	4.9581	0.588
2.1249	0.270	5.6664	0.682
2.8332	0.341	6.3747	0.768
3.5415	0.424	7.0830	0.860

Table 56: Adsorption isotherm data for (4-phosphonomethyl-benzyl)-phosphonic acid.

Initial concentration (10^{-3}) mol l^{-1}	Weight of $Al(OH)_3$ g	Absorbance	Dilution factor	Equilibrium concentration (10^{-3}) mol l^{-1}	Amount of ligand adsorbed (10^{-2}) mmol g^{-1}
0.1417	0.414	0.113	0	0.009	0.321
0.2853	0.390	0.682	0	0.056	0.588
0.4250	0.400	0.107	10	0.089	0.840
0.5666	0.390	0.222	10	0.184	0.981
0.7083	0.407	0.295	10	0.245	1.138
0.7083	0.390	0.290	10	0.241	1.198
1.4166	0.390	0.870	10	0.722	1.781
2.1249	0.390	0.802	20	1.331	2.036
2.8332	0.400	1.164	20	1.931	2.256
3.5415	0.401	0.624	50	2.588	2.378
4.2498	0.396	0.784	50	3.252	2.520
4.9581	0.419	0.940	50	3.899	2.528
5.6664	0.396	1.121	50	4.650	2.561
6.3747	0.407	0.636	100	5.276	2.700
7.0830	0.416	0.718	100	5.956	2.709

Table 57: Calibration curve data for 4-methyl-2,6-bis(phosphonomethyl)phenol.

Concentration (10^{-5}) Mole l^{-1}	Absorbance	Concentration (10^{-5}) Mole l^{-1}	Absorbance
0.3514	0.093	2.1084	0.544
0.7028	0.186	2.4598	0.641
1.0542	0.268	2.8112	0.734
1.4056	0.360	3.1628	0.822
1.7570	0.453	3.5140	0.910

Table 58: Adsorption isotherm data for 4-methyl-2,6-bis(phosphonomethyl)phenol.

Initial concentration (10^{-3}) mol l^{-1}	Weight of $Al(OH)_3$ g	Absorbance	Dilution factor	Equilibrium concentration (10^{-3}) mol l^{-1}	Amount of ligand adsorbed (10^{-2}) mmol g^{-1}
0.1405	0.397	0.026	0	0.010	0.329
0.2811	0.417	0.032	0	0.012	0.645
0.4216	0.407	0.243	0	0.093	0.804
0.5622	0.397	0.404	0	0.155	1.026
0.7027	0.408	0.611	0	0.235	1.145
0.7027	0.392	0.614	0	0.237	1.188
1.4054	0.404	0.193	10	0.743	1.640
2.1081	0.402	0.313	10	1.435	1.674
2.8108	0.415	0.530	10	2.116	1.674
3.5135	0.408	0.719	10	2.766	1.808
4.2162	0.401	0.909	10	3.494	1.801
4.9189	0.398	1.102	10	4.240	1.706
5.6216	0.413	0.630	20	4.894	1.762
6.3243	0.420	0.726	20	5.587	1.755
7.0270	0.409	0.820	20	6.310	1.753

Table 59: Calibration curve data for (3-oxo-3-*p*-tolyl-propyl)-phosphonic acid.

Concentration (10^{-5}) Mole l^{-1}	Absorbance	Concentration (10^{-5}) Mole l^{-1}	Absorbance
0.7000	0.096	4.2020	0.661
1.4010	0.217	4.9030	0.769
2.1010	0.319	5.6030	0.890
2.8020	0.429	6.3040	0.994
3.5020	0.542	7.0040	1.097

Table 60: Adsorption isotherm data for (3-oxo-3-*p*-tolyl-propyl)-phosphonic acid.

Initial concentration (10^{-3}) mol l^{-1}	Weight of $Al(OH)_3$ g	Absorbance	Dilution factor	Equilibrium concentration (10^{-3}) mol l^{-1}	Amount of ligand adsorbed (10^{-2}) mmol g^{-1}
0.1401	0.403	0.068	0	0.004	0.338
0.2802	0.395	0.100	0	0.006	0.694
0.4202	0.400	0.211	0	0.013	1.018
0.5603	0.400	0.802	0	0.050	1.276
0.7004	0.399	1.023	2	0.128	1.435
0.7004	0.397	1.007	2	0.126	1.447
1.4008	0.393	0.792	10	0.496	2.302
2.1012	0.405	0.909	20	1.139	2.376
2.8016	0.401	1.371	20	1.718	2.702
3.5020	0.395	0.772	50	2.419	2.742
4.2024	0.397	0.961	50	3.011	3.001
4.9024	0.394	1.181	50	3.701	3.050
5.6032	0.405	0.693	100	4.343	3.112
6.3036	0.398	0.806	100	5.051	3.147
7.0040	0.406	0.910	100	5.703	3.204

Table 61: Calibration curve data for (3-oxo-3-phenyl-propyl)-phosphonic acid.

Concentration (10^{-5}) Mole l^{-1}	Absorbance	Concentration (10^{-5}) Mole l^{-1}	Absorbance
0.8879	0.115	5.3274	0.698
1.7758	0.234	6.2153	0.822
2.6637	0.348	7.1032	0.929
3.5516	0.461	7.9911	1.033
4.4395	0.581	8.8790	1.161

Table 62: Adsorption isotherm data for (3-oxo-3-phenyl-propyl)-phosphonic acid.

Initial concentration (10^{-3}) mol l^{-1}	Weight of $Al(OH)_3$ g	Absorbance	Dilution factor	Equilibrium concentration (10^{-3}) mol l^{-1}	Amount of ligand adsorbed (10^{-2}) mmol g^{-1}
0.1421	0.399	0.039	0	0.003	0.349
0.2841	0.402	0.112	0	0.009	0.684
0.4261	0.398	0.244	0	0.019	1.023
0.5682	0.404	0.751	0	0.058	1.263
0.7103	0.400	0.774	2	0.119	1.478
0.7103	0.400	0.872	2	0.134	1.441
1.4206	0.401	0.697	10	0534	2.211
2.1309	0.398	0.734	20	1.125	2.527
2.8412	0.401	1.150	20	1.763	2.689
3.5150	0.401	0.622	50	2.384	2.911
4.2618	0.405	0.790	50	3.028	3.046
4.9721	0.401	0.977	50	3.745	3.060
5.6824	0.401	1.139	50	4.366	3.283
6.3927	0.403	0.670	100	5.136	3.118
7.1030	0.403	0.780	100	5.826	3.169

Table 63: Calibration curve data for (2-oxo-2-phenyl-ethyl)-phosphonic acid.

Concentration (10^{-5}) Mole l^{-1}	Absorbance	Concentration (10^{-5}) Mole l^{-1}	Absorbance
0.7000	0.094	4.2000	0.551
1.4000	0.188	4.9000	0.646
2.1000	0.274	5.6000	0.743
2.8000	0.370	6.3000	0.834
3.5000	0.455	7.0000	0.917

Table 64: Adsorption isotherm data for (2-oxo-2-phenyl-ethyl)-phosphonic acid.

Initial concentration (10^{-3}) mol l^{-1}	Weight of $Al(OH)_3$ g	Absorbance	Dilution factor	Equilibrium concentration (10^{-3}) mol l^{-1}	Amount of ligand adsorbed (10^{-2}) mmol g^{-1}
0.1400	0.404	0.051	0	0.004	0.337
0.2800	0.401	0.104	0	0.008	0.678
0.4200	0.401	0.136	0	0.010	1.022
0.5600	-	-	-	-	-
0.7000	0.396	0.146	10	0.111	1.487
0.7000	0.405	0.123	10	0.093	1.499
1.4000	0.402	0.667	10	0.507	2.221
2.1000	0.396	0.736	20	1.119	2.477
2.8000	0.397	1.175	20	1.786	2.554
3.5000	0.403	0.645	50	2.451	2.603
4.2000	0.397	0.824	50	3.131	2.693
4.9000	0.404	1.012	50	3.846	2.609
5.6000	0.402	0.597	100	4.537	2.644
6.3000	0.403	0.690	100	5.244	2.620
7.0000	0.403	0.781	100	5.936	2.640

Table 65: Calibration curve data for (3-phenyl-propyl)-phosphonic acid.

Concentration (10^{-5}) Mole l^{-1}	Absorbance	Concentration (10^{-5}) Mole l^{-1}	Absorbance
1.400	0.159	8.400	0.709
2.800	0.284	9.800	0.840
4.200	0.395	11.20	0.954
5.600	0.515	12.60	1.089
7.000	0.619	14.00	1.183

Table 66: Adsorption isotherm data for (3-phenyl-propyl)-phosphonic acid.

Initial concentration (10^{-3}) mol l^{-1}	Weight of $Al(OH)_3$ g	Absorbance	Dilution factor	Equilibrium concentration (10^{-3}) mol l^{-1}	Amount of ligand adsorbed (10^{-2}) mmol g^{-1}
0.1400	0.397	0.159	0	0.020	0.302
0.2800	0.400	0.447	0	0.055	0.563
0.4200	0.398	0.570	0	0.070	0.879
0.5600	0.395	0.617	0	0.076	1.231
0.7000	0.401	0.114	10	0.141	1.394
0.7000	0.396	0.114	10	0.141	1.414
1.4000	0.396	0.424	10	0.523	2.215
2.1000	0.396	0.910	10	1.123	2.467
2.8000	0.404	0.739	20	1.825	2.413
3.5000	0.399	1.006	20	2.484	2.546
4.2000	0.399	0.513	50	3.167	2.589
4.9000	0.395	0.627	50	3.870	2.608
5.6000	0.398	0.737	50	4.549	2.641
6.3000	0.403	0.849	50	5.241	2.628
7.0000	0.404	0.959	50	5.920	2.673

Table 67: R^2* values for the curve fitting of adsorption isotherm data as obtained from SigmaPlot 2000.

Ligand	R^2	
	Langmuir	Double Langmuir
2-hydroxypyridine	0.99162	-
uracil	0.94775	-
Irg-419	0.99125	-
Irg-78	0.93319	-
benzoic acid	0.97194	-
phenylphosphinic acid	0.97296	-
diphenylphosphinic acid	0.96449	-
phenylphosphonic acid	0.975532	-
benzylphosphonic acid	-	0.98299
4-nbpa	-	0.99160
2-pmbpa	-	0.98730
3-pmbpa	0.95841	0.99214
4-pmbpa	0.97284	0.99779
H_5mbpp	0.91735	-
P-bpa	0.92004	0.99530
P-419	0.90151	0.98892
2-opepa	0.92737	0.98885
3-pppa	0.98367	-

* R^2 is defined as the coefficient of determination and is a measure of how well a regression model describes the data. R^2 values near 1 indicate that the equation is a good description of the relation between the independent and dependent variables